



HAL
open science

The role of human-induced climate change on extreme convective precipitation events in the south of France: a high-resolution model simulation approach

Nhat Linh Luu

► To cite this version:

Nhat Linh Luu. The role of human-induced climate change on extreme convective precipitation events in the south of France: a high-resolution model simulation approach. Climatology. Université Paris-Saclay, 2020. English. NNT: 2020UPASV018 . tel-03104336

HAL Id: tel-03104336

<https://theses.hal.science/tel-03104336>

Submitted on 8 Jan 2021

HAL is a multi-disciplinary open access archive for the deposit and dissemination of scientific research documents, whether they are published or not. The documents may come from teaching and research institutions in France or abroad, or from public or private research centers.

L'archive ouverte pluridisciplinaire **HAL**, est destinée au dépôt et à la diffusion de documents scientifiques de niveau recherche, publiés ou non, émanant des établissements d'enseignement et de recherche français ou étrangers, des laboratoires publics ou privés.

The Role of Human-Induced Climate Change on Extreme Convective Precipitation Events in the South of France: A High-Resolution Model Simulation Approach

Thèse de doctorat de l'Université Paris-Saclay

École doctorale n° 129, Sciences de l'environnement d'Île-de-France SEIF
Spécialité de doctorat: Météorologie, océanographie, physique de l'environnement
Unité de recherche: Université Paris-Saclay, CNRS, CEA, UVSQ, Laboratoire des sciences du climat et de l'environnement, 91191, Gif-sur-Yvette, France
Réfèrent: Université de Versailles-Saint-Quentin-en-Yvelines

Thèse présentée et soutenue à Gif-sur-Yvette, le 26 juin 2020, par

Linh Nhat LUU

Composition du jury:

Matthieu Roy-Barman Professeur, LSCE/IPSL	Présidente
Erika Coppola Directeur de recherche, ICTP	Rapporteuse
Peter Stott Professeur, University of Exeter	Rapporteur
Aurélien Ribes Chargé de recherche, Météo France	Examineur
Robert Vautard Directeur de recherche, LSCE/IPSL	Directeur
Pascal Yiou Directeur de recherche, LSCE/IPSL	Codirecteur

Acknowledgements

First, I would like to show my massive thank to my two academic advisors, Dr. Robert Vautard and Dr. Pascal Yiou for all the advices and endless support they gave me over the last almost four years. Their expertise helps me shape my scientific perspectives, inspire ideas and improve many investigations presented in this work. Their help is not confined in only science, but also reach to many aspects of life.

I am deeply grateful to the two PhD reviewers, Dr. Erika Coppola, a leading scientist in convection-permitting modelling who I admire a lot, and Prof. Peter Stott, the pioneer scientist in extreme events attribution whom I lately (after my defense) noticed as a fan of Liverpool football club, the biggest rival of my favorite team, Manchester United. They have raised intriguing points and provided many recommendations to improve my work in their reports as well as during the PhD defense. I also want to express my special thanks to the other two jury members, Dr. Aurélien Ribes and Prof. Matthieu Roy-Barman for their critical comments during my defense and the helps for my preparation of the defense.

My heartfelt thanks to Geert Jan van Oldenborgh, Geert Lenderink, Michel Déqué, Phillipe Naveau, Davide Faranda, Soulivanh Thao and Lluís Fita Borrell for the scientific and technical discussions, other the colleagues and friends in LSCE, Dev, Carley, Trang, Audrey, John, Annemiek, Miriam, Aglaé, Florentin, Yushan, Florence, Mathieu, Masa, Jean-Yves, Nada, Jean-Claude, Meriem, Jérôme, Sheng, Fanny and many other names that I cannot mention explicitly here because of the limited space, for helps since the beginning of my PhD, for conversations about science and life we have had and for the time we have been together.

Special thanks to my Vietnamese friends, Hà, Nghi, Hoàn, Tiệp, Nương, Dũng, Hoàng Anh, Nam, Liên, Dũng, Tuyền, Tuấn, Linh, Bình, Hoa, Hoàng, Minh, Trung, Huệ and their little kids and enormous gratitude to my special friends, Elisa, Ronaldo, Théo and Gaia who are always ready and willing to provide helps and share every nice moment together. Thanks also to my colleagues and friends at IMHEN, who have immensely encouraged, supported and facilitated before and during my PhD.

The last, but most important, my deepest thanks to my dedicated wife Thơ, my daughter Tuệ Minh and my son Minh Đăng, who have always supported me and been with me anywhere I would go. I am always bearing in my mind that my dear wife has discontinued her career and devoted her plenty of time to follow me and take care of me as well as our adorable kids. Massive thanks to my great family in Vietnam for their love and endless encouragement.

Abstract

The France-Mediterranean area is frequently exposed to heavy precipitation events in the autumn whose daily accumulation can sometimes exceed 300 millimeters. There are a few studies showing the increasing trend in the frequency and intensity of these events (e.g. Ribes et al., 2019; Vautard et al., 2015). However, a formal extreme event attribution that links those changes to human-induced climate change for this area has never been done. This PhD subject aims at quantifying the role of human-induced climate change in altering the statistical properties of extreme convective precipitation event occurring over the France-Mediterranean focusing on the Cevennes mountain range and using a high-resolution model approach including convection-permitting model for the first time. I first analyze the EURO-CORDEX ensemble, which includes different combinations of global climate models and regional climate models. Then I conducted a set of numerical simulations with the WRF model at a convection-permitting resolution. I also compared the simulations with observations and high-resolution re-analyses. The results show that regional models can reproduce extreme convective rainfall events in better agreement with observations by increasing their horizontal resolution, especially to convection-permitting resolution (approx. 3 km). By using these simulations, I show that human-induced climate change consistently makes the 100-year of 3-hourly and daily precipitation event at least 2 times more likely under current climate. The results also suggest the need of using multi-model approach to reduce the uncertainties in this type of impact study.

Résumé

La zone France-Méditerranée est fréquemment exposée à de fortes précipitations en automne dont l'accumulation quotidienne peut parfois dépasser 300 millimètres. Quelques études montrent une tendance à l'augmentation de la fréquence et de l'intensité de ces événements (par exemple Vautard et al., 2015; Ribes et al., 2019). Cependant, une attribution formelle des événements extrêmes qui lie ces changements au changement climatique induit par l'homme pour cette région n'a jamais été faite. Ce sujet de thèse vise à quantifier le rôle du changement climatique induit par l'homme dans l'altération des propriétés statistiques des précipitations convectives extrêmes survenant sur la région France-Méditerranée, en se concentrant sur la chaîne de montagnes des Cévennes et en utilisant pour la première fois une approche de modèle à haute résolution incluant un modèle permettant la convection. J'analyse d'abord l'ensemble EURO-CORDEX, qui comprend différentes combinaisons de modèles climatiques globaux et de modèles climatiques régionaux. Ensuite, j'ai effectué une série de simulations numériques avec le modèle WRF à une résolution permettant la convection. J'ai également comparé les simulations avec les observations et les ré-analyses à haute résolution. Les résultats montrent que les modèles régionaux peuvent reproduire des événements extrêmes de pluie convective avec une meilleure concordance avec les observations en augmentant leur résolution horizontale, en particulier à une résolution permettant la convection (environ 3 km). En utilisant ces simulations, je montre que le changement climatique induit par l'homme rend les précipitations quotidiennes et trihoraires sur 100 ans au moins deux fois plus probables dans le climat actuel. Les résultats suggèrent également la nécessité d'utiliser une approche multi-modèle pour réduire les incertitudes dans ce type d'étude d'impact.

Table of Contents

Acknowledgements	i
Abstract	ii
Résumé.....	iii
Table of Contents	iv
Chapter 1. General Introduction.....	1
1.1. Introduction of the Mediterranean heavy rainfall events	1
1.2. Background	2
1.2.1. The science of Extreme Event Attribution (EEA)	2
1.2.2. Attribution of extreme precipitation	8
1.2.3. Convection-permitting simulation - a better tool for reproducing heavy precipitation events?	10
1.2.4. Research gaps and obstacles	13
1.3. Goal and Objectives of this research.....	14
1.4. Thesis Outline	15
Chapter summary	17
Résumé.....	18
Chapter 2. Attribution of Extreme Daily Rainfall Events in the South of France Using EURO – CORDEX Simulations	19
2.1. Article published in Geophysical Research Letters: Attribution of Extreme Rainfall Events in the South of France Using EURO-CORDEX Simulations	19
2.1.1. Abstract	20
2.1.2. Introduction	20
2.1.3. Evaluation of Model Simulation of Extreme Events	22
2.1.1. Attribution of Extreme Events	26
2.1.2. Discussion and Conclusion	31
2.1.3. Acknowledgments.....	32
2.1.4. Supporting Information.....	32
2.2. Synthesizing the results.....	34
2.3. Conclusion	37
Chapter Summary	38
Résumé.....	39
Chapter 3. Designing model configuration for simulation of extreme precipitation event using a case study.....	40
3.1. Introduction	40
3.2. Configuration and experiment design	41
3.2.1. The Weather Research and Forecast (WRF) model.....	41
3.2.2. Experiments design	42
3.2.3. Observations data	45
3.2.4. The description of autumn 2014 rainy season over the Cévennes	45
3.3. Results and discussion	49
3.3.1. Seasonal maximum daily rainfall (Rx1day).....	50
3.3.2. Seasonal maximum 3-hourly rainfall (Rx3hour)	52
3.3.3. Seasonal total rainfall (R_Total)	53
3.3.4. Daily rainfall (R_daily)	55
3.3.5. Daily maximum 3-hourly rainfall (Rx3hr_daily).....	61
3.3.6. Distribution of wet daily event (Prob_daily)	62
3.3.7. Moisture transport	63
3.4. Conclusion	69

Chapter summary	70
Résumé.....	71
Chapter 4. Evaluation of convection - permitting downscaling of new EURO-CORDEX simulations for the France – Mediterranean	72
4.1. Description of the simulations	72
4.2. Reference data and evaluation methods	73
4.3. Evaluation of extreme rainfall.....	76
4.3.1. Autumn maximum daily rainfall (Rx1day).....	76
4.3.2. Autumn maximum of daily maximum 3-hours rainfall (Rx3hour)	80
4.3.3. Scaling extreme rainfall with surface temperature	84
4.3.4. Distribution of wet events	86
4.3.5. Moisture sources	87
4.4. Conclusion	89
Chapter summary	92
Résumé.....	93
Chapter 5. Influence of anthropogenic climate change on extreme precipitation events in the south of France	94
5.1. Introduction	94
5.1.1. Objectives.....	94
5.1.2. Observations and simulations data.....	94
5.1.3. Framing of extreme event attribution.....	96
5.1.4. Method for detection and attribution	97
5.2. Investigating the change in extreme 3-hourly precipitation.....	100
5.2.1. Detecting the change in observations data	100
5.2.2. Analyzing the change of extreme rainfall using multi-model simulations method.....	101
5.3. Revisiting extreme daily precipitation	107
5.4. Discussion	109
5.5. Conclusion	110
Chapter summary	112
Résumé.....	113
Chapter 6. Conclusion and Perspectives	114
6.1. Conclusion	114
6.2. Perspectives.....	116
Supplementary for Chapter 4	118
Supplementary for Chapter 5	134
Bibliography.....	142

Chapter 1. General Introduction

This chapter presents a short overview of my PhD dissertation. At first, I will give a short introduction on the Mediterranean extreme precipitation events. Secondly, I will review the literature on extreme event attribution, attribution of extreme precipitation events and convection permitting simulation – a state-of-the-art approach expected to decrease the uncertainty in reproducing precipitation. Thirdly, I will point out some gaps in current studies as well as challenges that the community has been facing in this research. Next, I will propose the scientific questions and a few objectives to be done to answer those questions. The final part of this Chapter is to provide the outline of the whole dissertation.

1.1. Introduction of the Mediterranean heavy rainfall events

The Mediterranean coastal areas frequently undergo torrential rainfall events in the autumn which usually induce a lot of adverse social-economic consequences. This kind of event often leads to flash flooding, land-sliding or inundation causing human casualties, destruction of wealth and infrastructures such as bridges, houses, multi-story buildings or the interruption of power, communication, transportation, etc. (Fresnay et al., 2012; Nuissier et al., 2008). For example, a rainfall event reaching 220 mm in 3 hours occurred in the city of Vaison-La-Romaine, France in September 1992 (Sénési et al., 1996) and was followed by flash flooding causing the death of 32 people and the missing of 48 people¹. In September 2002, a flash flooding took place in the Gard region, France. This flooding was the result of record daily rainfall over 200mm covering 5500 km² of area with some place over 600 mm. Consequently, 24 people died and 1.2 billion euros of damage was estimated. Some other events happened over the Mediterranean basin such as in Gandia (Spain) in November 1987, in Piedmont (Italy) in November 1994, Aude (France) in 1999 and Algiers (Algeria) in 2001 with the amount of 24-to-48-hours rainfall ranging from 300 to 800mm resulting in extreme flash flood in those areas. These catastrophic events were responsible for the estimated lost and damage from 1 to 12 billion US dollars (Nuissier et al., 2008).

The devastating rainfall events listed above usually resulted from the formation and maintenance of quasi-stationary mesoscale convective system (Ducrocq et al., 2008;

¹ <https://www.theguardian.com/world/1992/sep/24/france.paulwebster>

Lee et al., 2018; Nuissier et al., 2008). This system is favored by typical large-scale dynamic system associating with a massive source of moisture above the sea level and steep orography in the Mediterranean basin. Specifically, there is usually a synoptic-scale trough in the vicinity (i.e. to the west of the area) producing southeastern low-level flows toward the threat area. These flows bring the moisture from the sea toward the relief of mountains to trigger the mesoscale convective system. This convective mechanism can be renovated at the same location as long as the large-scale dynamic is persistent. The rainfall following this convective system is characterized by its intense magnitude with lightning and thunder and lasts in a short period of time (within 30 minutes to a few hours) depending on the development of the mesoscale convective system. However, in many cases, the warm low-level moist flows can also associate and be lifted by the stalling or slowly moving cooler air mass over the area resulting in the persistent and less intense large-scale rainfall and sometimes the squall line structure. This pattern can be mixed together with the mesoscale convective system that makes the rainfall event lasting longer and being more intensive in a few hours.

Bindoff et al. (2013) in Chapter 10 of the IPCC Fifth Assessment Report stated that heavy precipitation at different timescales generally increases at global scale and is expected to continue with global warming. Recently, many studies also confirmed the increase in both frequency and magnitude of extreme precipitation for different regions including the Mediterranean basin (Chernokulsky et al., 2019; Mallakpour and Villarini, 2017; Ribes et al., 2019; Scherrer et al., 2016). A few climate projection studies showed that extreme precipitation events over the Mediterranean basin may increase in the future along with climate change (Jacob et al., 2014; Polade et al., 2017; Trambly and Somot, 2018). Given the catastrophic nature of this type of event, the role of human-induced climate change is always questioned whenever it happens. However, the link between anthropogenic climate change and current Mediterranean extreme precipitation events has not been formally established.

1.2. Background

1.2.1. The science of Extreme Event Attribution (EEA)

The field of science that copes quantitatively with how human-induced climate change affecting extreme events is called “extreme events attribution”. In many instances ill-posed questions have been raised by the medias such as “Did climate change cause that event?” or “Had that event resulted from climate change” because such extreme

events, by all means, have possibly already occurred without anthropogenic warming (Stott and Walton, 2013).

From a climate science perspective, “Extreme event attribution” (EEA) studies would satisfy the curiosity of understanding why and to what extent the probability and intensity of extreme weather event has been altered by anthropogenic climate change. This appeal of EEA is not only restricted in scientific community, but also appears from general public (Jézéquel et al., 2020). In addition, EEA states the challenges and raises the need of improvement of climate model in replicating the event of interest (Massey et al., 2015; National Academies of Sciences, 2016). For example, a global climate model with horizontal resolution of 60 km to 300 km and a regional climate model with its resolution of 10 km to 50 km are tools to understand human-induced climate change at global and regional scale, respectively. However, at those resolutions, many crucial processes at smaller scale, especially the clouds and deep convection in the formation of mesoscale convective system frequently happening over the Mediterranean coastal area and other areas in the tropic, still rely on parameterization schemes, which leads to large uncertainties in the reproduction of extreme rainfall in this case (Ban et al., 2014; Chan et al., 2013; Kendon et al., 2017). The enhancements that can be achieved from EEA studies include both knowledge and technological methods and stimulate the development of a better climate prediction and projection systems (Trenberth, 2008).

To a wider perspective, information from extreme event attribution is expected to raise the awareness for general public and policy-maker to make climate change and its impact more visible. It could also potentially play a role in climate change litigation and loss and damage (Marjanac and Patton, 2018) given that many difficulties remain unsolved for EEA on its way to the court of litigation (Jézéquel et al., 2020). Another motivation of EEA is that it could inform insurance companies not to rely on a stationary risk calculation and to tune their services, etc. (Stott et al., 2013; Stott and Walton, 2013). However, the information brought up by EEA results could be either insufficient or redundant to the needs of insurance sector, for example the unnecessary causality explanation for the event in EEA, the lack of attribution of general classes of events rather than a specific event, or only probability of extreme event provided by EEA rather the overall risks, which are the combination of probability of hazard, vulnerability and exposure (Jézéquel et al., 2020).

The history of attribution of a specific extreme weather event to anthropogenic climate change was first motivated by the article titled “Liability of climate change” published by *Allen* (2003) in *Nature*. Afterwards, the science of extreme event attribution, in which the question of “Was that extreme event caused by climate change” is translated to “how climate change altered the probabilities or intensities of that event” or “how climate change adjusted the physical mechanism (i.e. dynamic and thermodynamic) leading to that event”, has been growing up substantially. The former translated question is so-called risk-based approach and the latter one is well-known as storyline approach. These two approaches depend on diverse methodologies and provide different insights on the effect of climate change on the event of interest. The first extreme event attribution paper using the risk-based approach was defined by *Stott et al.* (2004). In this research, the authors showed that the summer heatwave in European region in 2003 was intensified by anthropogenic climate change. Its probability was estimated to increase at least by the factor of two under climate condition compared to natural forcing only with more than 90% of confidence interval. This key point was estimated after computing the fraction attributable risk (FAR), which is the deviation between P_1 and P_0 over P_1 . Here, P_1 is the exceedance probability of the event in a factual world – the real world where we are now and P_0 is that probability of the event in a counterfactual world – the world might have been without human-induced climate change.

Because of the raising need of extreme event attribution research, since 2012, the Bulletin of the American Meteorological Society (BAMS) published the annual - special report to explain extreme events of the previous year from a climate perspective (2019; 2018; 2016; 2015; *Herring et al.*, 2014; 2013; *Peterson et al.*, 2012). Those reports aim at publishing a number of case studies evaluating the link of human-induced climate change to the change in probability and intensity of an individual extreme event. The first report explaining the extreme event happening in 2011 contains only six papers. Then, extreme event attribution studies progressed quickly by many different research groups using variety of models and methods. These studies contributed considerably to the development of methods, data and scientific evidences of the influence of anthropogenic warming on different type of events including heat wave, rainfall, flooding, storms or wildfires, etc. (*Jézéquel et al.*, 2018).

Figure 1 shows with what confidence scientists could attribute the human impact to the change of any kind of extreme event. There is no doubt that scientific community

has the greatest understanding on extreme event relating to temperature and that climate model can reliably reproduce this type of event, therefore attribution of extreme temperature event obtains high confidence. Other type of extremes, e.g. heavy rainfall or drought, are combination of complicated large-scale dynamic and water vapor availability whose appreciation are moderate. In addition, the lack of long, qualitative and homogeneous observations of those events play a vital part in understanding and modelling them. As a result, quantifying the role of human impact on those extreme yields less confidence. For other extreme events (e.g. wildfires) associating with other factors (e.g. change in land-use, forest management, change in surface, etc.) additionally to climate system and anthropogenic warming, confidence in attribution studies varies slightly from little to zero extent (National Academies of Sciences, 2016).

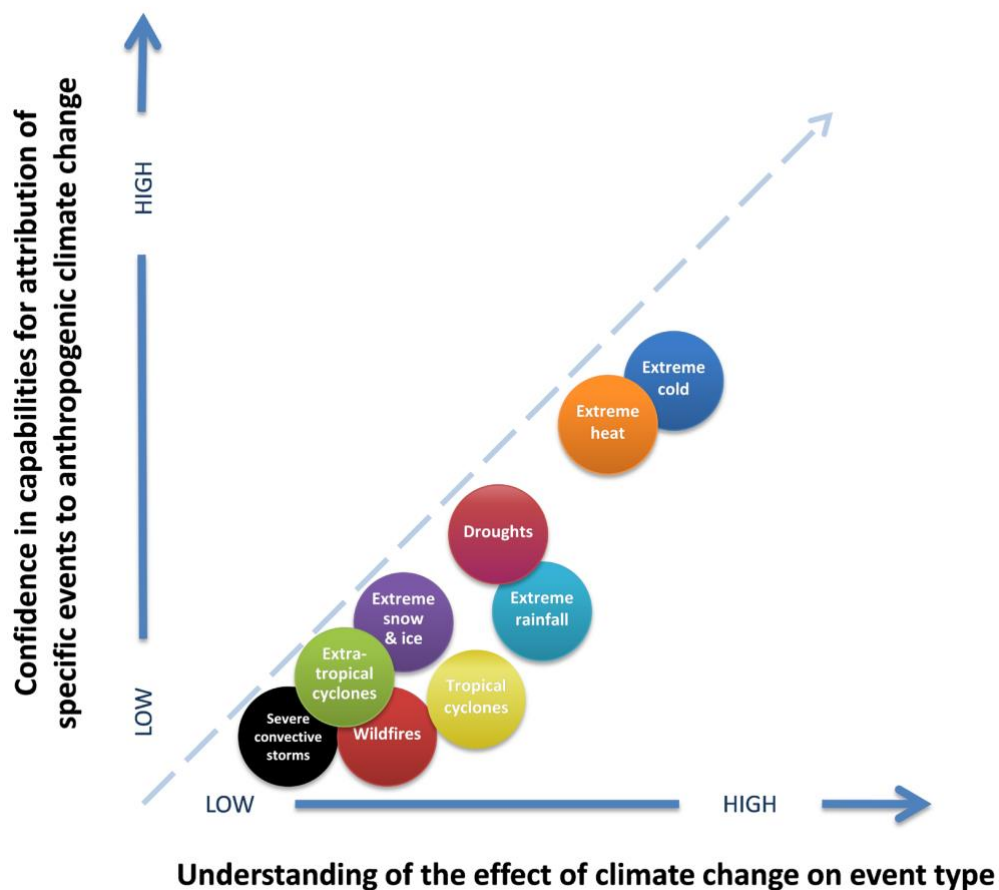


Figure 1. Schematic description of relation of confidence in attributing human – induced climate change to the change of specific type of extreme event to scientific understanding on that event. **Source: National Academies of Sciences (2016).**

Human – induced climate change undoubtedly plays role in the increase of likelihood and intensity of extreme temperature event all over the world. For example, Diffenbaugh and Scherer (2013) showed that the heatwave event in July 2012 in the

north-central and north-east of the US is four times likely in current climate in comparison with pre-industrial climate using CMIP5 simulations. Rahmstorf and Coumou (2011) concluded that the heatwave event in Russia in 2010 was five times more probable with the presence of climate change. Lewis and Karoly (2014) showed that the risk of September temperature anomalies in Australia in 2013 increased by five times by anthropogenic forcing using CMIP5 simulations. King et al. (2014) also analyzed the hot event in September 2012 in Australia but focused on the maximum daily temperature using CMIP5 simulations. They showed that the likelihood of occurrence of this type of event increased by 23 times in current climate compared to the late 19th century. In addition, they stated that the heatwave associated with drought condition was seven times more likely by human – induced climate change. Perkins et al. (2014) also analyzed a heatwave event occurring in Australia in the summer using 21 members of the CESM model. They showed that anthropogenic forcing increased the intensity of the event by two-fold and the frequency by three-fold. Min et al. (2015) showed that the risk of hot spring in 2014 in Korea increased by two to three times due to human impact. The anomaly warmer temperature happening in the Arctic during November – December of 2016 was investigated by Kam et al. (2018). They used CMIP5 simulations to confirm that human activities played a role in the occurrence of the event.

Flooding is a consequence of extreme rainfall events in either short or long durations. It has a direct impact on human life, properties, social economy and ecosystems. As a result, this type of event becomes one of the objects of extreme event attribution research. One of the seminal papers on attribution of flooding event is Pall et al. (2011) who estimated the contribution of anthropogenic warming to the likelihood of 2010 flooding event in England and Wales. The two different climate conditions were produced by large ensembles of atmospheric model HadAM3-N144 forced with sea surface and ice lower boundary with and without considering green-house gas effect. The results suggested that human-induced greenhouse gas concentration increased the likelihood of autumn 2000 flooding event by 20%. Schaller et al. (2016) is the first end-to-end attribution paper that investigated the changing probability of precipitation altering the probability of peak flows over Thames river in January 2014 in England under anthropogenic influence. The authors used January rainfall simulations from weather@home project and the CLASSIC hydrological model for flooding risk investigation. They showed that the likelihood of occurrence of 1-in-100-year January

rainfall event increased by 43% (0 to 164%) under man-made warming. This change was contributed roughly two third by thermodynamic changes and one third by dynamic changes. This finding was later confirmed by Vautard et al. (2016) using different methods. The change in likelihood of 1-in-100-year precipitation event led to the change in risk of 30-day peak river flows of 21% (12% to 133%) that was attributable to human-induced climate change. Kay et al. (2018) found consistency with Schaller et al. (2016) that the emissions by human activities increases the chance of occurrence of peak flow for duration of more than 10 days for the Winter 2013/2014 event in Great Britain.

Drought is another severe extreme condition that damages the ecosystem, agriculture and livestock affecting food security and increases risk of wildfire in some places. This type of extreme relates to the deficit of precipitation or water scarcity and probably combines with high temperature and fast evaporation. Because of this complex interaction, research on quantifying the role of anthropogenic climate change and natural variability affecting this extreme with certainty remains challenged and scarce, especially one taking into account land surface model (Hauser et al., 2017). For example, Diffenbaugh et al. (2015) investigated the link between anthropogenic warming and the 2012 drought event in California considering only temperature and precipitation using both observations data and simulations with and without human-induced external forcing. They confirmed that the probability of occurrence of dry condition co-occurring with warmer temperature has increased because of the impact of human activities. Gudmundsson and Seneviratne (2016) investigated the changes in meteorological drought frequency over Europe and Mediterranean. They showed that human influence increased the likelihood of occurrence of drought over the Mediterranean meanwhile it decreased the risk of drought over the northern Europe. They also found that there is no clear evidence for the central Europe. Uhe et al. (2018) conducted attribution analysis for drought event in Kenya in 2016 and Philip et al. (2018) investigated the role of climate change on Ethiopian drought in 2015. Both studies did not find significant impact of human-induced warming on those events. A recent study using land surface model to quantify the role of anthropogenic climate change on the drought event in the Horn of Africa in 2014 was done by Marthews et al. (2019). However, they cannot significantly attribute the trend of this event to human-induced climate change.

1.2.2. Attribution of extreme precipitation

Water vapor content in the atmosphere is expected to increase by 6-7% per degree of increase in temperature which is implied by the Clausius - Clapeyron relation, given that there is no or small change in relative humidity. The mean precipitation cannot increase globally at this rate because of the restraints in energy budget (Held and Soden, 2006). However, extreme rainfall, particularly at regional scale, does not depend on these restrictions, and therefore, it can increase at this adiabatic rate, even double times for hourly rainfall (Lenderink et al., 2017; Lenderink and Van Meijgaard, 2008). In fact, the intensity and frequency of heavy precipitation event tend to increase in most continents with high confidence (IPCC, 2014). However, in order to assess to what extent climate change has altered these characteristics of extreme rainfall, it is necessary to conduct attribution studies. In this section, I will give a few key findings from literature review of attribution of extreme precipitation.

Precipitation is a meteorological variable that is likely affected by human-induced climate change, especially heavy rainfall. Several studies showed that human impact modulated the probability of large – scale precipitation events in many areas with different levels of certainty. For instance, Christidis and Stott (2015) found that the extreme 10 days rainfall event in the winter 2013/14 in UK was seven times more likely due to human-induced climate change. However, this result was not statistically significant. Rosier et al. (2015) found medium confidence in their statement that anthropogenic climate change increased the likelihood of July maximum 5-day rainfall event like one in July 2014 over Northland, New Zealand. Sun and Miao (2018) suggested that El Niño and anthropogenic climate change both contributed to the increase in likelihood of occurrence of extreme 5-day rainfall event in Yangtze-Huai, China in June-July 2016 by ten times. In this case, the impact of human activities accounted for 35%. Yuan et al. (2018) found consistent result in evaluating extreme 10-day rainfall event in this period for the Yangtze River. They suggested that human-induced climate change made the event more likely from 17% to 59%, and up to 37% to 91% under El Niño conditions with large uncertainty. Those two factors including El Niño and human impact also increased the risk of 7-day extreme rainfall event in July 2016 over Wuhan, China (Zhou et al., 2018). Christidis et al. (2019) showed that extreme rainfall event (from daily, 5-day, 10-day to monthly time scale) in March 2017 in Peru was at least 1.5 times more likely to happen because of human-induced climate change. de Abreu et al. (2019)

indicated that likelihood of occurrence of two months (April - May) extreme rainfall event in 2017 in Uruguay river increased by a factor of 5 due to influence of climate change. Rimi et al. (2019) showed that human-induced warming has doubled the chance of extreme 6-day rainfall event in pre-monsoon season of 2017 in the northeast Bangladesh. In contrast to those examples, there are still a few studies showing no evidence of anthropogenic climate change affecting extreme rainfall events (e.g. Sparrow et al. (2013) for heavy 2013 summer rainfall event in UK, Imada et al. (2013) for rainy season 2012 in southwest Japan, Schaller et al. (2014) for the May – June 2013 rainfall event in upper Danube and Elbe basins in Germany, Hope et al. (2018) for extreme September 2016 rainfall event over the southeast of Australia).

The evidence of human-induced climate change influencing the change in extreme convective events were also found in several areas. Vautard et al. (2015) investigated the extreme daily rainfall happening in the Autumn 2014 over Cévennes mountain range in the South of France. They detected that the probability of the event increased by the factor of three due to climate change in observations – based analysis. However, the attribution part of this research using climate model has not been completed. Vautard et al. (2015) simply linked extreme precipitation in the area with the increasing in mean surface temperature. The completed attribution part of this research will be presented in the Chapter 2 of this dissertation. Eden et al. (2016) analyzed the influence of anthropogenic climate change on extreme rainfall event in September 2013 over Boulder, Colorado using both observations and model simulations. They found that the increase in likelihood of occurrence of extreme 1-day event can be attributable to global warming by human activities. In addition, they emphasized that using only the influence of thermodynamics change would lead to overestimate the likelihood of the event. Eden et al. (2018) used similar statistical method to Eden et al. (2016) to quantify the role of global warming in altering the probability of heavy rainfall event occurring on the 28th July 2014. They concluded that the changes in likelihood of occurrence of that event can be attributable to global warming, even though those changes from model simulations were somewhat underestimated the one from observation-based analysis. These differences can be explained by the lack of convection-permitting resolution to have a better trend reproduction. Zhang et al. (2017) analyzed the impact of increasing CO₂ on extreme daily and sub-daily rainfall for the whole world. They used 10 GCMs to simulate two differently idealized climate conditions including pre-industrial control

experiment and another one with CO₂ concentration increasing at the rate of 1% per year. The results showed that CO₂ increased the likelihood of occurrence of extreme sub-daily precipitation all over the world, except some regions in the subtropics. However, they emphasized the need of using higher-resolution model that can solve convection explicitly in order to minimize the uncertainty. In contrast, Tozer et al. (2020) found no clear evidence that anthropogenic warming had altered the event extreme daily rainfall event in Hobart, Australia in the autumn of 2018.

1.2.3. Convection-permitting simulation - a better tool for reproducing heavy precipitation events?

With the recent developments in high-performance computing capacity, it has become possible to refine the grid in regional climate model from greater than 10 km to convection-permitting or cloud-resolving resolution (i.e. horizontal resolution < 4 km) (Prein et al., 2015). This kind of configuration allows to remove the deep convection parameterization which is a well-known source of uncertainty in producing precipitation (Fosser et al., 2015; Hohenegger et al., 2008; Prein et al., 2013) and enables the model to solve explicitly the deep convection processes (Prein et al., 2015) and its interaction within a large-scale dynamic system (Feng et al., 2018). In addition, topography and variations of surface fields are better presented in the model (Prein et al., 2015). These advantages are expected to better simulate mesoscale convective system, short-time convection in relation with high and steep mountainous region, therefore, extreme precipitation in local area and sub-daily time scale would be better represented. The application of cloud-resolving models would provide a better understanding the underlying physic and micro-physics processes in connecting with precipitation, raising confidence for future projection and other field of impacts, particularly extreme event attribution (Prein et al., 2015). In this section, I provide a literature review on a few studies and mainly focus on the improvement of this high-resolution configuration in simulating precipitation. And hereafter, once the terminology “convection-permitting” is mentioned, it implies that the simulations run with the absence of convection parameterization scheme (i.e. the scheme is switched off and convective process is solved explicitly).

In the last two decades, the evaluation of simulations of precipitation at convection-permitting resolutions were done for different regions (e.g. the Alp, central Europe, UK, USA, etc.) and for different periods from a few months to a few decades by many research groups (Prein et al., 2015). Those research groups commonly share a

similar procedure that a regional climate model (RCM) is set up at convection-permitting resolutions to downscale the simulations from that model at coarser resolutions. These coarser resolutions are usually forced by reanalysis datasets (e.g. ERA-Interim from ECMWF) or Global Climate Model (GCM) outputs. These two steps can be done in either parallel or separated times. In general, those studies found the added values of convection-permitting resolutions in reproducing the extreme daily and hourly rainfall in both temporal and spatial distributions for different seasons (Ban et al., 2018; Ban et al., 2014; Chan et al., 2013; Chan et al., 2014; Fosser et al., 2015; Hodnebrog et al., 2019; Kendon et al., 2012; Knist et al., 2018; Prein et al., 2013). In addition, the convection-permitting simulations can provide a better performance for diurnal cycle of precipitation (Ban et al., 2014; Fosser et al., 2015; Knist et al., 2018; Langhans et al., 2013; Prein et al., 2013; Scaff et al., 2019). A few studies also found that the convection – permitting models can simulate the increase at super adiabatic rate of extreme hourly rainfall scaling with temperature (Ban et al., 2014; Knist et al., 2018). Kendon et al. (2012) also found that the use of such very high resolutions can avoid producing too many rainy days with a very low amount of rainfall and the timing of peak of convection was also better reproduced (Scaff et al., 2019).

The Mediterranean region is a hot-spot area under global warming and is prone to extreme precipitation events every year (Giorgi, 2006; Nuissier et al., 2008). In recent decade, this type of event has become the object of many scientific investigations under the framework of the Hydrological cycle in the Mediterranean eXperiment (HyMeX, Drobinski et al., 2014; Ducrocq et al., 2014). Many studies evaluated and investigated the convection – permitting models to have a better understanding about the event, how it responds to climate change and to improve the predictability of the event over this area. For example, some studies focused on the impact of lateral boundary condition and initial condition in convection – permitting simulation on reproducing extreme rainfall events in the area (Nuissier et al., 2012; 2012; Vié et al., 2011). Nuissier et al. (2016) showed that convection-permitting models had a good probabilistic skill in heavy rainfall forecasting and suggested that this approach was a favorable way to serve operational forecast. Armon et al. (2019) assessed the skill of WRF at convection-permitting resolution in simulating 41 individual heavy precipitation events in the eastern Mediterranean against radar data. They showed that convection-permitting model

reproduced accurately the structure and location of 95% the number of events and thus was able to give reliable long simulation.

The evaluation of long and large ensemble of simulations at convection-permitting resolution for the Mediterranean were done by a few studies. Zittis et al. (2017) investigated the added value of convection permitting resolution in simulating extreme precipitation events over the eastern Mediterranean region, specifically the Cyprus. They found that the 1-km domain without convection parameterization outperformed the coarser resolution, especially over a high altitude area. Fumière et al. (2019) investigated the added value of convection – permitting simulations with CNRM-AROME model to its parent domain from CNRM-ALADIN driven by ERA-Interim for the Mediterranean France. Even though the CNRM-AROME still underestimated some extremely heavy rainfall events, the enhancement in reproducing daily and hourly extreme rainfall in terms of intensity and place of occurrence was clearly proved. Coppola et al. (2018) introduced for the first time the evaluation of multi-model ensemble simulations using convection-permitting approach for three case studies of extreme precipitation events over Europe – Mediterranean area including the Hymex-IOP16 (from 23rd to 28th October 2012), the AUSTRIA (from 22nd to 25th June 2009) and the FOEHN (from 3rd to 7th November 2014). In general, the results showed that convection-permitting simulations reproduced well the three cases. The agreement among models is larger when the event was strongly driven by large-scale dynamics. In case that the event was constrained by weaker dynamics or contributed by interaction with orography, the inter-model spread was apparent. This research also emphasized the necessity of using ensemble approach in exploring convective events.

Because of its advantages in reproducing extreme precipitation, the convection-permitting simulations were also conducted for future projection of this variable. This approach was found essential in producing the increase in extreme precipitation more robust, especially in short durations (Hodnebrog et al., 2019; Kendon et al., 2017; Kendon et al., 2019; Vanden Broucke et al., 2019). Other studies also confirmed the advantages of this cloud – resolving model in simulating and projecting climate for other areas all over the world, for example Sun et al. (2016) for central U.S, Komurcu et al. (2018) for Northeastern U.S, Zhu et al. (2018) for China, Cannon and Innocenti (2019) for Canada and Karki et al. (2017) for the Himalayas.

The enhancements of convection-permitting approach could come from the explicit-solving convection processes and higher resolved atmospheric dynamics (Prein et al., 2013), meanwhile the convection parameterization failed in activating deep convection promptly (Langhans et al., 2013). However, because of the use of numerical methods and other parameterization schemes and the fact that the convection is still not fully resolved at the resolutions of 1.5 to 3km (Vanden Broucke et al., 2019), the model is still imperfect. Therefore, the systematic errors always exist in the simulations. For example, the convection – permitting model tends to overestimate or underestimate the extreme precipitation depending on regions, extend the duration of rainfall events with lower intensity, reproduce more extreme events than observations or provide location error of the heaviest events (Armon et al., 2019; Chan et al., 2013; Chan et al., 2014; Fosser et al., 2015; Fumière et al., 2019; Vanden Broucke et al., 2019).

1.2.4. Research gaps and obstacles

The results from extreme event attribution studies are sensitive to the choice of methods and data, definition of the event and framing (Hauser et al., 2017; Herring et al., 2018; Jézéquel et al., 2018). This means that different choices of those factors can lead to different results and certainties of the attribution analysis. For example, Dole et al. (2011) and Rahmstorf and Coumou (2011) concluded differently because of discrepancy in framing that was clarified in Otto et al. (2012). Vautard et al. (2018) or Eden et al. (2016) found different results when comparing between ensemble of individual models to the ensemble of all models. Yiou et al. (2017) discussed the choice of factual world, the world with human activities, and counter factual world, the world could have been without anthropogenic climate change. In the model-based approach, the counter-factual world can be obtained by setting the atmospheric state, greenhouse gases concentration or SSTs level to pre-industrial period. However, it is difficult to evaluate the realism of those counter-factual simulations because of the lack of observations and therefore, it remains uncertain. In the observation – based approach to detect the changes of extreme event, the counter factual world can be the beginning of the 20th century. However, it is necessary to note that green-house gases still exist during that period and the fact that they are larger in current climate (or factual world).

Climate models play an important role in attribution studies because they can provide a longer and homogeneous dataset under different climate conditions (i.e. factual and counter factual world). However, the realism of extreme events reproduced by these

simulations contains large uncertainty. These could come from different sources of error and exist in diverse aspects including both natural variability and climate change signal. One of the key challenge in attribution studies is to quantify this external signal and then to link it to the change of the extreme event distinctively to the noise of variability (Hegerl and Zwiers, 2011; Stott et al., 2013). Hauser et al. (2017) also suggested the need of using multi-model simulations and multi-methods in extreme event attribution study.

The attribution of extreme precipitation, especially at sub-daily scale, is more challenging than what has been done with temperature (van Oldenborgh et al., 2013). The first difficulty comes from the lack of long and homogeneous observations data. Moreover, the gridded observational reference data is often a combination of disparate sources including in situ measurement and radar, therefore, it contains many uncertainties (Isotta et al., 2014). The second obstacle is the capability of regional models in reproducing precipitation because this variable is the result of processes that are not resolved explicitly inside the model. One of the promising and prominent ways to solve the difficulty concerning the ability of model mentioned above is to use convection-permitting resolution. However, this raises another challenge for scientific community, which is how to set up the long runs with an appropriate spatial resolution for attribution study but still save the cost of computational resource. Doing this efficiently is a complex issue (Trenberth, 2008). One can restrict the domain size to focus only on a small area, however, it can lead to strong influence of the boundary conditions on solutions of convection – permitting domain (Prein et al., 2013). Bellprat et al. (2019) also emphasized the need of bridging climate model developer and extreme event attribution community to produce a more robust assessment on how human activities affected the extreme weather and climate events.

1.3. Goal and Objectives of this research

Given the fact that the impact of human-induced climate change on the Mediterranean events has not been well established and the fact that model simulation using convection-permitting approach at climate scale remains limited and poorly evaluated for any area in the Mediterranean basin, this PhD dissertation is designed to deal with those research gaps. This work is going to answer two scientific questions including: i) What is the added value of convection-permitting model in reproducing extreme rainfall events in the autumn in comparison with the existing EURO-CORDEX simulations; ii) How human-induced climate change does alter the statistical properties

of extreme precipitation events (in daily and sub-daily scale) in the autumn using EURO-CORDEX simulations and the new convection-permitting simulations. This research focuses on the Cévennes mountain range in the South of France, an area with particularly extreme precipitations in the Mediterranean basin. Below are three objectives proposed to answer those two questions:

- To investigate quantitatively how human-induced climate change affects the probabilities of occurrence and intensity of extreme daily rainfall in the interest area. For this purpose, three ensembles of EURO-CORDEX simulations including 0.44 and 0.11 degree of horizontal resolutions and the bias corrected of 0.11 degree of resolution are employed.
- To simulate autumn extreme rainfall in the Mediterranean focusing on the south of France and evaluate the results at convection-permitting resolution (approx. 3km) and at both daily and sub-daily time scale.
- To attribute the change in autumn extreme hourly rainfall in Cévennes mountain range to anthropogenic climate change using convection – permitting simulations. The analysis consists of two tasks. Firstly, changes in frequency and intensity of extreme rainfall event is detected in observation dataset. Secondly, those changes are analyzed from very high horizontal simulation datasets.

The outcomes of this research not only match the scientific and social need, but also make up significantly to my own knowledge and experience. Those achievements could help me to contribute to the sustainable development, adaptation and mitigation of my country, Vietnam, one of the most vulnerable countries to climate change and natural hazards in the world.

1.4. Thesis Outline

Following this section, Chapter 2 presents my paper published in Geophysical Research Letters (Luu et al. (2018)). The paper is an initiative to clarify the first objective proposed in previous section which examines the degree to which the probabilities and intensities of extreme daily rainfall events in the Cévennes mountain range changes. Those changes come from the comparison between current (2001-2030) and historical (1971-2000) climates which are also called factual and counterfactual, respectively by scientific community.

Chapters 3 and 4 are dedicated to the second objective. In chapter 3, I present the configuration of WRF and set up a few experiments to simulate rainfall for the South of France in the autumn. The simulations are driven by ERA-Interim and done at convection-permitting resolution (approx. 3km). The assessment is then conducted to confirm whether a higher resolution is able to reproduce a more realistic extreme rainfall event over a complex topography area. In chapter 4, all configuration used in chapter 3 are applied to WRF model to downscale directly new EURO-CORDEX simulations which are also done by WRF and forced by three different global models including IPSL-CM5A-MR, HADGEM2-ES and NORESM1-M. Those 3-km simulations are afterwards analyzed and statistically evaluated and will play a substantially important part in the next chapter.

Chapter 5 is devoted for the attribution of extreme hourly rainfall event using convection – permitting and EURO – CORDEX simulations. This chapter adapts the same method presented in Chapter 2. However, I shift the counter factual period backward in time from 1971-2000 to 1951-1980. Because of the lack of boundary condition from CMIP5, the counter factual period cannot be shifted backward further. However, this change is still expected to determine clearer climate change signal in the tail of extreme hourly rainfall distributions between the factual and counterfactual climates.

The last part of this thesis concludes and emphasizes all scientific points and objectives proposed from the beginning, state again the challenges that Extreme Event Attribution studies in general and Extreme Precipitation Event Attribution studies in specific that have been confronting, suggest the implication of these attribution results, and eventually plan further research.

Chapter summary

This chapter presents two scientific questions: i) What is the added value of convection-permitting model in reproducing extreme rainfall events in the autumn in comparison with the existing EURO-CORDEX simulations; ii) How human-induced climate change alter the statistical properties of extreme precipitation events (in daily and sub-daily scale) in the autumn using EURO-CORDEX simulations and the new convection-permitting simulations. Three objectives are designated to answer the two scientific questions.

Objectives of the thesis

- Using EURO-CODEX simulations in attributing the change of extreme daily rainfall in the South of France to human activities influence on climate.
- Configuring, running and evaluating simulations of extreme precipitation events in the Mediterranean France using convection-permitting approach.
- Investigating the role of human-induced climate change on extreme hourly rainfall event for the South of France using convection-permitting model outputs.

Structure of the thesis

- Chapter 1 provides the general introduction, goal and objectives of the PhD
- Chapter 2 presents the attribution of extreme daily rainfall for the south of France using EURO-CODEX simulations
- Chapter 3 and 4 are dedicated for testing, running and assessing the convection – permitting simulations
- Chapter 5 investigates the role of human – induced climate change on extreme hourly rainfall event for the South of France using convection – permitting and EURO – CORDEX simulations
- Conclusions and perspectives

Résumé

Ce chapitre d'introduction propose deux questions scientifiques: i) Quelle est la valeur ajoutée du modèle permettant la convection dans la reproduction des événements pluviométriques extrêmes de l'automne par rapport aux simulations EURO-CORDEX existantes; ii) Comment le changement climatique induit par l'homme modifie les propriétés statistiques des événements de précipitations extrêmes (à l'échelle quotidienne et infra-journalière) à l'automne en utilisant les simulations EURO-CODEX et les nouvelles simulations permettant la convection. Trois objectifs sont conçus pour répondre aux deux questions scientifiques.

Objectifs de la these:

- Utilisation des simulations EURO-CODEX pour attribuer l'évolution des précipitations journalières extrêmes dans le sud de la France à l'influence des activités humaines sur le climat.
- Configurer, exécuter et évaluer des simulations d'événements de précipitations extrêmes en France méditerranéenne en utilisant une approche permettant la convection atmosphérique.
- Etudier le rôle du changement climatique induit par l'homme sur les événements pluviométriques horaires extrêmes pour le sud de la France en utilisant les sorties du modèle permettant la convection.

Structure de la these:

- Le chapitre 1 présente l'introduction générale, le but et les objectifs du doctorat
- Le chapitre 2 présente l'attribution des précipitations journalières extrêmes pour le sud de la France à l'aide de simulations EURO-CODEX
- Les chapitres 3 et 4 sont dédiés au test, à l'exécution et à l'évaluation de la convection - permettant des simulations
- Le chapitre 5 étudie le rôle du changement climatique induit par l'homme sur les événements pluviométriques horaires extrêmes pour le sud de la France en utilisant des simulations de convection et des simulations EURO-CORDEX
- Conclusions et perspectives

Chapter 2. Attribution of Extreme Daily Rainfall Events in the South of France Using EURO – CORDEX Simulations

The French Mediterranean is regularly prone to heavy precipitation events in the autumn whose daily accumulation can exceed a hundred millimeters. The magnitude of 1-in-10-year daily rainfall event in this area is two-to-four-fold higher compared to the mainland France (Ribes et al., 2019). These heavy rainfall events are often followed by other type of hazards such as flash floods or landslides that may have profound impact to the society around the area. The investigation of trend in extreme rainfall over a large area of the Mediterranean is conducted by many studies. However, a former extreme event attribution study focusing on a small area, for example the Cévennes, has never been done.

In this chapter, I will conduct the first extreme event attribution study focusing on the extreme daily rainfall event on the Cévennes mountain range using EURO-CORDEX simulations. The chapter contains: i) a research article published in Geophysical Research Letters that attributing the change in probability and intensity of extreme daily rainfall to human-induced climate change using multi-model approach, ii) an additional section that analyzes results from individual simulation. The overall conclusion and chapter summary are given at the end of this chapter.

2.1. Article published in Geophysical Research Letters: Attribution of Extreme Rainfall Events in the South of France Using EURO-CORDEX Simulations

Linh Nhat Luu², Robert Vautard², Pascal Yiou², Geert Jan van Oldenborgh³, and Geert Lenderink²

Received 12 March 2018; Accepted 12 June 2018

©2018. American Geophysical Union. All Rights Reserved.

Citation: Luu, L. N., Vautard, R., Yiou, P., van Oldenborgh, G. J., & Lenderink, G. (2018). Attribution of extreme rainfall events in the South of France using EURO-

²Laboratoire des Sciences du Climat et de l'Environnement, UMR 8212 CEA-CNRS-UVSQ, Université Paris-Saclay and IPSL, Gif-sur-Yvette, France

³Royal Netherlands Meteorological Institute (KNMI), De Bilt, Netherlands

2.1.1. Abstract

This study investigates how climate change affects the daily extreme precipitation events that occur in the autumn in Cévennes mountain range (South of France). We use an ensemble of 10 EURO-CORDEX model simulations with two horizontal resolutions (0.11° and 0.44°). Those data sets, after pooling all models together, are fitted by stationary generalized extreme value and empirical distributions for several periods to estimate a climate change signal in the tail of distribution of extreme rainfall. We find that the exceedance probability of a 1-in-100-year event in the historical climate has increased by a factor of 2.5 ± 0.8 under the current climate. The results show that higher-resolution simulations with bias adjustment provide a robust and confident increase in the intensity and likelihood of occurrence of the events in the current climate in comparison with the historical climate. These changes are in agreement with an observations-based analysis in a previous study.

Plain Language Summary: This paper investigates the connection between autumn high precipitation events in the South of France and climate change. From an ensemble of regional climate simulations and observations, we show that the probability of exceeding 100-year precipitation events has more than doubled, due to temperature increase.

Key Points:

- The attribution of extreme rainfall events in the South of France is made by using model simulations and observations
- The change of extreme precipitation distribution is significant under climate change
- We verify the Clausius-Clapeyron relation for precipitation events

2.1.2. Introduction

The Mediterranean region often undergoes thunderstorms in the autumn, which generate convective rainfall in coastal areas leading to more than 100 mm of precipitation in a day. Dedicated research programs have been devoted to understand these impactful phenomena (Drobinski et al., 2014; Ducrocq et al., 2014). In France, the Cévennes mountain range, which is located in the south of the country with its weather and climate

strongly influenced by Mediterranean Sea, undergoes the highest amounts of daily precipitation in the autumn. In this region numerous extreme rainfall events in 2014, one of them with an intensity of more than 300 mm/day occurring on different days, raised the question of the role of climate change in increasing likelihood and intensity of such events. Observations show a roughly 4% per decade increasing trend of autumn daily maxima over the past 60 years (Vautard et al., 2015). They also showed that the return period of 2014 amounts declined by a factor of 3 (95% confidence interval: 1 to 13) since the middle of the twentieth century. This change was shown to be linked to the warming trend in the region. These results were later confirmed by an analysis over an extended region (Ribes et al., 2019). However, a formal attribution of this change to human influence on climate could not be done from an observational analysis only.

The attribution of such convective extreme precipitation events is emerging as a key challenge and has received substantial efforts in weather and climate sciences. Several previous studies have used large regions to aggregate events and infer human influence on past events. Min et al. (2011) showed a contribution of increased anthropogenic greenhouse gases (GHGs) to the intensification of convective rainfall events in the Northern Hemisphere using observation and multi-model simulation from Coupled Model Inter-comparison Project phase 3, even though these models have resolutions of a few hundred kilometers and therefore cannot represent convective events. Zhang et al. (2013) determined the contribution of human influence on the increase in annual maxima daily rainfall and 5-day consecutive rainfall (i.e., Rx1day and Rx5day, respectively) over the Northern Hemisphere land areas. Those indices were analyzed by observations covering the period 1951–2005 and several coupled model simulations from the Coupled Model Inter-comparison Project phase 5, again with resolutions of hundreds of kilometers. The results showed a 3.3% increase in Rx1day with 90% uncertainty of 1.1% to 5.8% that is attributed to anthropogenic forcing. Fischer and Knutti (2015) showed that 18% of daily heavy rainfall events over continents can be mainly attributed to a human-induced warming trend since the pre-industrial period.

Less robust results could be obtained in attributing extreme daily amounts over a limited region. However, Eden et al. (2016) used a multimethod approach to find higher confidence in the attribution of the extreme heavy rainfall event in September 2013 in Boulder (Colorado, USA). The authors determined the change in probabilities of the event in observations and an ensemble of two general circulation model simulations for

daily amounts. Their results allowed them to draw a robust conclusion on the anthropogenic influence on such events. van der Wiel et al. (2017) found the increase in both intensity and probability of annual maximum 3-day consecutive precipitation of heavy rainfall event in 2016 in the central U.S. Gulf Coast under 2016 climate conditions compared to 1900 climate conditions due to anthropogenic climate change. The results show strong confidence with a good agreement between observations and model simulation with multiple horizontal resolutions. In addition, the more realistic higher resolution model (25 km) produced a more significant increase in probability of the event of interest.

One of the issues that can be raised for short-lived convective rainfall attribution studies using climate models is that of resolution, as the phenomena involved have an intrinsically small scale. Recently, Prein et al. (2016) showed that the new EURO-CORDEX high-resolution (12 km) ensemble has a better ability to capture high precipitation events in mountainous areas. Ruti et al. (2016) presented the results from the Med-CORDEX ensemble showing a clear improvement in extreme rainfalls in the mountain ranges surrounding the Mediterranean Sea with higher resolutions. This provides hope for better attributing the extreme daily events in the areas where orography plays a key role on such events.

In this article, we focus on the attribution of extreme Mediterranean rainfall using 14 stations in the Cévennes mountain range (as in Vautard et al., 2015) using EURO-CORDEX simulations. We verify that regional climate model simulations in the EURO-CORDEX project can reproduce statistical features of such events in the historical period and investigate their projections in future scenarios. This study completes the paper of Vautard et al. (2015), which was based on observations. The evaluations of model simulations of extreme rainfall are presented in Section 2.1.3. Section 2.1.1 shows the attribution of extreme rainfall events in the Cévennes range. Discussion and conclusions are drawn in Section 2.1.2.

2.1.3. Evaluation of Model Simulation of Extreme Events

2.1.3.1. Autumn Maxima Rainfall (Rx1day)

We evaluate the ability of the models in simulating SON (September–November) daily maximum rainfall over the Cévennes mountain range. Three different data sets from EURO-CORDEX with six regional models driven by five different boundary conditions

forming 10 simulations are investigated. The simulations were run under Representative Concentration Pathway 8.5 (Meinshausen et al., 2011) and cover the 1951–2100 period with two horizontal resolutions including 12 and 50 km (EUR-11 and EUR-44). For the finer resolution, we also use Cumulative Distribution Function transform (CDFt) bias-corrected simulations whose method was described in Michelangeli et al. (2009) and Vrac et al. (2012; ensemble denoted BC-EUR-11). Bias correction is made using the WFDEI reference gridded reanalyzes corrected by observations (Weedon et al., 2014). The detail of the 10 model simulations are given in supporting information Table S1. We use daily observational precipitation data of 14 stations in Cévennes mountain (Vautard et al., 2015) as reference.

We use quantile-quantile (q-q) plots to compare modeled SON rainfall maxima (Rx1day) with observations. From the gridded model data set, we use nearest neighbor interpolation to derive the simulation at 14 stations. This method avoids smoothing extreme values from a gridded model. Then, both SON rainfall values from models and observations are sorted in ascending order and compared for each station separately. Thus, the quantiles of each simulation at a station are compared to the observational quantiles. For each q-q plot between observations and models, we fit a linear regression ($Y = AX + B$) to all the data points. In the regression, the model quantiles are considered as independent variables (X) and observed quantiles are dependent variables (Y). Ideally, the slope (A) should be 1 and the intercept (B) should be 0. Those parameters (slope and intercept) indicate how the biases are distributed among models. An idealized linear model, with exponential distributions for the variables and a Gaussian perturbation with a standard deviation that is as large as the largest residual standard error of the fits described above, gives a 90% confidence interval of 0.6 to 1.1 for the slope (A) and -14 to 25 for the intercept (B). This allows comparing how the simulation-observation regression differs from the ideal case.

Figure 2 summarizes the evaluation of the model skill in simulating SON Rx1day over 14 stations in the Cévennes region for the period of 1971–2005. For EUR-44, the slopes have much higher values than 1 (Figure 2b). Therefore, the simulated values of SON Rx1day are generally lower than the observations. We can point out the worst simulations in this case (RCA4 driven by IPSL-CM5A and MPI-ESM-LR). For EUR-11, the slope A of the linear fit ranges from 0.5 to 3.5 (Figure 2a). This indicates a better agreement of model simulations to observations, in particular for the worst cases of EUR-

44. The slope A from BC-EUR-11 is in the range of 0.5 and 2, and approximately 10% of all models and stations show a slope lower than 1 (Figure 2c). As a result, most of the simulations tend to underestimate SON-Rx1day. In addition, we find that the residual standard errors range almost from 10 to 20 mm in the three model ensemble data sets.

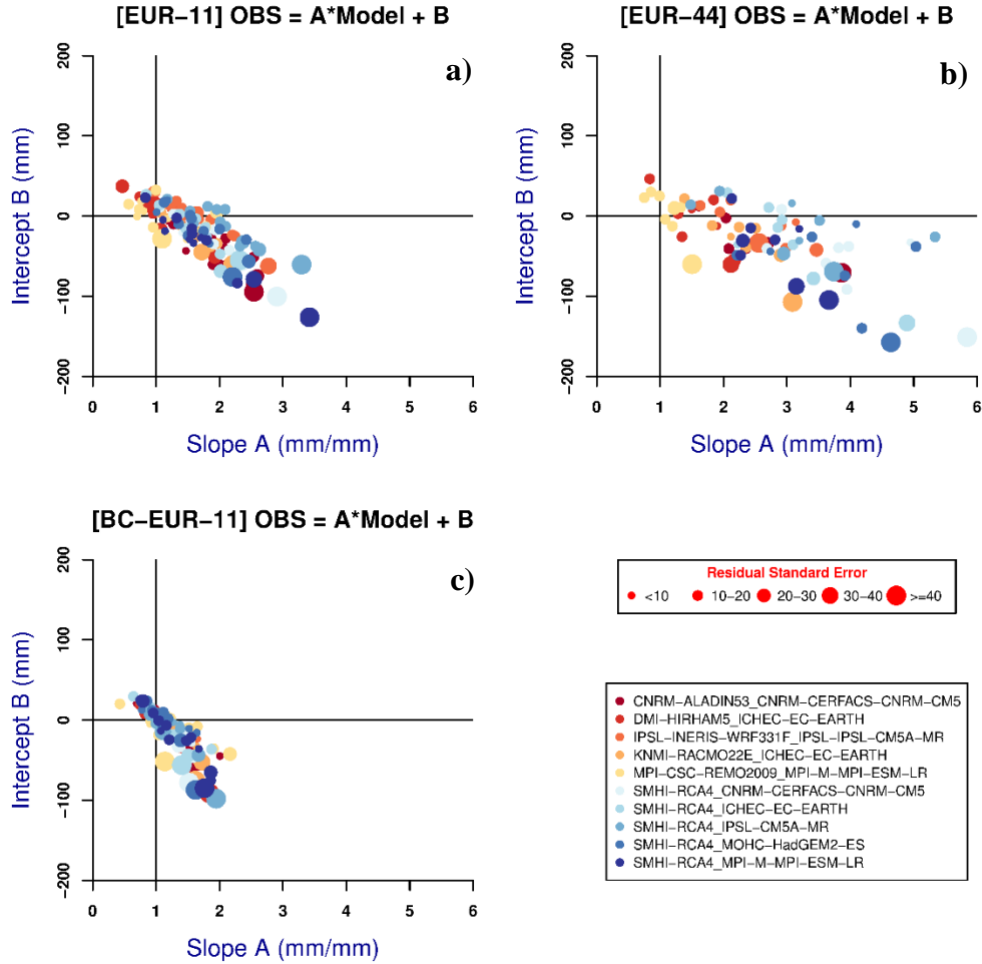


Figure 2. Summary of q - q plot comparison of model and observation for the period of 1971–2005; colors denote different models, and size of dots denotes the residual standard error of the linear fit. The horizontal and vertical axes show the slope A (mm/mm) and intercept B (mm) of the fit described in section 2.1. (a) EUR-11, (b) EUR-44, and (c) BC-EUR-11.

2.1.3.2. Dependence of Daily Rainfall on Temperature

An increase in temperature raises the water capacity holding of the atmosphere with 6–7% per degree warming, following the Clausius-Clapeyron relation (Clapeyron, 1834; Clausius, 1850). This increase in water-holding capacity, and the fact that relative humidity changes are relatively small in climate change simulations, leads to the expected increase in heavy precipitation with warming. While the sensitivity of extremes to

warming should be ideally derived from long climatic periods, deriving the dependency from short-term variability can also provide useful information (Lenderink and Attema, 2015; O’Gorman, 2012; Westra et al., 2014). Therefore, we evaluate the models with a scaling method as described by Lenderink and Van Meijgaard (2008) for the period of 1971 to 2005. This evaluation also enables us to confirm the attribution of change in extreme precipitation to human influence by linking it with temperature changes present in the model simulations, as was done by observations Vautard et al. (2015). For this purpose, we pair daily mean temperature and precipitation at each station together and then pool all stations together. Then, this pooled data set is sorted in ascending order of temperature. Next, we divide the data into several bins with their width of 2 °C and 1 °C overlap between two successive bins as in Lenderink and Van Meijgaard (2008). In each bin, we calculate the 99th percentile of precipitation and the median of temperature of the bin. The 90% confidence interval is estimated by 2,000 nonparametric bootstrap samples. This analysis is conducted by using daily rainfall at 14 stations from observations and interpolated from the three model ensembles. For 2-m temperature, we compute the mean of a box bounded by 2.5–5°E and 43.5–45°N from the CORDEX ensembles and from ENSEMBLES daily gridded observational dataset (E-OBS) (Haylock et al., 2008).

Figure 3 shows extreme daily rainfall scaling with 2-m temperature from different simulations and observations. Table S2 presents the slopes of the linear fit to each curve in Figure 3, which gives the average increasing rate of daily rainfall following the increase in 2-m temperature. We find that the dependencies from observations follow the Clausius-Clapeyron relation for temperature ranging from 4 to 14 °C with an average increasing rate of 4.1%/°C. This rate is a bit lower than the 6–7%/°C and also different from what was found for individual months in Vautard et al. (2015). This discrepancy could be due to the sensitivity of extreme rainfall response to warming being lower in mountainous regions where different dynamics control the vertical motion of air current (Shi and Durran, 2016). Generally, the intensity of daily rainfall from EUR-44 is underestimated in comparison with observations. The best average dependent rate is 4.2%/°C from ALADIN53 driven by CNRM-CM5 compared to 4.1%/°C from observation. The intensity for rainfall from EUR-11 is also underestimated, and BC-EUR-11 has a better agreement with observations. The results of extreme rainfall intensity found here are consistent with what we found out in the previous section.

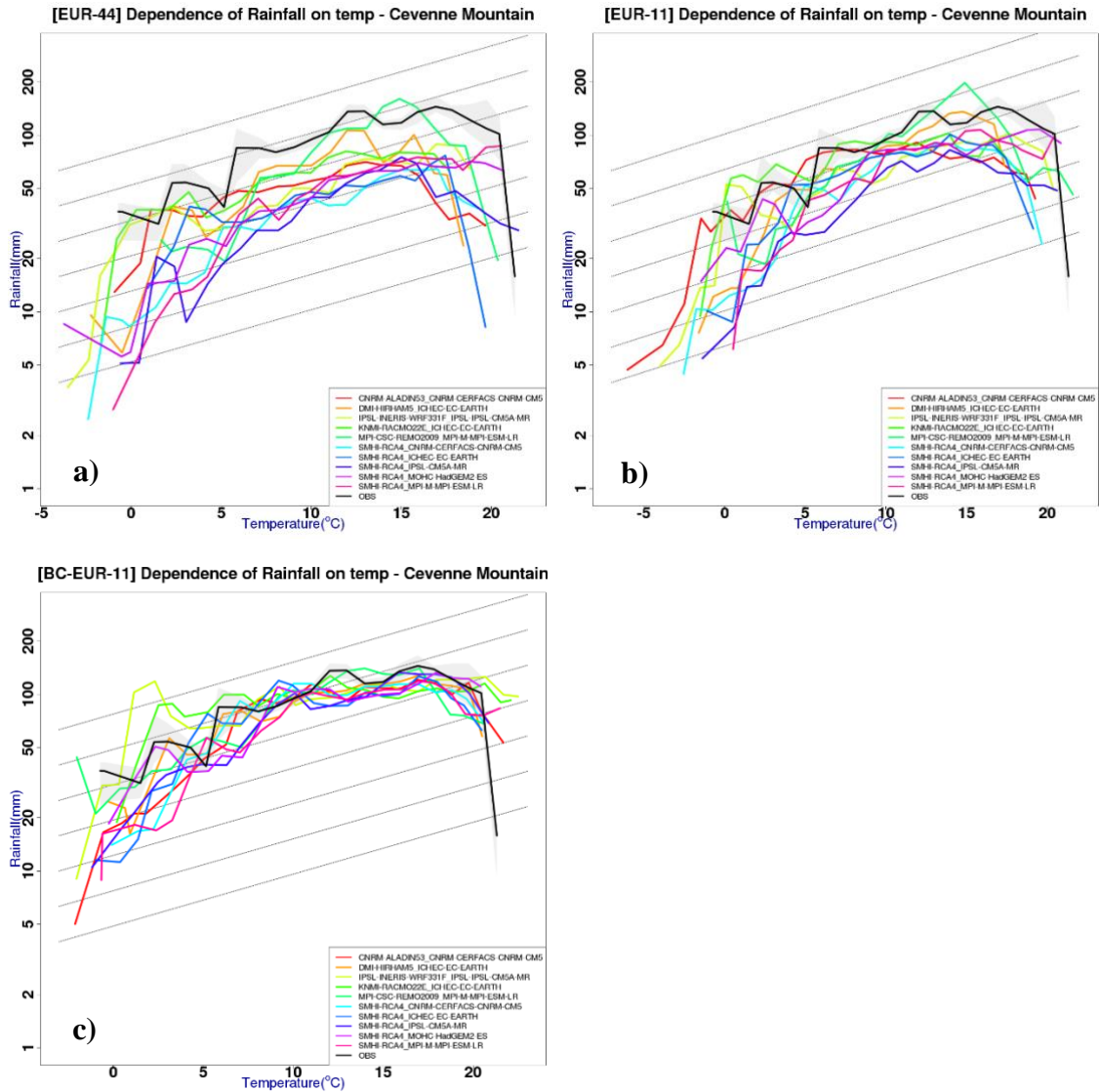


Figure 3. Dependency of extreme daily precipitation on 2-m temperature in the autumn (SON); (a) EUR-44, (b) EUR-11, and (c) BC-EUR-11; the gray bar shows 90% confidence interval of dependency from OBS; the dotted black lines denote Clausius-Clapeyron relation. SON = September–November.

2.1.1. Attribution of Extreme Events

We pool together SON Rx1day from the 14 stations and 10 models from each ensemble separately for the historical (1970–2000) and current (2001–2030) climates, which are both scaled with observations over the historical period (i.e., each model value at a given station is multiplied by the mean over time of all 14 observed stations divided by the mean over time of that model at that station) in order to obtain a pooled distribution that is as homogeneous as possible. We then make the assumption, as in Vautard et al. (2015), that this scaled and pooled data set represents a single distribution of daily rainfall events in the area. Events are, however, not

independent from one station to another, a fact that is taken into account for confidence interval estimation (see below). Each 30-year model period is described by $14 \times 10 \times 30$ years of simulations, and the 58-year period of observations (1957–2014) is expressed by 14×58 years. The distribution of extreme precipitation of each period is modeled statistically by fitting a stationary generalized extreme value (GEV) distribution (Coles, 2001) to SON maxima daily precipitation (R_{x1day}) of pooled data for each ensemble. The 95% confidence interval is estimated by using bootstrapping with a moving block technique (Eden et al., 2016) in order to take into account the spatial dependence among 14 stations and the dependence among 10 models of each data set. For each bootstrap sample, we randomly pick values from the pooled data set that could be any model or station and also take all values from other models and stations that were highly correlated with the initial picked model and station. This allows us to take into account the correlation among stations and models, as was done in Vautard et al. (2015). The total size of each bootstrap experiment is 2000.

One question with model pooling is whether extremes are represented by only one or a few models with a significantly heavier tail than others, even after scaling or bias correction. To address this, we count the number of different models of the pooled data in the distribution tail corresponding to different return periods (Figure 4), and compare the curve obtained with the 95% confidence interval taken from 1000 nonparametric bootstrap samples which were randomly drawn from complete pooled data sets. We count the number of models whose values are equal to or greater than a return value at a specific return period. For each return period, we repeat the same procedure 1000 times to estimate the reference for comparison. We find that for the EUR-11 data set, the distribution tail includes an insufficient number of models as compared to random picking for return periods larger than about 100 years under the 1971–2000 climate, indicating heavier tails in some models than in others (Figure 4a). The BC-EUR-11 simulations do not seem to suffer from this potential problem after pooling, which is not surprising because the simulation distribution is corrected across the distribution. We also find the same result with EUR-44 data set (not shown) as for the historical climate from the EUR-11 data set.

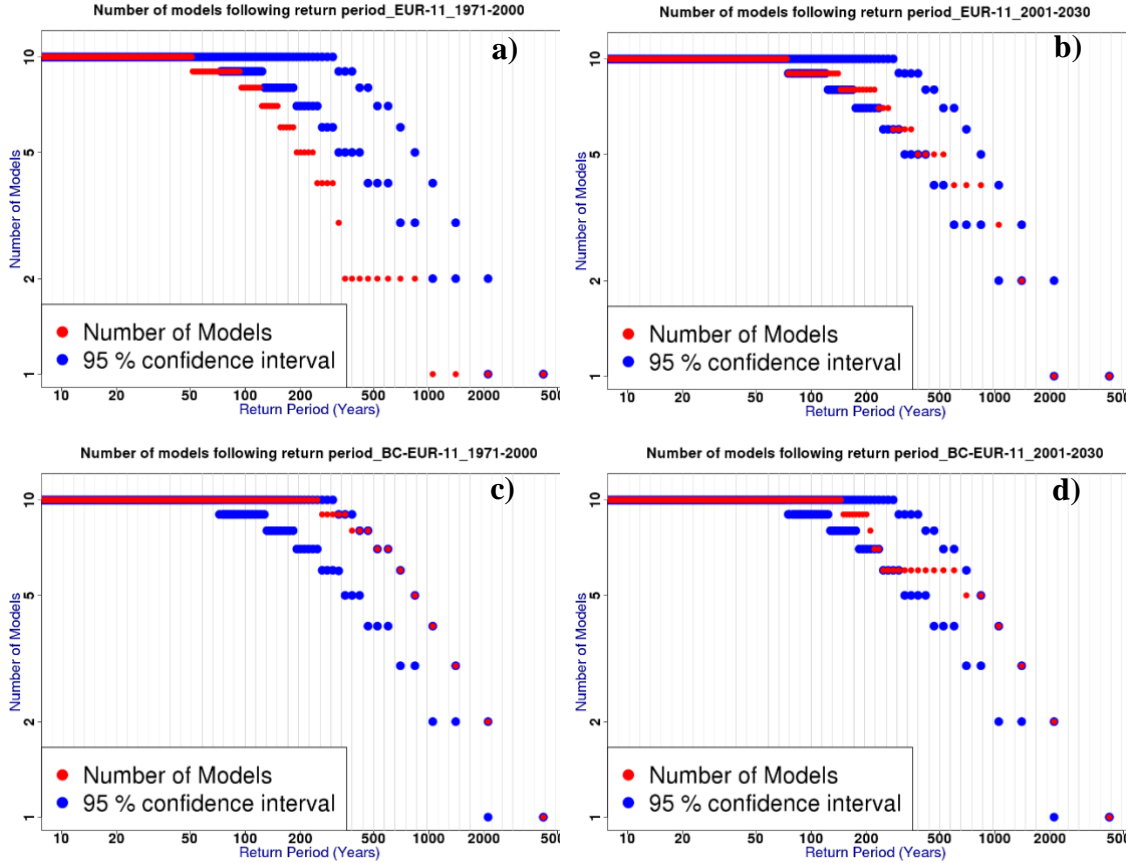


Figure 4. The number of models (red points) contributing to pooling distribution; the blue points denote 95% confidence interval from 1,000 nonparametric bootstrap sampling from complete pooled data sets; (a) historical and (b) current period of EUR-11; (c) historical and (d) current period of BC-EUR-11.

The parameters of GEV fits of each data set are shown in Table S3. We find that the location and scale parameters increase in the current climate as compared to the historical climate for all three ensembles. These increases indicate that the distribution of extreme rainfall shifts toward higher level (location) and stretches (scale) more widely under the current climate in comparison with the historical climate. The shape parameter increases inducing a larger increase of time-dependent return values in the tail of distribution. Figure 5 shows return level plots for observations in 1957–2014, model historical simulations (1971–2000), model simulation of the current climate (2001–2030), and near (2021–2050) and far future (2041–2070). We discuss mainly the historical and current climate, which are assumed to represent counterfactual and factual climate, respectively. In attribution studies, we use factual climate terminologies to imply the world with anthropogenic effect where we are now, and counterfactual climate is of the world that might have been with only natural change and variability and the absence

of human-induced climate change (i.e., preindustrial climate). We bear in mind that the historical period used still includes a significant amount of human forcing through GHGs and that most EURO-CORDEX simulations (i.e. except those from ALADIN and RACMO) only include changes in GHGs and not aerosols. We also note that global temperature under historical climate would be more or less 0.5 °C higher than the preindustrial period.

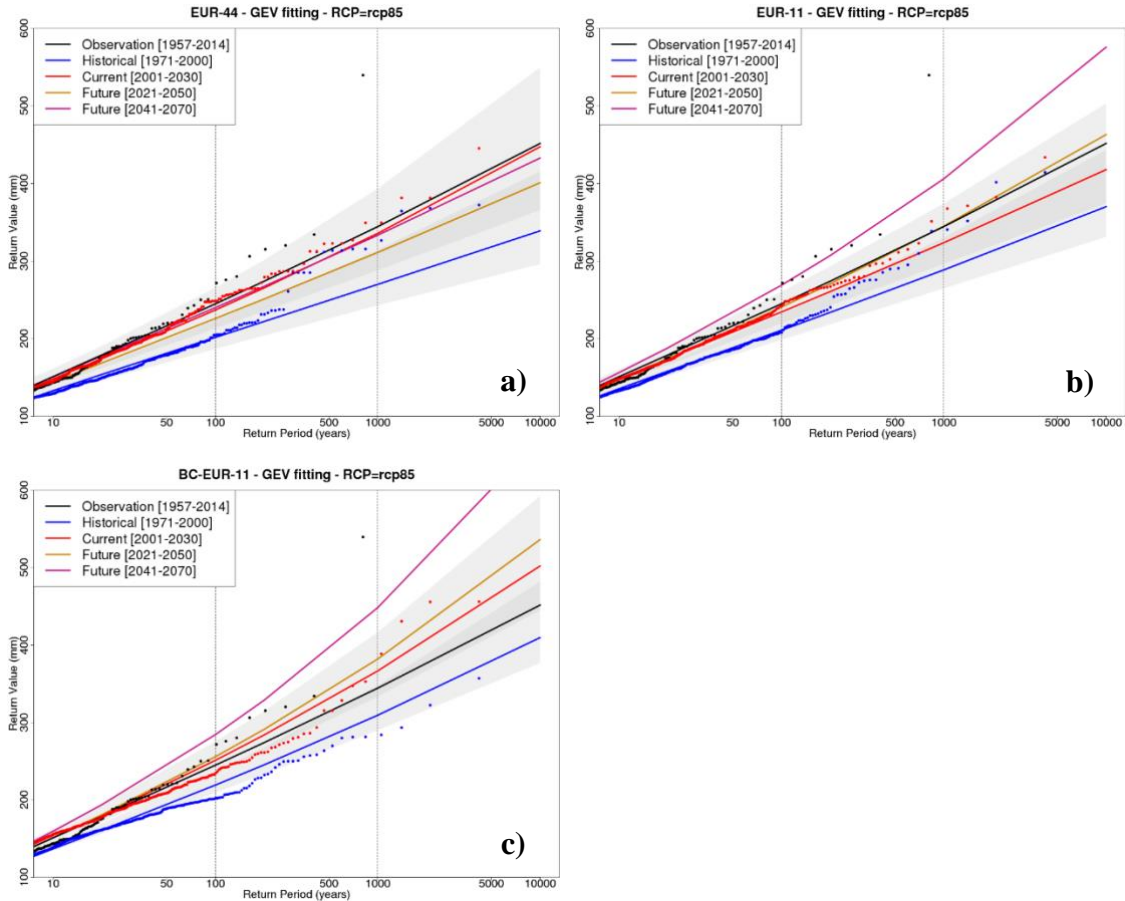


Figure 5. Return level plot from stationary GEV-fitted to model SON maxima of 1-day precipitation; (a) EUR-44, (b) EUR-11, and (c) BC-EUR-11. The blue and red shadings show 95% confidence interval for historical and current climate, respectively. GEV = generalized extreme value; SON = September–November.

The risk ratio is defined by the fraction between exceedance probability of rainfall events under current (factual) and historical (counterfactual) climate. These ratios represent the increase in likelihood of occurrence of extreme rainfall events in the factual climate and are summarized in Table S4 using three ensembles. For example, the YYYY-Years (column label in Table S4, e.g., 1000-Years) implies the event with its intensity equal to or greater than 1000-year return value at any among 14 stations in the

counterfactual climate. Here we do not show the real return values corresponding to the return period because they are different among three data sets and two types of distributions including sorted (Empirical) and GEV-fitted pooling data set. We mainly discuss risk ratios and changes in rainfall intensity following empirical distribution because The GEV distribution seems unable to generate return values at large return period (Figure 5) for the three pooled data sets.

In the EUR-44 case (Figure 5a), the intensity of a 1-in-100-year event increases by 22% but with an extensive range of 5% to 36%. Similarly, the likelihood of occurrence of a 1-in-100-year event of historical climate may have increased by a factor of 2.4 (1.3 to 4) under the current climate. This means that the event with intensity equal to or greater than 100-year return value in historical climate may occur every 40 years in the current climate at any among 14 stations (i.e., approximately 600 years at a given station).

The comparison between return level plots of historic and current climate EUR-11 is shown in Figure 5b. The intensity of a 1-in-100-year event in the historical climate may increase by 17% (1 to 27), and the likelihood of this event in the historical climate appears to increase by a factor of 2.2 (from 1.1 to 3.1) in current climate. For BC-EUR-11 (Figure 5c), the likelihood of occurrence of 1-in-100-year events between historical and current climate increases by a factor of 2.5 within a confidence range of 1.8 and 3.4. In addition, the magnitude of this event appears to increase 16% in current climate compared to historical climate. The uncertainty in this circumstance ranges from 10% to 24%. When taking rarer events, the significance of results becomes lower in most experiments. For a 1-in-1000-year event, the intensity of Rx1day increase 7% (-19% to 51%) from the EUR-44 ensemble and the return period of this event decreases by a factor of 1.7 (0.4 to 14.9) under current climate. For EUR-11, the likelihood of occurrence of events of comparable intensity to a 1-in-1000-year event in historical climate may increase by a factor of 1.4 (0.7 to 4.5) in the current climate. The magnitude of this event increases by 8% within a range of -16 and 29%. For BC-EUR-11, the increase in intensity of a 1-in-1000-year event is 37% (4% to 63%). The likelihood of this event in current climate increases by a factor of 3.1 with a range of 1.8 to 7.1.

The change in likelihood (Table S4) and intensity of extreme daily events (Table S5) is consistent among three ensembles for return periods lower than 100 years. The 95% confident interval in these cases are similar, but BC-EUR-11 provides the most

robust result. However, the higher return period (e.g. 1000 years) shows less agreement in changes given their uncertainty margin, specifically the change in intensity. The most reliable increase is produced by BC-EUR-11 ensemble because there are at least three to four models contributing to the tail of pooled distribution.

Generally, all three ensembles show an increase in both intensity and probability (exceedance probability) of extreme rainfall under current climate, although not all are significant. This agrees well with the results of Vautard et al. (2015) which were obtained from observational data sets only. They find that the return period of a 1-in-1000-year event of climate of 1950 may have decreased by a factor of 4 under climate of 2014 and for a 1-in-100-year event, it might decline by a factor of about 2. There is a small difference between our study and Vautard et al. (2015) because the periods considered and methods used are not the same.

2.1.2. Discussion and Conclusion

We have investigated the changes that occurred over the past 30 years in the likelihood in extreme daily precipitation over the Cévennes mountain range. We first evaluated the capacity of the models to simulate these extreme events, using three ensembles with a different resolution (12 and 50 km). We find here that a higher horizontal resolution of the model improves the quality of simulation of precipitation magnitudes because of its ability to capture complex topography and large-scale convection, as this was shown by Prein et al. (2016). We also find that a bias reduction with CDFt using a large-scale gridded data set (WFDEI) as a reference significantly improves the statistical properties of extreme precipitation on daily scale even though reference observation-based data are of relatively low resolution. In addition, a finer grid with bias correction can produce a better dependency (average dependent rate and intensity) of daily rainfall on 2-m temperature. These findings reinforce the confidence in our analysis of changes in the probability and intensity of extreme rainfall event.

The likelihood of occurrence and intensity of extreme daily rainfall events show an increasing trend in the interest region. The increase is found to be more confident with EUR-11 and the most confident with BC-EUR-11, especially in more rare events (e.g. 1000-year event) because these events are produced by at least three to four models. This indicates a robust estimate of the increase of probability. For instance, a 1-in-100-year

event undergoes a probability change of 2.5 (1.8 to 3.4) and 2.2 (1.1 to 3.1) for BC-EUR-11 and EUR-11, respectively, which are both significant increases in frequency.

The changes between the two time periods used in model simulations can only be explained by the changes in GHGs as no other external factor is changing in most EURO-CORDEX simulations. This difference in GHGs is smaller than the difference between factual and natural simulations, but we can reasonably assume that if a significant human influence can be detected in this case, it would be detected in factual versus natural experiments. These changes are found consistent with the physical relation between the extreme daily precipitation and the increase in regional mean temperature as shown in section 2. Besides, regional mean temperature is strongly concerned with a larger scale (i.e., subcontinental or continental scale) for which formal attribution studies of anthropogenic forcing on increasing in mean temperature were done (Stott, 2003 and Christidis et al., 2012a for the European continent; Christidis et al., 2010 2012b for the Mediterranean basin). We, therefore, confirm that human influence plays an indispensable part in altering the likelihood and intensity of daily extreme rainfall events in the Cévennes mountain area. In addition, we also find the advantage of high resolution in constraining the uncertainty margin of the distribution of extreme precipitation.

These results highlight the importance of the increasing resolution in order to improve the estimation of change in odds of extreme rainfall events. However, further improvements could be obtained using convection-permitting models, which allow computing convective rainfall directly in a small area.

2.1.3. Acknowledgments

This work was supported by EC grant 162227-EUPHEME. L. N. Luu was supported by the Commissariat à l’Energie Atomique et aux énergies alternatives. The EURO-CORDEX simulation can be found at <https://esgfnode.ipsl.upmc.fr/search/cordex-ipsl>.

2.1.4. Supporting Information

Table S1. Information on EURO-CORDEX models are employed in this study

No.	Institute	RCMs	GCMs - Boundary Condition	Ensemble
1	National Centre for Meteorological Research (CNRM), France	ALADIN53	CNRM-CM5	EUR-44 EUR-11 BC-EUR-11
2	Danish Meteorological Institute (DMI), Denmark	HIRHAM5	ICHEC-EC-EARTH	

No.	Institute	RCMs	GCMs - Boundary Condition	Ensemble
3	Institute Pierre Simon Laplace (IPSL), France	WRF331F	IPSL-CM5A-MR	
4	Royal Netherlands Meteorological Institute (KNMI), Netherland	RACMO22E	ICHEC-EC-EARTH	
5	Max Planck Institute (MPI), Germany	REMO2009	MPI-M-MPI-ESM-LR	
6	Swedish Meteorological and Hydrological Institute (SMHI), Sweden	RCA4	CNRM-CM5	
7			ICHEC-EC-EARTH	
8			IPSL-CM5A-MR	
9			MOHC-HadGEM2-ES	
10			MPI-M-MPI-ESM-LR	

Table S2. The best estimate values of dependent rate (%/°C) of 99th percentile daily rainfall on 2m temperature from observation and different model simulations for Cévennes area.

Models	BC-EUR-11	EUR-11	EUR-44
Observation	4.1		
CNRM-ALADIN53_CNRM-CERFACS-CNRM-CM5	5.9	4.2	2.4
DMI-HIRHAM5_ICHEC-EC-EARTH	5.6	9.1	6.7
IPSL-INERIS-WRF331F_IPSL-IPSL-CM5A-MR	3.4	5.9	7.1
KNMI-RACMO22E_ICHEC-EC-EARTH	2.3	3.5	5.8
MPI-CSC-REMO2009_MPI-M-MPI-ESM-LR	5.3	4.4	6.2
SMHI-RCA4_CNRM-CERFACS-CNRM-CM5	5.5	6.6	7.6
SMHI-RCA4_ICHEC-EC-EARTH	5.4	5.8	2.9
SMHI-RCA4_IPSL-CM5A-MR	7.0	6.1	5.5
SMHI-RCA4_MOHC-HadGEM2-ES	6.3	6.5	7.4
SMHI-RCA4_MPI-M-MPI-ESM-LR	6.3	7.1	8.4

Table S3. Summary of GEV parameters of extreme precipitation for observations and models including the location (μ), the scale (σ) and the shape (ξ) parameter; Ranges inside parentheses denote 95% confident interval estimated from bootstrap.

Maximum Likelihood Estimators		Location (μ)	Scale (σ)	Shape (ξ)
Observation (1957-2014)		67.8	35.6	0.033
Historic	EUR-44	68 (66.5 to 69.4)	28.7 (27.4 to 30.1)	0.005 (-0.024 to 0.044)
	EUR-11	66.8 (65.5 to 67.7)	29.8 (29 to 30.9)	0.021 (-0.002 to 0.055)
	BC-EUR-11	65.8 (64.9 to 66.2)	29.9 (29.1 to 30.5)	0.047 (0.032 to 0.08)
Current	EUR-44	73.1 (70.4 to 76.3)	31.4 (29.9 to 33.2)	0.054 (0.014 to 0.087)
	EUR-11	70.7 (68.4 to 72.3)	33.6 (32.2 to 35.9)	0.024 (0.005 to 0.056)
	BC-EUR-11	69.8 (68 to 71.7)	33.4 (32.1 to 35.1)	0.07 (0.05 to 0.096)

Table S4. Risk Ratio between factual (2001-2030) and counterfactual (1971-2000) climate for Cévennes region.

Risk Ratio		100-Years	200-Years	1000-Years
Empirical Distribution	EUR-44	2.4 (1.3 to 4)	3 (0.6 to 5.5)	1.7 (0.4 to 14.9)
	EUR-11	2.2 (1.1 to 3.1)	2.1 (0.7 to 3.6)	1.4 (0.7 to 4.5)
	BC-EUR-11	2.5 (1.8 to 3.4)	2.1 (1.5 to 4.9)	3.1 (1.8 to 7.1)
GEV Distribution	EUR-44	2.4 (1.5 to 3.9)	2.9 (1.5 to 5.2)	4.5 (1.7 to 11)
	EUR-11	1.9 (1.1 to 2.7)	2 (1.1 to 3.3)	2.4 (0.8 to 5.1)
	BC-EUR-11	2 (1.5 to 2.7)	2.3 (1.6 to 3.3)	3 (1.8 to 5.3)

Table S5. Change in return value (%) between factual (2001-2030) and counterfactual (1971-2000) climate for Cévennes region.

Intensity (%)		100-Years	200-Years	1000-Years
Empirical Distribution	EUR-44	22 (5 to 36)	21 (-8 to 39)	7 (-19 to 51)
	EUR-11	17 (1 to 27)	11 (-4 to 24)	8 (-16 to 29)
	BC-EUR-11	16 (10 to 24)	13 (6 to 30)	37 (4 to 63)
GEV Distribution	EUR-44	18 (7 to 31)	20 (7 to 37)	32 (7 to 71)
	EUR-11	11 (2 to 19)	12 (1 to 22)	13 (-6 to 32)
	BC-EUR-11	15 (8 to 22)	16 (9 to 25)	23 (9 to 44)

2.2. Synthesizing the results

In this section, I will give the syntheses of Probability Ratio (**PR**) (i.e. Risk Ratio as mentioned in Section 2.1.1 of this chapter) and Intensity Change (**IC**) for the 100-year daily rainfall event in the Cévennes region. These syntheses of the **IC** and **PR** results of all individual simulations and model pooling of each ensemble (e.g. BC-EUR-11) are estimated by taking the average. The confidence interval of this average number is estimated using non-parametric bootstrap technique. In this procedure, 2000 samples are randomly picked with replacement. Each sample provides **PR** or **IC** values of all simulations to estimate the average of that sample. Finally, the 95% uncertainty margin is obtained from those 2000 average values.

The syntheses of **PR** for the 100-year daily rainfall event from BC-EUR-11 and EUR-11 ensembles are shown in Figure 6 and Figure 7, respectively. The results from EUR-44 ensemble is not discussed here because of its poor ability in reproducing extreme daily rainfall in the Cévennes (as shown in Section 2.1.3). In general, the two ensembles give similar results for each simulation and the model pooling case that the probability of the event increases under factual climate, except those from the SMHI-RCA4 driven by HadGEM2-ES and DMI-HIRAM5 driven by EC-EARTH. The **PR** from most of the simulations are statistically insignificant. In average, the two ensembles show consistent

results that probability of the 100-year daily rainfall event increases significantly by factor of 2.6 (2.2 to 3.9) from BC-EUR-11 and 2.2 (1.5 to 3.4) from EUR-11. These changes are also consistent with the model pooling dataset.

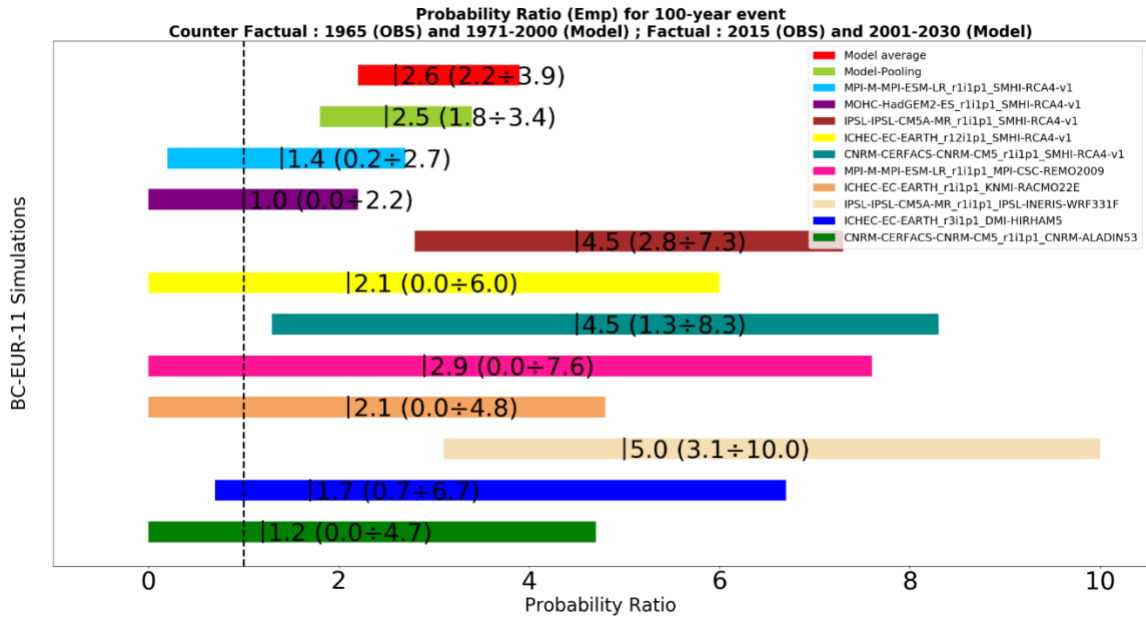


Figure 6. The syntheses of Probability Ratios of Rx1 day for 100-year event of model pooling and individual simulations from BC-EUR-11 ensemble

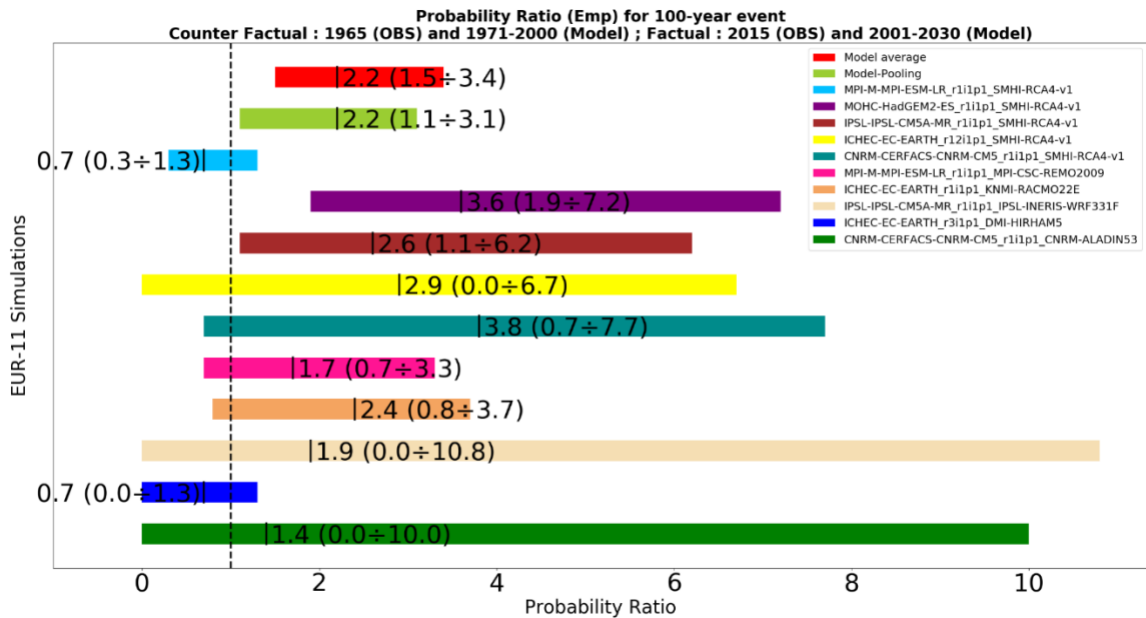


Figure 7. The syntheses of Probability Ratios of Rx1 day for 100-year event of model pooling and individual simulations from EUR-11 ensemble

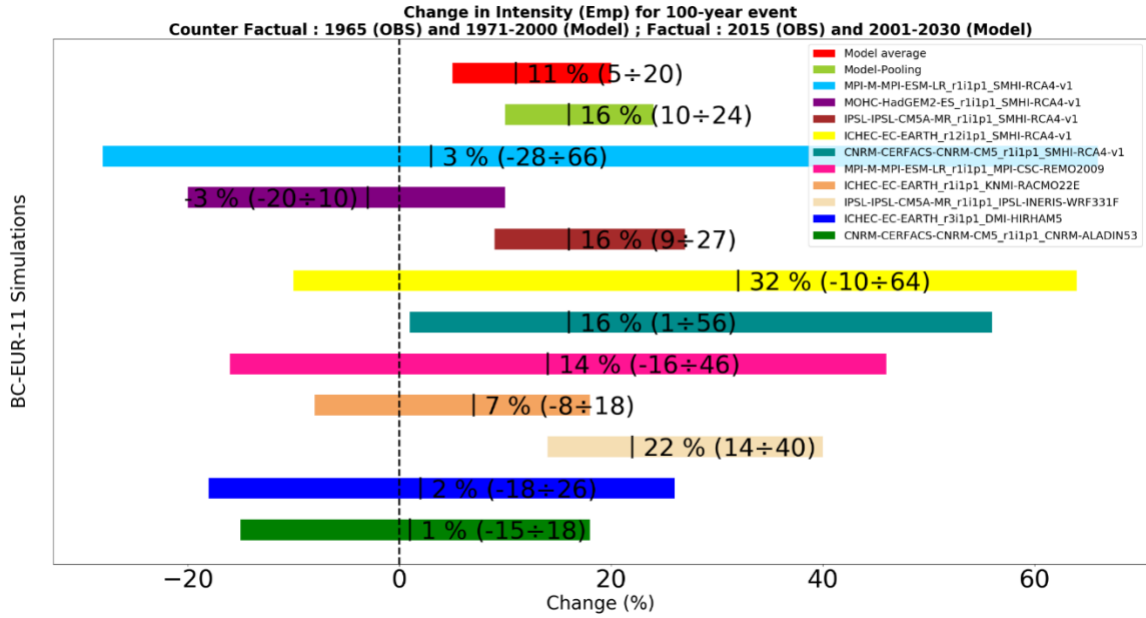


Figure 8. The syntheses of Intensity Changes of $Rx1day$ for 100-year event of model pooling and individual simulations from BC-EUR-11 ensemble

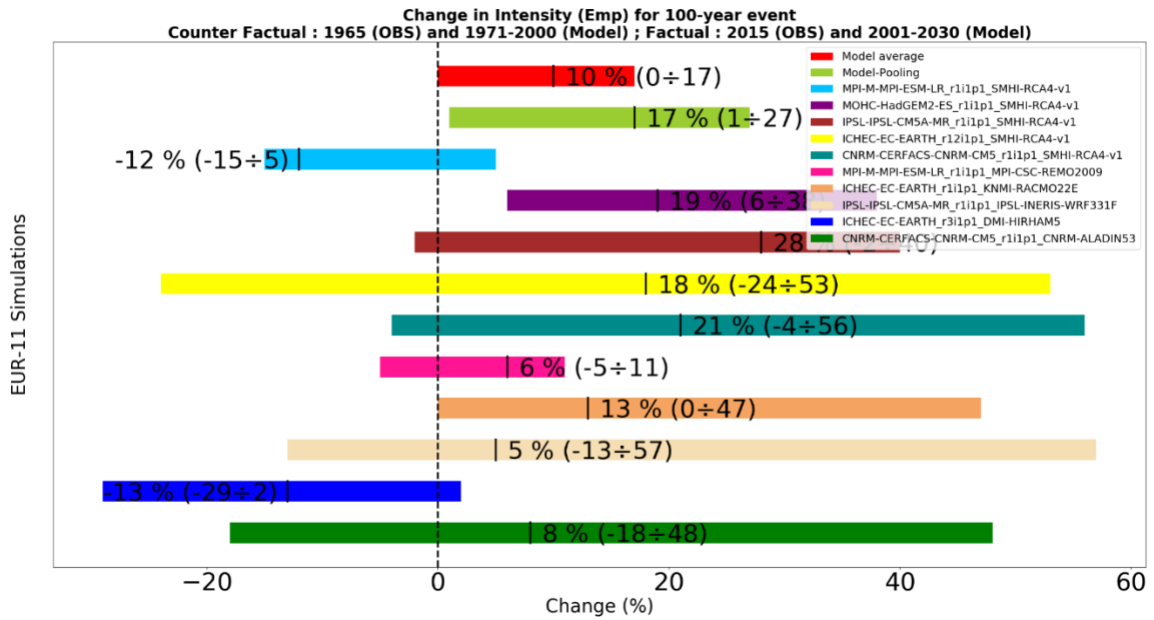


Figure 9. The syntheses of Intensity Changes of $Rx1day$ for 100-year event of model pooling and individual simulations from EUR-11 ensemble

Figure 8 and Figure 9 shows the syntheses of changes in intensity of the 100-year daily rainfall event from BC-EUR-11 and EUR-11 ensembles, respectively. The results of IC here are found similar to what was found in PR analysis that the two ensembles provide roughly consistent changes. The averages of ICs are 11% (5 to 20%) from BC-EUR-11 and 10% (0 to 17%) from EUR-11. Those averages are also closed to the model pooling cases. It is also worth noting here that different regional climate models (RCM) forced by the same boundary condition (GCM) can give different results. For instance, in

the EUR-11 ensemble, the SMHI-RCA4, KNMI-RACMO22E and DMI-HIRAM5 are forced by the same EC-EARTH. The SMHI-RCA4 shows large increase, but not significant, in intensity of the event (Figure 9), while the KNMI-RACMO22E shows smaller and significant increase. In contrast, the DMI-HIRAM5 shows a declined trend in rainfall intensity. These differences indicate the need of using multi-models (i.e. different RCMs and different GCMs) to take into account the internal variability of each model.

2.3. Conclusion

This chapter investigates the change in probability and intensity of extreme daily rainfall event in the French Mediterranean area. Three ensembles of EURO-CORDEX simulations are used including one with horizontal resolution of 0.44 degree (approx. 50 km, EUR-44), one with resolution of 0.11 degree (approx. 12km, EUR-11) and the bias-corrected version of EUR-11 (BC-EUR-11) using the cumulative distribution function transform (CDFt) method. I find that the higher resolution simulations show improvement in reproducing extreme daily rainfall events and the relation of extreme daily rainfall and mean surface temperature, especially the bias-corrected simulations. These results emphasize the need of using higher-resolution simulations in Extreme Event Attribution (EEA) studies.

The syntheses of Probability Ratio (**PR**) and Intensity Change (**IC**) show significant changes in likelihood of occurrence and intensity of extreme daily rainfall event. The results are found consistent between EUR-11 and BC-EUR-11 ensembles. I can conclude that these changes can be attributed to anthropogenic climate change because the difference between the counterfactual and factual climate in most simulations is only the greenhouse gas emission. This attribution result will motivate the investigation of the role of human-induced climate change on extreme rainfall in sub-daily time scale that will be conducted in the next chapters of this PhD.

By analyzing the **PR** and **IC** of individual simulations in each ensemble, I also find the variation of results among different models. This suggests that multi-model approach is of great importance in quantifying the uncertainty caused by model biases and internal variability in the attribution results.

Chapter Summary

Objective:

This chapter investigates the impact of human-induced climate change on the extreme daily rainfall event in the south of France using EURO-CORDEX simulations including a coarse resolution of 0.44 degree (EUR-44), a higher resolution of 0.11 degree (EUR-11) and a bias-corrected EUR-11. The capability of these simulations in reproducing extreme daily rainfall event is evaluated before conducting the attribution step.

Method:

The autumn blocks maxima of daily rainfall over the Cévennes mountain range from simulations are compared with in situ observations. In addition, the scaling of extreme daily rainfall with mean surface temperature is verified for each simulation and compared to observations.

The risk-based approach is used to for the attribution task. The Probability Ratio is calculated to reflect the change of likelihood of occurrence of extreme daily rainfall between factual (2001-2030) and counter factual (1971-2000) climate.

Results:

The bias-corrected EUR-11 reproduce well the extreme daily rainfall but non bias-corrected simulations underestimate the events amplitude.

The probability and intensity of the 1-in-100-year daily event increase under the factual climate by a factor of 2.5 (1.8 to 3.4). These increases are attributable to human-induced climate change.

Résumé

Objectif:

Ce chapitre étudie l'impact du changement climatique induit par l'homme sur les événements pluviométriques quotidiens extrêmes dans le sud de la France à l'aide de simulations EURO-CORDEX incluant une résolution grossière de 0,44 degré (EUR-44), une résolution plus élevée de 0,11 degré (EUR-11) et un EUR-11 corrigé du biais. La capacité de ces simulations à reproduire un événement pluviométrique quotidien extrême est évaluée avant de procéder à l'étape d'attribution.

Méthode:

Les blocs de maxima des précipitations quotidiennes d'automne sur le massif des Cévennes issues des simulations sont comparés aux observations in situ. La mise à l'échelle des précipitations quotidiennes extrêmes avec la température moyenne de surface est vérifiée pour chaque simulation et comparée aux observations.

L'approche basée sur les risques est utilisée pour la tâche d'attribution. Le ratio de probabilité est calculé pour refléter le changement de probabilité d'occurrence de précipitations quotidiennes extrêmes entre le climat factuel (2001-2030) et contre-factuel (1971-2000).

Résultats:

L'EUR-11 corrigé du biais reproduit bien les précipitations quotidiennes extrêmes mais les simulations non corrigées du biais sous-estiment l'amplitude des événements.

La probabilité et l'intensité d'un événement quotidien sur 100 ans augmentent dans le climat factuel d'un facteur 2,5 (1,8 à 3,4). Ces augmentations sont attribuables aux changements climatiques d'origine humaine.

Chapter 3. **Designing model configuration for simulation of extreme precipitation event using a case study**

In this chapter, I first give a short description of the Weather Research and Forecast (WRF) model which is used for dynamical downscaling in this PhD thesis. Next, the design of experiments for reproducing extreme rainfall events occurring in the South of France in the Autumn of 2014 is provided. An evaluation of these experiments is then carried out. These results play an important part in the selection of an ultimate configuration for long simulations that will be introduced in the next chapter.

3.1. Introduction

Deep convection is an important driver of heavy rainfall events in many regions over the world. This process often occurs in sub-grid scale and interacts with different processes from microscale to synoptic scale such as cloud micro-physic, planetary boundary layer near the surface or radiation. However, deep convection has been parameterized in climate simulation as well as weather forecast for a long time because of the lack of computational capacity. This parameterization often represents the properties of convection process over a grid box that is underlined by the empirical distribution or equation interacting with prognostic variables such as temperature, moisture (Kendon et al., 2012). In addition, the convection schemes are designed for coarse resolution RCMs and not able to represent thunderstorms or an extreme rainfall event at local scale. Therefore, this parameterization procedure takes up large uncertainty in climate model results and leads to defect in representation of a few characteristics of rainfall, especially the underestimation of extreme daily and hourly rainfall (Kendon et al., 2012; Kendon et al., 2019; Lenderink and Van Meijgaard, 2008; Prein et al., 2013). As a result, convection-permitting model with a higher horizontal resolution (i.e. 4 km or less) is expected to replace the convection parameterization scheme and solve explicitly deep convection process to improve the quality of simulations (Ban et al., 2014; Karki et al., 2017; Kendon et al., 2012; Prein et al., 2015).

Along with the physics of the model, specifically deep convection processes, the size and position of the nested domain can play a role in reproducing precipitation (Colin et al., 2010; Dash et al., 2015; Giorgi and Mearns, 1999; Seth and Giorgi, 1998). If the domain covers an area with a specific atmospheric conditions where the physics of model work improperly, the generated errors can be conveyed to the rest of the domain (Miguez-

Macho et al., 2004). Liang et al. (2001) showed that the non-homogeneous uncertainty in lateral boundary condition can degrade the quality of the simulations if the nested domain's boundary is located over this poor forcing condition. The over-specification of lateral boundaries for the nested region can also impact the solutions. This over-specified pattern is organized by the errors accumulating near the boundary and depends on the domain geometry and location as well as the atmospheric circulation. These errors in small scale are relaxed effectively into the forcing field within the buffer zone meanwhile the long waves part from these errors are not treated correctly, then impose to the boundary and reflect back to the nested domain. Consequently this reflection modifies the large scale dynamic in the inner domain (Miguez-Macho et al., 2004). However, the selection of domain is subject to regions and experiment and there is no strict criterion for every region (Giorgi and Mearns, 1999).

The objective of this chapter is to set up a few configurations of convection permitting model for sensitivity tests of domain size and positions. These experiments are then evaluated with a focus on extreme rainfall over the Cévennes mountain range in the South of France during three months of the autumn in 2014.

3.2. Configuration and experiment design

3.2.1. The Weather Research and Forecast (WRF) model

The Weather Research and Forecasting (WRF) is a limited-area atmospheric model developed to serve multiple purposes including research and weather and climate forecast. The efforts to develop WRF were first initiated in late 1990s by collaboration between the National Center for Atmospheric Research (NCAR) and the National Centers for Environmental Prediction (NCEP). The model was designed to inherit the advantages and abolish the shortcomings of numerical models at that time such as MM5, ETA, etc. Therefore, WRF was expected to have many improvements in terms of accuracy, computational efficiency and flexibility in expanding and adapting to different parallel platforms.

The version WRF used in this PhD dissertation is 3.8.1 with the Advanced Research WRF (ARW) dynamical core which has been developed and maintained by NCAR's Mesoscale and Microscale Meteorology Division (MMM). Some key features of this version include:

- Solving fully compressible non-hydrostatic equations with hydrostatic option
- Arakawa C-grid staggering grid
- Complete Coriolis and curvature effect
- Available one-way and two-way nesting with multiple nests, nest levels and moving nest options
- Grid spacing vertically varying with height
- Scalar-conserving flux form for prognostic variables
- Four options for map projections: Lambert-conformal, Mercator, polar stereographic and latitude and longitude (rotated availability)
- Runge-Kutta second and third order time integration
- Second to sixth order of horizontal and vertical advection
- Grid and spectral nudging
- Full physics options and improvements compared to previous versions for land-surface, planetary boundary layer, radiation, microphysics and cumulus convection

3.2.2. Experiments design

In this chapter, WRF-ARW is configured to perform simulations for the autumn (September – October - November) of 2014. A large domain which covers the European region is, at first, set up and run following the European Coordinated Regional Climate Downscaling Experiment (EURO-CORDEX, hereafter mentioned as EUR-11) domain (Jacob et al., 2014). The horizontal resolution is 0.11 degree (approx. 12km) and the size of the domain is 503 grid points in west-east direction and 491 grid points in north-south direction. The time step for integration is 60 seconds and the number of hybrid sigma vertical levels is 32. This domain is driven by ERA-Interim reanalysis with boundary condition updated every 6 hours. The simulation for this domain is done alone with the start time at 2014-09-01_00 and end time at 2014-11-30_18. Map projection used for this simulation is ‘lat-lon’ with rotated option. Three parameters concerning the option include the POLE_LAT, POLE_LON and STAND_LON whose values are of 39.25, -162 and -18, respectively. This domain is depicted in Figure 10 and all physics parameters used for the simulation are provided in Table 6. In addition, spectral nudging method is applied to prevent the regional information from going far away the driving reanalysis. The nudging terms are only added to upper zonal and meridional directions of wind (i.e. levels above the 12th model level) in the prognostic equations. The numbers of waves in both x and y direction are set to 5, which means that only the five longest waves are

nudged toward the forcing data. The nudging coefficient weighting the model solution to correct the error is set to $5 \cdot 10^{-5}$. The simulation using this domain configuration is done to provide boundary condition for the convection-permitting domains close to reanalysis data as much as possible. I will not provide further discussion on the results of simulated precipitation from this domain.

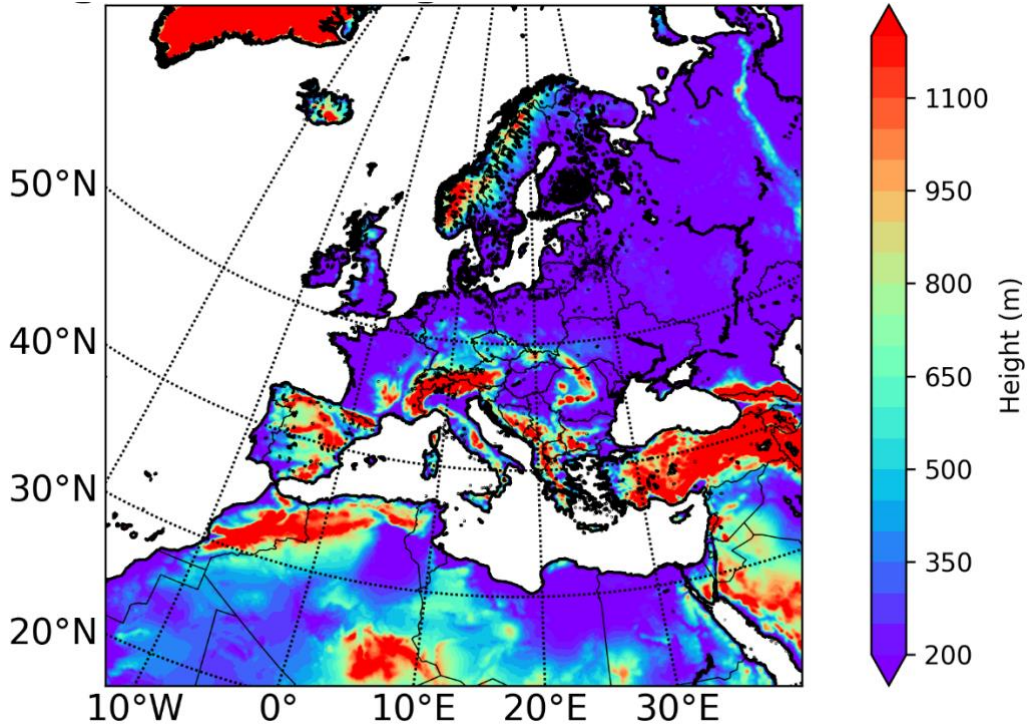


Figure 10. The location of the EURO-CORDEX domain and its topography information

Table 6. Physics parameterization used for this simulation

No.	Physics	Option
1	Microphysics	Thompson scheme (Thompson et al., 2008)
2	Longwave radiation	rrtmg scheme (Iacono et al., 2008)
3	Shortwave radiation	rrtmg scheme (Iacono et al., 2008)
4	Surface-layer option	Monin-Obukhov (Janjic) scheme (Janjic, 1996)
5	Land-surface option	Unified Noah land-surface model
6	Boundary-layer	MYNN 2.5 level TKE scheme (Nakanishi and Niino, 2006)
7	Cumulus option	New GFS simplified Arakawa-Schubert scheme from YSU
8	SST updating	every 6 hours

For the convection permitting simulations (hereafter mentioned as CPS), four different nested domains inside the EUR-11 domain are conducted with the horizontal resolution and time step of a fourth of the parent domain (i.e. $dx = 3\text{km}$ and $dt = 15\text{s}$). This choice achieves a trade-off between maximizing quality (i.e. select the resolution/domain size as high/large as possible) for the domain and the cost of computation (Giorgi and Mearns, 1999). These domains are run independently and forced

by EUR-11's results, which are prepared for WRF to read by the `ndown.exe` program. All physic parameters, map projection, number of vertical levels and time of updating boundary in these nested domains remain the same as the EUR-11 domain except that either cumulus parameterization or spectral nudging are switched off. Three out of four CPS including WRF-01, WRF-02 and WRF-03 (see Figure 11 and Table 7) have the same size of 301 by 301 grid points but they are located at different places. The WRF-01, whose center of the domain located roughly over the country of Andorra, covers a part of the north-western Mediterranean Sea and a small part of the eastern Atlantic. The WRF-02 moves north-eastward from WRF-01 and covers mainly continent and the western part of the Alps. The WRF-03 moves south-eastward from the WRF-01 and therefore it contains a larger part of the Mediterranean Sea including Corsica. This helps in evaluating the effect of position of the domain and the presence of the Mediterranean Sea in the domain in reproducing heavy rainfall events in the Cévennes mountain range. The last nested domain (i.e. WRF-003) has a smaller size of 201 by 201 grid points which helps investigating how size of domain affects simulation of extreme rainfall events.

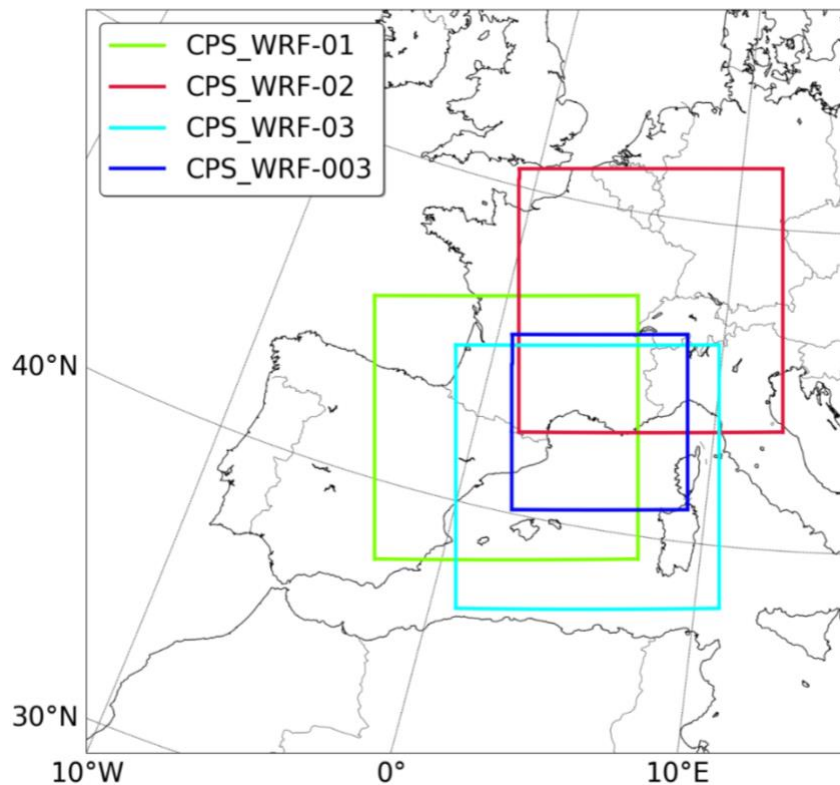


Figure 11. Location of four CPS domains.

Table 7. Description of the four nested domains

No.	Label	No. of grid points	i_parent_start	j_parent_start
1	WRF-01	301x301	150	155

No.	Label	No. of grid points	i_parent_start	j_parent_start
2	WRF-02	301x301	191	191
3	WRF-03	301x301	173	141
4	WRF-003	201x201	189	169

3.2.3. Observations data

Daily rainfall and daily maximum 3-hourly rainfall datasets at stations are used to evaluate the simulations from the four CPS domains. The two datasets provided by the METEO-FRANCE cover the coastal area in the South of France and include different number of stations and different lengths. The daily data starts from 1950 at several stations and 1961 at a few stations. This dataset spans until 2014. Meanwhile, the 3-hourly data starts in range of 1982 to 1998 depending on stations and lasts until 2018. The detail of all stations is given in Figure 12 and the table in Supplementary. In addition to in-situ observations, the high-resolution analysis of precipitation over France named SAFRAN (Quintana-Seguí et al., 2008; Vidal et al., 2010) is also used for model assessment. The data is gridded in 8x8 km and interpolated to 1-hour interval for the period of 1958 – 2018. However, in this chapter, I use only the data of three months in the autumn in 2014 for both in-situ observations and SAFRAN. In this chapter, I use only the data of three months in the autumn in 2014 for evaluation.

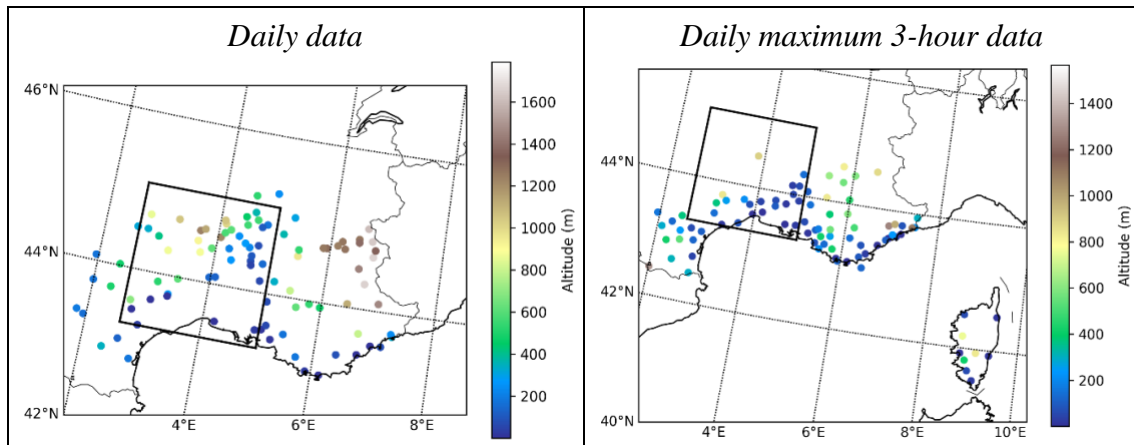


Figure 12. Spatial distribution of stations for daily data and 3-hourly data and their elevation. The black rectangular box covers the Cévennes mountain range and is defined by the minimum and maximum of longitude and latitude among 14 stations used in Luu et al. (2018).

3.2.4. The description of autumn 2014 rainy season over the Cévennes

Figure 13 shows the evolution of daily rainfall in the autumn 2014 for Cévennes mountain range. The daily boxplots are created from pooling 14 stations (Vautard et al.,

2015) over Cévennes mountain range. Figure 13 shows that rainfall occurred over a half of the season with three principal heavy rainfall events with maximum values of at least one among 14 stations exceeding 150mm per day. The first event started in September 15th of 2014 and terminated in September 20th of 2014 and the maximum value was 320mm/day. The second event lasted from the 6th October 2014 to the 15th October 2014 with its maximum value of 193 mm/day. The last went from the 1st to the 5th November 2014 with the peak value of 220 mm/day.

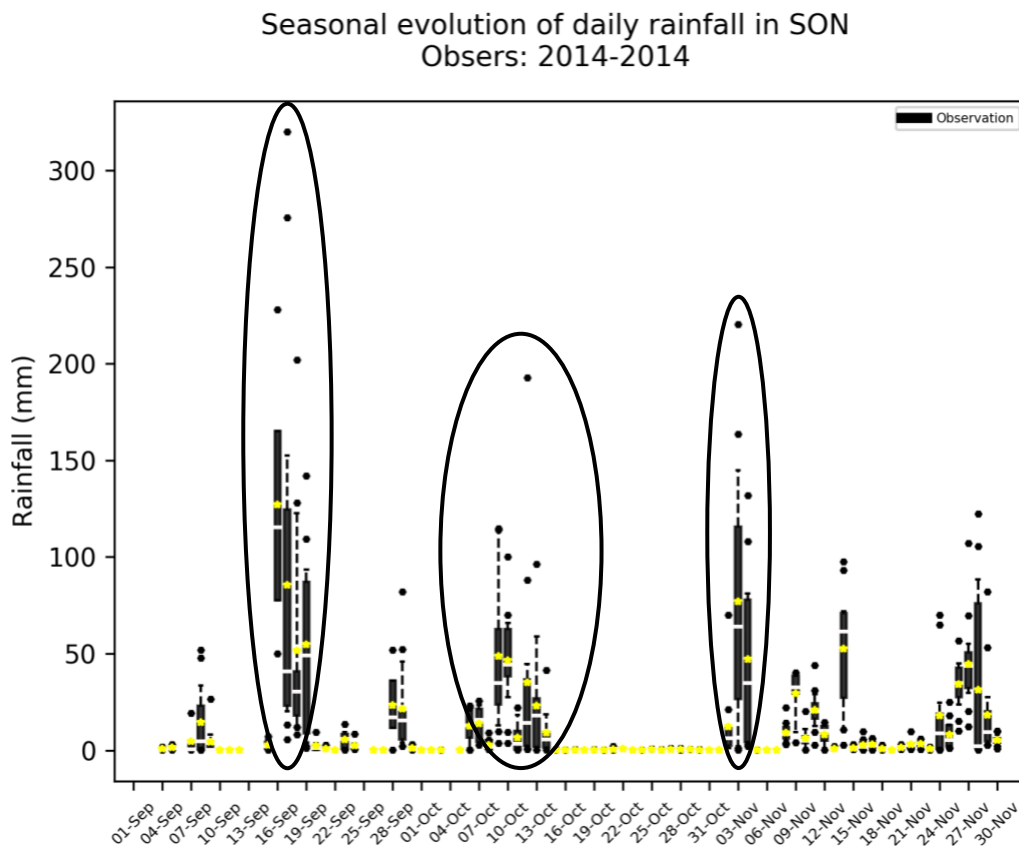


Figure 13. Time Series of daily rainfall of Cévennes mountain range in the autumn of 2014; the boxplots show the range of data from the 1st to 3rd quartile of 14 stations pooling, the cap shows the 10th and 90th percentile, the white line and the yellow star in the middle of each box are the median and mean, respectively and the rest are outliers.

For the event in September (see Figure 14), heavy rainfall started on the 16th with the maximum amount of 228 mm/per in the south upwind side of Cévennes mountain range. On the 17th, the convective system moved northward along the mountain leading to highest amount of rainfall of 320 mm/day in the middle of the range. The convective system kept moving northward on the 18th September. The amount of rainfall from 250mm to 350mm/day was observed at some stations and the peak was 362 mm/day. On the 19th, the convective system stayed over the middle of upwind side of Cévennes mountain range. The highest daily rainfall amount observed in that area was 142 mm/day.

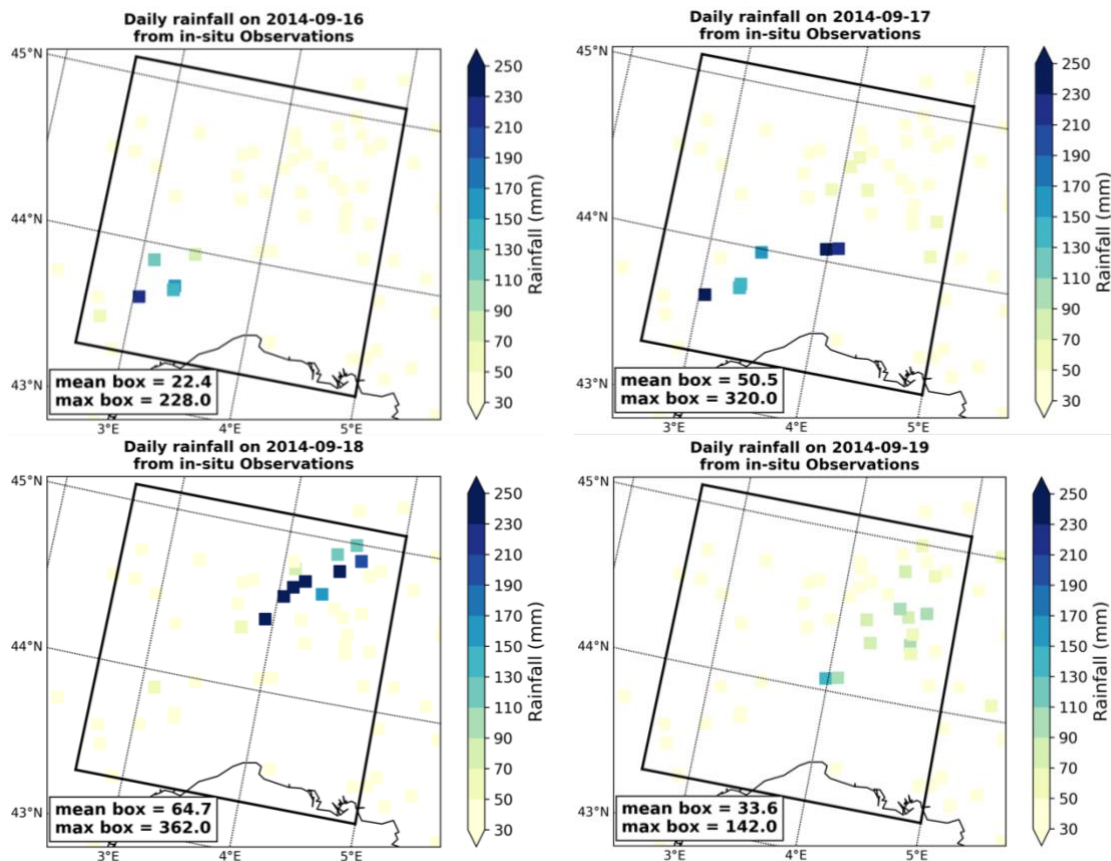
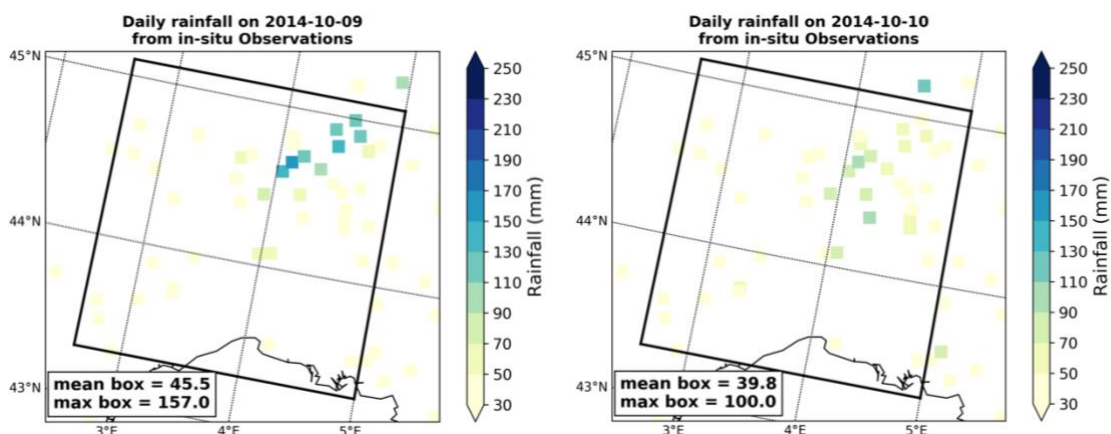


Figure 14. Daily amount of rainfall of the events occurring in September

Figure 15 shows the evolution of daily rainfall of a few principal rainy days during the second event in October. Heavy rainfall started on the 9th of October over the north part the mountain. The heaviest amount observed was 157 mm/day. In the next day, the convective system remained at the same place and produced rainfall amount from 80 to 100mm/day at some stations. The peak value of daily rainfall during this event was observed on the 12th October with the value of 316 mm/day over the same place as previous days. The convective system tended to stay over that area in the next day and generated rainfall amount from 60 to 100 mm/day in a few stations.



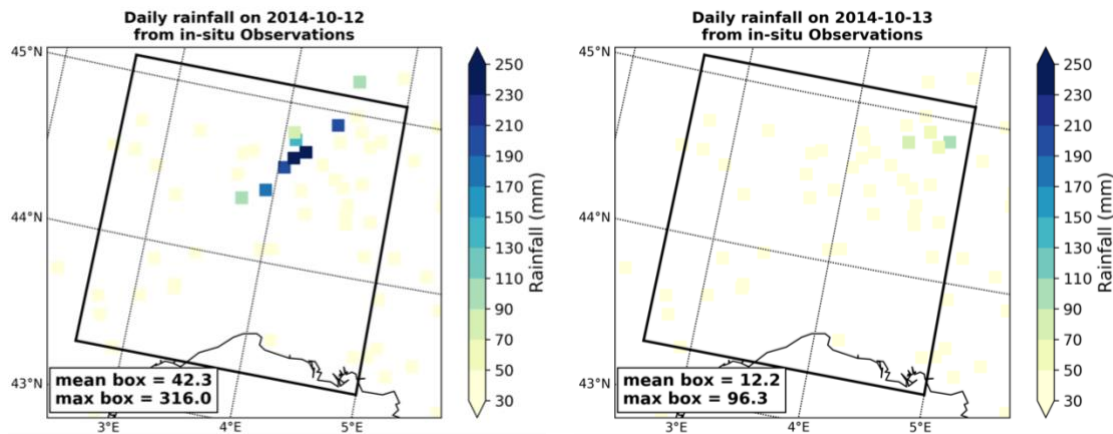
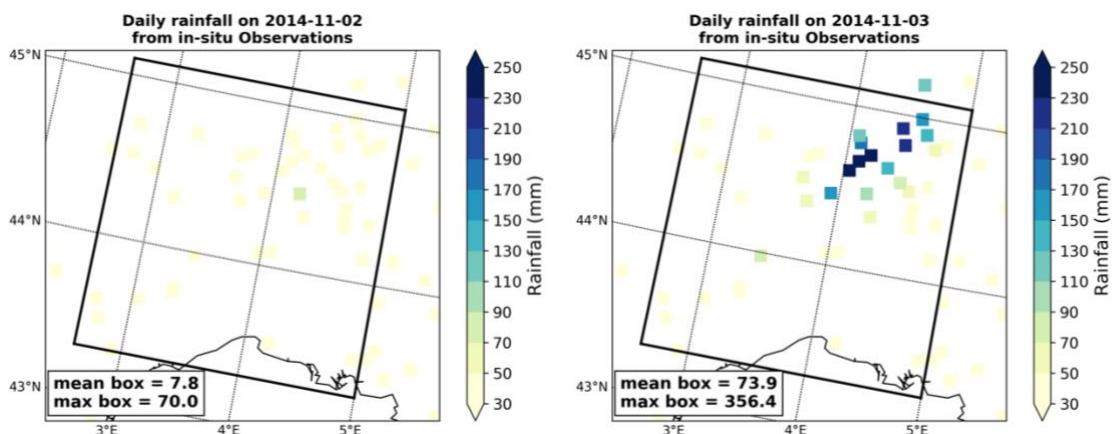


Figure 15. Daily amount of rainfall of the events occurring in October

The behavior of daily rainfall during the last event (Figure 16) was roughly the same as the second event. The convective system mainly stayed over the north part of the Cévennes mountain range. Heavy rainfall started on the 2nd November with the highest value at a station of 70 mm/day. The peak of this event occurred on the 3rd of November. An amount of 356 mm/day was observed at a station closed to the highest station in previous day. In addition, there were several stations whose observed values exceeded 100 mm/day. On the 4th of November, the convective system tended to move eastward into the Alps. However, heavy rainfall with the amount over 100mm/day was still observed at a few stations on the upwind side of Cévennes range.



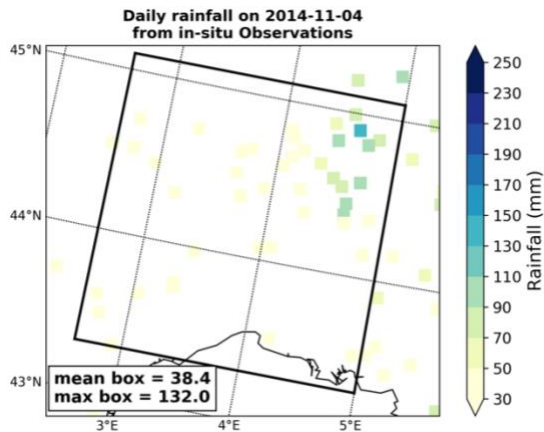


Figure 16. Daily amount of rainfall of the events occurring in November

3.3. Results and discussion

In this section, I propose a matrix of six rainfall indices to evaluate the simulations from four different nested domains against in situ observations and SAFRAN dataset for the autumn 2014. These indices are maximum daily rainfall in the autumn of 2014 (Rx1day), maximum 3-hourly rainfall in the autumn of 2014 (Rx3hour), total rainfall of the autumn 2014 (R_Total), daily rainfall for a specific day (R_daily), daily maximum 3-hourly rainfall for a specific day (Rx3hr_daily) and exceedance probability distribution of daily wet events (Prob_daily). The detail of each index is given on Table 8. It has to be noted that for two indices with 3-hourly rainfall, only heavy rainfall events happening in the southern part of Cévennes mountain range is considered because of the availability of the stations (i.e. there is no station on the northern part of the mountain that is collected). The analyses of those 3-hourly rainfall are not performed by SAFRAN because hourly rainfall from this dataset was interpolated from daily data based on analyzed hourly specific humidity and other factors (Vidal et al., 2010), therefore does not show a sufficient quality. Besides, to serve the evaluation, a Cévennes box is defined based on the maximum and minimum of the latitudes and longitudes of the 14 stations used in Vautard et al. (2015). Roughly, this box is confined from 2.6°E to 5°E and from 43.3°N to 45.1°N.

The western Mediterranean (e.g. south of France) is always exposed to heavy rainfall events in the autumn because several meteorological conditions that facilitate the forming of mesoscale convective systems can occur at the same time. These conditions contain: i) warm sea surface temperature supporting the swap of heat and moist processes between the sea and the atmosphere above; ii) a synoptic-scale trough in vicinity (i.e. to the west of the area) producing southeastern flows toward the threat area; iii) steep-high

mountainous range which is normal to the impinging moist air mass brought by the southeastern flows (Nuissier et al., 2008). Because the first condition is obvious in all simulations and the third condition is a natural feature that can be well represented in high-resolution models, in this section, I will focus on investigating the second factor from all simulations and comparing them against ERA5 data. The moist flow moving forward the Cévennes is estimated using method in Lélé et al. (2015):

$$\vec{Q} = -\frac{1}{g} \int_{ps}^{pu} \overline{q\vec{U}} dp$$

In this equation, \vec{Q} is the zonal and meridional moisture transport vector ($\text{kg}\cdot\text{m}^{-1}\cdot\text{s}^{-1}$), g denotes the standard gravitational acceleration at mean sea level ($9.81 \text{ m}\cdot\text{s}^{-2}$), q is specific humidity (kg/kg), \vec{U} is zonal and meridional wind vector ($\text{m}\cdot\text{s}^{-1}$), ps and pu are surface and upper pressure level. In this case, I selected 1000 mb and 700 mb, respectively.

Table 8. Description of all indices used for model evaluation

No.	Index	Description
1	Rx1day	Maximum daily rainfall at each station or grid point over the autumn 2014
2	Rx3hour	Maximum 3-hourly rainfall at each station or grid point over the autumn 2014
3	R_daily	Daily rainfall at each station or grid point for a specific day/event
4	R_Total	Accumulated rainfall of the autumn 2014 at each station or grid point
5	Rx3hr_daily	Daily maximum 3-hourly rainfall at each station or grid point for a specific day/event
6	Prob_daily	Exceedance Probability distribution of wet daily events from stations pooling (14 stations used in Vautard et al. (2015)) dataset. Wet daily event is defined by the amount exceeding 0.1mm/day
7	Moisture flux	Zonal and meridional moisture transport vector estimated from horizontal wind vectors and specific humidity

3.3.1. Seasonal maximum daily rainfall (Rx1day)

Figure 17 shows the maximum daily rainfall of the autumn 2014 from observations at stations, SAFRAN and all CPS simulations. In general, all CPS simulations (Figure 17a-d) perform a good agreement with observations in terms of spatial distribution of extreme values. The most extreme value occurs in the north upwind side of the Cévennes range, meanwhile the less heavy (but still extreme) precipitation occurs in the south of the mountain. However, all simulations underestimate the observed maximum values. The WRF-003 reproduces the intensity of Rx1day most closely to observations with the mean absolute bias of all stations within the Cévennes box of 39% (Figure 18). The WRF-03 and WRF-003 are the two cases that are able to reproduce 6

stations within the box with rainfall amount higher than 200 mm per day (compared to 8 stations from observations) even though their intensities are lower than those from observations and the places of occurrence are different from observations (Figure 18). The SAFRAN is also slightly lower than the in-situ observations (Figure 17). This difference can come from the optimal interpolation method or the lack of station contributing to the interpolation process (i.e. the station observing the heaviest rainfall value was not taken into account during the interpolation procedure).

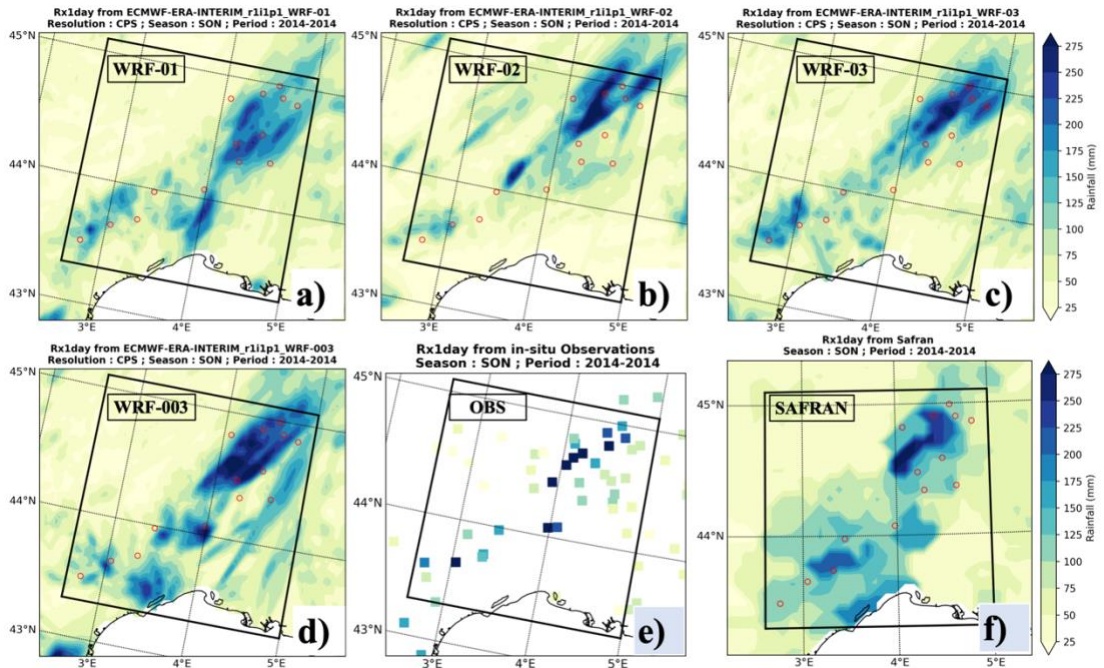


Figure 17. Rx1day from in-situ observations and four CPS simulations for the autumn of 2014 focusing on the Cévennes area. The red-empty circles in each panel from a to d and f denote 14 stations within the Cévennes box.

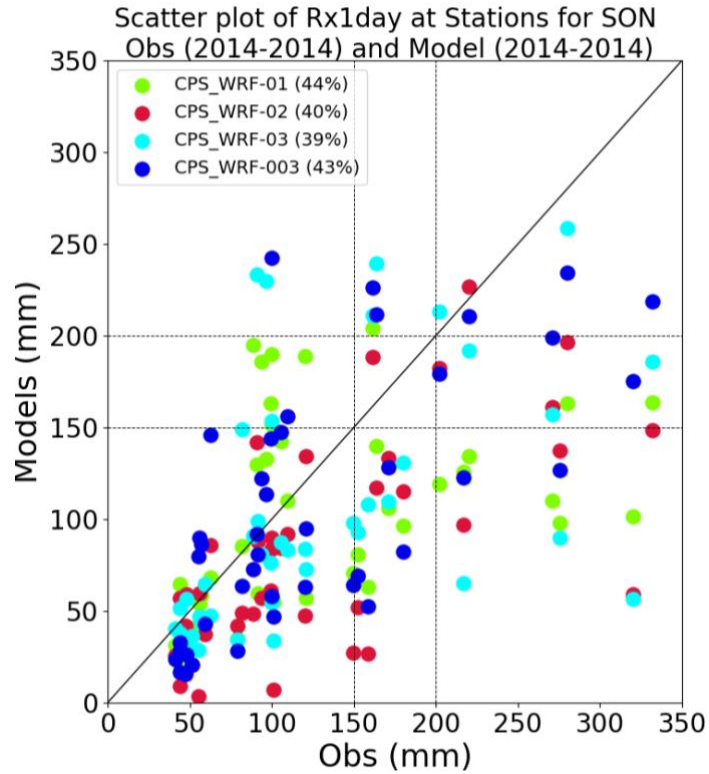


Figure 18. Comparison of Rx1day at all stations within the Cévennes box between CPS simulations and Observations; Dots denote different stations and colors denote different simulations. The numbers on the legend show the mean bias among all stations within the Cévennes box from simulations against in-situ observations.

3.3.2. Seasonal maximum 3-hourly rainfall (Rx3hour)

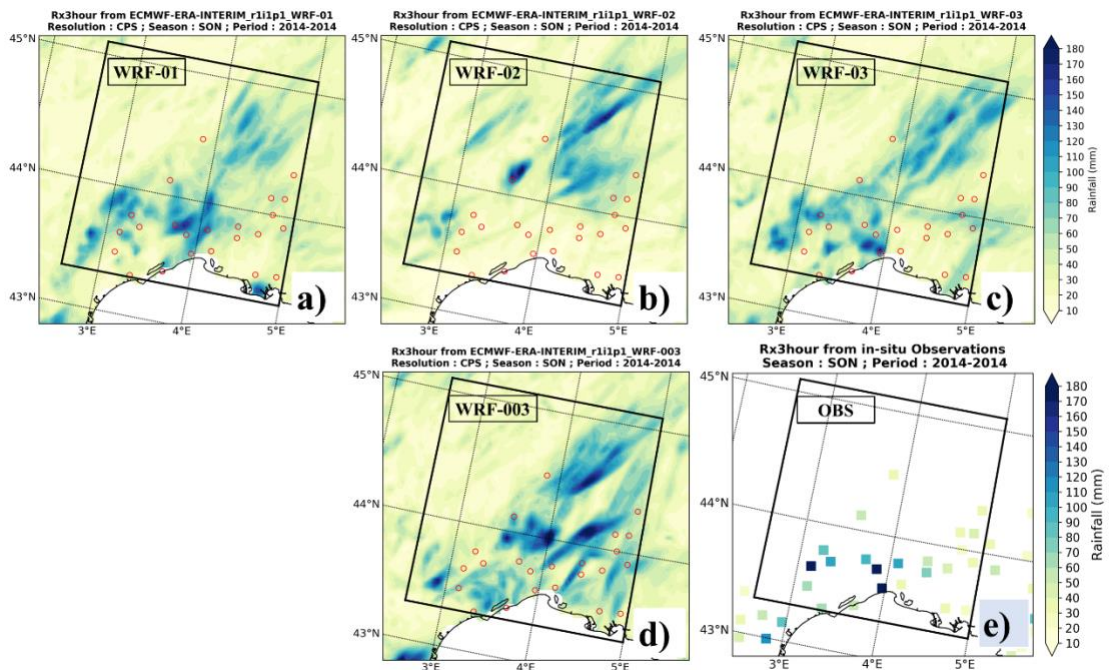


Figure 19. Rx3hour from in-situ observations and four CPS simulations for the autumn of 2014 focusing on the Cévennes area. The red-empty circles in each panel from a to d denote 23 stations within the Cévennes box.

The maximum 3-hour rainfall in the autumn of 2014 from in-situ observations and CPS simulations are shown in Figure 19. The coverage of stations with availability of hourly data over the Cévennes mountain range is restricted to the southern part. Therefore, I only focus on the evaluation for Rx3hour in the southern part of the mountain (i.e. from the latitude of 44°N to the south). Figure 19 shows that Rx3hours at some observed stations in the southern part of the Cévennes and near the coast exceed 180 mm with the maximum value of 252 mm in 3-hour. The WRF-01 and WRF-03 reproduce well this spatial distribution of Rx3hour, but underestimate with their mean absolute bias of all stations within the Cévennes box of 32% and 53%, respectively (Figure 20). The WRF-02 and WRF-003 tend to show more intensified rainfall over the middle and the northern part of the Cévennes. The mean absolute bias of stations from these two cases are 68% and 53%, respectively (Figure 20).

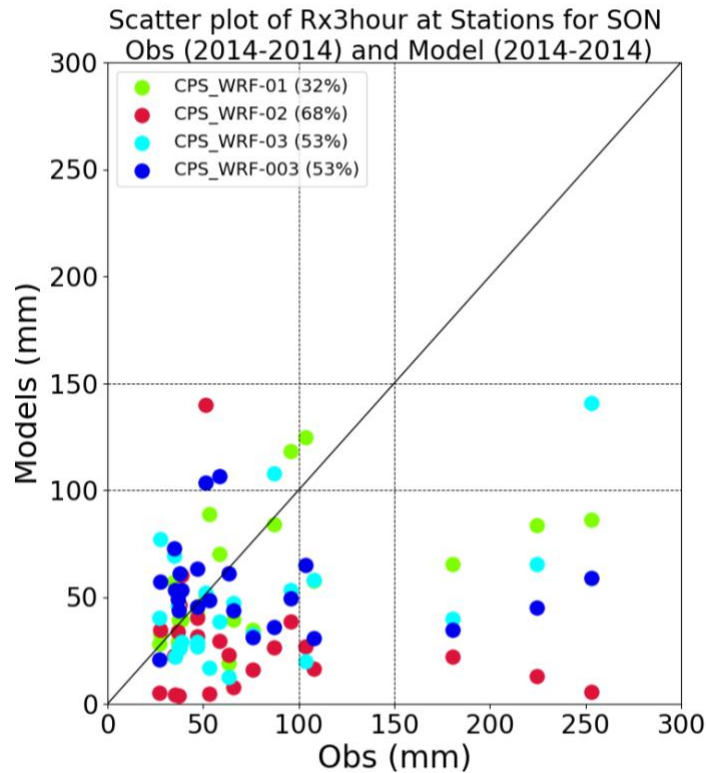


Figure 20. Comparison of Rx3hour at all stations within the Cévennes box between CPS simulations and Observations; Dots denote different stations and colors denote different simulations. The numbers on the legend show the mean bias among all stations within the Cévennes box from simulations against in-situ observations.

3.3.3. Seasonal total rainfall (R_{Total})

Figure 21 shows the accumulated rainfall in three months from observations, SAFRAN and all simulations. The observations indicate that large amount of monthly accumulated rainfall extends over from the north to the south of the Cévennes range (i.e.

the diagonal line of the Cévennes box). The highest total amount of rainfall is observed in the northern part of the mountain. The peak value is over 2000 mm/month and a few stations have the monthly amount ranging from 1500 to 2000mm. Meanwhile in the southern part, accumulated rainfall ranges from a few hundreds to 1000 mm. This spatial coverage feature is well reproduced by all CPS simulations. However, the amount of total rainfall from these simulations are lower than both in situ observations and SAFRAN data. The mean absolute biases of all stations within the Cévennes box from WRF-01, WRF-02, WRF-03 and WRF-003 are 33%, 50%, 35% and 39%, respectively (Figure 22). The SAFRAN appears to show overestimation of the peak value.

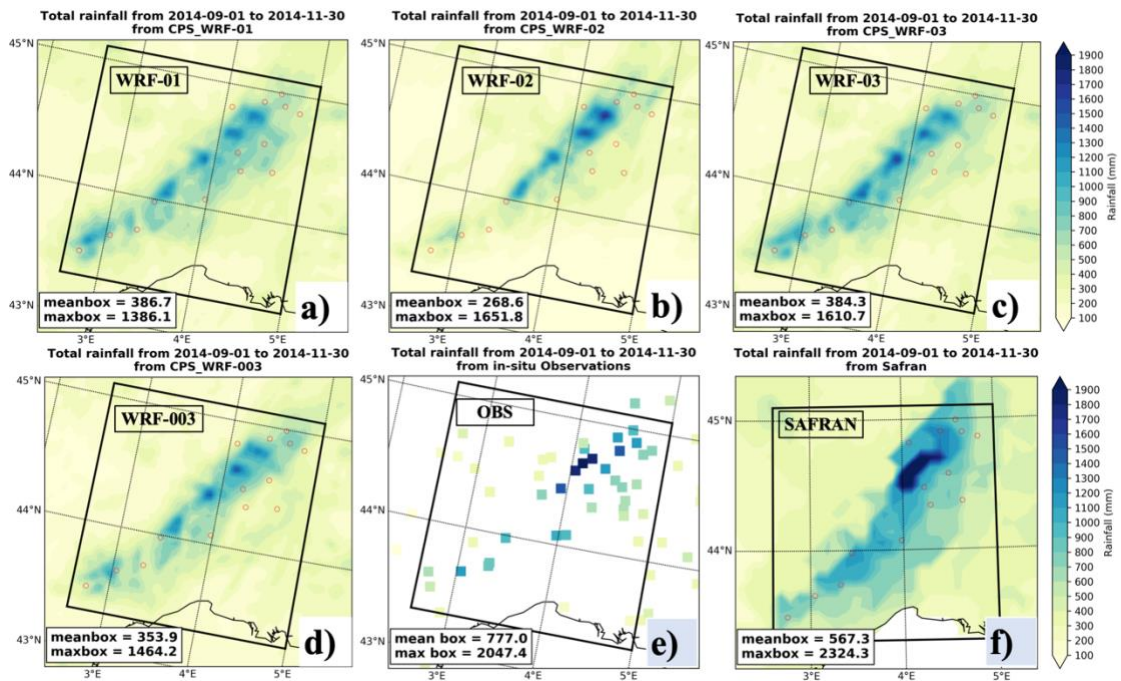


Figure 21. R_{Total} from in-situ observations, SAFRAN dataset and four CPS simulations for the autumn of 2014 focusing on the Cévennes area. The red-empty circles in each panel from a to d and f denote 23 stations within the Cévennes box.

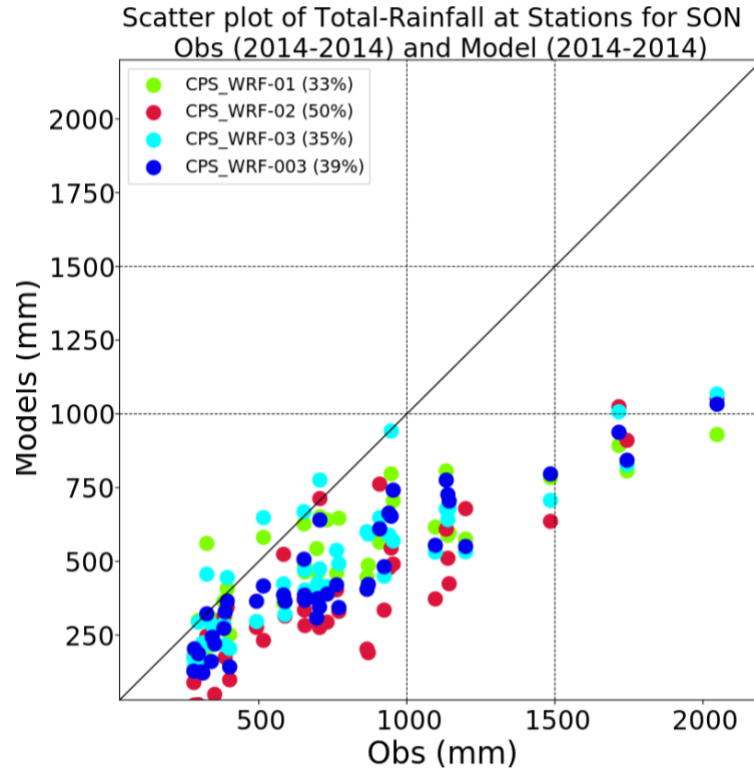


Figure 22. Comparison of R_{Total} at all stations within the Cévennes box between CPS simulations and Observations; Dots denote different stations and colors denote different simulations. The numbers on the legend show the mean bias among all stations within the Cévennes box from simulations against in-situ observations.

3.3.4. Daily rainfall (R_{daily})

In this part, I will focus on the heaviest rainy days of the three events occurring in the autumn 2014. This will help in assessing the ability of models in re-generating heavy rainfall correctly in places, time of occurrence and intensity. The heavy rainfall events were observed mainly on three days including 16th, 17th and 18th of September (Figure 14). In the first day, heavy rainfall occurred in the southern part of the Cévennes. In the next day, the convective system moved to the middle part of the mountain. In the last day, it occurred over the northern part. The peak of this event was observed on the 18th with the value of 362 mm in the northern part of the Cévennes. SAFRAN data underestimates this value and is not able to represent heavy rainfall on the 16th (Figure 23). For CPS simulations, they are not able to reproduce heavy rainfall on the 16th and the 19th of September. The WRF-01, WRF-03 and WRF-003 shows the same distribution that heavy rainfall is mainly reproduced on two days of 17th and 18th of September. Heavy rainfall is distributed in the southern part of the Cévennes (from the latitude of 44°N to the south) on the 17th and around the 44°N on the 18th. The WRF-02 can only reproduce heavy rainfall on the 18th, however, the place of occurrence is also over the 44°N rather than

over the north part of the Cévennes as shown in observations and SAFRAN. In terms of rainfall intensity, all CPS simulations show underestimation. The WRF-01 and WRF-03 reproduce better the peak of rainfall on the 17th than other simulations. The maximum intensity on the 18th produced by WRF-02 and WRF-003 is closer to observations than others (Figure 23).

For the event in the middle of October, heavy rainfall occurs mainly on four days including the 9th, 10th, 12th and 13th (as shown in Figure 15 for the observations and Figure 24 for SAFRAN) and covers mainly the northern part of the Cévennes (from the latitude of 44°N to the north). The SAFRAN shows a good agreement with in-situ observations in most of the days except the peak event on the 12th of October. The maximum daily rainfall within the Cévennes box on this day from SAFRAN is only 186 mm, which is far from the value of 316 mm in Observations. All CPS simulations produce the heaviest rainfall on the 10th of October, which is two days earlier than observations (i.e. the peak is on the 12th). In addition, the place of occurrence of these events from all simulations is closed to what is observed. However, the rainfall intensity on the peak day of this event gives a large difference among simulations. The WRF-01 and WRF-03 underestimate the observations with their maximum values of 256 mm and 297 mm, respectively. The WRF-02 and WRF-003 tend to intensify the rainfall amounts, which are 369 mm for the former simulations and 336 mm for the latter (Figure 24).

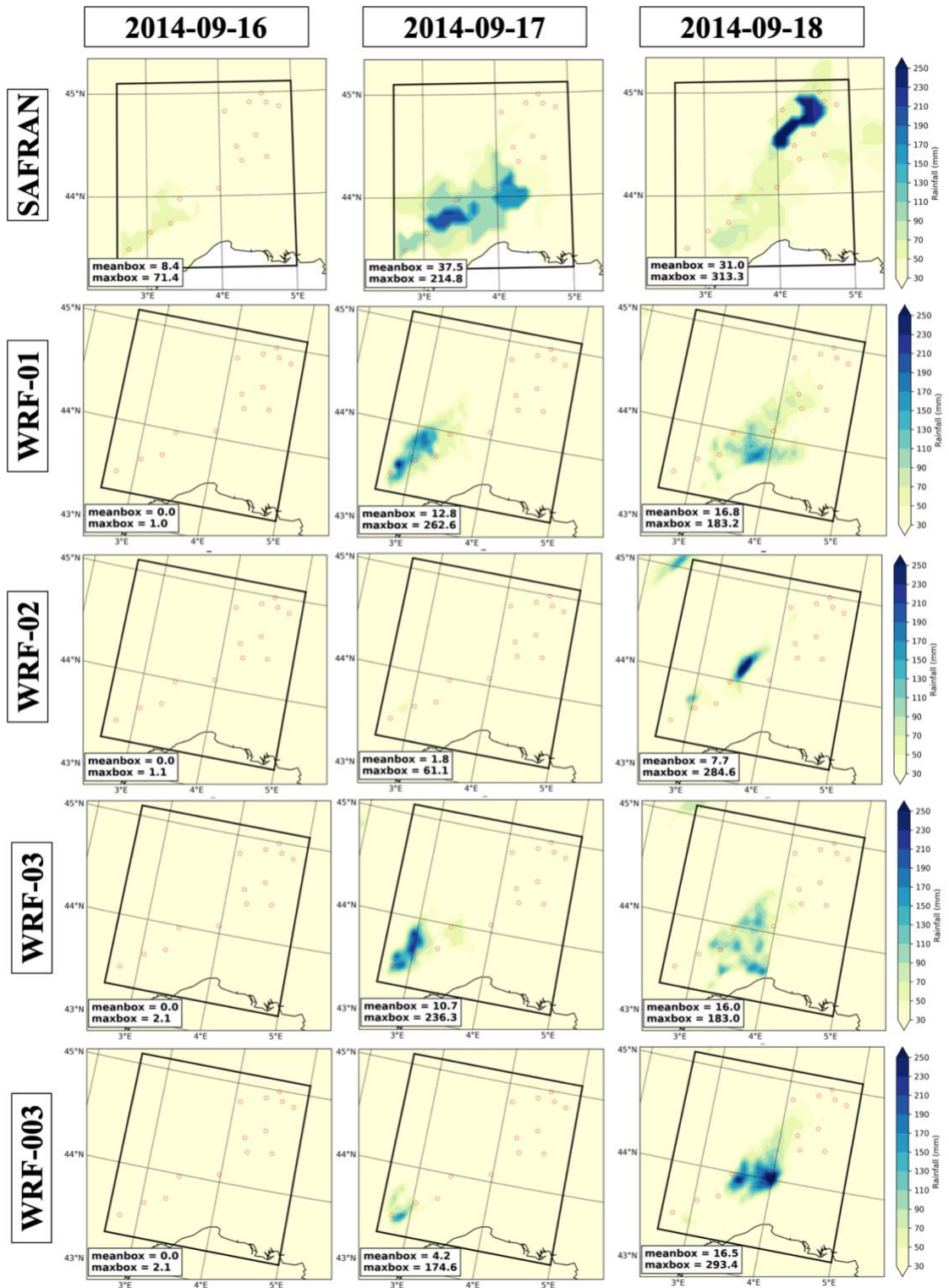
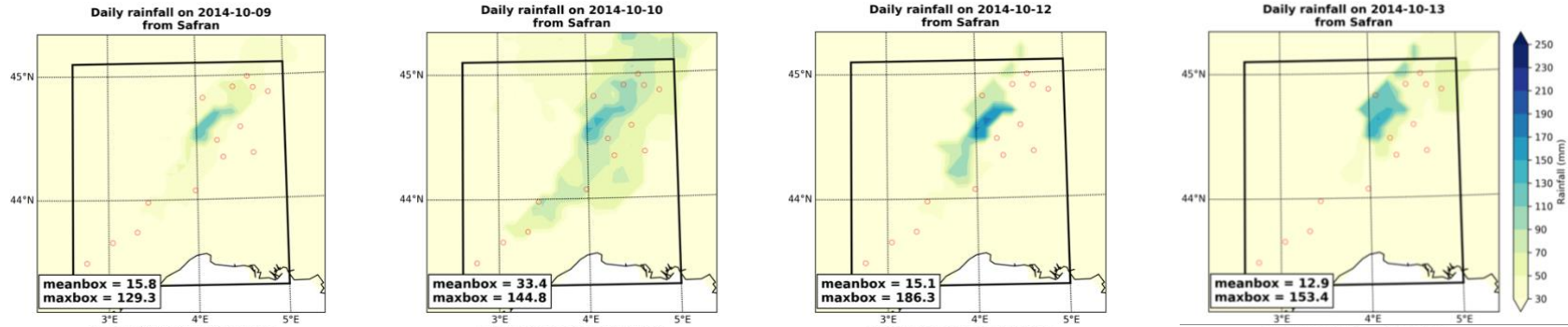
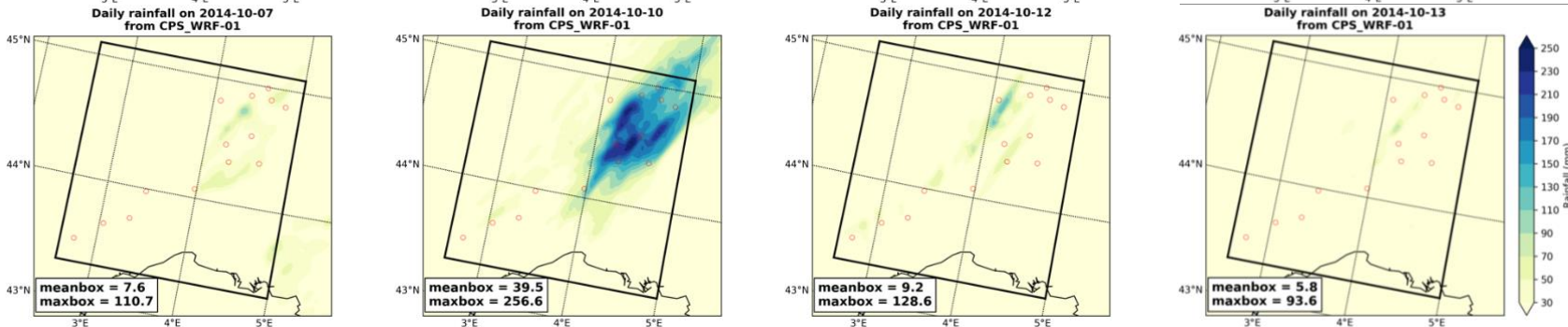


Figure 23. R_{daily} from SAFRAN and CPS simulations for the 16th, 17th and 18th of September; different days are shown in different columns; SAFRAN and different CPS simulations are shown in different rows

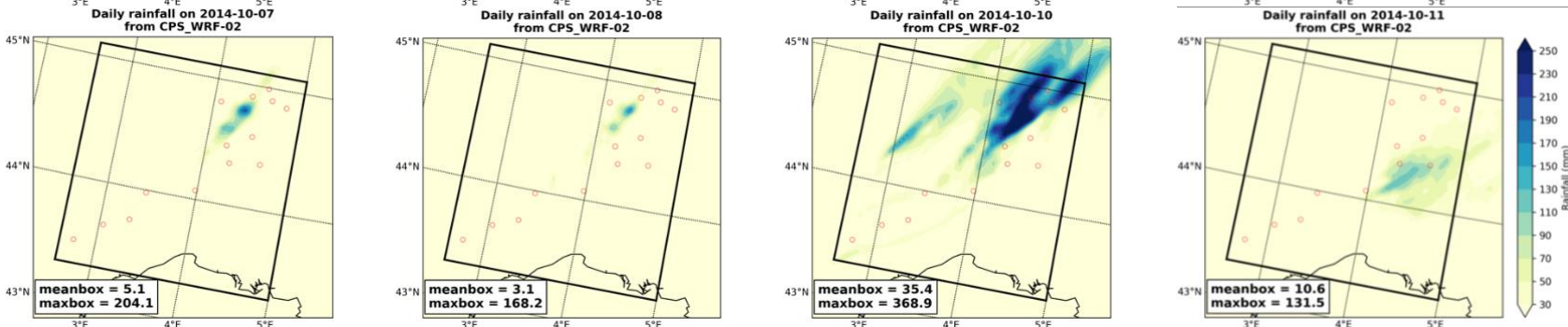
SAFRAN



WRF-01



WRF-02



WRF-03

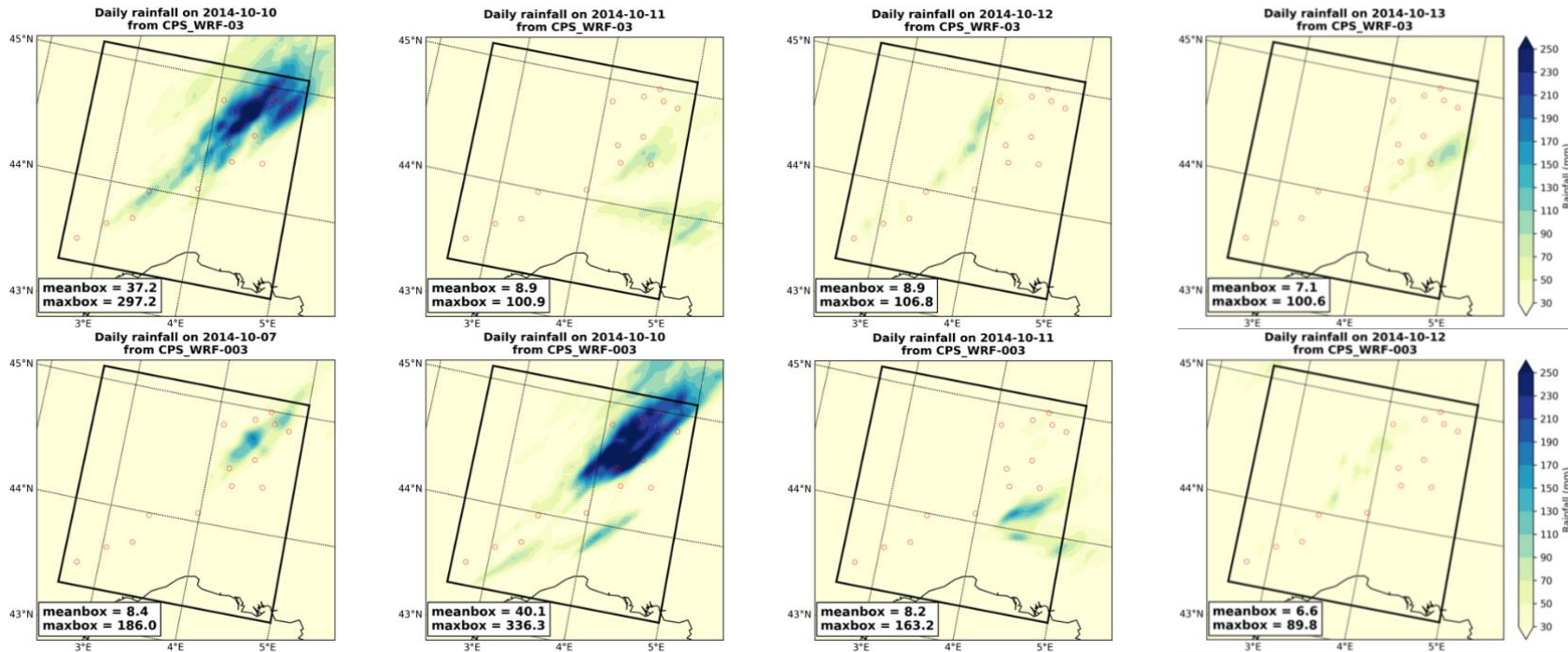
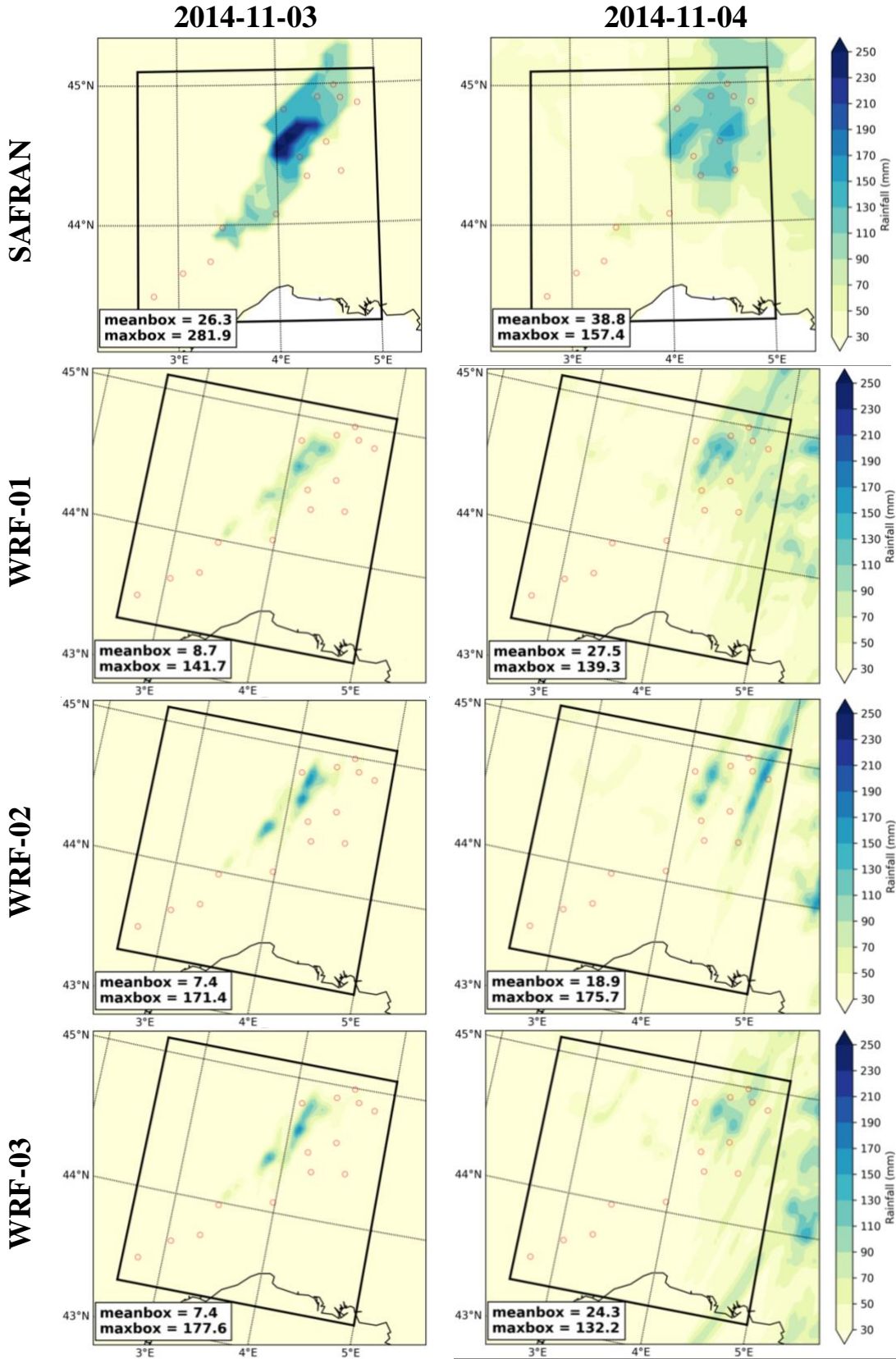


Figure 24. *R_daily* from SAFRAN and CPS simulations for the event in October; different days are shown in different columns; SAFRAN and different CPS simulations are shown in different rows



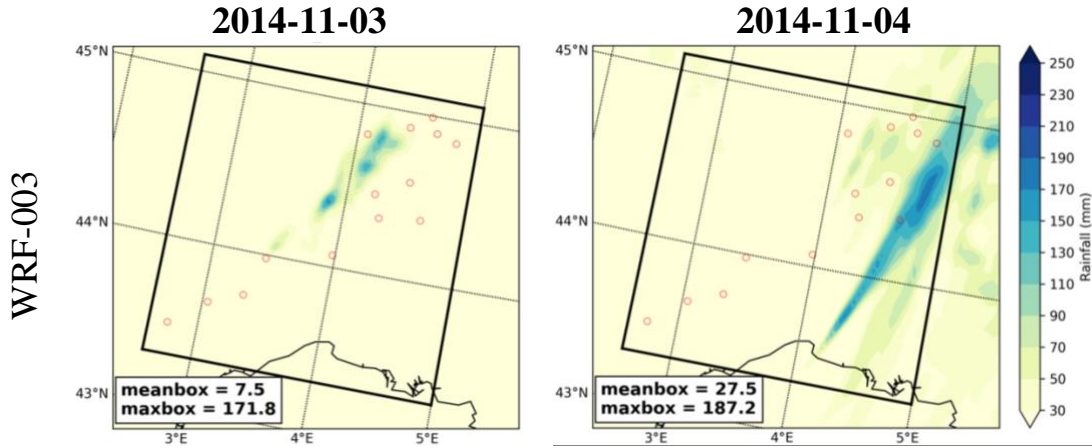


Figure 25. R_daily from SAFRAN and CPS simulations for the event in November; different days are shown in different columns; SAFRAN and different CPS simulations are shown in different rows

For the event in the beginning of November (Figure 25), there is a consensus among observations, SAFRAN and simulations from nested domains that heavy rainfall occurs on two days including the 3rd and 4th of November. In addition, the torrential rainfall occurs only over the northern part of the Cévennes. On the 3rd of November, the WRF-02, WRF-03 and WRF-003 show the same highest amounts of rainfall ranging from 170 mm to 180 mm and they are a half of what is observed at stations. The peak value from WRF-01 on this day is lower than other nested domains. The maximum value from SAFRAN, which is 282 mm, is also underestimated the in-situ observations. On the 4th of November, the peaks amount of rainfall reproduced by WRF-01 and WRF-03 (around 130 mm) are in good agreement with the observations (132 mm), meanwhile the results from WRF-02 (175 mm) and WRF-003 (187 mm) are overestimated. SAFRAN data also overestimates the peak value of in-situ observations.

3.3.5. Daily maximum 3-hourly rainfall ($Rx3hr_daily$)

In this part, I only focus on the extreme rainfall event happening in the 17th of September because this event occurred over the southern part of the Cévennes where hourly in-situ observations are available. Most CPS simulations reproduce amount of the peak intensity closely to observations on the 17th of September. These values are 160 mm, 144 mm and 177 mm for WRF-01, WRF-03 and WRF-003 respectively, which are comparable to 180 mm from observations (except the WRF-02 with its peak value of 117 mm). However, the WRF-01 and WRF-03 show a better coverage of extreme rainfall area over the southern part of the Cévennes and along the 44°N latitude than what is reproduced by the WRF-003 (Figure 26).

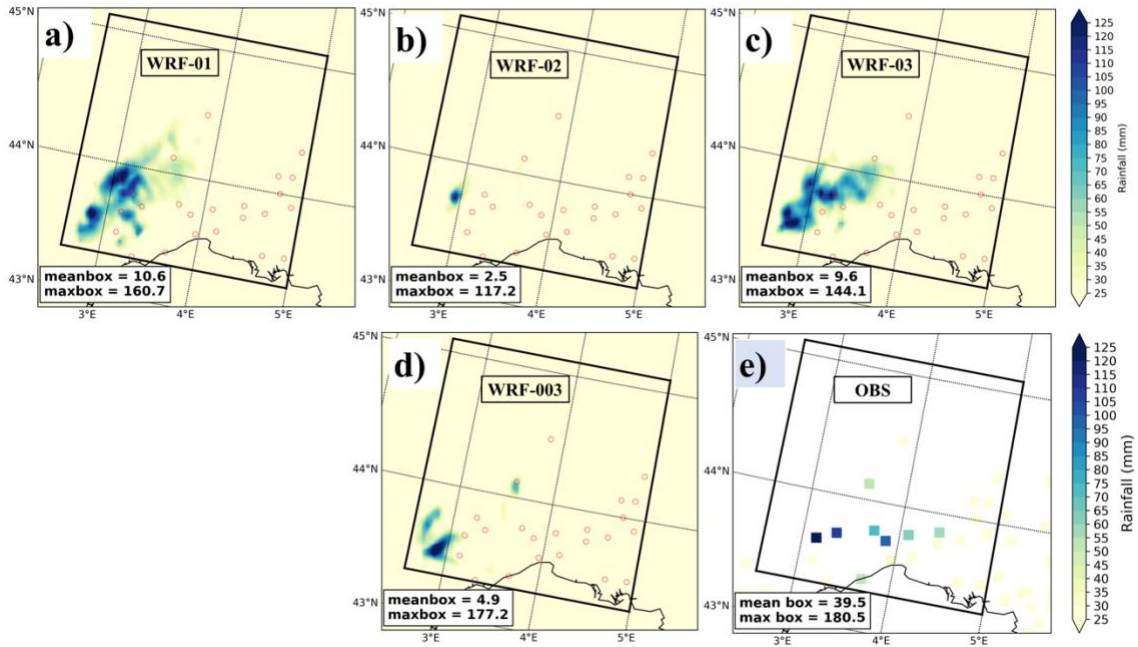


Figure 26. *Rx3hr_daily* from observations and simulations for the 17th of September
3.3.6. Distribution of wet daily event (*Prob_daily*)

Figure 27 shows the comparison of CPS simulations and observations in terms of distributions of pooling 14 stations as used in Vautard et al. (2015). The left panel (Figure 20a) shows the exceedance probability distributions of all simulations and observations. Those distributions are obtained by pooling all daily rainfall values higher than 1 mm from 14 stations. The right panel (Figure 27b) shows the boxplot of bias of 10% of values in the tail of each distribution against observations. In the boxplot, the box shows the range from the 1st to the 3rd quartile, the caps show the range for 10th and 90th percentile, the white line and the yellow star in the middle of the box are median and mean values, respectively. It can be inferred from Figure 27 that the distribution of wet daily events from the four CPS simulations are comparable to each other and underestimate wet daily events from observations in either the middle or the right tail of the distributions. To be more specific for the right tail of the distribution, the WRF-01, WRF-03 and WRF-003 reproduce extreme values closest to observations. Their mean and median biases ranged from -30% to -25%. The WRF-03 and WRF-01 seem to be the best case because their range of bias is the smallest. However, the box from WRF-03 is closer to 0 compared to the WRF-01. The WRF-02 underestimates the extreme from observations.

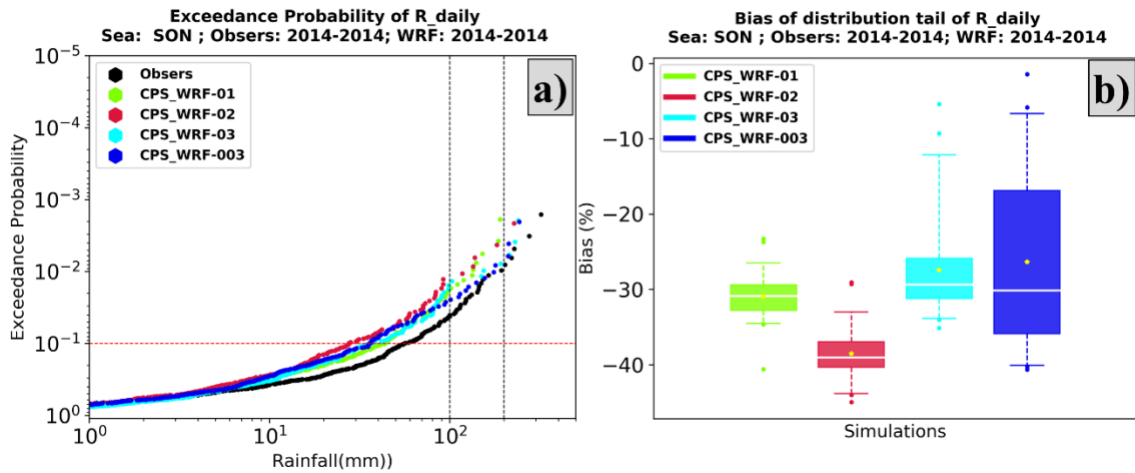


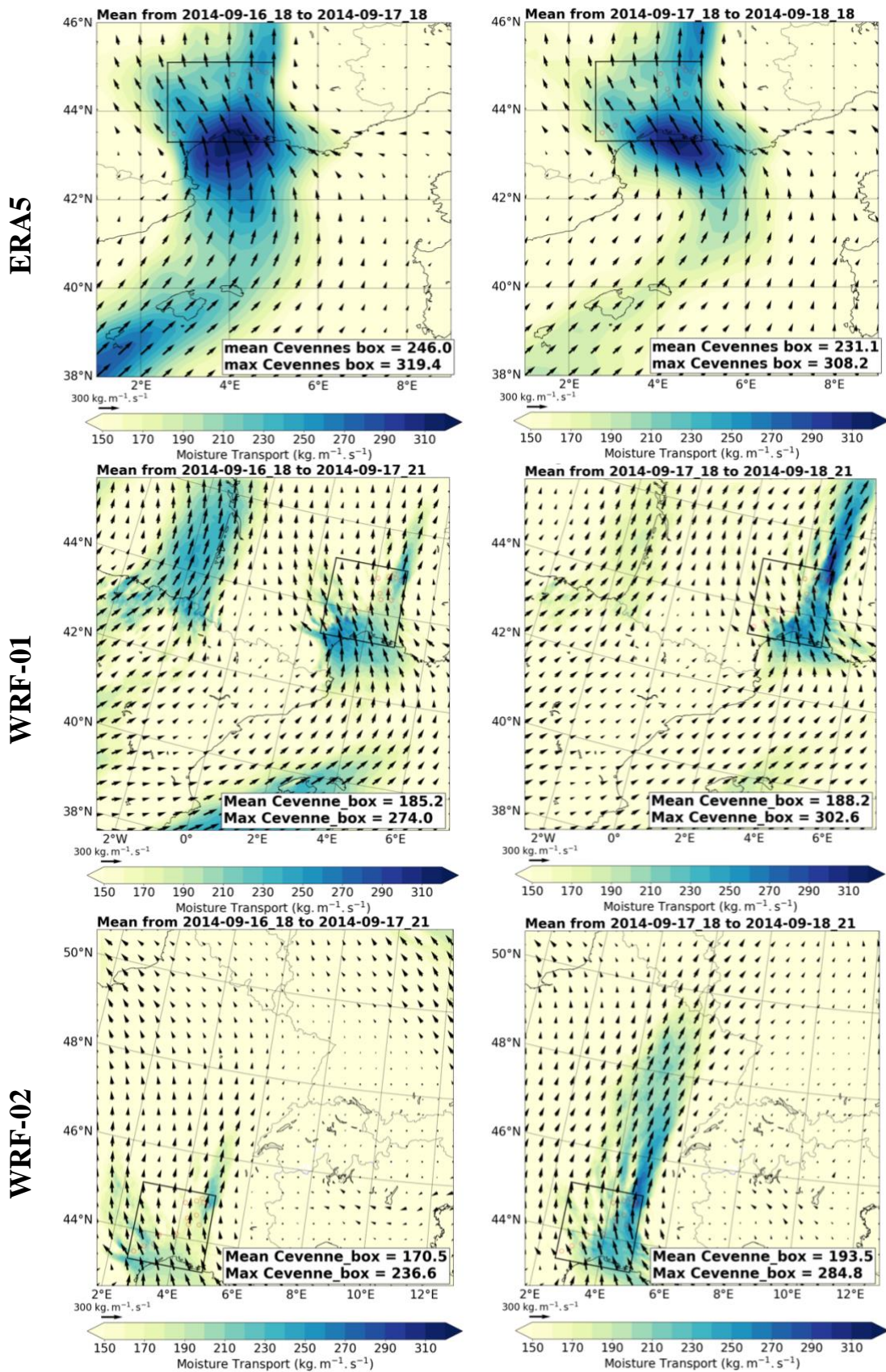
Figure 27. Comparison of distributions of daily wet events between observations and CPS simulations; Left panel is exceedance probability distributions; Right panel is box plot showing the bias of extreme value of wet daily events (>Percentile 90th) of each simulation against observations.

3.3.7. Moisture transport

This section investigates the moisture source impinging to the Cévennes in those three considered events by the method proposed in the beginning of section 3.3. The moisture transport is estimated every 3 hours for the simulations and every 6 hours for ERA5 reanalysis. Here I will show the mean moisture transport of the days when the highest extreme rainfall events are occurring over the Cévennes in each simulation or observations. This mean value is calculated for all time steps ranging from the 18Z of previous day to 18Z of the event's day for ERA5 (every 6 hours) and from the 18Z of previous day to 21Z of the event's day for simulations (every 3 hours).

The four CPSs can reproduce well the moisture transport from the Mediterranean moving toward the Cévennes mountain range in all three events. Figure 28 shows the moisture transport in two days including the 17th and 18th of September from ERA5 and all simulations because the two heaviest rainfall events in September occurring in those two days in observations and simulations. The results from ERA5 indicate that low-level moisture flow covers the whole Cévennes box and concentrates at the coastal area in the south of the mountain range on both two days. The moisture source coming to the area is underestimated on the 17th of September by the WRF-02 and WRF-003. On the next day, the moisture is intensified only on the right side of the Cévennes box by those two simulations. The WRF-01 and WRF-03 simulations seem to reproduce the best estimate of ERA5 even though the intense moisture does not cover the whole area as in ERA5.

However, these two cases tend to produce intensified moisture flow on the 18th (Figure 28).



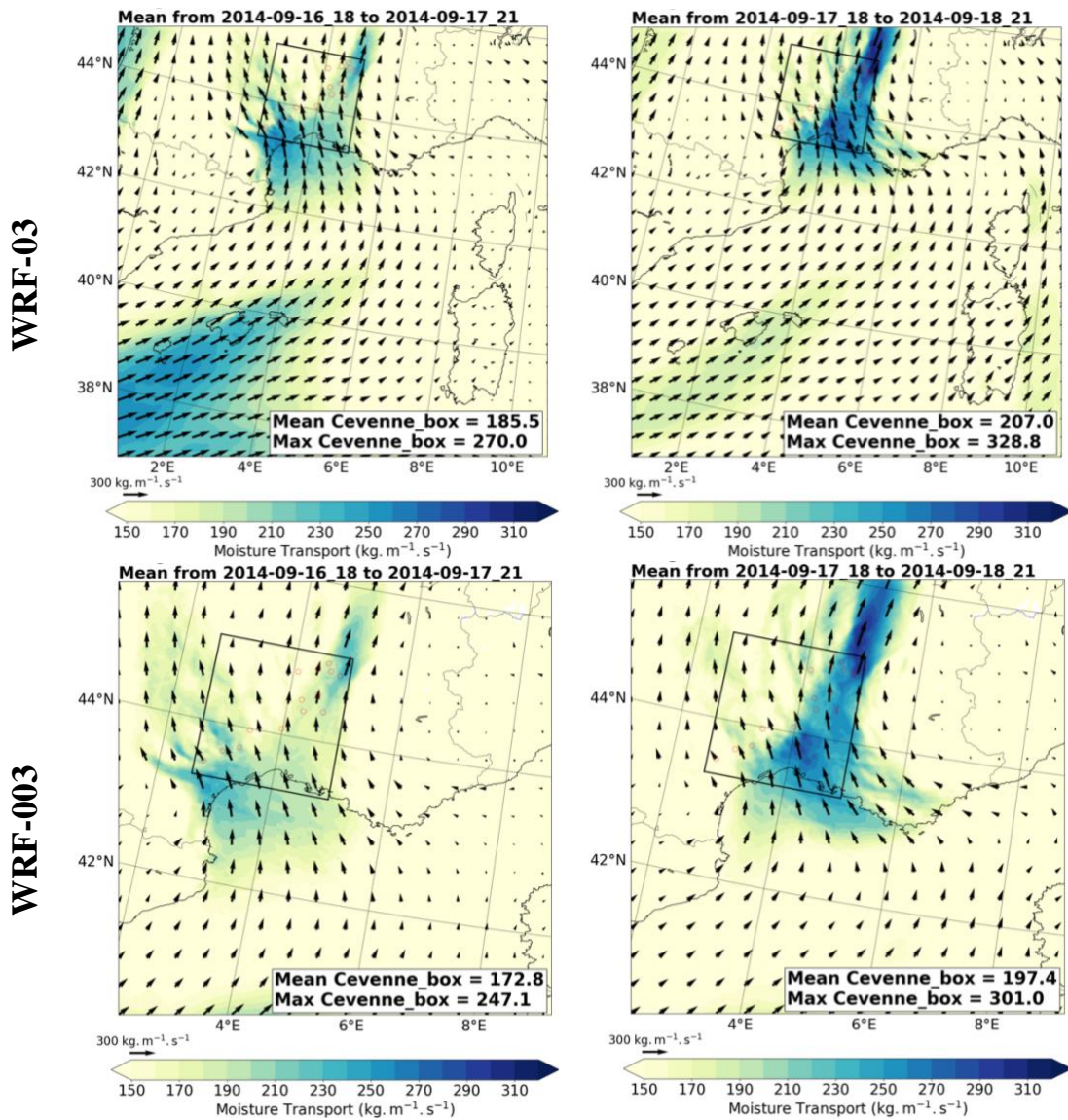
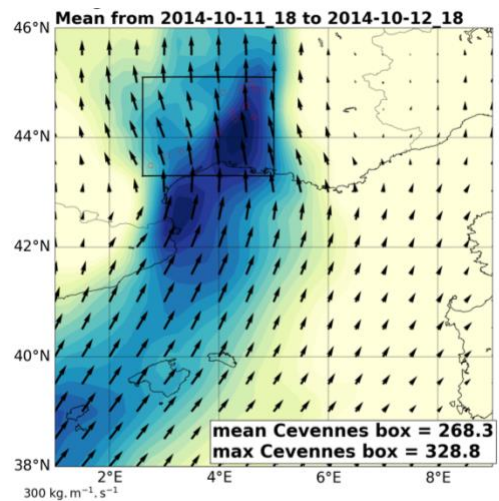
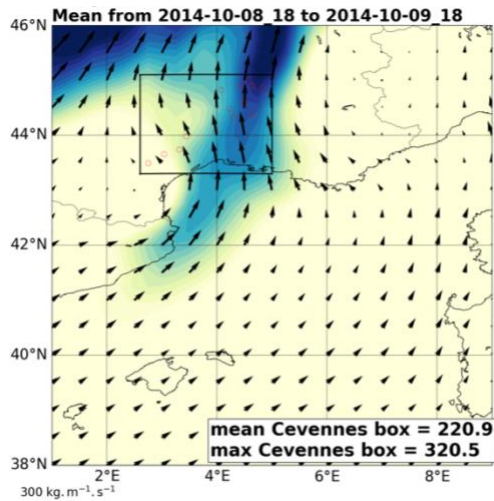


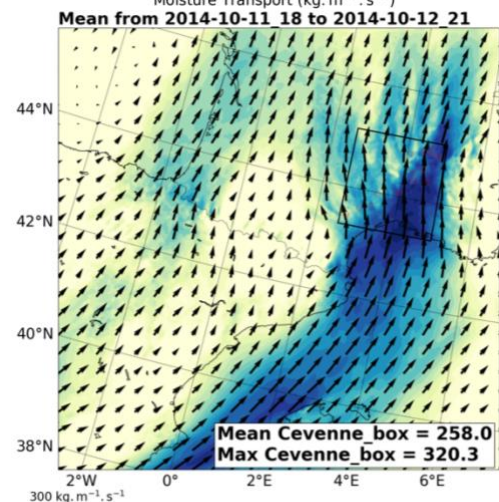
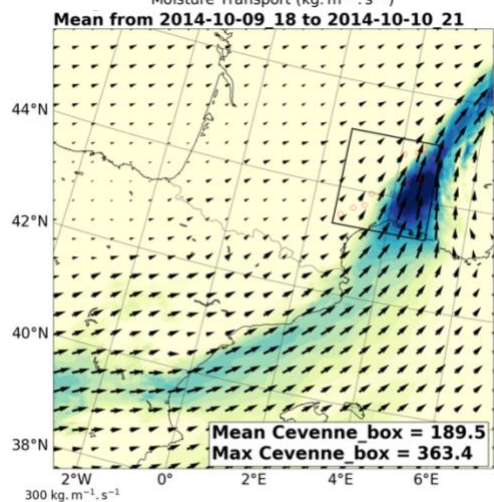
Figure 28. Mean moisture transport over the Cévennes from ERA5 and CPS simulations for the two heaviest daily rainfall events in September.

Figure 29 shows the same information as Figure 28 except for the events in October. Here I also select only two days with the heaviest rainfall occurring over the Cévennes box. The dates of these two days can be different among simulations and observations. The dates investigated are the 9th and 12th of October for ERA5, the 10th and 12th for WRF-01 and WRF-03, 7th and 10th for WRF-02 and WRF-003. However, all simulations can reproduce similar feature as ERA5 that is the coverage of intensified moisture over the right-hand half of the Cévennes box. These features remain the same for the event in November on two days including the 3rd and the 4th (Figure 30).

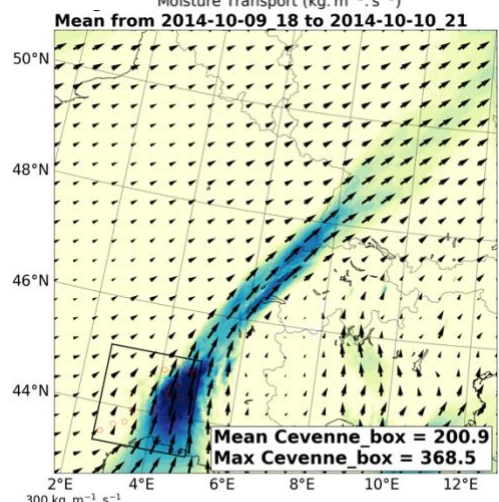
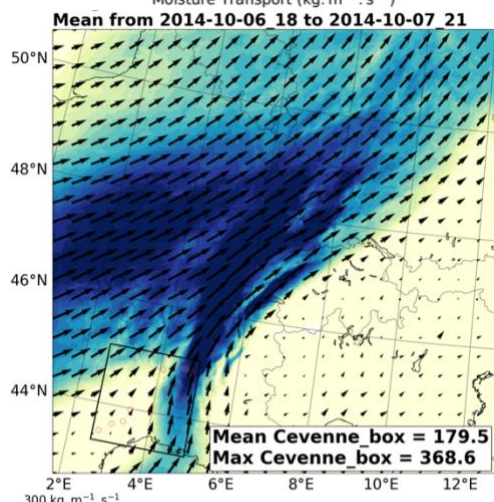
ERA5



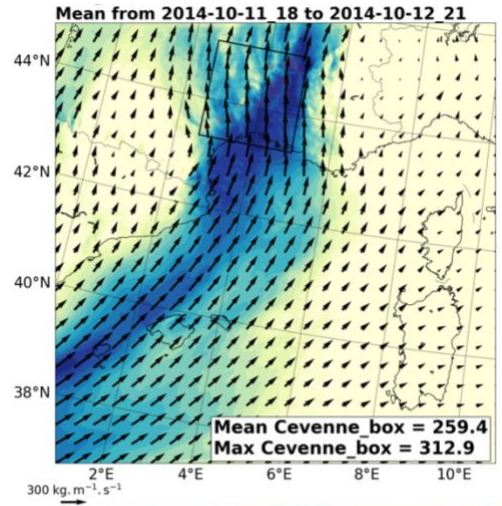
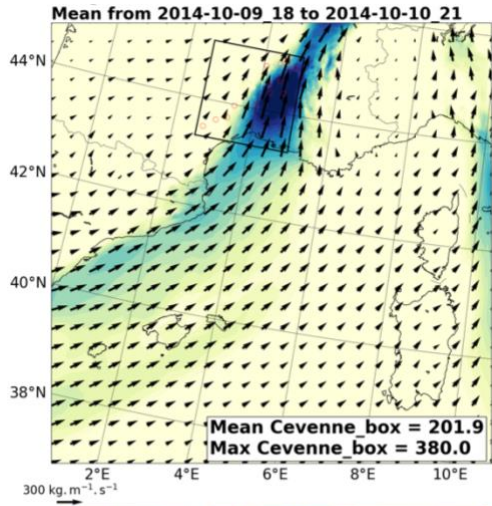
WRF-01



WRF-02



WRF-03



WRF-003

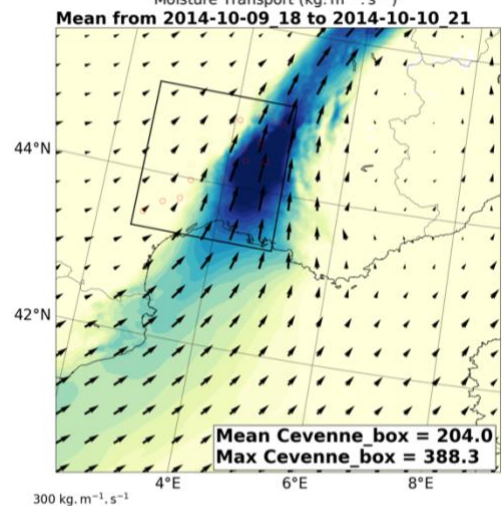
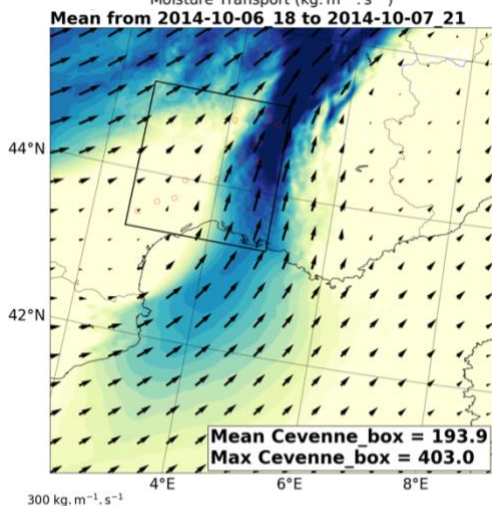
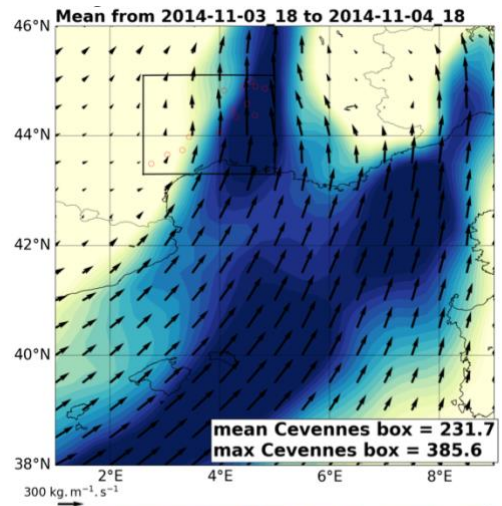
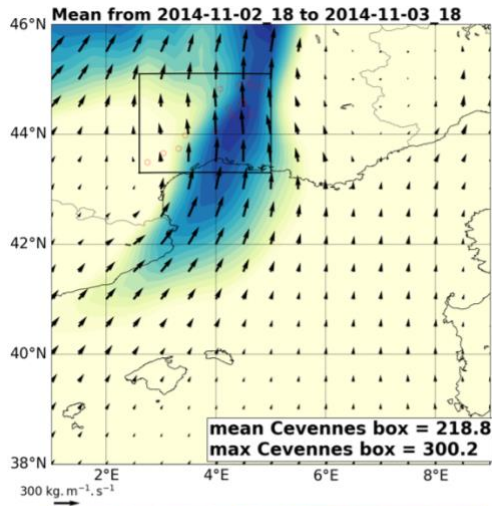
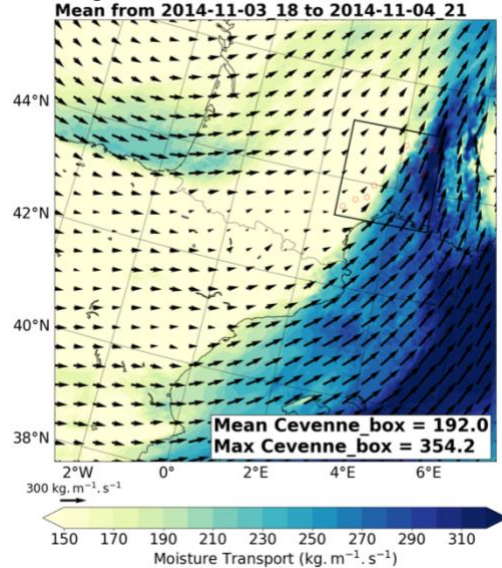
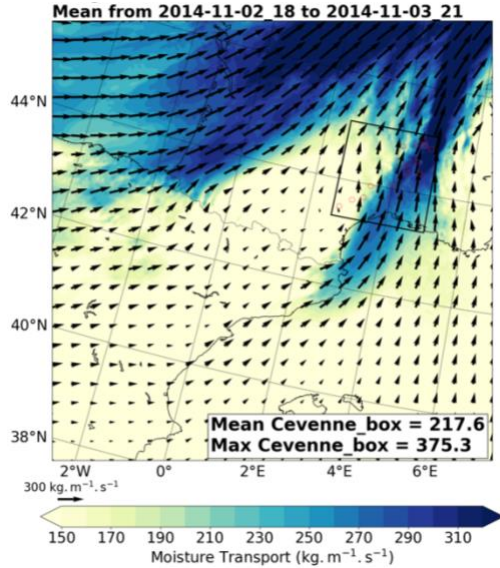


Figure 29. Mean moisture transport over the Cévennes from ERA5 and CPS simulations for the two heaviest daily rainfall events in October.

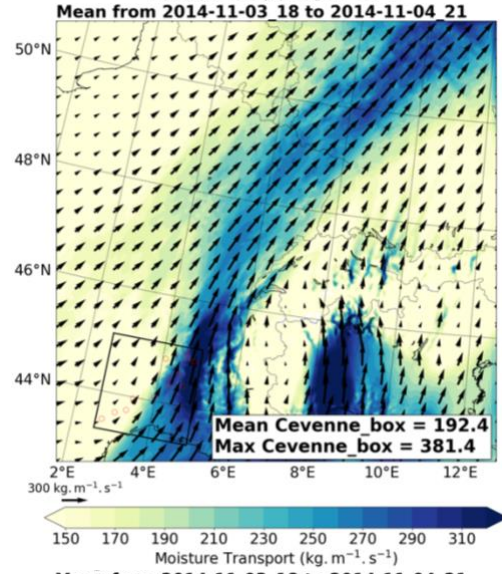
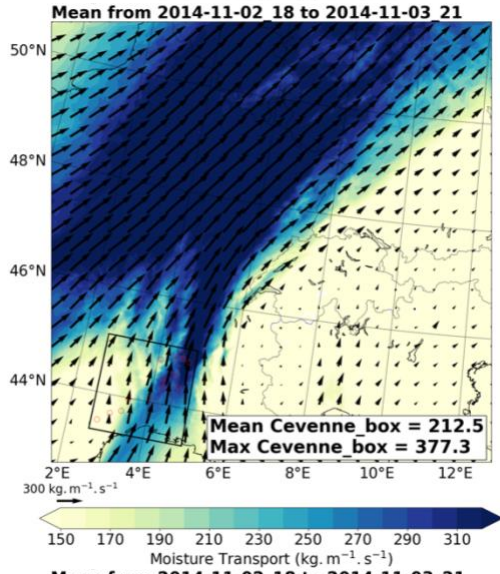
ERA5



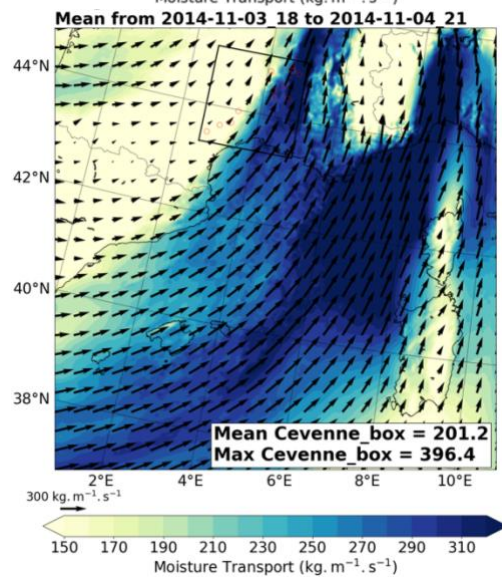
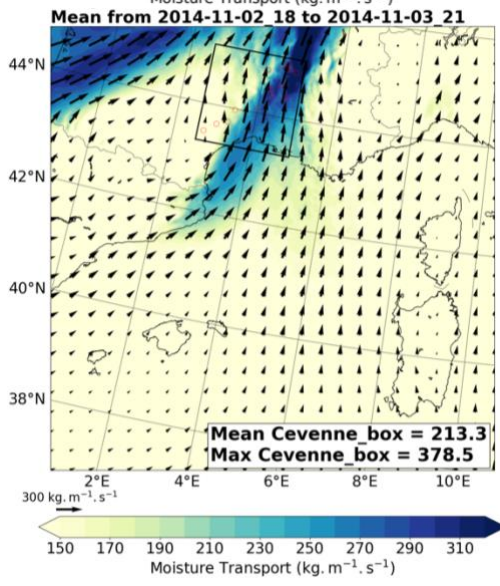
WRF-01



WRF-02



WRF-03



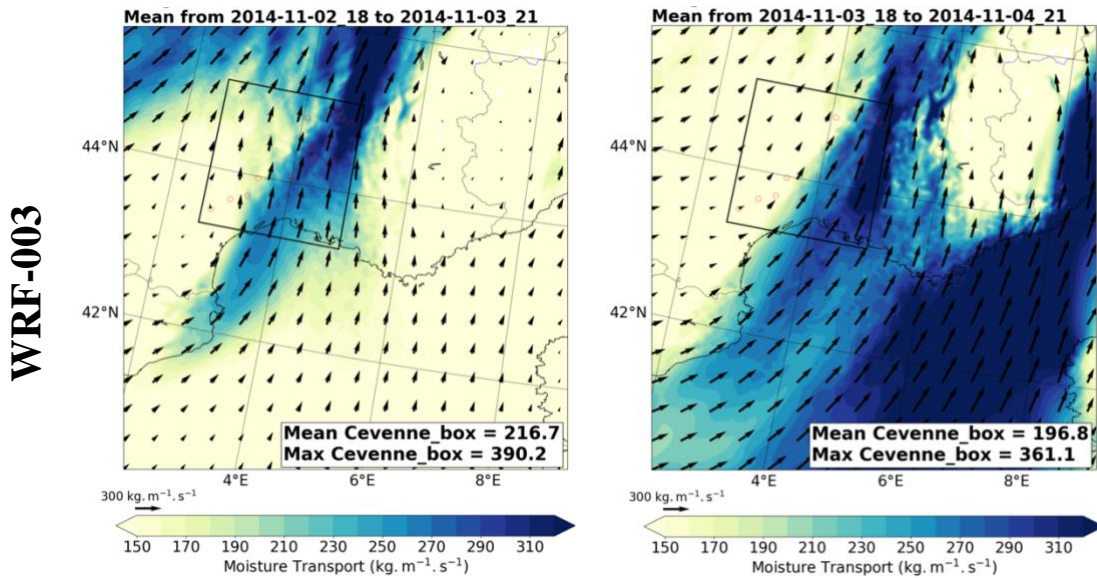


Figure 30. Mean moisture transport over the Cévennes from ERA5 and CPS simulations for the two heaviest daily rainfall events in November.

3.4. Conclusion

In this chapter, five different experiments are conducted for the autumn of 2014 to simulate rainfall focusing on the south of France. These experiments include a EURO-CORDEX domain whose configuration is the similar to EURO-CORDEX framework, and four nested domains at convection-permitting resolution driven by this EURO-CORDEX simulation. For evaluating these simulations, I propose six different rainfall indices including daily rainfall (R_daily), daily maximum 3-hour rainfall (Rx3hr_daily), maximum daily rainfall over a period (Rx1day), maximum 3-hour rainfall over a period (Rx3hour), total rainfall over a period (R_total) and probability distribution of daily rainfall (Prob_daily) and an additional analysis for moisture transport from the Mediterranean toward the Cévennes.

The change of position of four nested domains relative to EURO-CORDEX domain alters the results concerning extreme rainfall significantly. These disparities are shown in different aspects such as intensity, coverage, time and place of occurrence of the events. Even though the CPSs can, to some extents, reproduce those rainfall indices and the moisture transport, among those four CPS domains, the WRF-03 shows the best overall skills in capturing convective rainfall events over the Cévennes mountain range. However, the timing and place of occurrence of heavy rainfall event is a remaining limitation in all simulations.

Chapter summary

Objective:

The objective of this chapter is to find an appropriate configuration of convection-permitting domain that can be used to conduct simulations at climate scale.

Method:

I propose a set of four different configurations of convection-permitting domains which are different in sizes and positions relative to the EURO-CORDEX domain. These configurations are then used to simulate the real autumn of 2014 focusing on the Cévennes mountain range. The simulation results are evaluated against in-situ observations using a matrix of six different indices concerning daily and 3-hourly rainfall events and a moisture flux index.

Results:

The change of position of nested domains relative to parent domain alters the results concerning extreme rainfall significantly. Among those four convection-permitting configurations, the WRF-03 shows the best overall skills in capturing convective rainfall events over the Cévennes mountain range. This domain covers a larger part of the Mediterranean in comparison with others and Corsica.

Résumé

Objectif:

L'objectif de ce chapitre est de trouver une configuration appropriée du domaine permettant la convection qui peut être utilisée pour effectuer des simulations à l'échelle du climat.

Méthode:

Je propose un ensemble de quatre configurations différentes de domaines permettant la convection qui sont de tailles et de positions différentes par rapport au domaine EURO-CORDEX. Ces configurations sont ensuite utilisées pour simuler le véritable automne 2014 en se concentrant sur le massif des Cévennes. Les résultats de la simulation sont évalués par rapport aux observations in-situ à l'aide d'une matrice de six indices différents concernant les événements pluviométriques quotidiens et sur 3 heures et un indice de flux d'humidité.

Résultats:

Le changement de position des domaines imbriqués par rapport au domaine parent modifie considérablement les résultats concernant les précipitations extrêmes. Parmi ces quatre configurations permettant la convection, le WRF-03 présente les meilleures compétences globales pour capturer les événements de pluies convectives sur le massif des Cévennes. Ce domaine couvre une plus grande partie de la mer Méditerranée par rapport aux autres et à la Corse.

Chapter 4. Evaluation of convection - permitting downscaling of new EURO-CORDEX simulations for the France – Mediterranean

This chapter is dedicated to evaluate the performance of a unique regional climate model with convection-permitting (CPS) set-up and its driving EURO-CORDEX (EUR-11) simulations in reproducing extreme daily and hourly rainfall during the autumn. These assessments focus on the Cévennes mountain range in the South of France. The conclusion of all findings is presented at the end of this chapter.

4.1. Description of the simulations

The objective of this chapter is to produce and evaluate an ensemble of long simulations with the convection-permitting horizontal resolution and investigate the added value of this resolution over the highest resolution (approx. 12km) of EURO-CORDEX simulations (Jacob et al., 2014; Kotlarski et al., 2014). To obtain the CPSs, WRF model version 3.8.1 is used to downscale the recently-finished EURO-CORDEX simulations (C3S PRINCIPLES⁴) from 12km to 3 km. Unless otherwise specified we use the configurations presented in Chapter 3. This downscaling strategy is provided in detail steps below:

- The three EURO-CORDEX downscaling experiments at 12 km resolution were done under EURO-CORDEX framework. They were run using WRF version 3.8.1 and forced by three different global climate models (GCM) including IPSL-CM5A-MR (IPSL/France), HADGEM2-ES (MOHC/UK) and NORESM1-M (NCC/Norway) for the period from 1951 to 2100. For the years after 2006, the downscaling experiment from IPSL-CM5A-MR was done for two scenarios including RCP4.5 and RCP8.5. Meanwhile, the two others were done for RCP8.5 only.
- The results from three EURO-CORDEX simulations were processed and prepared as initial and boundary condition to force WRF version 3.8.1 at convection-permitting resolution (approx. 3km) by using ndown.exe program provided in the WRF software suite. These simulations use the same domain as WRF-03 case described in Chapter 3 that covers the France – Mediterranean area with its focus on the Cévennes mountain range in the south of France. These CPS runs are conducted for two

⁴ Copernicus Climate Change Service Contract #C3S_34b_Lot2.4.3.1

separated periods including a historical climate of 1951 – 1980 and a current climate of 2001 – 2030. After the year of 2006, only RCP8.5 scenario is selected for CPS downscaling experiments.

- These CPSs focus only on three months in the autumn when many extreme rainfall events were observed over the Cévennes. Each autumn simulation is initialized in the August 26th and kept running until the 1st of December with the forcing from the lateral boundary updated every three hours from EURO-CORDEX output. Given that the same regional model (WRF) is used in EURO-CORDEX and this CPS simulations, the six days at the end of August are used as spin-up time for the model after being forced by a set of initial variables interpolated from 12 km to 3 km in the previous steps.
- One of the important factors for initializing the climate simulation is to initialize soil properties (e.g. moisture and temperature). These two variables are interpolated from EURO-CORDEX results to CPS resolution for the initial condition of each season run instead of considering directly from GCM results. By doing so, it is expected to save computational expense of running several to ten years for soil moisture spin-up (as mentioned in Yang et al., 2011) because the soil moisture spin-up is taken into account in EURO-CORDEX simulations, and that allows the model to be re-initialized in every August without perturbing too much in the land surface parameterization/model of WRF. However, we are aware that soil moisture may not be fully in balance with the high-resolution set-up.
- All physics, dynamics, boundary layer schemes remain the same as what were proposed in Chapter 3 except that spectral nudging is eliminated for both EURO-CORDEX and CPSs.
- The CPSs are run in a single domain that is different from being nested inside EURO-CORDEX simultaneously. The results are stored every hour.

4.2. Reference data and evaluation methods

In this chapter, the CPS and EURO-CORDEX simulations are evaluated against four reference datasets. The first dataset is in situ observations including daily and daily maximum of 3-hour precipitation that are described in Chapter 3. Because of the availability of these two observational datasets, the 30 years of daily precipitation from historical simulations are compared to the period of 1961-1990 of daily precipitation in observations. Meanwhile, the daily maximum of 3-hour precipitation is only available

from 1982 and a few stations start in 1998, therefore, the period of 1998 to 2018 is used to evaluate the hourly simulation in current climate (see Table 9). The second reference dataset is SAFRAN (Quintana-Seguí et al., 2008; Vidal et al., 2010), which is used to evaluate daily precipitation from simulations. The dataset starts in 1958, therefore, I select the period from 1961 to 1990 that is consistent with in situ observations. The third dataset used here is COMEPHORE (**CO**mbinaison en vue de la **Meilleure Estimation de la Précipitation **HO**rai**RE****⁵) (Tabary et al., 2012). This dataset is a combination between rain gauge observations and radar information that makes the quality of the data, despite existing limitation from uncertainty in radar and rain gauge measurement, higher than any other gridded observation dataset, especially over the complex topography area such as the Cévennes (Fumière et al., 2019). Besides, this dataset has high spatial (1 km) and temporal (1 hour) resolution. However, the availability of this data only last from 1997 to 2007, that can be used to evaluate the 3-hour precipitation from current climate simulations. The last reference dataset is the new high-resolution atmospheric reanalysis ERA5 (ECMWF, 2017) which replaces the ERA-Interim operationally stopped in August 2019. In this section, the ERA5 dataset in pressure level is collected for a few variables including zonal and meridional winds and specific humidity with their time interval of 6 hours. This dataset is stored for the period of 30 years from 1989 to 2018 to serve the moisture transport analysis that is described below in this section.

To evaluate the CPSs and EURO-CORDEX simulations, several indices are selected consisting of Rx1day, Rx3hour, distribution of wet events, which are introduced in Chapter 3. Moreover, I also consider the moisture source impinging on the Cévennes mountain range and the relationship of extreme 3-hourly and daily rainfall scaling with daily mean temperature at 2meter. For the moisture index, the Cévennes box is determined at first similarly to what is used in Chapter 3 by extracting the maximum and minimum latitude and longitude information of the 14 stations used in (Vautard et al., 2015). Roughly, it is confined from 2.6°E to 5°E and from 43.3°N to 45.1°N. Next, the 12 heaviest daily rainfall events occurring in this Cévennes box in 30 years of simulations and observations are defined. The period of simulations used in this analysis is 2001 – 2030 and that of observations is 1989 – 2018 because of the availability of ERA5 that starts from 1979. For each event, the mean moisture transport of several time steps from

⁵ https://donneespubliques.meteofrance.fr/?fond=produit&id_produit=103&id_rubrique=34

18 UTC of the previous day to 21 UTC of the day when the event occurred is estimated. The time interval for this analysis from simulations is every 3 hours and for reanalysis is every 6 hours. Finally, the mean moisture transports of those 12 events from simulations are computed and compared against the one from ERA5. The moisture transport is estimated using the method in L  l   et al. (2015) and similar to what is used in Chapter 3:

$$\vec{Q} = -\frac{1}{g} \int_{ps}^{pu} q \vec{U} dp$$

In this equation, \vec{Q} is the zonal and meridional moisture transport vector ($\text{kg}\cdot\text{m}^{-1}\cdot\text{s}^{-1}$), g denotes the standard gravitational acceleration at mean sea level ($9.81 \text{ m}\cdot\text{s}^{-2}$), q is specific humidity (kg/kg), \vec{U} is zonal and meridional wind vector ($\text{m}\cdot\text{s}^{-1}$), ps and pu are surface and upper pressure level. In this case, I selected 1000 mb and 700 mb, respectively.

For the scaling of extreme rainfall on surface temperature, the method in Lenderink and Van Meijgaard (2008) is employed. The daily (or daily maximum 3-hour rainfall) data at stations in C  vennes box, which are 14 stations for daily rainfall (or 23 stations for hourly rainfall) highlighted in Table 11 (or Table 12), are pooled together. This dataset is then paired with corresponding daily mean temperature at 2m which is the average of the C  vennes box (the observed temperature is taken from the version 19.0e of E-OBS⁶ (Corn  s et al., 2018)). Next, this data is sorted in the ascending order of temperature and divided into several bins with its width of 2  C and 1  C overlapping between the two successive bins. In each bin, the 99th percentile of rainfall and mean temperature are estimated as representative values for that bin. To obtain the statistical inference for this analysis, the non-parametric bootstrap is used. For each bin, 1000 samples of temperature and rainfall values are randomly picked with replacement from the original bin. The size of each sample remains similar to the size of the original bin. Then the same procedure of calculating the 99th percentile of rainfall is repeated for each sample. Finally, the 90% confidence interval is computed based on those statistics from the 1000 samples.

The detail of which period selected for evaluation of simulation and for reference corresponding to each index is given in Table 9 below.

⁶ <https://www.ecad.eu/download/ensembles/downloadversion19.0eHOM.php>

Table 9. The selection of periods for evaluation of each index

No.	Indices	Period for each Dataset			
		OBS	WRF	COMEPHORE	ERA5
1	Rx1day	1961-1990	1951-1980	1997-2007	-
2	R-T Scaling (daily rainfall)			-	-
3	Distribution of wet events (daily rainfall)			-	-
4	Rx3hour	1998-2018	2001-2030	1997-2007	-
5	R-T Scaling (daily maximum 3-hour rainfall)			-	-
6	Distribution of wet events (daily maximum 3-hour rainfall)			-	-
7	Moisture source	1989-2018	2001-2030	-	1989-2018

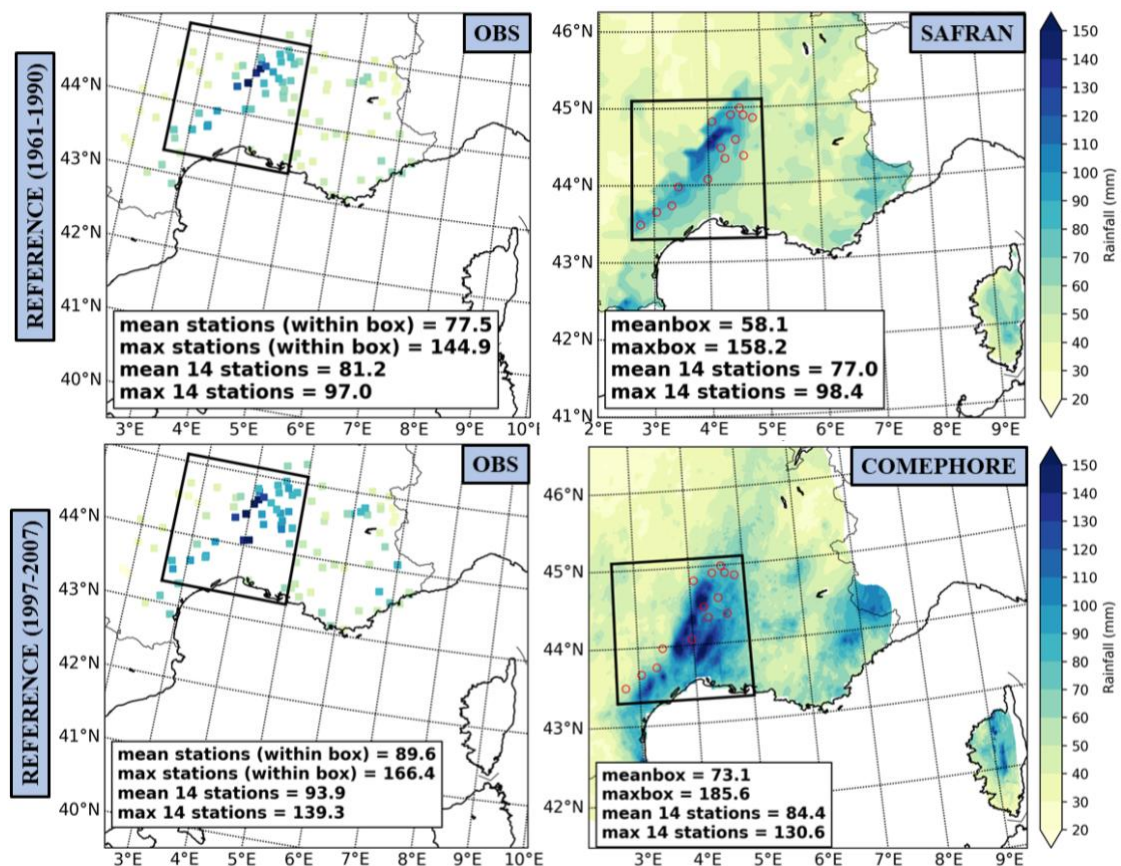
4.3. Evaluation of extreme rainfall

4.3.1. Autumn maximum daily rainfall (Rx1day)

The 30-year (11-year for COMEPHORE) mean of autumn maxima daily rainfall (Rx1day) is computed to evaluate simulations from EURO-CORDEX and CPS against reference data. Figure 31 shows spatial distribution of Rx1day from observations and simulations. It is indicated from two periods of in situ observations that extreme daily rainfall tends to occur along the Cévennes mountain range (i.e. the diagonal of the Cévennes box), especially the northern part (i.e. from 44°N upward to the north). The SAFRAN data shows similar feature for Rx1day in the period of 1961 – 1990 with the max/mean of 14 stations of 98mm/77mm against 97mm/81mm from in situ observations. This can be explained by the fact that SAFRAN is an interpolation product based on observations at stations. The spatial distribution of Rx1day in COMEPHORE in the period of 1997-2007 also has agreement with observations, at least where the station data is available. The magnitude of max/mean of 14 stations in COMEPHORE is slightly different from observations, 131mm/84mm in COMEPHORE versus 139mm/94mm in observations. The COMEPHORE data also shows the extreme values on the right of the Cévennes range where in situ measurement is unavailable. This information can be the added value coming from the radar product or from the stations that are not collected in this dissertation.

Because the EURO-CORDEX and CPS simulations share the RCM (WRFv3.8.1) and all configurations (e.g. physic, micro-physic, etc.), hereafter they will be shortly

mentioned by their resolutions (e.g. EUR-11 or CPS) and driving GCMs (e.g. EUR-11-IPSL-CM5A-MR for replacing its long name EUR-11-IPSL-IPSL-CM5A-MR_r1i1p1_IPSL-WRF381P). The EUR-11 and CPS simulations can reproduce heavier rainfall along the Cévennes mountain range than other areas in the Cévennes box (Figure 31). However, the magnitude of Rx1day from EUR-11 and CPS simulations are largely different. The simulated results from three EUR-11 simulations are largely underestimated the observations in the Cévennes box. The mean bias of the Cévennes box from EUR-11-IPSL-CM5A-MR, EUR-11-HadGEM2-ES and EUR-11-NorESM1-M and their ensemble mean are -43%, -33%, -47% and -41%, respectively (Figure 32). However, they show overestimation (from 10% to 40%) of Rx1day over the Alps in the boulder between France and Switzerland. Similarly, the three CPSs show underestimation of Rx1day over the Cévennes box, but these results have a better agreement with in situ observations, especially the CPS-HadGEM2-ES. The mean absolute (dry) bias in the box from CPS-IPSL-CM5A-MR, CPS-HadGEM2-ES and CPS-NorESM1-M and their ensemble mean are 24%, 12%, 28% and 18%, respectively (Figure 32). These CPSs also reproduce heavier rainfall over the Alps similarly to EUR-11.



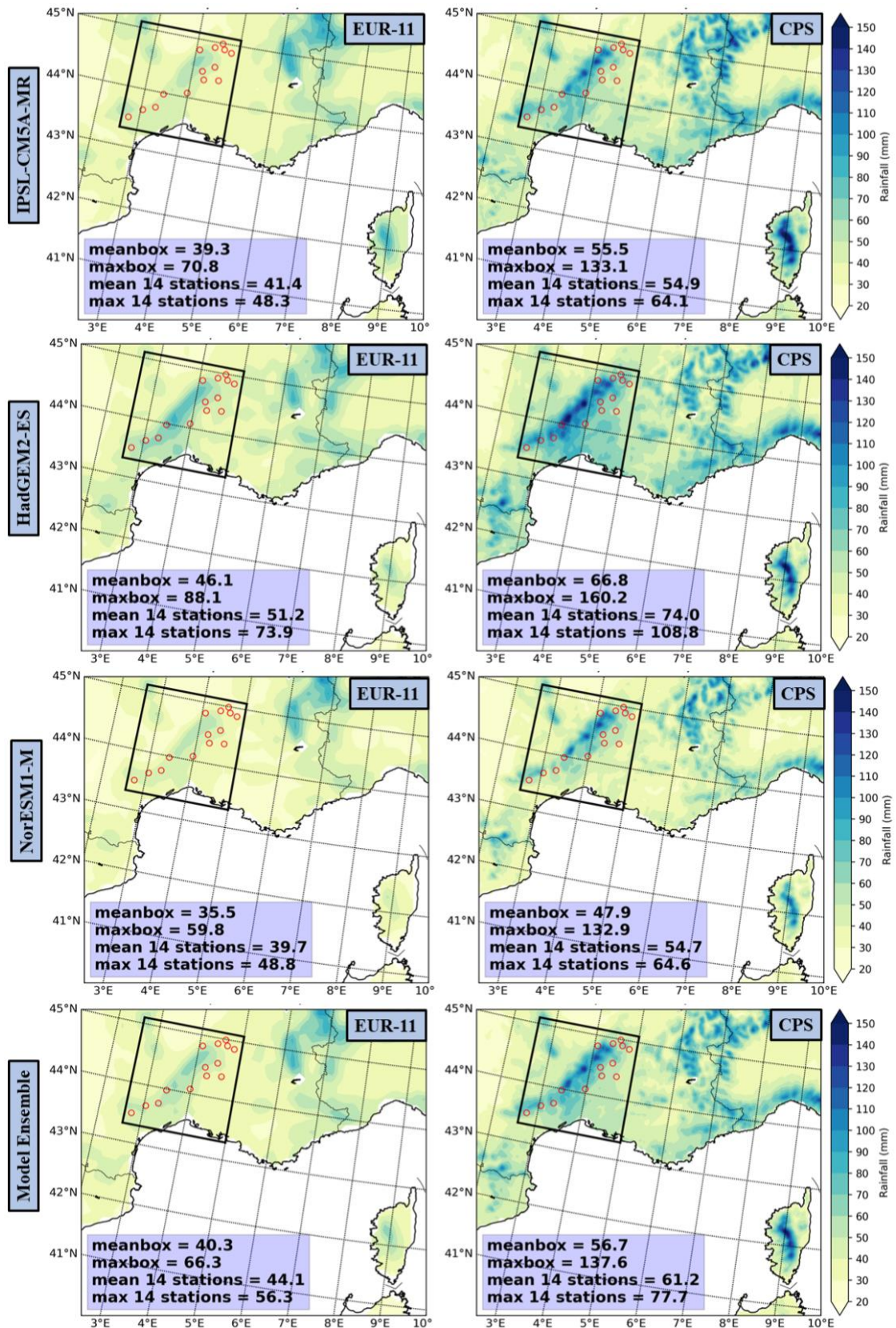
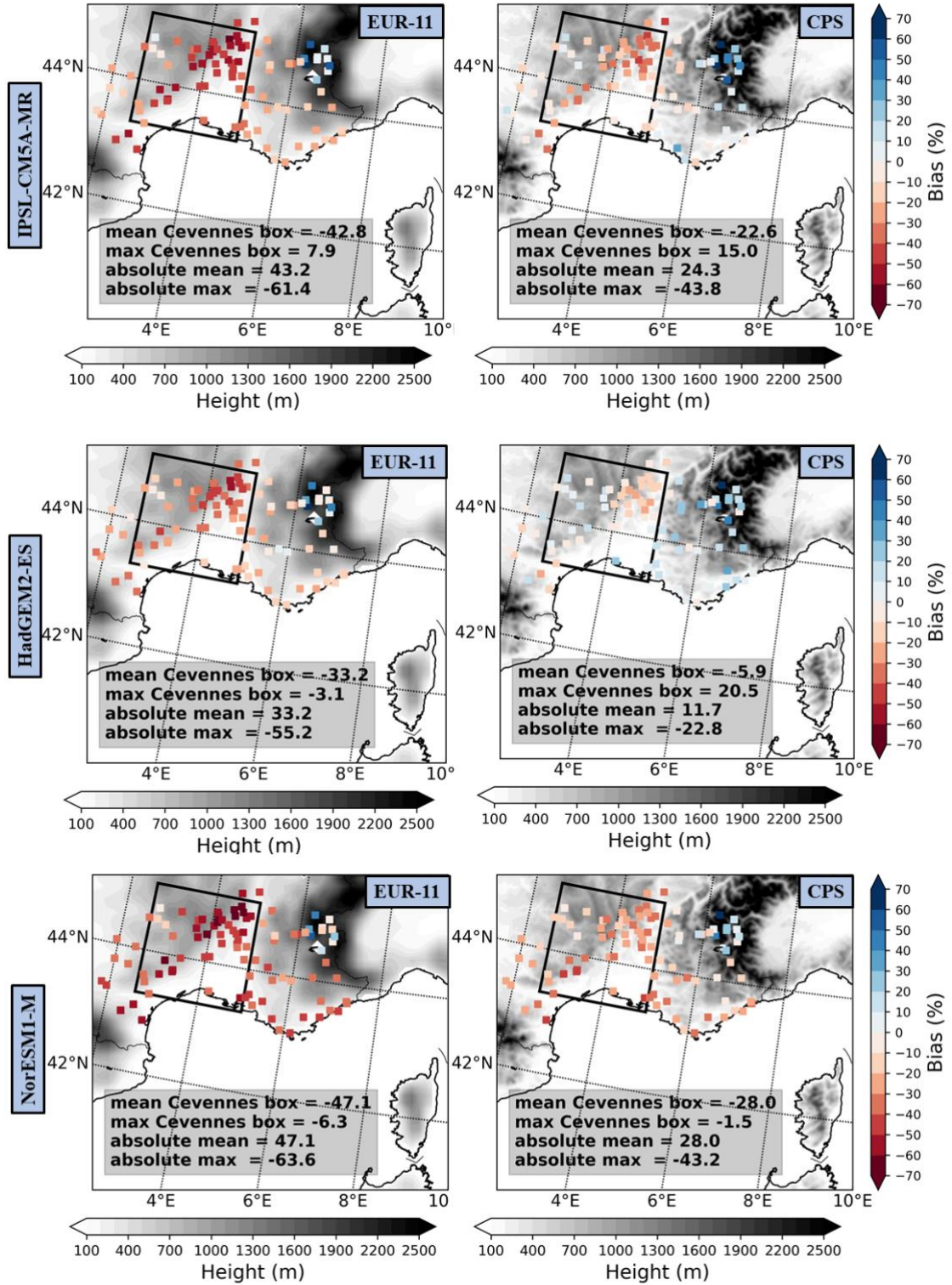


Figure 31. The Autumn maximum daily rainfall ($Rx1day$) from simulations (1951 - 1980), observations (1961-1990), SAFRAN (1961-1990) and COMEPHORE (1997-2007) data; observations in 1997-2007 is also provided to compare to COMEPHORE

data. The empty-red circles in every panel of simulations and gridded reference datasets denote 14 stations used in Vautard et al. (2015).



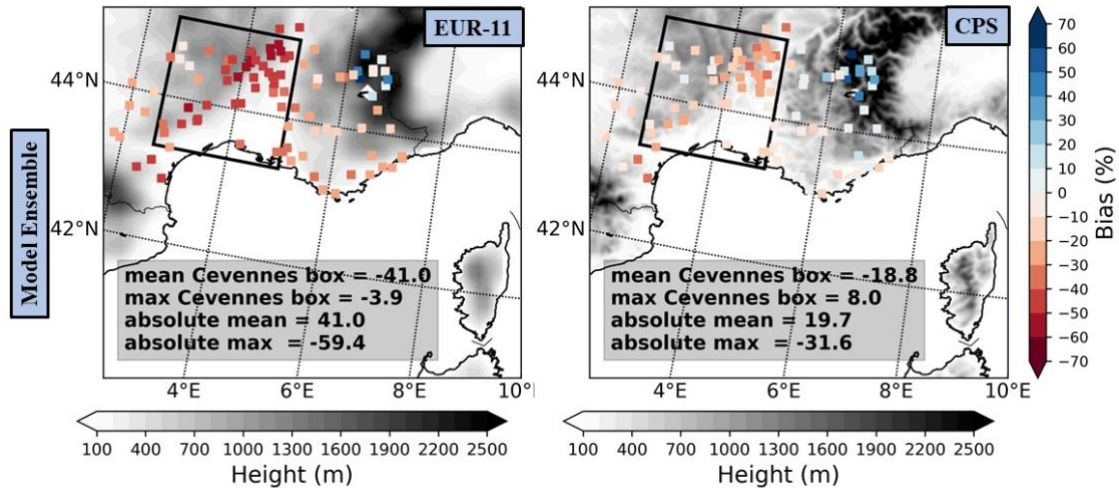


Figure 32. Bias of $Rx1day$ simulations from EURO-CODEX (left) and CPS (right) in comparison with in situ observations. The light-to-dark shaded color denotes the elevation from each simulation.

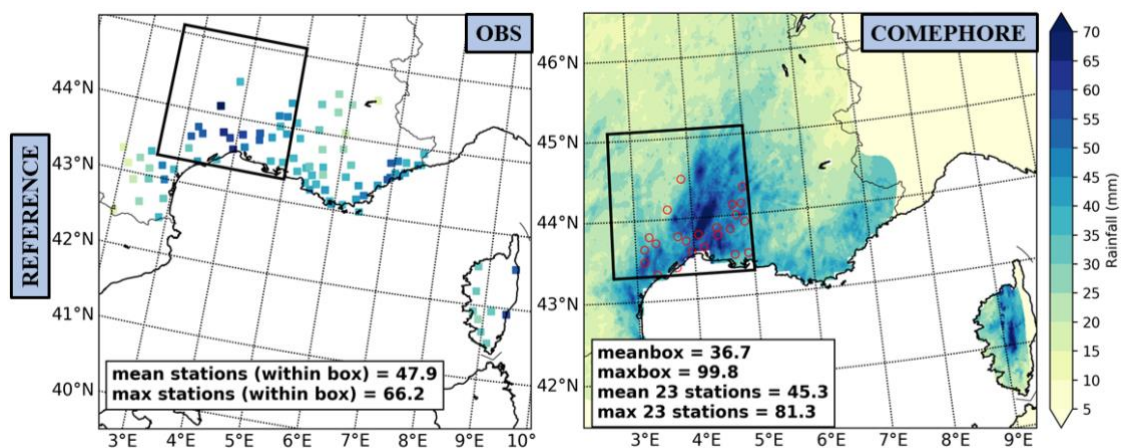
4.3.2. Autumn maximum of daily maximum 3-hours rainfall ($Rx3hour$)

An important feature that is expected to be improved in convection permitting model is the deep convection process. The development of this process can produce heavy precipitation over an area in a short period of time (e.g. hourly scale). Here I use the autumn maximum 3-hour rainfall ($Rx3hour$) to evaluate whether convective rainfall simulation is improved in CPSs compared to the coarser resolution EUR-11. The reference data used in this section is gauge measurement and COMEPHORE data. The SAFRAN data is eliminated because of its lack of quality in sub-daily timescale.

The spatial distributions of interannual mean of the autumn $Rx3hour$ from in situ observations, COMEPHORE, EUR-11 and CPS simulations are shown in Figure 33. The biases at stations of those simulations against rain gauge measurement are given in Figure 34. The pattern that heavy rainfall is observed in the northeast – southwest orientation in this $Rx3hour$ analysis remains the same as what is shown in $Rx1day$ analysis. In addition, 3-hour heavy rainfall event occurs in the plain on the south-east of the Cévennes in both in situ observations and COMEPHORE data (Figure 33). The spatial max/mean of $Rx3hour$ of 23 stations inside the Cévennes box from observations and COMEPHORE are 66mm/48mm and 81mm/45mm, respectively. The mean values from the two references are closed, meanwhile the maximum values show almost 30% wet bias of the COMEPHORE. This discrepancy can come from the radar information or the method combining radar and gauge measurements. This also proves the uncertainty in

COMEPHORE data in the complex topography area although the Cévennes is an area with good coverage of radar system.

Figure 33 shows that EUR-11 simulations are not able to reproduce the Rx3hour over Cévennes. Even though these simulations can generate more rainfall over the Cévennes compared to other areas, the magnitudes of the events are largely underestimated. The mean bias over 23 stations within the Cévennes box of EUR-11-IPSL-CM5A-MR, EUR-11-HadGEM2-ES and EUR-11-NorESM1-M and their ensemble mean are -64%, -57%, -66% and -63%, respectively (Figure 34). In contrast to EUR-11, the CPSs can reproduce the northeast – southwest orientation of heavy rainfall over the Cévennes. They can also provide heavy rainfall pattern over the plain on the south-east of the Cévennes, as well as the eastward coastal area similarly to observations and COMEPHORE (Figure 33). Generally, all CPS simulations are underestimated over the Cévennes. The spatial mean biases of Rx3hour over the Cévennes box from CPS-IPSL-CM5A-MR, CPS-HadGEM2-ES and CPS-NorESM1-M and their ensemble mean are respectively -11%, -6%, -28% and -17%. However, these CPS simulations perform differently for the plain and coastal area on the south-east of the Cévennes and the Alps. The CPS-IPSL-CM5A-MR reproduces heavier rainfall compared to observations with its bias ranging from 20% to 60%. The CPS-HadGEM2-ES shows the best agreement among the three CPSs with observations. The bias in this case ranges from -20% to 20%. The last CPS simulation underestimates the heavy rainfall at most stations with its bias ranging from -10% to -40% (Figure 34).



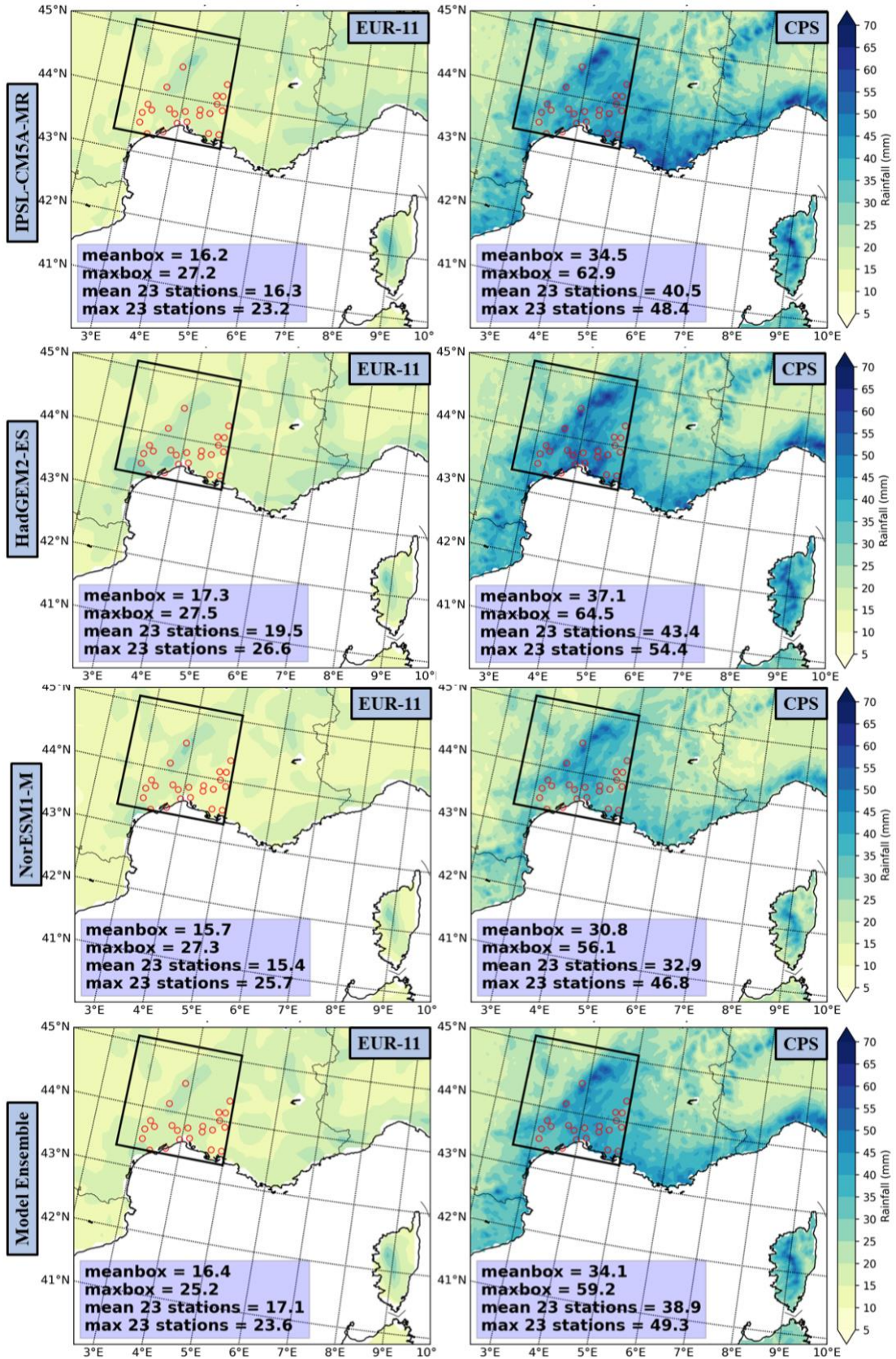
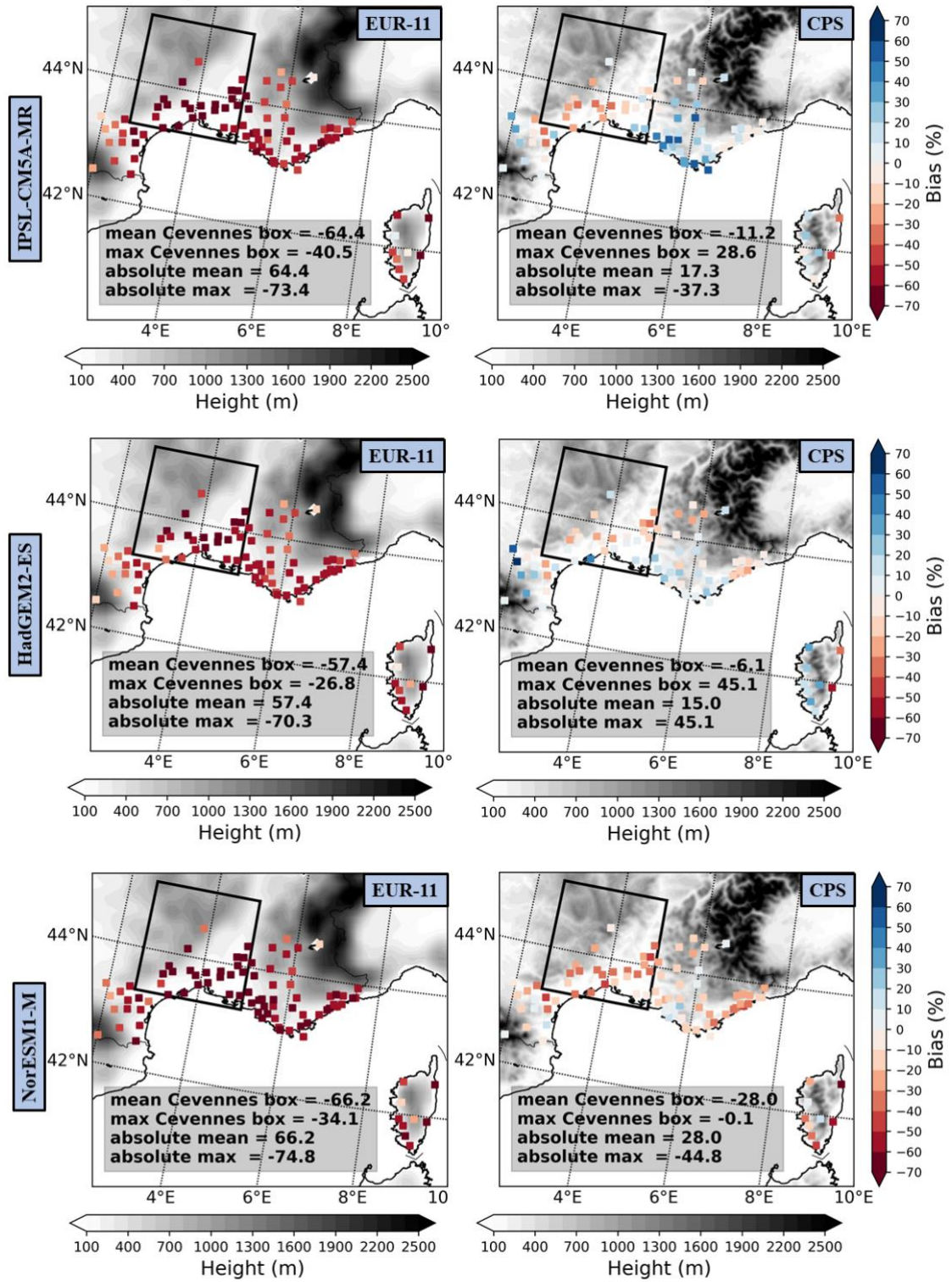


Figure 33. The Autumn maximum 3-hour rainfall (R_{x3hour}) from simulations (2001 - 2030), observations (1998-2018) and COMEPHORE (1997-2007) data. The empty-red

circles in every panel for simulations and COMEPHORE denote 23 stations within the Cévennes box.



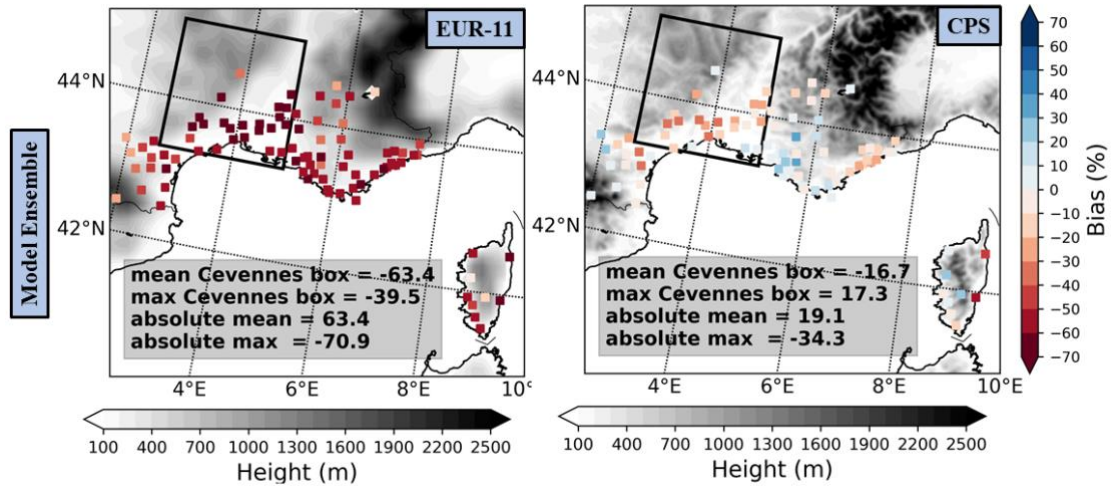


Figure 34. Bias of Rx3hour simulations from EURO-CODEX (left) and CPS (right) in comparison with in situ observations. The light-to-dark shaded color denotes the elevation from each simulation.

4.3.3. Scaling extreme rainfall with surface temperature

In theory, the Clausius – Clapeyron relation states that the water holding capacity of the atmosphere increases by 7% when temperature increases by 1 Kelvin (Celsius). This means that in the absence of significant changes of relative humidity, the moisture source available for convective process may increase by 7% per degree Kelvin (Celsius) of increasing in temperature (Lenderink and Attema, 2015). This relation has a close link to the increase in extreme precipitation in both daily and sub-daily time scale in the warming climate (Lenderink et al., 2017; Pall et al., 2007; Westra et al., 2014). In this section, the Clausius - Clapeyron relation is reflexed by a non-parametric scaling model of daily/daily maximum 3-hour rainfall and surface temperature for the Cévennes area by the method described in Section 4.2. This scaling is conducted for all EUR-11 and CPS simulations to compare to one obtained from observations. This evaluation plays an important part in attributing the change in extreme rainfall to global warming resulting from human activities.

Figure 35a shows extreme daily precipitation as a function of surface temperature for all simulations and in situ observations. The observations show that extreme daily rainfall in the Cévennes area is close to the Clausius – Clapeyron relation (the black dot line in Figure 35a) for the surface temperature ranging from 3° to 16° degree Celsius. Similarly, all the simulations can reproduce this scaling behavior as observation in different range of temperature. The CPS-IPSL-CM5A-MR, CPS-HadGEM2-ES and CPS-NorESM1-M roughly show the Clausius – Clapeyron relation for temperature range

of 4° to 16°C, 4° to 18°C and 5° to 15°C, respectively. The three EUR-11 simulations tend to show approximately similar temperature range for this scaling behavior but lower rainfall intensity than their corresponding CPS simulations.

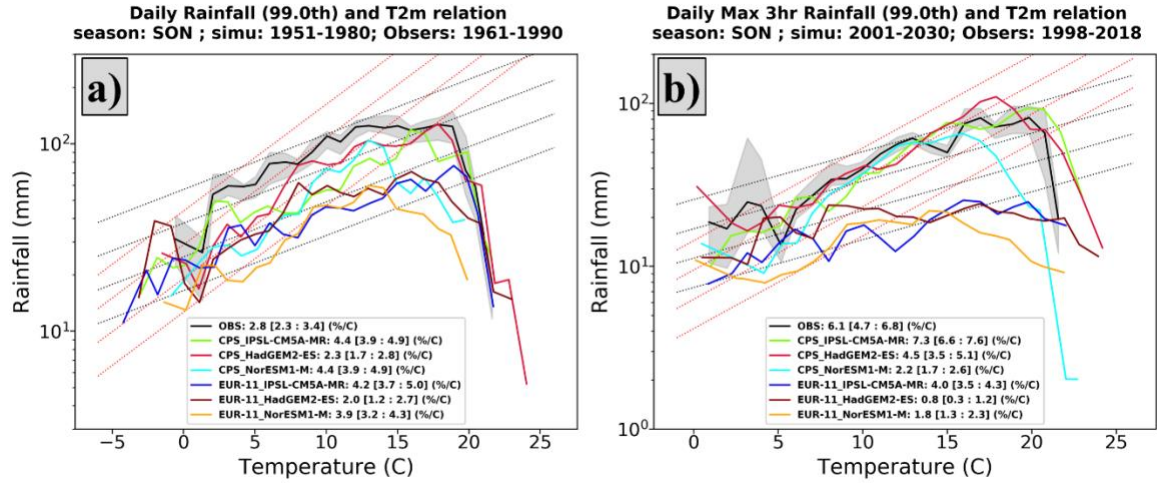


Figure 35. Extreme daily precipitation (a) and extreme daily maximum of 3-hourly rainfall (b) as a function of daily temperature at 2m from simulations (1951-1980 for daily rainfall and 2001-2030 for 3-hourly rainfall) and observations (1961-1990 for daily rainfall and 1998-2018 for 3-hourly rainfall); the black dot lines show Clausius-Clapeyron relation and the red dot lines show the super Clausius – Clapeyron relation; the grey band denotes 90% confident interval of observational scaling.

Figure 35b shows the same information as Figure 35a but for daily maximum 3-hour rainfall. The improvement of CPSs in reproducing convective rainfall is shown in this analysis that only three CPSs can reproduce the double (or super) Clausius – Clapeyron relation (the red dot lines in Figure 35b) similarly to observation for temperature ranging roughly from 5° to 16°C or 20°C. This super Clausius – Clapeyron can be explained simply that the releasing of latent heat during the condensation of water vapor has feedback and enhances the convergence of moisture in lower level (Lenderink et al., 2017; Trenberth et al., 2003). In addition to the ability to reproduce super Clausius – Clapeyron scaling behavior, the intensity of extreme 3-hour rainfall from the three CPSs also show a better agreement with observations. The three EUR-11 simulations fail to reproduce this relationship in either the scaling behavior or intensity. One of the reason for this underestimation is that the convective parameterization scheme uses a more simplified description of cloud process which is not able to represent the real complex dynamic of cloud (Lenderink and Attema, 2015). The decreasing trend of extreme rainfall in high temperature in both Figure 35a and Figure 35b is caused by the lack of real

moisture in the atmosphere when the condition of constant of relative humidity is not matched.

4.3.4. Distribution of wet events

The advantage of CPSs in reproducing extreme rainfall over the EURO-CORDEX simulations is obvious when the distributions of wet events (rainfall amount greater or equal to 0.1 mm) from simulations are compared against in situ observations. The distribution of daily wet events from observations and simulations are shown in Figure 36. All simulations are clearly underestimated, especially in the tail of the distributions. However, the CPSs have a better agreement with observations that is indicated by the bias of the tail of distribution (Figure 36 right panel). The best reproduction of the tail of distribution comes from CPS-HadGEM2-ES with its mean bias of -20%. The mean biases of CPS-IPSL-CM5A-MR and CPS-NorESM1-M are roughly -40%; the biases from EUR-11 simulations are larger that ranges from -60 to -50%. The enhancement in skill of reproducing convective rainfall events from CPSs is more obvious in Figure 37. The distributions of daily maximum 3-hour rainfall are separated apparently into 2 groups including one of EUR-11 simulations and one of CPS simulations and observations, especially the tail of those distributions. The mean biases of the three CPSs range from -20% to -5%, meanwhile the biases from EUR11 simulations are approximately -60% for all three cases. For both daily and sub-daily events, the downscaling experiments from HadGEM2-ES always show the best skills compared to other simulations with the same resolution. These results are also consistent with what are found in the previous sections of this Chapter.

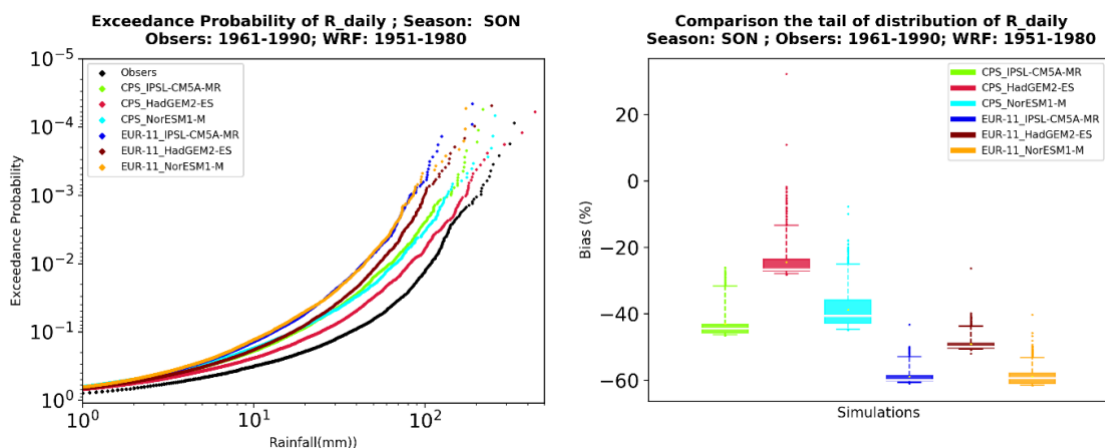


Figure 36. Exceedance probability distribution (left) for daily rainfall in the autumn from observations (1961-1990) and simulations (1951-1980) and the bias (right) of 10% in the tail of simulations against observations

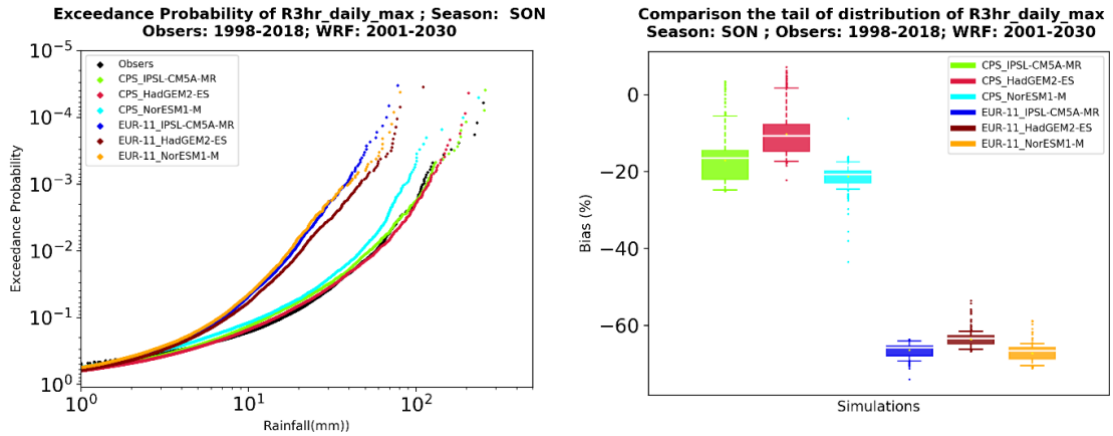
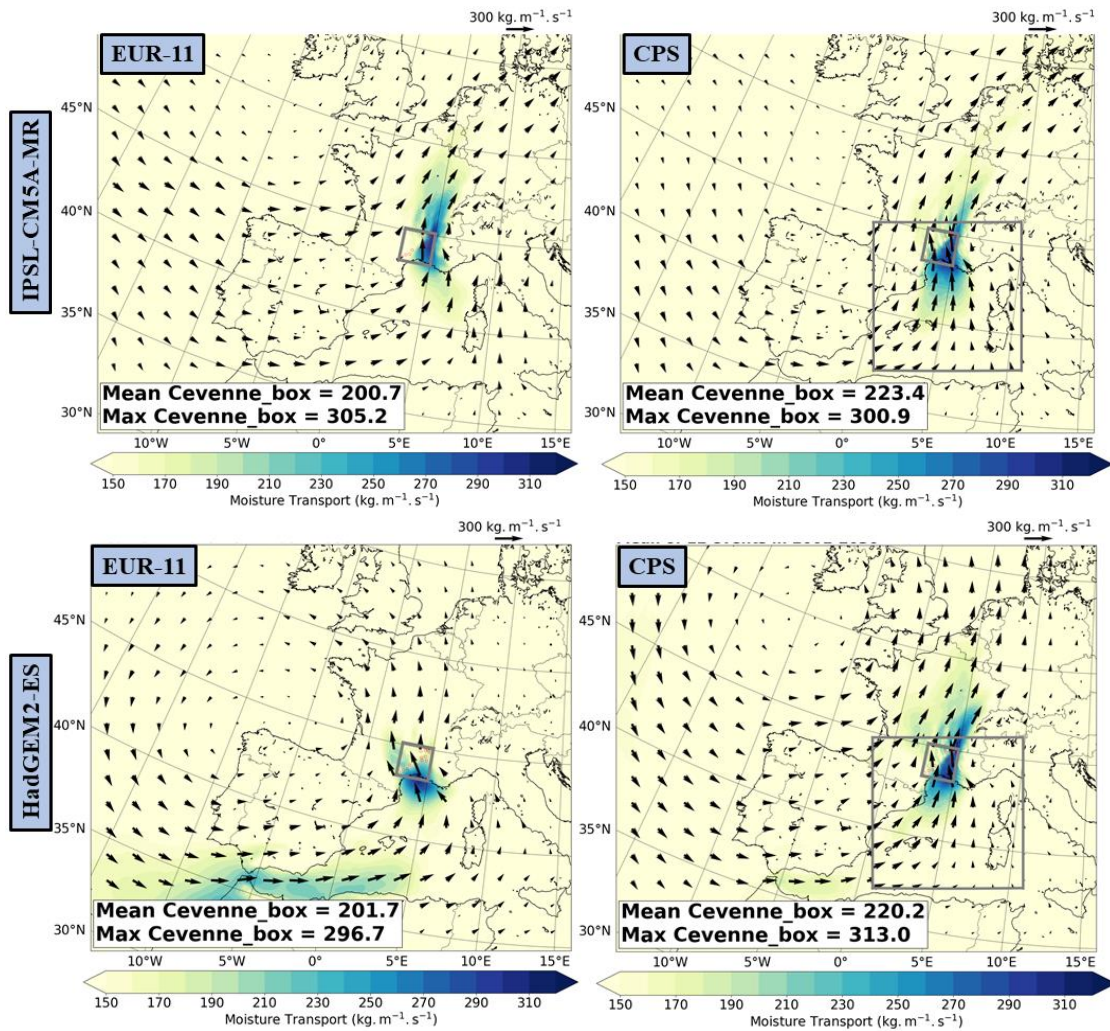


Figure 37. Exceedance probability distribution (left) for daily maximum of 3-hour rainfall in the autumn from observations (1998-2018) and simulations (2001-2030) and the bias (right) of 10% in the tail of the distributions of simulations against observations.

4.3.5. Moisture sources



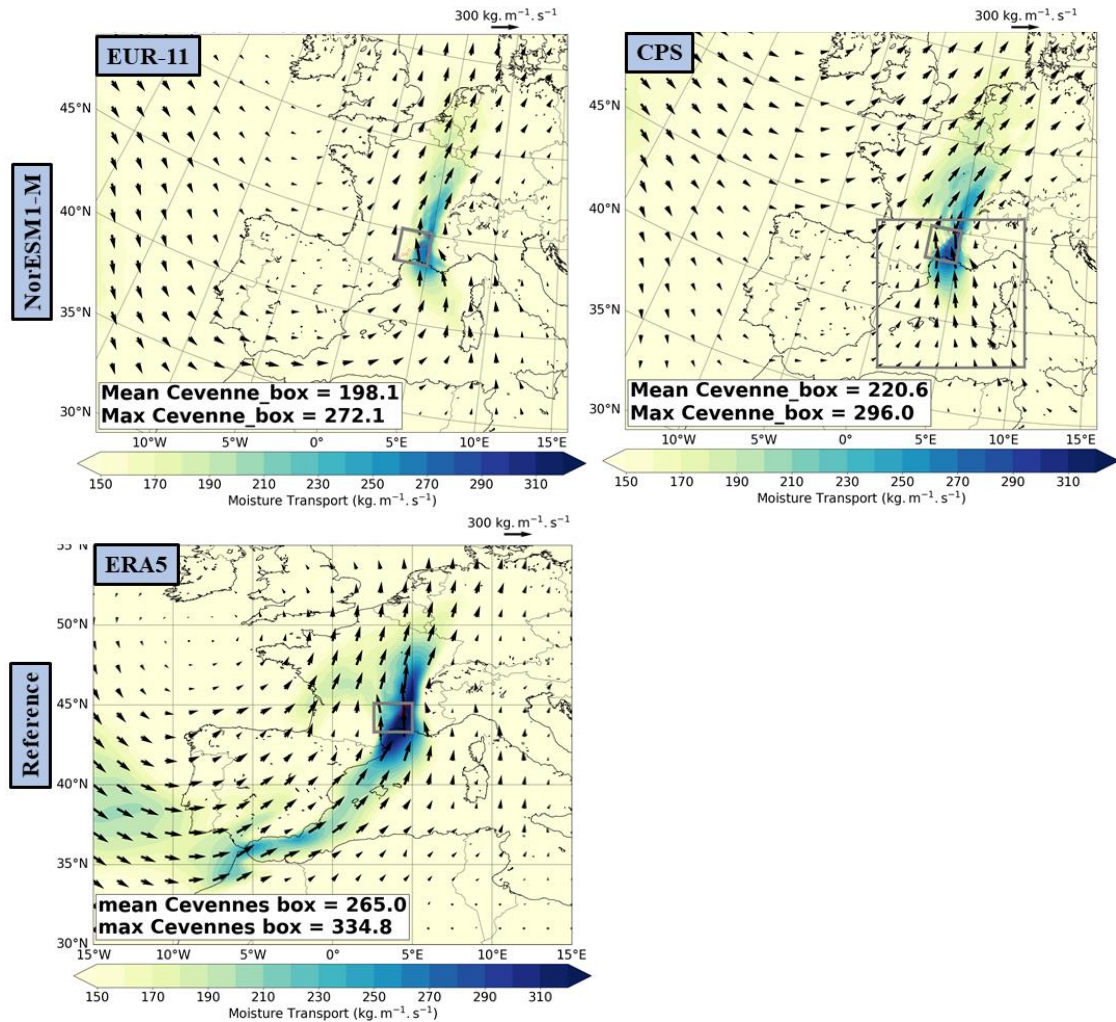


Figure 38. Mean moisture transport of the 12 heaviest daily rainfall events from simulations (2001-2030) and ERA5 (1989-2018)

The heavy precipitation events in the autumn with their intensity exceeding 100 mm in a few hours is of regular occurrence in the south of France and other countries in the western Mediterranean. One of the most important ingredients contributing to the mechanism of these severe events is the water vapor transported from the Mediterranean by unstable low-level flow that is persistent and intensified in several consecutive hours. This immense moisture source combining with the high topography of the mountain ranges (the Cévennes in this case) triggers the mesoscale convective system which is frequently reinforced at the same location (2014; Ducrocq et al., 2008; Lee et al., 2018; 2008; Nuissier et al., 2011). In this section, I will investigate how the moisture source transported by the southeastern flow from the Mediterranean is reproduced by all simulations, then compare them against analysis of ERA5 reanalysis. The method to estimate moisture transport from the 12 heaviest precipitation events is given in Section

4.2 and those heaviest rainfall events from all simulations and observations are given in the Supplementary.

Figure 38 shows the moisture transport averaged from the 12 heaviest rainfall events occurring over the Cévennes mountain range from 30 years of all simulations and reanalysis ERA5 data. Because the domain of CPSs is much smaller than what is needed for this investigation, they are embed inside their EUR-11 parent domains in each figure of CPSs (the right column of Figure 38). This means that the mean moisture transport investigations are estimated for each CPS and its driving EUR-11 to perform those plots. Hence, the information of moisture transport of each EUR-11 simulations may differ from between the analyses of EUR-11 themselves (the left column of Figure 28) and analyses of CPSs (the right column of Figure 28). The ERA5 reanalysis shows that a low-pressure system locates around 50N and 9W in the Atlantic with its trough deeply expanding to the south. This synoptic system generates southerly to easterly flows bringing moisture from the Mediterranean and striking the Cévennes. The EUR-11 simulations, in either investigation of themselves or investigation of their nested CPSs plot, appear to reproduce well these large-scale features. The low-pressure system tends to locate in between 45N to 50N and 5W to 10W and facilitate the low-level jet toward the Cévennes. The amount of moisture brought to the Cévennes box is obviously larger than surrounding areas and in agreement with what is shown by ERA5. The mean moisture on the Cévennes box reproduced by EUR-11 simulations is roughly 25% underestimated in comparison with ERA5 reanalysis. The CPS forced by EUR-11 simulations, despite their limitation of domain size, can also reproduce the moist flows impinging on the Cévennes and in better agreement with what is shown in ERA5. The mean moisture on the Cévennes box from CPS simulations is also underestimated by approximately 17% against ERA5. In addition, the CPS simulations also reproduce the position of the maximum moisture closer to ERA5, especially the CPS-HadGEM2-ES. These findings suggest that given the fact that both EUR-11 and CPS can reproduce fairly good moisture features over the Cévennes, the added values of CPS in providing realistic extreme daily and sub-daily precipitation robustly come from the increase in horizontal resolution and explicitly-resolving convective process.

4.4. Conclusion

In this chapter, I conduct three downscaling experiments with WRF version 3.8.1 in convection-permitting (CPS) resolution (approx. 3km) for two different periods

including historical (1951-1980) and current (2001-2030) climate conditions. These simulations are forced by the output of EURO-CODEX (EUR-11) simulations (approx. 12km) which were also downscaled with WRFv3.8.1 from three different Global Climate Models from CMIP5 including IPSL-CM5A-MR, HADGEM2-ES and NORESM1-M. All CPS simulations are conducted for three months in the Autumn and focus on the South of France and Mediterranean Sea. This downscaling strategy results in energy efficiency and saves time because simulations for different autumns and experiments can be run at the same time.

The results show that convection-permitting simulations reproduce more realistic extreme rainfall in terms of intensity and spatial coverage and statistical distributions compared to EURO-CORDEX simulations. This improvement is more pronounced for sub-daily extreme rainfall, for example daily maximum 3-hour rainfall. In particular, the CPSs are able to reproduce the scaling of sub-daily extreme rainfall on surface temperature at the rate of double Clausius-Clapeyron relation, which is definitely missed in EUR-11 simulations with convection parameterization scheme. These added values are consistent to other researches with convection – permitting simulations driven by reanalysis data for the different areas (Armon et al., 2019; Ban et al., 2018; Fumière et al., 2019; Kendon et al., 2012; Knist et al., 2018). I also find that the behavior of CPS simulations is modulated by their driving GCM simulations given that they share the same regional climate model. For example, the downscaling experiment of the HadGEM2-ES show the best performance compared to others at the same resolution.

Both EUR-11 and CPS simulations can reproduce the moisture transport hitting the Cévennes with slightly better agreement of CPS with ERA5 in terms of mean amount of moisture on the Cévennes box. Even though the moisture source is well presented in all simulations, only three CPS simulations are able to reproduce realistic sub-daily extreme precipitation over the Cévennes. It can be deduced that cloud-solving feature, higher resolution, better representation of complex topography and a better supply of moisture source (in terms of intensity and location of the peak) can all play a role in the added values of convection – permitting simulations.

One of the inherent problems in evaluating long simulations at hourly time scale is the uncertainty in observations (as mentioned in Ban et al., 2014). The 3-hourly observational dataset used in this research started at different times among stations. In addition, the coverage of stations, especially inside the Cévennes box, is limited only to

the southeastern part of the area. A large part in the north of Cévennes range where a lot of heavy rainfall value happened is missing (as shown by COMEPHORE data). The COMEPHORE data, which is the combination of Rader measurement and in situ observation, is also used as a solution for a better representation of spatial distribution of heavy rainfall. Even though this data also contains a lot of uncertainty which comes from poor observations and radar information because of the complex topography, its quality over the Cévennes is sufficient (as discussed in Fumière et al., 2019). However, the length of this dataset is quite short and its observation period is different from the simulations in this research.

In conclusion, convection-permitting approach appears to reproduce more realistic statistical properties of extreme daily and 3-hourly rainfall simulations compared to the EURO-CORDEX simulations, at least with the WRF model. This improvement calls for a use for climate change studies and their impacts. However, I suggest to use multi-model approach to have a better consideration in the sensitivity of this variable on different model dynamics or micro-physic schemes.

Chapter summary

Objective:

The goal of this chapter is to evaluate the added value of using convection-permitting approach in reproducing the autumn extreme daily and 3-hourly rainfall events for the south of France in regional climate simulations downscaled from GCMs.

Method:

A single regional climate model (WRFv3.8.1) is used to downscale three different EURO-CORDEX simulations to convection-permitting resolution.

Seven indices containing Rx1day, Rx3hour, distribution of wet events for daily and daily maximum 3-hour rainfall data, extreme rainfall – 2m temperature scaling (T-P scaling) and moisture source are used to evaluate the results from simulations against in-situ observations, SAFRAN and COMEPHORE data.

Results:

The convection-permitting simulations (CPS) show a better skill in reproducing the statistical properties of extreme daily and 3-hourly rainfall compared to their driving EURO-CORDEX simulations. This improvement can be partly explained by the cloud-solving feature, higher resolution, better representation of complex topography and a better supply of moisture source.

Résumé

Objectif:

L'objectif de ce chapitre est d'évaluer la valeur ajoutée de l'utilisation de l'approche par convection pour reproduire les événements pluviométriques extrêmes quotidiens et 3 heures d'automne pour le sud de la France.

Méthode:

Un modèle climatique régional unique (WRFv3.8.1) est utilisé pour réduire l'échelle de trois simulations EURO-CORDEX différentes à une résolution permettant la convection.

Sept indices contenant Rx1day, Rx3hour, la distribution des événements humides pour les données de précipitations quotidiennes et quotidiennes maximales sur 3 heures, les précipitations extrêmes - échelle de température de 2 m (mise à l'échelle TP) et la source d'humidité sont utilisés pour évaluer les résultats des simulations par rapport aux observations in-situ, SAFRAN et données COMEPHORE.

Résultats:

Les simulations permettant la convection (CPS) montrent une meilleure aptitude à reproduire les propriétés statistiques des précipitations extrêmes journalières et 3 heures par rapport à leurs simulations EURO-CORDEX. Cette amélioration peut être en partie expliquée par la fonction de résolution des nuages, une résolution plus élevée, une meilleure représentation de la topographie complexe et un meilleur approvisionnement en source d'humidité.

Chapter 5. **Influence of anthropogenic climate change on extreme precipitation events in the south of France**

5.1. Introduction

5.1.1. Objectives

This chapter investigates to what extent anthropogenic human-induced climate change might affect the behavior of extreme precipitation in the Cévennes mountain range in the south of France. I propose a twofold strategy to analyze the extremes for two different time scales:

- Analyze the change in likelihood of occurrence and intensity of extreme 3-hourly rainfall event in the Autumn in observations, convection-permitting simulations and EURO-CORDEX simulations.
- Analyze the change in likelihood of occurrence and intensity of extreme daily rainfall event in the Autumn in observations and convection-permitting simulations. This investigation complements what was concluded in Luu et al. (2018) using EURO-CORDEX simulations.

5.1.2. Observations and simulations data

In this chapter, the same set of rain gauges (as in Chapter 4) with 3-hourly data starting consistently from 1998 to 2018 is used. By the definition of the Cévennes box (as defined in Chapter 4), 23 stations within this box are selected to calculate the block maxima of 3-hourly rainfall (Rx3hour) in the autumn. Given that these stations are not completely independent from one to other and some of them may not be located at the greatest rainfall area in the Cévennes (e.g. near the edge or corner of the Cévennes box where the rainfall amount is much less than along the upwind side of the mountain range), a subsample out of these 23 stations is selected by two conditions: (i) There is no pair of any two stations with a temporal correlation of autumn block maxima of 3-hourly data greater than 0.7; (ii) The average of block maxima of each station during the period of 1998 - 2018 ranges from 40 to 70 mm. These conditions give a subsample of 13 stations inside the Cévennes box, which are shown in Figure 39. Note that these 13 stations are different from the 14 stations used in Vautard et al. (2015).

For the daily time scale, a set of autumn maximum daily rainfall at 14 stations (i.e. the same stations as in Vautard et al. (2015) and Luu et al. (2018)) ranging from 1960 to 2014 is used for the detection of change analysis. In addition, the annual global mean

surface temperature anomaly for the period of 1955 to 2018 is used as covariate of the model for detection of climate change signal in observations (as in Vautard et al., 2015). These data are explored in NASA's Goddard Institute for Space Studies (GISS)⁷ database.

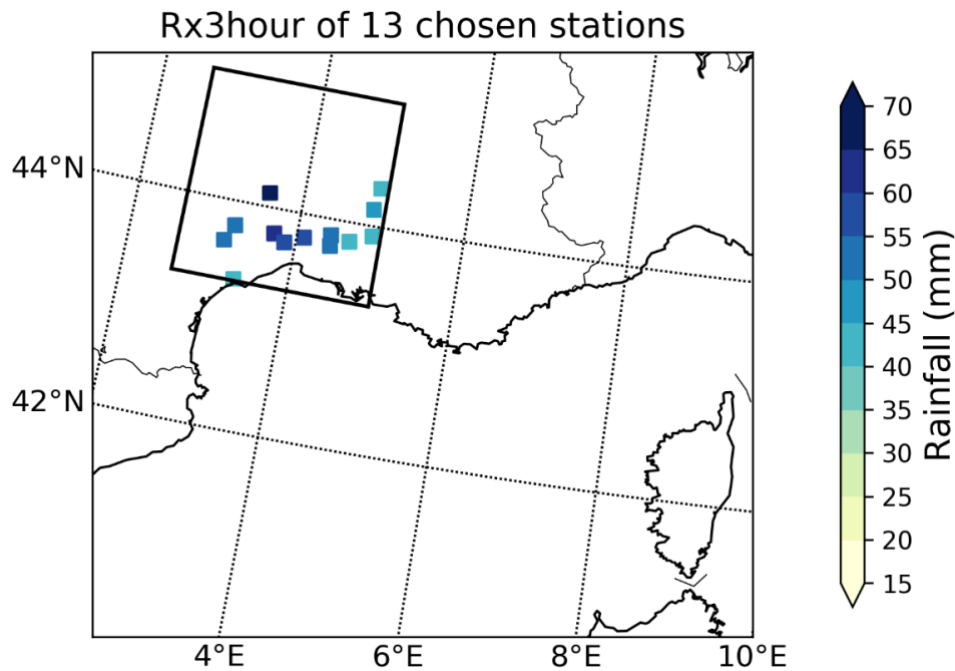


Figure 39. Location and mean of Rx3hour in the autumn for the period of 1998-2018 of 13 designated stations

Extreme rainfall simulations from two different high-resolution datasets for two periods of 1951-1980 and 2001-2030 are collected for the investigation in this chapter. The first dataset contains the state-of-the-art convection-permitting simulations with horizontal resolution of approximately 3 km which are evaluated in Chapter 4. The second dataset contains simulations from 9 different experiment runs of EURO-CORDEX with horizontal resolution of 0.11° (approx. 12km) which are downloaded from ESGF data server⁸ and collected by contacting to the research groups conducting the simulations. In fact, the number of these EURO-CORDEX simulations which are collected is larger. However, only 9 experiments whose length of 3-hourly and daily data starts at least from 1951 or earlier (i.e. to have a consistent historical period with convection – permitting simulations) are used. These EURO-CORDEX simulations are the latest and different from those used in Luu et al. (2018) in terms of models and periods used. The three EURO-CORDEX simulations driving the three convection-permitting simulations which

⁷https://data.giss.nasa.gov/gistemp/graphs/graph_data/Global_Mean_Estimates_based_on_Land_and_Ocean_Data/graph.txt

⁸<https://esgf-node.ipsl.upmc.fr/search/cordex-ipsl/>

are evaluated in Chapter 4 are included in those 9 simulations. The detail of EURO-CORDEX simulations employed in this chapter is given in Table 10 and hereafter, the convection – permitting and EURO-CORDEX simulations are abbreviated as CPS and EUR-11, respectively.

Table 10. Detail of simulations used in this chapter

No.	RCMs	GCMs	Resolution	Ensemble
1	WRF381P (Institut Pierre-Simon Laplace)	IPSL-CM5A-MR (Institut Pierre-Simon Laplace)	3 km and 12 km	r1i1p1
2		HadGEM2-ES (Met Office and Hadley Center)		
3		NorESM1-M (Norwegian Climate Centre)		
4	REMO2015 (Climate Service Center Germany GERIC)	MPI-ESM-LR (The Max Planck Institute for Meteorology)	12 km	r3i1p1
5		NorESM1-M (Norwegian Climate Centre)		
6	ALADIN63 (National Centre for Meteorological Research)	CERFACS-CNRM-CM5 (National Centre for Meteorological Research)		r1i1p1
7	CCLM4-8-17 (Climate Limited-area Modelling Community)	HadGEM2-ES (Met Office and Hadley Center)		
8		MPI-ESM-LR (The Max Planck Institute for Meteorology)		
9	HIRHAM5 (Danish Meteorological Institute)	EC-EARTH (Irish Centre for High-End Computing)		r3i1p1

5.1.3. Framing of extreme event attribution

Framing the question of extreme event attribution is important. This framing process consists of event definition, the scientific question and the choice of analysis method, which have impacts on the results of this kind of study, then consequently affect the outcomes and outreaches to the stakeholder or decision makers (Eden et al., 2018; Kirchmeier-Young et al., 2019; Otto et al., 2012). In this chapter, I first define the two different worlds (i.e. climates) including 1951 – 1980 as counterfactual world (climate), which is the world that yielded with a moderate human impact and 2001 – 2030 as factual

world (climate), which is the world we are living in with high anthropogenic emissions. It is worth noting that additional anthropogenic concentrations have been already existing in the atmosphere during the period of 1951 – 1980, therefore this period cannot be the “real” counterfactual climate, i.e. without climate change. However, we use this period as a counterfactual climate and always bear in mind that the difference in global mean surface temperature between this period and the 1900s is around 0.3°C, i.e. about one third of the current warming (based on NASA/GISS database used in this research). The event that will be analyzed is determined here as a 100-year (or 50-year) event that is estimated from station-pooling distributions (pooling 13 stations showed in Figure 39 for 3-hourly rainfall and pooling 14 stations as in Vautard et al. (2015) for daily rainfall). This means that the event has an intensity greater or equal to the return value corresponding to 100-year (50-year) return period from the distribution of counterfactual climate over the Cévennes area, when the probability ratio is discussed. And when the intensity change of 100-year event is discussed, this means the comparison of two return values corresponding to 100-year return period from the distributions of the two climates.

In this study, block maxima of daily rainfall and 3-hourly rainfall in the autumn are considered. These selections of season and time scale are the principal constraints of the event definition to convective rainfall over the Cévennes. For the spatial scale, block maxima of 3-hourly rainfall from 13 stations are pooled together. The same procedure is applied to block maxima of daily rainfall of 14 stations. Eventually, the question to be addressed in this attribution study is “Has human-induced climate change altered the likelihood and intensity of 100-year (50-year and 20-year) rainfall (e.g. both daily and 3-hourly scale) event?”

5.1.4. Method for detection and attribution

To quantify the impact of increasing in temperature (i.e. anthropogenic climate change) on the observational distribution of extreme rainfall, a non-stationary Generalized Extreme Value (GEV) distribution (Coles, 2001) is fitted to the station-pooling observations datasets (as in Eden et al., 2018; Eden et al., 2016; van der Wiel et al., 2017; Vautard et al., 2015). In this procedure, the dependence on global mean temperature is reflected in two parameters of the GEV distribution: the location (μ) and scale (σ) parameters. The probability density function (PDF) of GEV and the scaling of μ and σ by an exponential function of temperature anomaly are given below:

$$F(x) = \exp \left[- \left(1 + \xi \frac{x-\mu}{\sigma} \right)^{-\frac{1}{\xi}} \right] \quad (Eq. 1)$$

$$\mu = \mu_0 \cdot \exp \left(\frac{\alpha T}{\mu_0} \right) \quad (Eq. 2)$$

$$\sigma = \sigma_0 \cdot \exp \left(\frac{\alpha T}{\mu_0} \right) \quad (Eq. 3)$$

The parameters μ_0 , σ_0 and α are obtained from a maximum likelihood estimation, α is the linear trend of rainfall block maxima as a function of 5-year running mean of annual global mean temperature anomalies T , which is a proxy for human-induced climate change. The shape (ξ) and dispersion (σ/μ) parameters are assumed to be constant. By applying this procedure, the original distribution of observations (1998 - 2018) is then scaled to the year of 1965 and 2015 by their corresponding global mean surface temperature anomalies. These years are in the middle of two periods of simulations and can represent for those two periods, therefore they are consistent in defining factual and counter factual climate between detection of changes in observations and attribution analysis using model simulations. For the statistical significance, a non-parametric bootstrap with moving block technique is then applied with 2000 samples. In each bootstrap sample, a station is picked randomly followed by other stations that are positively correlated with it (correlation coefficient $> 1/e$). Because of the use of block maxima data, the temporal auto-correlation can be negligible.

For the attribution using model results, a stationary Generalized Extreme Value (GEV) distribution is fitted to the station-pooling from each simulation as well as the model-pooling dataset (Luu et al., 2018) for two separated periods including counter factual (1951-1980) and factual climate (2001-2030). The GEV is fitted to either raw dataset or dataset normalized by a scaling factor that is a fraction of mean of observations over mean of simulation at each station. The detail of normalization process is given in Equation (4). The procedure for quantifying the uncertainty margin remains the same as what is presented for detection in previous paragraph.

$$R_{t,m,j}^* = R_{t,m,j} \times \frac{\overline{O_{ref}}}{\overline{R_{ref,m,j}}} \quad (Eq. 4)$$

In Equation (4), \mathbf{R} and \mathbf{R}^* are rainfall value before and after normalization respectively; $\overline{O_{ref}}$ and $\overline{R_{ref,m,j}}$ are mean of observations over all stations and simulation at each station; \mathbf{m} denotes different simulations and \mathbf{t} represents for the iteration of different years in each simulation and \mathbf{j} denotes different stations. From Equation (4),

each raw simulated rainfall value at each station is shifted by a factor equivalent to the fraction of the constant mean of observations over all stations divided by the mean of simulation at that station. Because the 3-hourly rainfall is available only from 1998 to 2018, that scaling fraction is estimated by this observations period (1998 - 2018) and the factual climate of each simulation (2001 - 2030). In contrast, the two periods used for this scaling fraction for daily block maxima are 1961 – 1990 for observations and the counter factual climate 1951 – 1980 for simulations.

In addition to the stationary GEV fit technique, the empirical distribution of the station-pooling of each simulation and model-pooling datasets is used to estimate the probability of a precipitation value and the intensity of an event corresponding to a specific return period. The exceedance probability is estimated by counting the number of rainfall values in the distribution with intensity greater than the magnitude of the given event divided by length of the dataset. The intensity of an event (i.e. return value) corresponding to a specific return period is computed by simple numerical percentile method. Even though each period lasts only 30 years (i.e. 30 autumns), we can still estimate this empirical probability of rare event (e.g. 100-year event) for each simulation because we pool all stations together. This transforms the distribution of 30 values to 390 values (30 years x 13 stations) for 3-hourly rainfall.

The effect of a different climate on extreme rainfall is determined by two indices including Probability Ratio (**PR**) and Intensity Change (**IC**). The **PR** shows to what extent the event in consideration becomes more (or less) probable between the two climates. The **IC** shows how much the magnitude of an event with similar probability changes when the climate is changing. The detail of calculation of those two indices is given in the equations below:

$$PR = \frac{P_1}{P_0} \quad (Eq. 5)$$

$$IC (\%) = \frac{R_1 - R_0}{R_0} \times 100 \quad (Eq. 6)$$

In those equations, **P₁** and **P₀** are exceedance probabilities of the amount of rainfall in consideration under factual and counter factual world, respectively. The **R₁** and **R₀** denotes rainfall magnitude for a specific return period under factual and counter factual climate, respectively. For the **PR**, a value greater/lower than 1 shows the increase/decrease in frequency of the event. The value of 1 denotes that the event remains unchanged in terms of probability of occurrence between the two climates. For the **IC**, a

positive/negative value gives an increasing/decreasing trend in terms of magnitude of the event.

The **IC** and **PR** results of all individual simulations and model pooling of each ensemble (i.e. CPS or EUR-11) are then synthesized by taking the average. The confidence interval of this average number is estimated using non-parametric bootstrap technique. In this procedure, 2000 samples are randomly picked with replacement. Each sample provides **PR** or **IC** values of all simulations to estimate the average of that sample. Finally, the 95% uncertainty margin is obtained from those 2000 average values.

5.2. Investigating the change in extreme 3-hourly precipitation

5.2.1. Detecting the change in observations data

The detection of change in extreme 3-hourly precipitation event is performed by comparing return value as a function of return period curves of factual (2015) and counterfactual (1965) climate. These two curves are results of the non-stationary GEV fitted to block maxima of Rx3hour with global mean temperature anomaly as covariate. Figure 40 indicates that the likelihood of occurrence of an event with its intensity greater or equal to a 100-year return value under climate of 1965 (hereafter this will be mentioned shortly as 100-year event) increases by a factor of 1.2 under climate of 2015. However, this change is not significant with a 95% of confidence interval of 0.3 to 2.2. The probability ratio of 50-year events behaves similarly as that of 100-year event even though their uncertainty margins are trivially different (0.4 to 2.1). The intensity of these 2 events increase by similar magnitude of 5% (-22% to 27%) under climate of 2015 compared to climate of 1965.

This covariate-dependent GEV fitting method relies on the correlation of block maxima of precipitation and the increase in global mean surface temperature. Because of the short length of 3-hourly precipitation observations (21 years), this correlation is found positive (i.e. 3-hourly precipitation increases following the increase in global mean temperature) but uncertain. This leads to uncertainties in the result of detection analysis. Therefore, I cannot make a robust conclusion on this investigation.

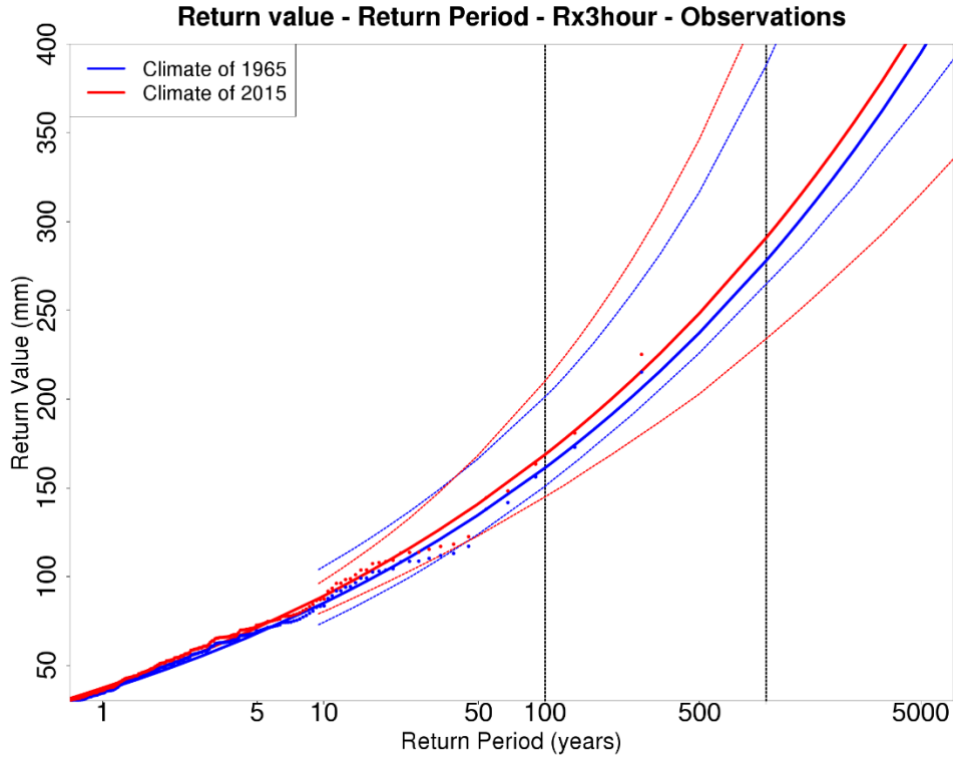


Figure 40. Return value as a function of return period obtained from non-stationary GEV fitted to block maxima of observations of Rx3hour. The blue and red curves are scaled fit of climate of 1965 and 2015, respectively. The blue/red dotted curves are 95% confidence interval of the two climates. The blue/red points are obtained by multiplying each original precipitation value with the scaling factor given in Equation 2 and 3 for the difference of global mean surface temperature between the year that precipitation value was observed and the year of 1965/2015.

5.2.2. Analyzing the change of extreme rainfall using multi-model simulations method

In this section, the stationary GEV distribution is fitted to the normalized block maxima of 3-hourly precipitation from model simulations for two different periods including 1951-1980 (counterfactual climate) and 2001-2030 (factual climate). Two sets of simulations are employed consisting of EURO-CORDEX simulations (EUR-11) with horizontal resolution of 12 km and convection-permitting simulations (CPS) with a resolution of 3 km. The higher resolution ensemble is expected to reduce the uncertainty in simulating extreme rainfall events in comparison with the coarser one. The change in intensity of 3-hourly rainfall and probability ratio is then estimated for the comparison between those two different climates. Even though the stationary GEV technique is used, I mainly discuss those two indices obtained from empirical (non-parametric) distribution rather than the fitted GEV distribution because the GEV fit is sometimes poor. In this section, only the return level – return period plots from model-pooling are shown. The

results from individual simulations are still analyzed in the syntheses plots. However, their return level – return period plots are shown in the Supplementary 0. For the discussion below, simulations will be mentioned by the syntax of RCM with information about forcing GCM in a square bracket (e.g. WRF381P [HadGEM2-ES]). The information on the ensemble (e.g. r1i1p1) is excluded here because there is no RCM driven by a GCM with two or more different members or physic schemes or initial conditions. This information in detail is synthesized in Table 10.

The return value – return period plots of 3-hourly rainfall from simulations pooling of CPSs, the three EUR-11 driving CPSs and all EUR-11 simulations are shown in Figure 41, Figure 42 and Figure 43, respectively. These figures also show that almost simulations contribute to the tail of each pooling distribution (e.g. 100-year return period but very tail like 1000-year return period). This indicates that there is no model completely dominating the heavy tail of those distributions and that all simulations can reproduce extreme rainfall values at least in their ensembles (e.g. CPS or EUR-11 ensemble). Roughly speaking, all empirical distributions of factual climate lie above those of counter factual climate. This means extreme 3-hourly rainfall tends to increase in both frequency and intensity. The detail of these changes with their confidence intervals is discussed in the next paragraphs. It can also be deduced from those figures that the normalization step (the left panel in each figure) considerably helps matching the distributions of simulations to the observations, especially for EUR-11 (see Figure 42 and Figure 43 and the Supplementary 0 for individual simulations).

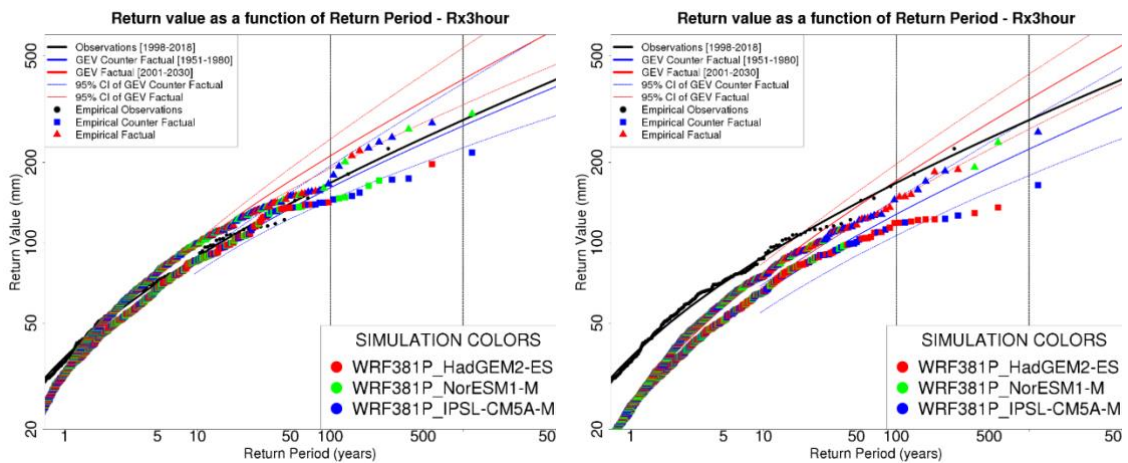


Figure 41. Return value as a function of return period of Rx3hour from the 3 convection – permitting simulations pooling; Left/right panels are normalized/raw dataset; The black/blue/red curves denote the GEV fits of Observations/Counter Factual/Factual climates; The dashed blue/red curves denote 95% confidence interval of the GEV fits of

counter factual/factual climates; The circle/square/triangle points denote precipitation values from observations/counter factual/factual climates; The different colors of points denote different simulations contributing to the pooling procedure; The name of each simulation is shortened to **RCM_GCM**.

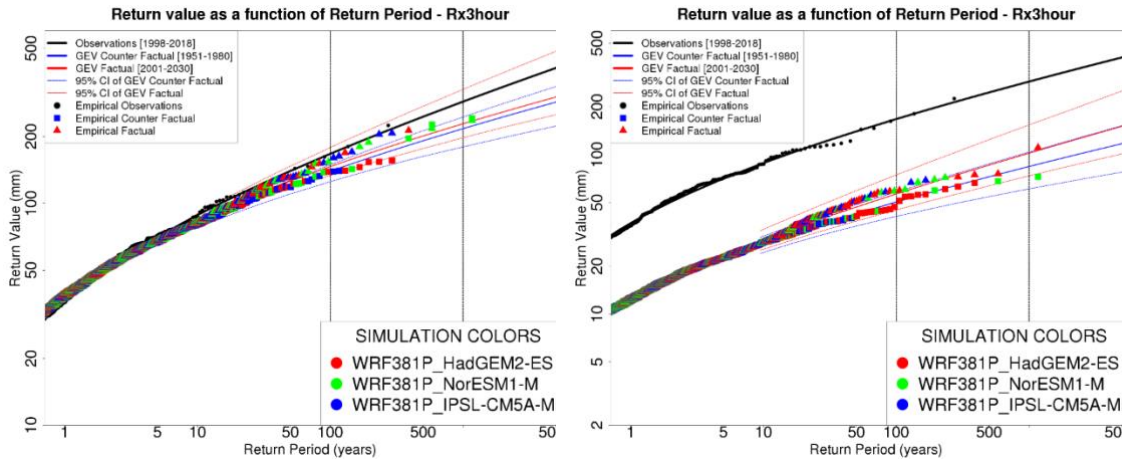


Figure 42. The same as Figure 41 but for the pooling of three EURO – CORDEX simulations driving the three convection – permitting simulations.

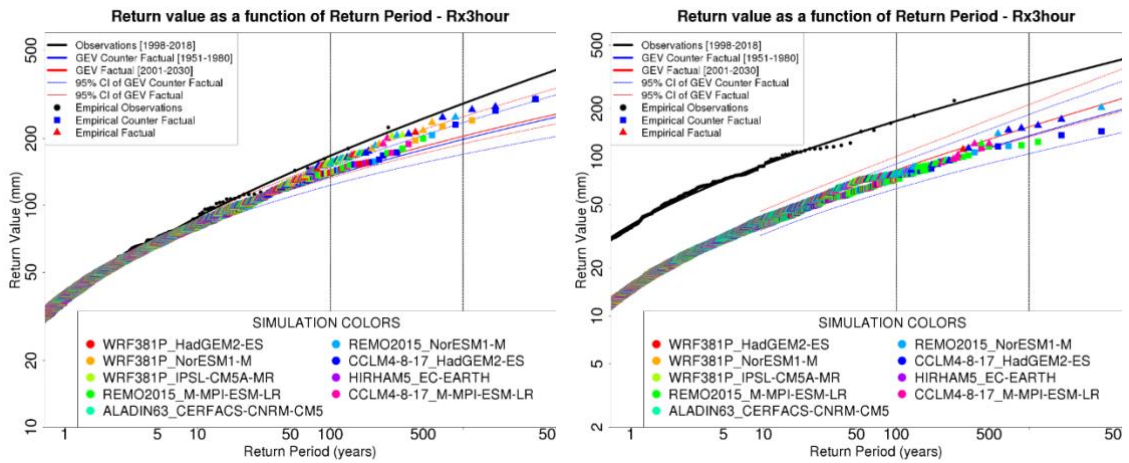


Figure 43. The same as Figure 41 but for all EURO – CORDEX simulations pooling.

The syntheses of results of Probability Ratio (**PR**) for a 100-year event from three ensembles including the CPSs, the ensemble of three EUR-11s driving CPS, and the ensemble of all EUR-11 are shown in Figure 44. Using these three ensembles enable the fair comparison between two different resolutions (i.e. between three CPSs and their three driving EUR-11s) and between two different number of members in the ensemble (i.e. nine EUR-11s and its subset of three driving CPSs). In general, the magnitudes of **PR** are slightly modified by the normalization procedure in most of the simulations. The **PR** of most of the individual simulations are not significant in either with or without normalization. However, a few simulations from EUR-11 ensemble obtain significant reduction in uncertainty margin after being normalized, for instance the WRF381P

[HadGEM2-ES] and REMO2015 [MPI-ESM-LR]. Therefore, hereafter, I will discuss only the results from normalized ensemble. The results of raw dataset can be referred to the Supplementary 0. The average of **PR** of all simulations and model pooling from CPS ensemble suggests that the 100-year event is 2.5 times more likely in the factual climate with its confidence interval of 1.6 to 4.3. Results from average of all EUR-11 simulations and of only three EUR-11 simulations show similar trend that the event is more likely with PR values of 1.7 (1.3 to 2.6) and 1.8 (1.3 to 3.3). By comparing the results of CPSs and their three driving EUR-11, it indicates that higher resolution produces a clearer signal in probability ratio. On the other hand, by comparing an ensemble of the three EUR-11 and all EUR-11, a larger ensemble makes the results more robust by narrowing the uncertainty margin.

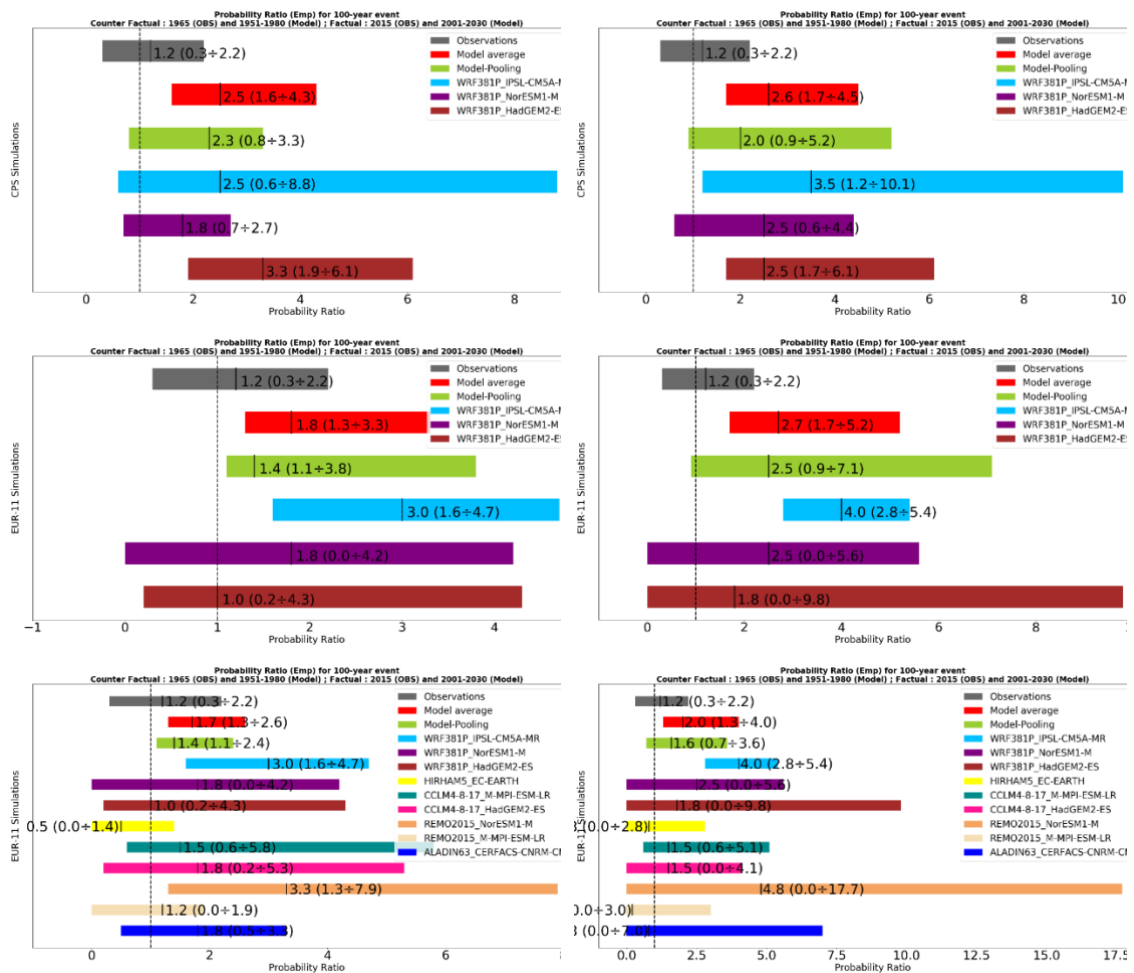


Figure 44. The syntheses of Probability Ratios of Rx3hour for 100-year event from model pooling and individual simulations; the top row shows results of the three CPS simulations; the middle row shows results of the three EUR-11 simulations driving the three CPSs; the bottom row shows results of all EUR-11 simulations; the left column shows results of normalized ensembles; the right column shows results of raw ensembles.

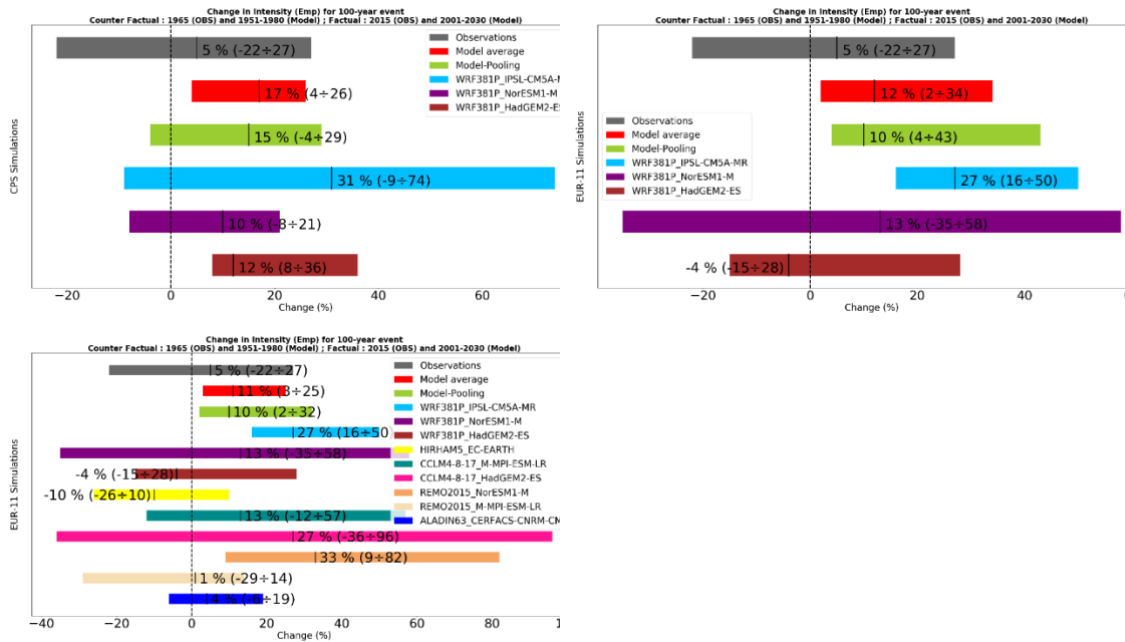
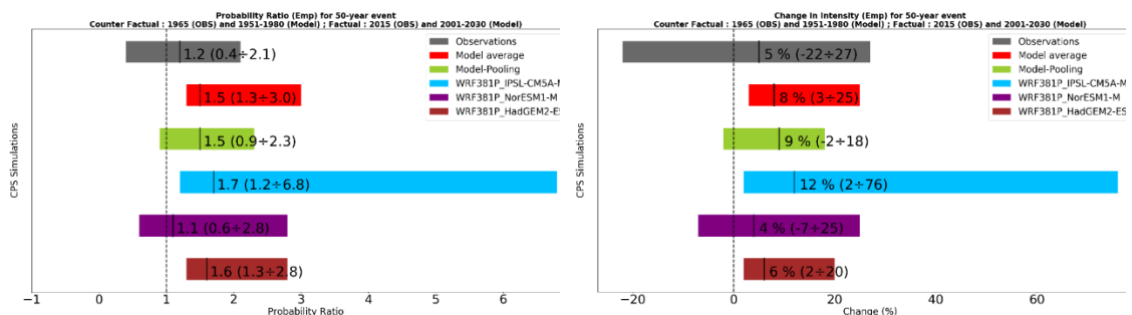


Figure 45. The syntheses of Intensity change of Rx3hour for 100-year event from model pooling and individual simulations after normalization; the top left panel shows results of CPS ensemble; the top right panel shows results of the three EUR-11 driving CPSs; the bottom left shows results of all EUR-11 simulations.

The changes in intensity of the 100-year event of 3-hourly rainfall in the Cévennes area between factual and counter factual climate is shown in Figure 45. The results of CPS ensemble (Figure 45 top left panel) indicate that all simulations and the model pooling generate an increasing trend in intensity of 100-year event, but only WRF381P [HadGEM2-ES] has statistical significance. The model average shows a 17% (4% to 26%) increase in the magnitude of the event under factual climate. The simulations from EUR-11 ensemble also show an increasing trend of intensity of 3-hourly rainfall, except WRF381P [HadGEM2-ES] and HIRAM5 [EC-EARTH] which show negative intensity change (IC). The average ICs of the three EUR-11 driving CPSs and all EUR-11 are 12% (2% to 34%) and 11% (3% to 25%), respectively. All of those changes are significant and they are similar to PR analysis that CPS simulations produce more substantial signal and a larger ensemble reduces considerably the uncertainty margin.



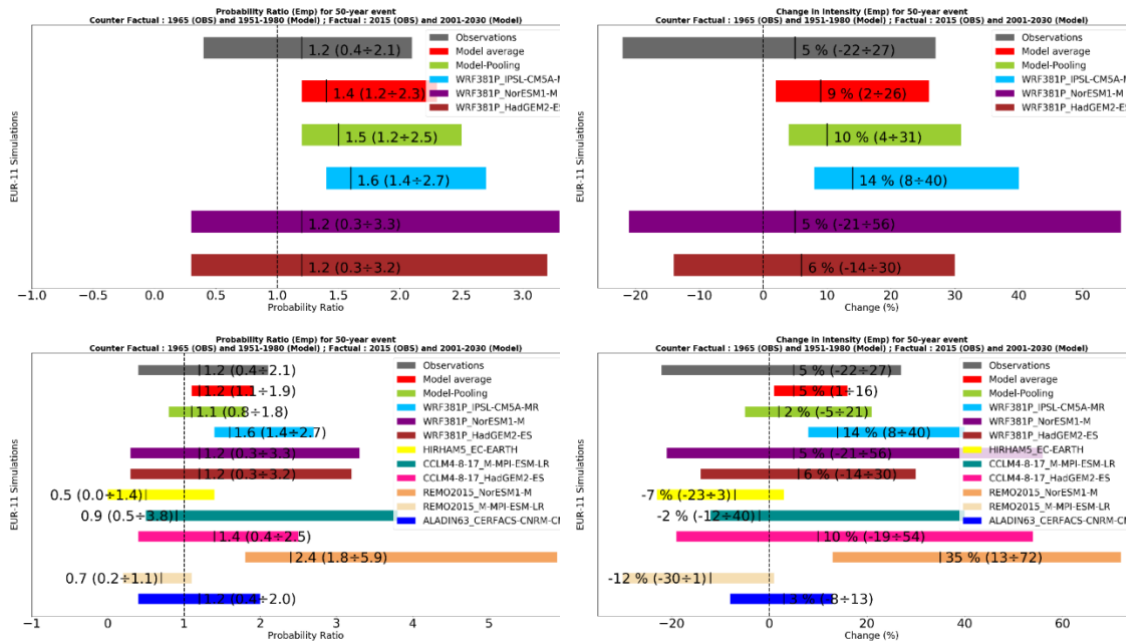


Figure 46. The syntheses of Probability Ratio (left column) and Intensity change (right column) of Rx3hour for 50-year event from model pooling and individual simulations after normalization; the top row shows results of the three CPS simulations; the middle row shows results of the three EUR-11 simulations driving the three CPSs; the bottom row shows results of all EUR-11 simulations.

The Probability Ratio (**PR**) and Intensity Change (**IC**) between the factual and counterfactual climates from all normalized ensembles are shown in Figure 46 for the 50-year event. All CPS simulations including three individual members and a model pooling dataset show that the 50-year event increases in both intensity and probability of occurrence under factual world. However, the results from model pooling and WRF381P [NorESM1-M] are not significant. The average **PR** and **IC** of this ensemble are 1.5 (1.3 to 3) and 8% (3% to 25%), respectively. For EUR-11 ensemble, most of simulations show **PRs** greater than 1 and positive **IC** values, except the HIRAM5 [EC-EARTH] and the two regional models including CCLM4-8-17 and REMO2015 driven by MPI-ESM-LR. However, these results are almost not statistically significant, except the WRF381P [IPSL-CM5A-MR] and the REMO2015 [MPI-ESM-LR]. The average of **PRs** of the three EUR-11 simulations driving the CPSs and all simulations ensemble are 1.4 (1.2 to 2.3) and 1.2 (1.1 to 1.9), respectively. The former ensemble shows 9% (2% to 26%) increase in intensity of the 50-year event and the latter ensemble shows smaller increase of 5% (1% to 16%) in intensity of the event. For this 50-year event, a less rare event compared to the 100-year event, we do not find any clear difference in average **IC** and **PR** between CPS ensemble and the three EUR-11 driving the CPSs. However, we still find that the larger EUR-11 ensemble can provide a smaller confidence interval. By comparing to the

100-year event, we find that the change in intensity and frequency of extreme 3-hourly rainfall is larger for rarer event under the factual climate.

5.3. Revisiting extreme daily precipitation

The question of how climate change affects the likelihood of occurrence and intensity of daily rainfall event over the Cévennes has already been addressed in Luu et al. (2018) and the Chapter 2 of this manuscript using EURO-CORDEX simulations. In this section, this question is re-considered by using state-of-the-art convection-permitting simulations. The comparison of the extreme daily rainfall distributions between climate of 1965 and 2015 from observations is shown in Figure 47. This return level – return time plot shows an obvious changing signal between the two climates. Specifically, the 100-year event is intensified by 26.7 % [19% to 30%] under the climate of 2015. The change in intensity of 50-year event remains similar to 100-year event. In terms of frequency, a warmer 2015 climate makes the 100-year event 3.5 times more likely with the confident interval of 2.8 to 3.9. The Probability Ratio (**PR**) of 50-year event is 3.1 [2.5÷3.4]. All of those changes are statistically significant.

The analysis of return level – return period of extreme daily rainfall using normalized convection-permitting simulations pooling is given in Figure 48. This figure indicates that all individual simulations contribute to the heavy tail of the pooling distribution (e.g. 100-year event). The increase in intensity and probability of extreme daily event can be inferred from Figure 49. The model-pooling and two other individual simulations including WRF381P [IPSL-CM5A-MR] and WRF381P [HadGEM2-ES] produce increasing trend for both frequency and intensity of the 100-year event. However, only WRF381P [IPSL-CM5A-MR] shows significant results with the **PR** of 3.6 (3 to 6.7) and the **IC** of 43% (17% to 61%). The WRF381P [NorESM1-M] reduces the intensity and lowers the probability of occurrence of the event under factual climate. However, none of these changes is statistically significant at 95% confidence interval. In average, the CPS simulations produce the 100-year event of daily rainfall over the Cévennes 2 times (1.6 to 3.1) more likely and intensify the event by 19% (4% to 24%). These changes are significant, consistent but lower than what is found from observations analysis.

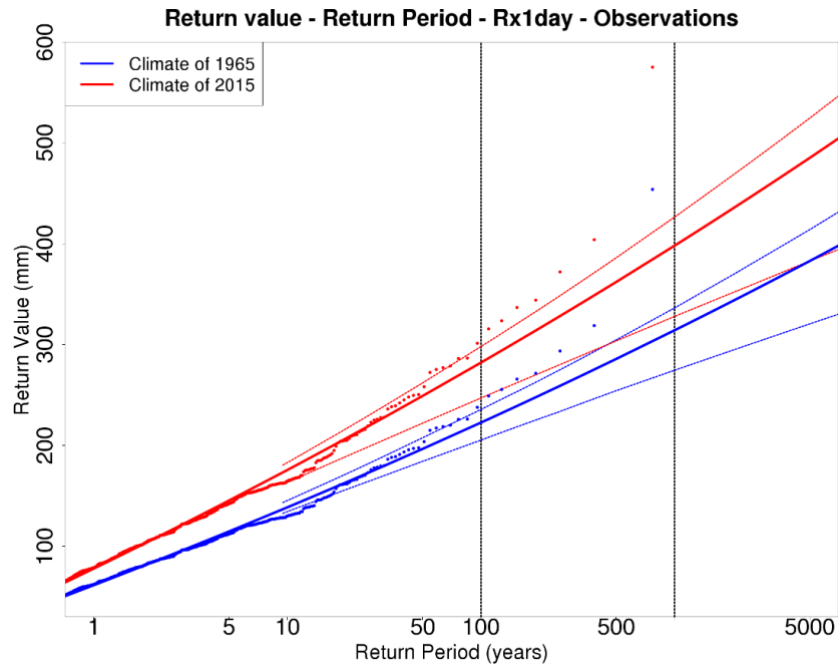


Figure 47. Return value as a function of return period obtained from non-stationary GEV fitted to block maxima of observations of Rx1day. The blue and red curves are scaled fit of climate of 1965 and 2015, respectively. The blue/red dotted curves are 95% confidence interval of the two climates. The blue/red points are obtained by multiplying each original precipitation value with the scaling factor given in Equation 2 and 3 for the difference of global mean surface temperature between the year that precipitation value was observed and the year of 1965/2015.

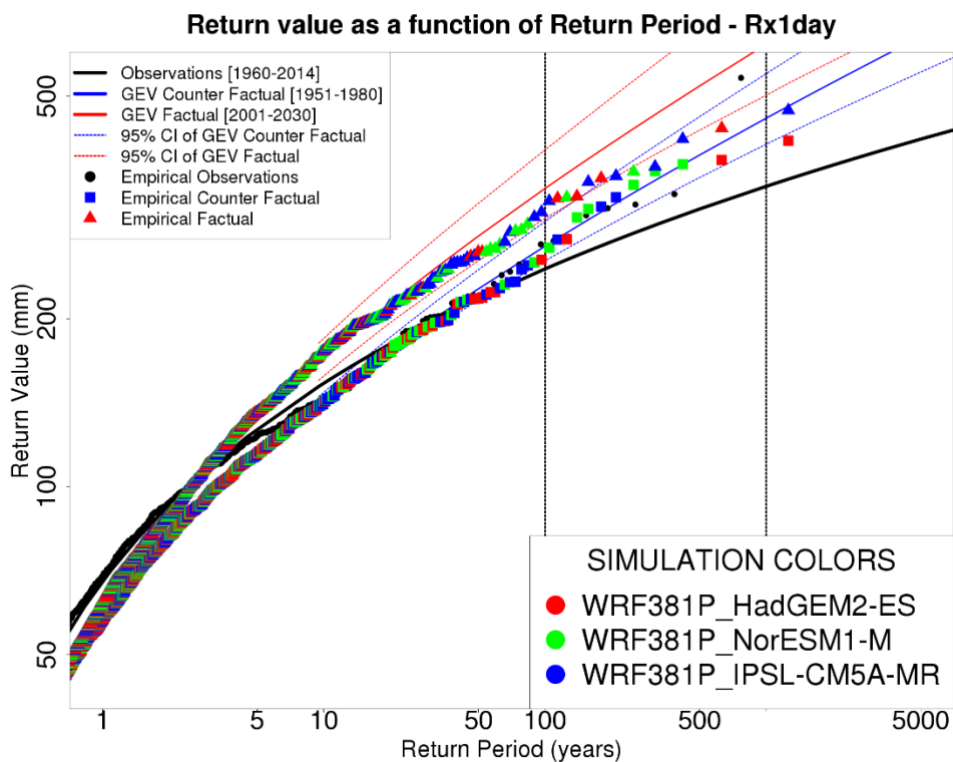


Figure 48. Return value as a function of return period of Rx1day from the three normalized convection – permitting simulations pooling; The black/blue/red curves

denote the GEV fits of Observations/Counter Factual/Factual climates; The dashed blue/red curves denote 95% confidence interval of the GEV fits of counter factual/factual climates; The circle/square/triangle points denote precipitation values from observations/counter factual/factual climates; The different colors of points denote different simulations contributing to the pooling procedure.

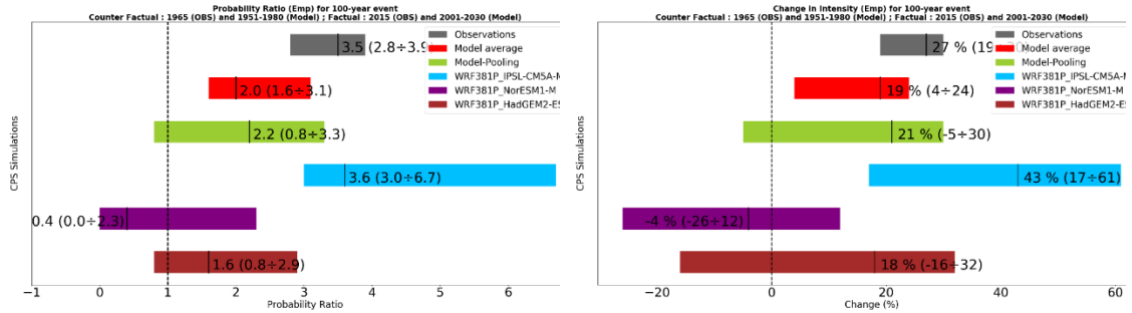


Figure 49. The syntheses of Probability Ratio (left) and Intensity change (right) of $Rx1day$ for 100-year event from normalized CPS simulations.

5.4. Discussion

In this chapter, the detection of change in probability and intensity of extreme daily and 3-hourly rainfall is investigated from in situ observations dataset. We only find clear and statistically significant increase for extreme daily rainfall event. The lack of statistical confidence in the detection analysis for 3-hourly rainfall data could come from the short length of observations data (i.e. only 21 years). The lack of data leads to an insignificant linear trend of extreme 3-hourly rainfall. We also find that the changes in both likelihood and intensity remain similar for different return periods for example a 100-year or less rare event. Imposing a multiplicative scaling of exponential function to location and scale parameters shifts the distribution upward in a warmer climate that makes the change in intensity and probability ratio independent on magnitude of the event.

The three convection – permitting simulations produce larger changes in the heavy tail (e.g. 100-year return period) of the distribution of 3-hourly rainfall in comparison with the three EURO – CORDEX simulations driving them. This larger signal is reliable because the CPSs with their higher resolution and ability to solve explicitly deep convection process can reproduce extreme 3-hourly rainfall with better agreement with observations compared to those three EUR-11 simulations (Chapter 4). We also find that the internal variability of WRF strongly affects the attribution results by forcing different boundary conditions to the CPS simulations. Given this fact and the fact that a larger ensemble can help reducing the uncertainty margin, the attribution can

be more robust if a larger ensemble of different regional models driven by different global models can be used.

Even though there are confirmations of improvement in extreme sub-daily precipitation simulations for some areas in Europe from EURO-CORDEX experiments (e.g. Dyrddal et al., 2018; Prein et al., 2016) and convection-permitting simulations (e.g. Ban et al., 2018; Fumière et al., 2019), we cannot avoid the systematic error in the simulations. This shortcoming leads to the uncertainty in Probability Ratio and Intensity Change for both CPS and EUR-11 simulations in this study. Therefore, an application of bias correction or ensemble calibration methods is then suggested to obtain more reliable results in attribution studies and climate change impact studies (Bellprat and Doblas-Reyes, 2016; Sippel et al., 2016). The enhancement in extreme event attribution by using bias-corrected simulations is also proved in Luu et al. (2018) or Bellprat et al. (2019).

5.5. Conclusion

In this chapter, the question of how climate change affects extreme 3-hourly and daily rainfall event over the Cévennes mountain range is addressed using two ensembles of simulations including convection-permitting (3-km) and EURO-CORDEX (12-km) simulations. The detection of change in probability and intensity of extreme rainfall is also conducted for observations.

The results from observations analysis show that the change in intensity and likelihood of daily rainfall between climate of 1965 and climate of 2015 are clear and significant. However, this signal in 3-hourly rainfall event is less significant. This comes from the difference in length of observations data of the two durations that leads to different confidence in estimating the trend of daily/3-hourly rainfall as a function of the increasing surface temperature, probably due to a larger variability in 3-hourly events.

The CPS simulations shows larger change in intensity and frequency of 100-year event of 3-hourly rainfall compared to EUR-11. This difference comes from the better reproduction of 3-hourly rainfall distribution as shown in Chapter 4. In addition, the change in daily rainfall is found clear, significant and consistent with what was found in Luu et al. (2018). However, these changes in daily rainfall are smaller than what was found in the analysis of observations. Given that the CPS simulations reproduce well the scaling of extreme daily/3-hourly rainfall on the increase in surface temperature (Clausius – Clapeyron/double Clausius – Clapeyron) and that the increase in global mean

temperature is the response of climate system to anthropogenic emission on most simulations (except the ALADIN63 with changing in aerosol), the change in probability and intensity of extreme rainfall, especially the 3-hourly time scale, in the Cévennes can be attributed to human-induced climate change.

We also find that a large model ensemble plays important role in the significance of attribution result. This suggests that a more robust conclusion can be made if more CPS simulations with different RCMs and GCMs are used.

Chapter summary

Objective:

This chapter investigates to what extent anthropogenic human-induced climate change might alter the intensity and likelihood of occurrence of extreme precipitation (3-hourly and daily) in the Cévennes mountain range in the south of France.

Method:

The impact of anthropogenic climate change on observed extreme precipitation in daily and 3-hourly scale is detected by using a Generalized Extreme Values (GEV) model with global mean temperature anomalies as covariate. Then the attribution of those detected climate change signal is done by using two ensembles of simulations including EURO-CORDEX (12-km) and convection-permitting simulations (3-km).

Results:

In observations, the climate change signal is only found for daily rainfall rather than 3-hourly rainfall in the observations-based analysis, due to too short observational records. By contrast, models exhibit a clear signal in sub-daily precipitation: the syntheses of CPS and EUR-11 ensemble show that the 100-year 3-hourly rainfall event increases under the impact of anthropogenic climate change with larger signal from CPS ensemble than for EUR-11. The analysis for daily rainfall using CPS simulations obtain similar results to sub-daily event. These changes are statistically significant.

Résumé

Objectif:

Ce chapitre examine dans quelle mesure le changement climatique anthropique d'origine humaine pourrait modifier l'intensité et la probabilité d'occurrence de précipitations extrêmes (3 heures et quotidiennes) dans le massif des Cévennes, dans le sud de la France.

Méthode:

L'impact du changement climatique anthropique sur les précipitations extrêmes observées à l'échelle quotidienne et à l'échelle de 3 heures est détecté en utilisant un modèle de valeurs extrêmes généralisées (GEV) avec des anomalies de température moyenne globale comme covariable. Ensuite, l'attribution de ces signaux de changement climatique détectés est effectuée en utilisant deux ensembles de simulations comprenant EURO-CORDEX (12 km) et des simulations permettant la convection (3 km).

Résultats:

Le signal de changement climatique n'est trouvé que pour les précipitations quotidiennes plutôt que pour les précipitations de 3 heures dans l'analyse basée sur les observations. Les synthèses de l'ensemble CPS et EUR-11 montrent que l'événement pluviométrique de 100 ans sur 3 heures augmente sous l'influence du changement climatique anthropique avec un signal plus important de l'ensemble CPS. L'analyse des précipitations quotidiennes à l'aide de simulations CPS permet d'obtenir des résultats similaires à ceux d'un événement sous-quotidien. Tous ces changements sont statistiquement significatifs.

Chapter 6. Conclusion and Perspectives

6.1. Conclusion

The ultimate goal of this PhD is to quantify the role of human-induced climate change on the autumn convective extreme precipitation event in the south of France. This goal is divided into two main tasks including the model simulations and the attribution of extreme convective precipitation event to anthropogenic climate change. The former part is given in Chapter 3 and Chapter 4, while the latter part is investigated in Chapter 2 and Chapter 5. This conclusion will summarize the novel achievements that are obtained through every single chapter.

In Chapter 2, I collect three ensembles of EURO-CORDEX simulations including a coarse horizontal resolution (approx. 50km, EUR-44), a finer resolution (approx. 12km, EUR-11) and a bias-corrected version of the EUR-11. These simulations are evaluated against in situ observations and then used to investigate how human-induced climate change modulate the probability and intensity of extreme daily rainfall event. I show that anthropogenic climate change leads the 100-year event in the counterfactual climate to become 2.6 (2.2 to 3.9) times more likely and 11% (5% to 20%) intensified according to the bias-corrected EUR-11. I also suggest that convection-permitting simulation can be employed to obtain further improvements in attribution event, especially the sub-daily time scale event.

Chapter 3 and Chapter 4 are designed to set up and evaluate long climate simulations at convection-permitting resolution. In Chapter 3, I propose four configurations of convection-permitting resolution to simulate the autumn of 2014 when several heavy precipitation events were observed over the Cévennes mountain range. These four configurations share the use of the WRF model, a EURO-CORDEX parent domain driven by the ERA-Interim and all physics schemes except the size and position of the domain. I find that these convection-permitting models primarily show added value in reproducing observed extreme event where explicitly resolving the convection process can play a role. The results also show the influence of boundary condition on the domain that is small or close to the boundary. Finally, these testing configurations help choosing an optimal domain among four options (at least in the framework of this PhD) that will be used to conduct long simulations at convection-permitting resolution. Chapter 4 uses the optimal configuration that is selected in the conclusion of Chapter 3 to downscale the

three EURO-CORDEX simulations from the resolution of 12 km to 3 km. These EURO-CORDEX simulations were done by WRF model driven by three different CMIP5-GCMs including IPSL-CM5A-MR, HADGEM2-ES and NORESM1-M. Each downscaling experiment is done for two separated periods including 1951-1980 and 2001-2030, focus on the French Mediterranean area and the autumn. I show that the reproduction of statistical properties of extreme rainfall, especially in sub-daily time scale, over the Cévennes is substantially improved by convection-permitting model. The improvement can be contributed by a finer resolution, elaborate complex topography, the explicitly-resolving convection process and enhancement in moisture transport to the Cévennes area.

Chapter 5 fulfills my PhD ultimate goal by investigating the extent to which human-induced climate change alter the probability and intensity of extreme 3-hourly rainfall over the Cévennes using the three convection-permitting simulations obtained in Chapter 4 and another ensemble of EURO-CORDEX simulations with the horizontal resolution of 0.11 degree. This ensemble contains latest version of EURO-CORDEX, which is different from what were used in Chapter 2. In addition, this chapter revisits the question posed in Chapter 2 about extreme daily rainfall using the same set of convection-permitting simulations. I find that human-induced climate change plays a role in the change in probability and intensity of extreme daily/sub-daily rainfall. These changes are more or less consistent between the two different time scale (daily and 3-hourly scale).

The innovative achievement of this PhD, to the best of my knowledge, is the use of convection-permitting simulations in extreme event attribution study for the first time. This PhD brings me the chance to learn a new field science that engages a specific meteorological event to the general appreciation of influence of human-induced climate change through using statistical method. In addition, I have an opportunity to manage and make several long climate simulations with regional climate model at convection-permitting resolution that require a lot of effort in designing, finding optimal configuration to save computer resource and monitoring the experiments. This gives me valuable experiences in a state-of-the-art climate modelling approach that is expected to develop considerably in the future. The combination of these two big tasks in this PhD subject also brings me some new perspectives that will be presented in the next section.

6.2. Perspectives

Extreme event attribution study aims at quantifying the degree to which human-induced climate change influences the probability and intensity of the observed event. Even though the further outreach of this type of study is under debate, it is worth to conduct the study, at least, to enlarge the scientific understanding on the causality of extreme event, especially in the context of climate change. In addition to the risk-based approach used in this PhD, the storyline approach will bring a different point of view to the cause and effect of human-induced climate change and heavy rainfall relationship. This aims at highlighting how climate change may alter the large-scale atmospheric circulation leading to the heavy rainfall event, or how heavy rainfall may change in terms of probability and intensity conditional upon the same atmospheric circulation between the two different climates (e.g. counterfactual and factual climates). This approach requires a large domain of climate simulation which is a potential hurdle in running convection-permitting model. However, with the significantly improved performance of graphic processing unit (GPU) in high-resolution climate simulation test compared to the conventional CPU (Demeshko et al., 2013; Fuhrer et al., 2018), the possibility of this experiment become more obvious.

The downscaling strategy used in this PhD dissertation has showed advantages in saving computing resource meanwhile reproduced high-quality simulations for the French Mediterranean. This suggests that the approach can be applied to other Mediterranean coastal area where the mechanism of heavy precipitation events in the autumn is similar (e.g. Italy or Spain). In addition, the advantages of convection-permitting model provided in this PhD may shed the new light on how weather and climate extreme event may respond to a warming climate in the future. Given the capability of the model in capturing heavy rainfall in the past climate, sufficient confidence can be obtained in analyzing the change of this extreme event in future climate projection. The multi-model ensemble approach can be used to reduce the uncertainty, limitations and the lack of other factors (e.g. aerosol) in climate models.

The impact of heavy rainfall event becomes worse when it interacts with other hazards (e.g. storm surge). Bevacqua et al. (2019) shows that the compound flooding event over the Mediterranean coasts is the most probable in the current climate and is expected to become more likely in the future. Other studies also found similar results for different areas (Bevacqua et al., 2017; Wahl et al., 2015). However, the formal link

between this increase in probability of this compound flooding and human-induced climate change is remaining scarce or even lacking. Therefore, attribution of this compound event can be a direction that can share the approach with the research study targeted in this PhD subject.

Supplementary for Chapter 4

12 Heaviest Daily Rainfall Events from Observation Season: SON ; Period: 1989-2018

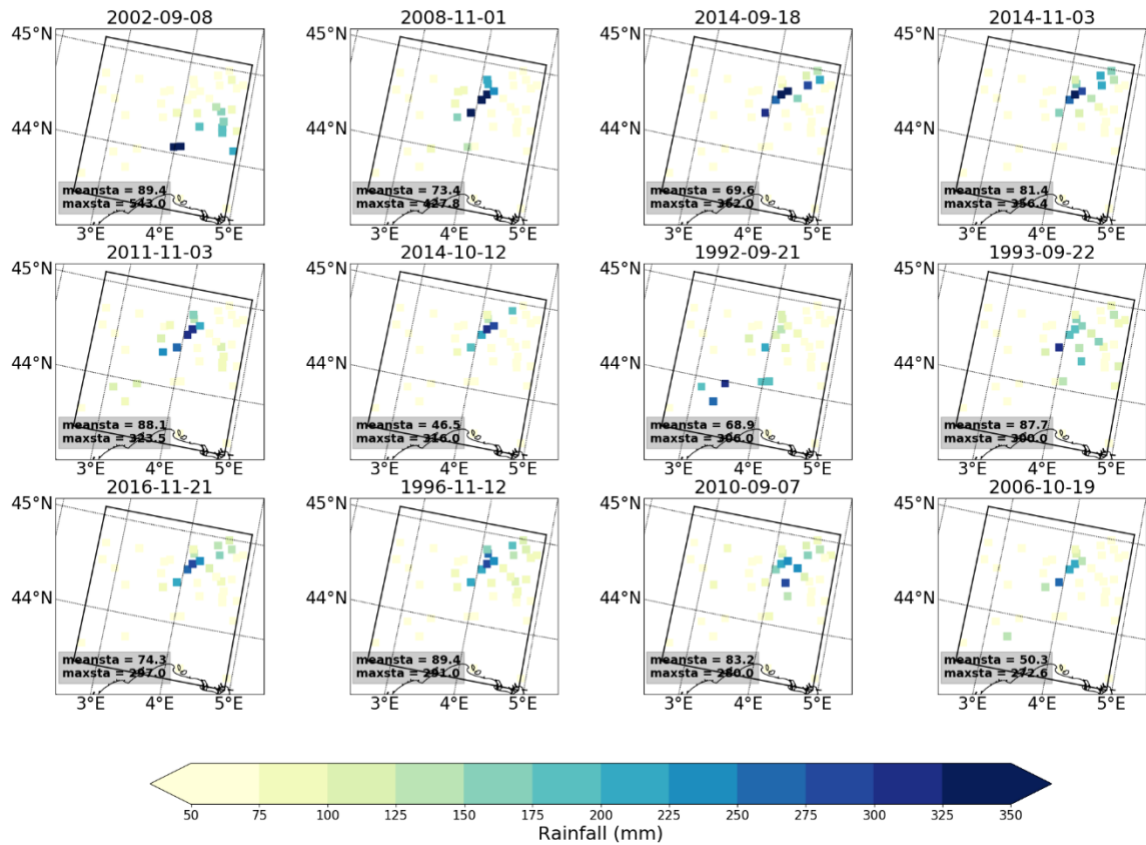


Figure 50. The 12 heaviest daily precipitation events occurring in the Cévennes box from in situ observations in the period of 1989 – 2018

**12 Heaviest Daily Rainfall Events from CPS-IPSL-IPSL-CM5A-MR_r1i1p1_IPSL-WRF381P
Season: SON ; Period: 2001-2030**

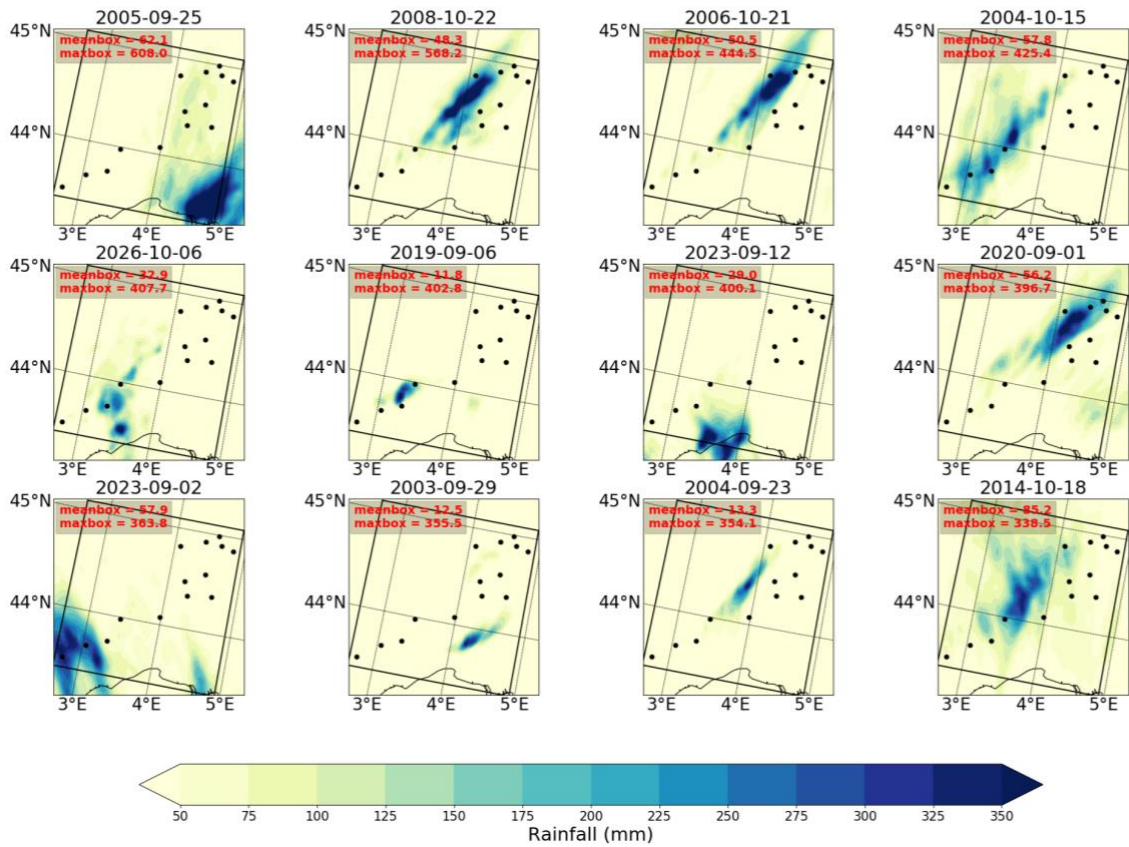


Figure 51. The 12 heaviest daily precipitation events occurring in the Cévennes box from CPS_IPSL-IPSL-CM5A-MR_r1i1p1_IPSL-WRF381P (3 km) in the period of 2001 – 2030

**12 Heaviest Daily Rainfall Events from CPS-MOHC-HadGEM2-ES_r1i1p1_IPSL-WRF381P
Season: SON ; Period: 2001-2030**

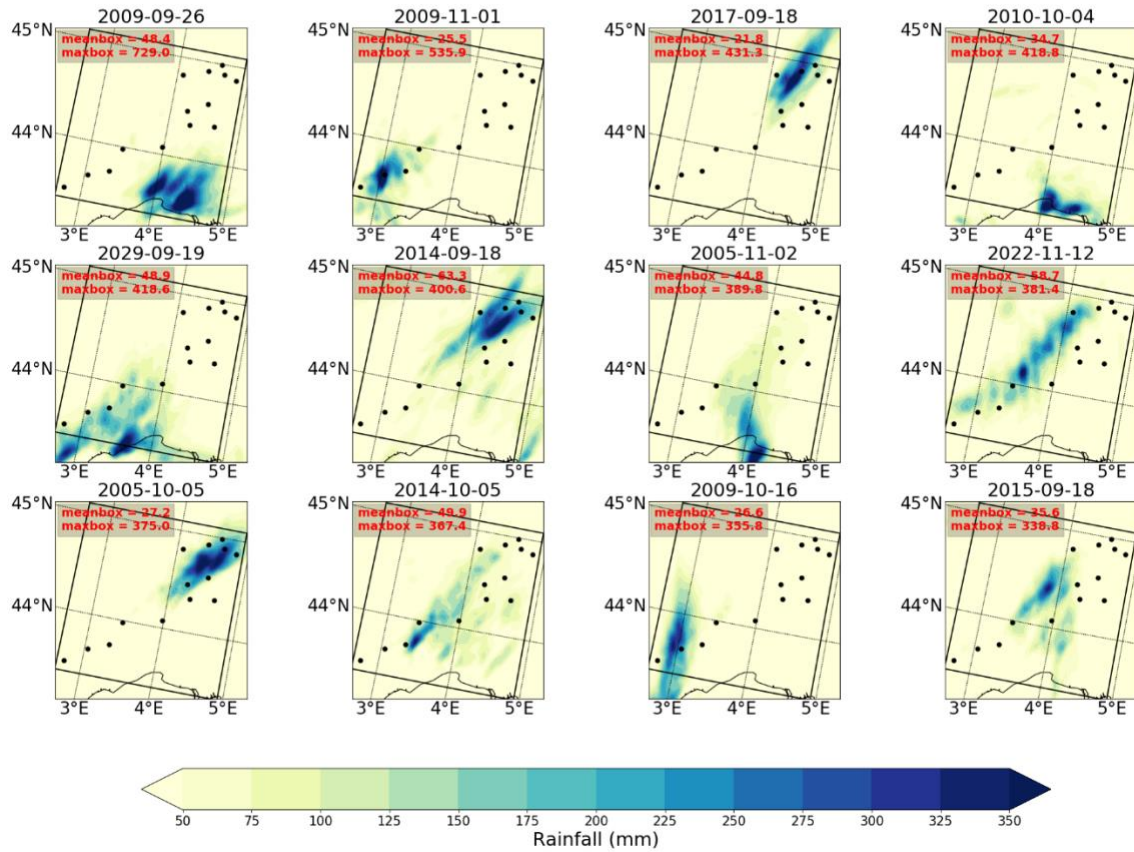


Figure 52. The 12 heaviest daily precipitation events occurring in the Cévennes box from CPS_MOHC-HadGEM2-ES_r1i1p1_IPSL-WRF381P (3 km) in the period of 2001 – 2030

**12 Heaviest Daily Rainfall Events from CPS-NCC-NorESM1-M_r1i1p1_IPSL-WRF381P
Season: SON ; Period: 2001-2030**

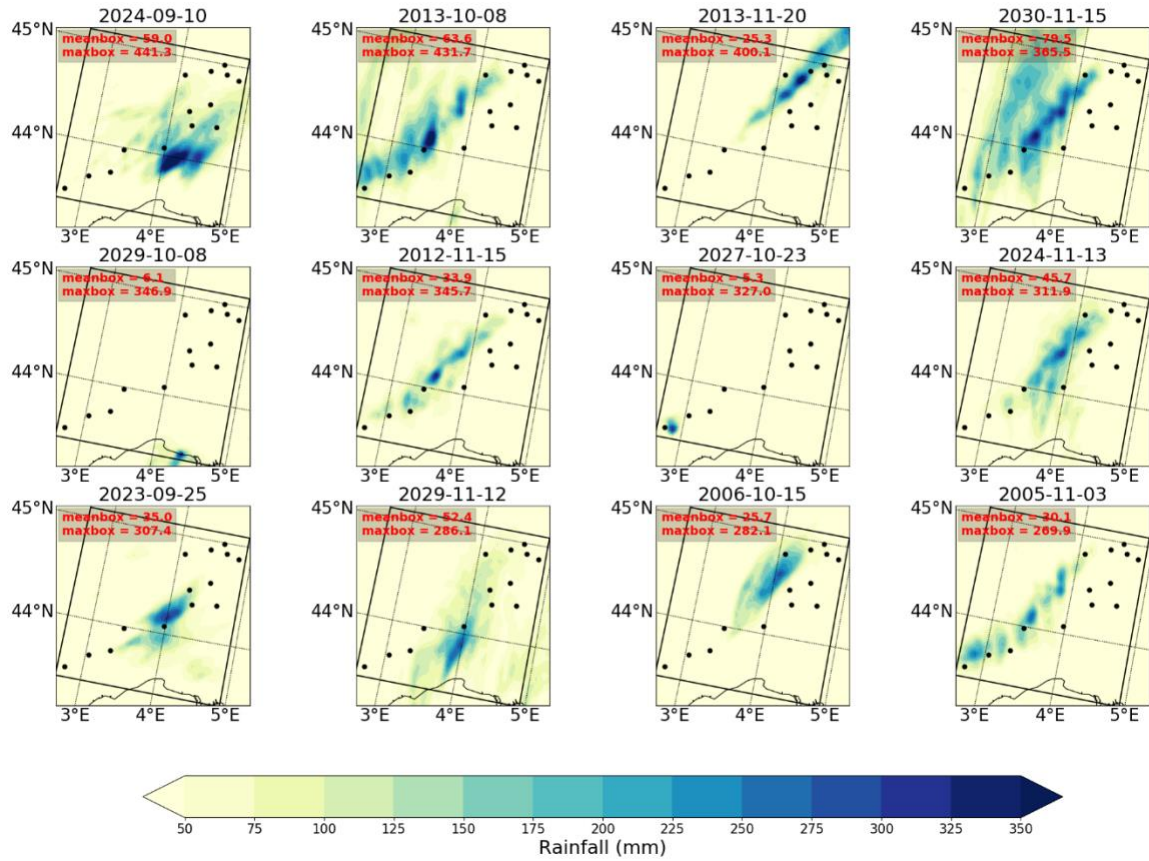


Figure 53. The 12 heaviest daily precipitation events occurring in the Cévennes box from CPS_NCC-NorESM1-M_r1i1p1_IPSL-WRF381P (3 km) in the period of 2001 – 2030

**12 Heaviest Daily Rainfall Events from EUR-11-IPSL-IPSL-CM5A-MR_r1i1p1_IPSL-WRF381P
Season: SON ; Period: 2001-2030**

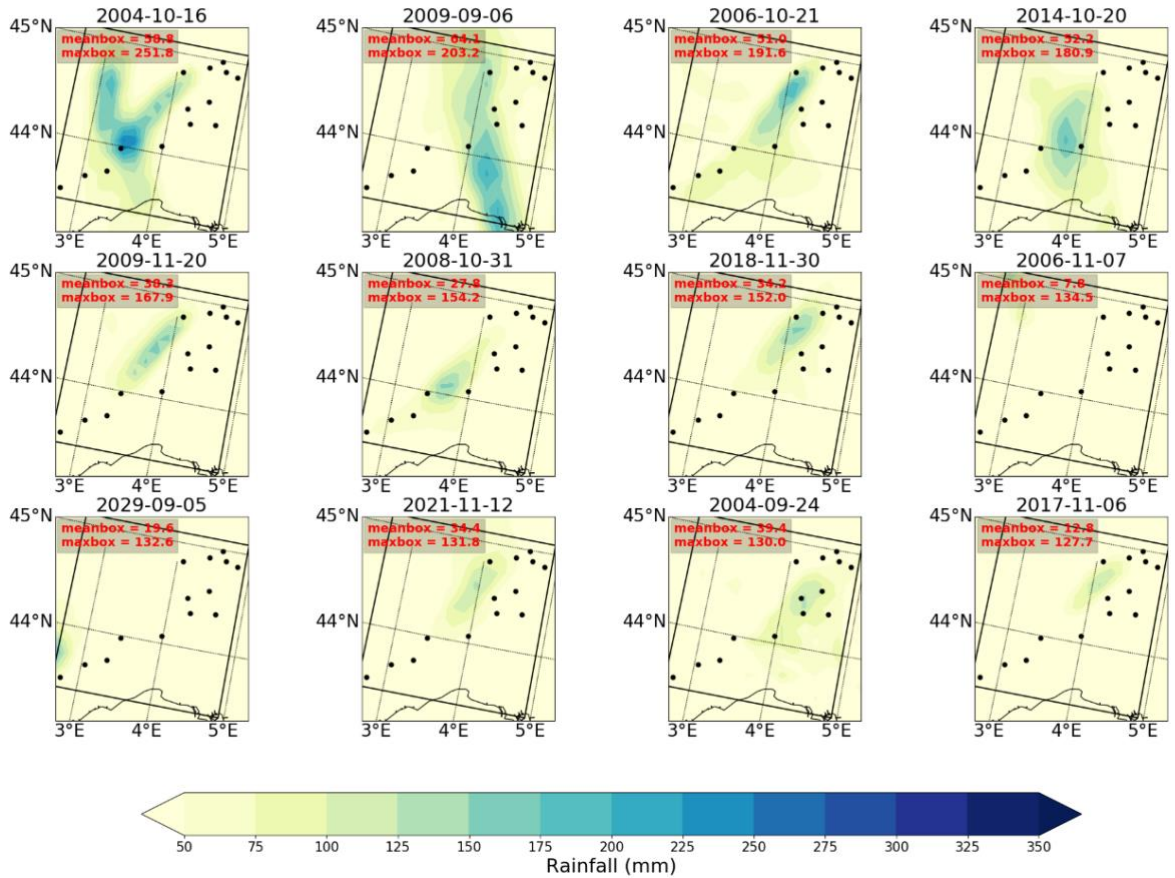


Figure 54. The 12 heaviest daily precipitation events occurring in the Cévennes box from EUR-11_IPSL-IPSL-CM5A-MR_r1i1p1_IPSL-WRF381P (12 km) in the period of 2001 – 2030

**12 Heaviest Daily Rainfall Events from EUR-11-MOHC-HadGEM2-ES_r1i1p1_IPSL-WRF381P
Season: SON ; Period: 2001-2030**

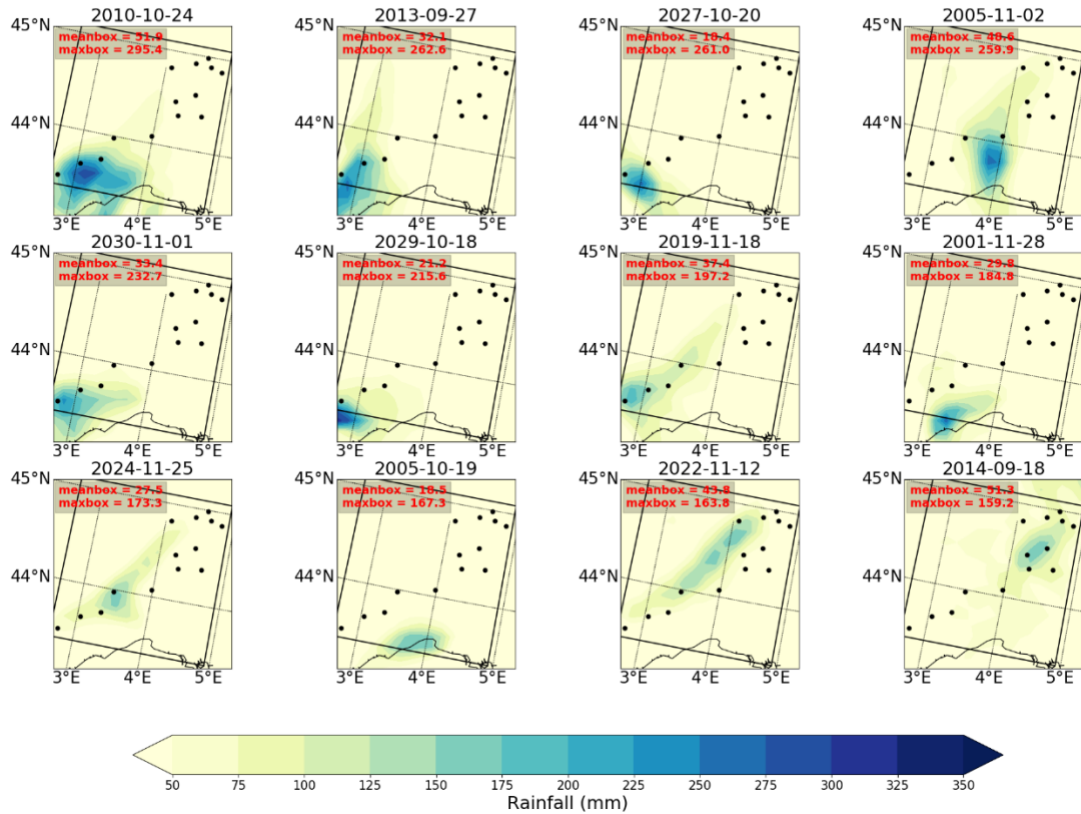


Figure 55. The 12 heaviest daily precipitation events occurring in the Cévennes box from EUR-11_MOHC-HadGEM2-ES_r1i1p1_IPSL-WRF381P (12 km) in the period of 2001 – 2030

**12 Heaviest Daily Rainfall Events from EUR-11-NCC-NorESM1-M_r1i1p1_IPSL-WRF381P
Season: SON ; Period: 2001-2030**

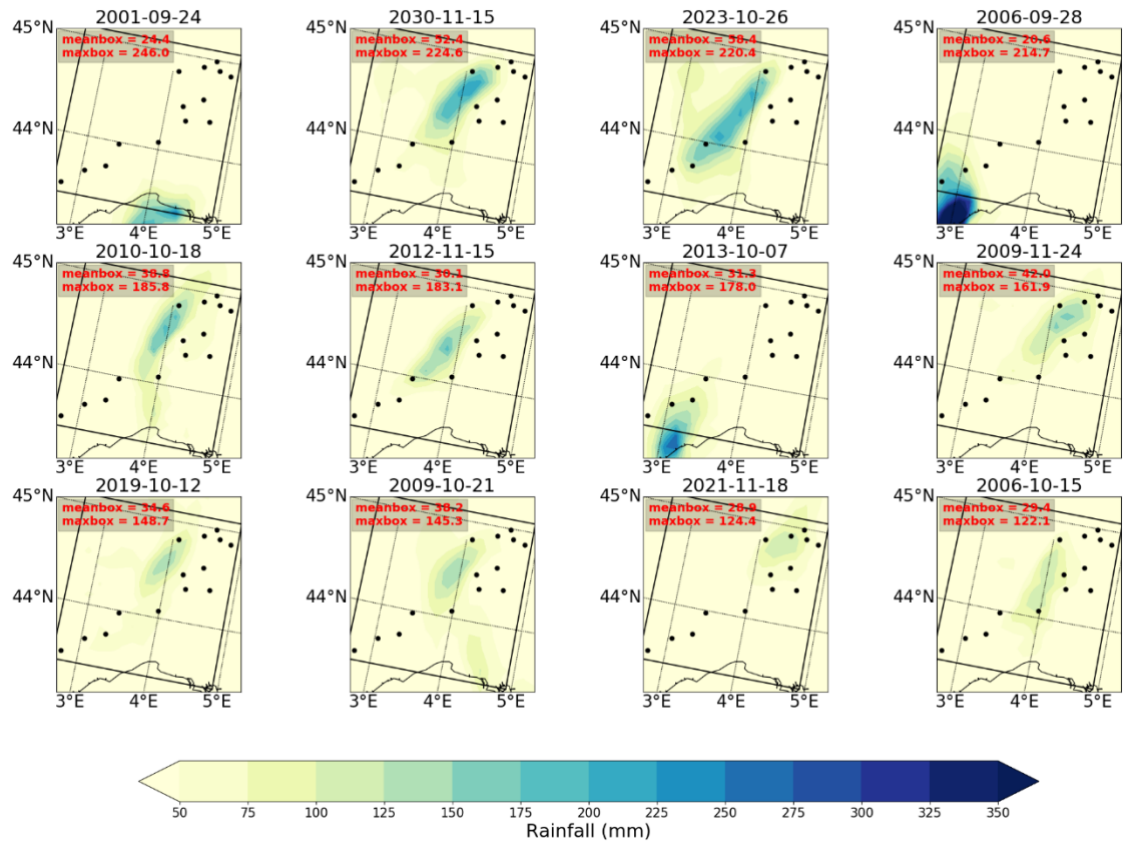


Figure 56. The 12 heaviest daily precipitation events occurring in the Cévennes box from EUR-11_NCC-NorESM1-M_r1i1p1_IPSL-WRF381P (12 km) in the period of 2001 – 2030

Table 11. List of stations for daily rainfall data; the 14 stations in the Cévennes box are highlighted in yellow

No.	ID	Name	Altitude (m)	Start_year	End_year	Latitude	Longitude
1	4041001	LE_CASTELLET	473	1958	2018	43.94	5.98
2	4088001	FORCALQUIER	535	1950	2018	43.96	5.78
3	4099001	LAMBRUISSE	1123	1953	2018	44.04	6.45
4	4226001	UVERNET-FOURS	1660	1955	2018	44.32	6.69
5	5026001	CEILLAC	1665	1950	2018	44.67	6.78
6	5027001	CERVIERES	1637	1956	2018	44.87	6.72
7	5032002	CHAMPOLEON	1275	1950	2018	44.72	6.26
8	5038001	CHATEAU-VILLE-VIEILLE	1355	1950	2018	44.76	6.80
9	5063001	LA_GRAVE	1790	1950	2018	45.05	6.29
10	5064001	LA_CHAPELLE-EN-VALGAUDEMAR	1270	1950	2018	44.81	6.20
11	5090002	LA_MOTTE-EN-CHAMPSAUR	1250	1956	2018	44.75	6.12
12	5093001	NEVACHE	1603	1950	2018	45.02	6.62
13	5098001	LES_ORRES	1445	1952	2018	44.50	6.55
14	5101001	PELVOUX	1270	1950	2018	44.87	6.49
15	5110001	PUY-SAINT-VINCENT	1380	1956	2018	44.83	6.49
16	5139002	DEVOLUY	1300	1950	2018	44.69	5.94
17	5139006	DEVOLUY	1262	1950	2018	44.69	5.87
18	6004002	ANTIBES	72	1950	2018	43.56	7.13
19	6016001	BEUIL	1460	1950	2018	44.10	6.99
20	6029001	CANNES	2	1950	2018	43.56	6.95
21	6088003	NICE	333	1950	2018	43.71	7.30
22	6088007	NICE	238	1950	2018	43.74	7.28

No.	ID	Name	Altitude (m)	Start_year	End_year	Latitude	Longitude
23	7005001	ALBA-LA-ROMAINE	223	1951	2018	44.54	4.58
24	7033001	BESSAS	261	1951	2018	44.34	4.30
25	7042001	BOURG-SAINT-ANDEOL	74	1951	2018	44.37	4.64
26	7064001	LE_CHEYLARD	450	1951	2018	44.91	4.44
27	7075001	CROS-DE-GEORAND	1011	1952	2018	44.78	4.10
28	7110001	JOYEUSE	212	1951	2018	44.48	4.23
29	7119001	LE_LAC-D'ISSARLES	1053	1952	2018	44.82	4.08
30	7129001	LAMASTRE	367	1955	2018	44.99	4.59
31	7144001	LOUBARESSÉ	1220	1951	2018	44.60	4.05
32	7153001	MAYRES	577	1955	2018	44.67	4.11
33	7159001	MIRABEL	278	1957	2018	44.58	4.50
34	7161001	MONTPEZAT-SOUS-BAUZON	606	1951	2018	44.72	4.21
35	7240001	SAINT-GEORGES-LES-BAINS	170	1951	2018	44.86	4.83
36	7261001	SAINT-LAURENT-DU-PAPE	106	1951	2018	44.82	4.75
37	7279001	SAINT-MONTAN	103	1951	2018	44.44	4.64
38	7286002	SAINT-PIERREVILLE	559	1953	2018	44.81	4.48
39	7331001	VALS-LES-BAINS	250	1951	2018	44.66	4.37
40	7338001	VERNOUX-EN-VIVARAIS	560	1951	2018	44.90	4.65
41	7347001	VOCANCE	529	1951	2018	45.20	4.55
42	11012001	ARGELIERS	31	1950	2018	43.31	2.91
43	11015001	ARQUES	350	1950	2018	42.95	2.37
44	11076001	CASTELNAUDARY	160	1950	2018	43.31	1.95
45	11185001	LAGRASSE	130	1961	2018	43.09	2.62

No.	ID	Name	Altitude (m)	Start_year	End_year	Latitude	Longitude
46	11243001	MONTFERRAND	190	1950	2018	43.35	1.82
47	12096001	ESPALION	334	1955	2018	44.53	2.76
48	12116001	HUPARLAC	860	1955	2018	44.71	2.76
49	12212001	SAINT-BEAULIZE	525	1957	2014	43.90	3.11
50	12224001	SAINT-GENIEZ-D'OLT	420	1956	2018	44.46	2.97
51	12298001	VILLECOMTAL	318	1956	2018	44.53	2.57
52	13001009	AIX-EN-PROVENCE	173	1960	2018	43.53	5.42
53	13030001	CUGES-LES-PINS	180	1950	2018	43.27	5.70
54	13047001	ISTRES	23	1950	2018	43.52	4.92
55	13054001	MARIGNANE	9	1950	2018	43.44	5.22
56	13092001	SAINT-CHAMAS	10	1950	2018	43.54	5.04
57	13103001	SALON-DE-PROVENCE	58	1950	2018	43.60	5.10
58	26035001	BEAUFORT-SUR-GERVANNE	370	1951	2018	44.78	5.14
59	26047001	BELLEGARDE-EN-DIOIS	965	1961	2018	44.54	5.45
60	26167001	LUC-EN-DIOIS	537	1953	2017	44.62	5.45
61	26198001	MONTÉLIMAR	73	1951	2018	44.58	4.73
62	26211001	MONTSEGUR-SUR-LAUZON	150	1951	2018	44.36	4.86
63	26307001	SAINT-JEAN-EN-ROYANS	308	1951	2018	45.01	5.29
64	26330001	SAINT-SORLIN-EN-VALLOIRE	245	1951	2018	45.27	4.93
65	30003001	AIGUES-MORTES	1	1956	2018	43.54	4.21
66	30009001	ALZON	611	1950	2018	43.98	3.44
67	30129001	GENERARGUES	139	1950	2018	44.07	3.98
68	30243001	SAINT-CHRISTOL-LES-ALES	129	1950	2018	44.09	4.08

No.	ID	Name	Altitude (m)	Start_year	End_year	Latitude	Longitude
69	34212001	POUJOLS	276	1959	2018	43.76	3.33
70	34293001	LA_SALVETAT-SUR-AGOUT	693	1950	2018	43.60	2.70
71	34142001	LODEVE	191	1960	2014	43.74	3.32
72	34260001	SAINT-GERVAIS-SUR-MARE	320	1950	2014	43.66	3.05
73	34284001	SAINT-PONS-DE-THOMIERES	363	1950	2014	43.49	2.76
74	48009001	AUMONT-AUBRAC	1055	1950	2018	44.72	3.27
75	48014001	BAGNOLS-LES-BAINS	918	1955	2018	44.51	3.67
76	48043001	CHATEAUNEUF-DE-RANDON	1238	1950	2018	44.64	3.68
77	48045001	CHAUDEYRAC	1140	1952	2018	44.67	3.76
78	48094001	LE MASSEGROS	873	1950	2018	44.31	3.18
79	48116001	LE PONT-DE-MONTVERT	875	1950	2018	44.37	3.74
80	48198001	VILLEFORT	620	1950	2018	44.44	3.93
81	66127001	OPOUL-PERILLOS	180	1957	2017	42.87	2.88
82	81069001	CORDES-SUR-CIEL	175	1949	2018	44.07	1.96
83	81105002	GRAULHET	171	1949	2013	43.76	2.00
84	81182001	MONTREDON-LABESSONNIE	495	1957	2018	43.72	2.32
85	81308001	VALENCE-D'ALBIGEOIS	470	1949	2013	44.02	2.40
86	83031001	LE_CANNET-DES-MAURES	80	1950	2018	43.38	6.39
87	83061001	FREJUS	7	1950	2018	43.42	6.74
88	83069001	HYERES	2	1959	2018	43.09	6.15
89	83080001	MONS	796	1950	2018	43.69	6.71
90	83137001	TOULON	23	1950	2018	43.12	5.90
91	84054001	L'ISLE-SUR-LA-SORGUE	64	1961	2018	43.90	5.05

No.	ID	Name	Altitude (m)	Start_year	End_year	Latitude	Longitude
92	84064001	LAPALUD	46	1959	2018	44.32	4.66
93	84069001	MALAUCENE	340	1957	2018	44.17	5.12
94	84087001	ORANGE	57	1953	2018	44.14	4.86
95	84123001	SAULT	792	1959	2017	44.09	5.42
96	84144001	VIENS	620	1959	2018	43.90	5.57

Table 12. List of 89 stations for daily maximum 3-hour rainfall data; the 23 stations in Cévennes box are highlighted in yellow

No.	ID	Name	Altitude (m)	Start_year	End_year	Latitude	Longitude
1	11004001	ALAIGNE	293	1998	2018	43.11	2.10
2	11016003	ARQUETTES-EN-VA	240	1992	2018	43.10	2.50
3	11069001	CARCASSONNE	128	1984	2018	43.22	2.29
4	11076001	CASTELNAUDARY	160	1998	2018	43.31	1.95
5	11081003	CAUNES-MINERVOI	371	1990	2017	43.33	2.48
6	11124003	DURBAN-CORBIERE	120	1990	2018	42.99	2.82
7	11168001	GRANES	420	1992	2018	42.91	2.25
8	11203004	LEZIGNAN-CORBIE	60	1995	2018	43.17	2.73
9	11260002	MOUTHOMET	538	1990	2018	42.96	2.53
10	11262005	NARBONNE	110	1989	2018	43.15	2.96
11	13001006	AIX-LES_MILLES	106	1993	2015	43.51	5.36
12	13001009	AIX_EN_PROVENCE	173	1988	2018	43.53	5.42
13	13004003	ARLES	1	1991	2018	43.51	4.69
14	13005003	AUBAGNE	130	1991	2018	43.31	5.60
15	13022003	CASSIS	212	1994	2018	43.22	5.50

No.	ID	Name	Altitude (m)	Start_year	End_year	Latitude	Longitude
16	13047001	ISTRES	23	1982	2018	43.52	4.92
17	13054001	MARIGNANE	9	1982	2018	43.44	5.22
18	13055001	MARSEILLE-OBS	75	1982	2010	43.31	5.39
19	13062002	MIMET	416	1993	2018	43.42	5.50
20	13103001	SALON_DE_PROVEN	58	1982	2018	43.60	5.10
21	13108004	TARASCON	15	1991	2018	43.83	4.64
22	13110003	TRETS	264	1991	2018	43.45	5.70
23	13111002	VAUVENARGUES	565	1993	2018	43.55	5.68
24	20004002	AJACCIO	5	1982	2018	41.92	8.79
25	20050001	CALVI	57	1982	2018	42.53	8.79
26	20114002	FIGARI	20	1982	2018	41.51	9.10
27	20148001	BASTIA	10	1982	2018	42.54	9.48
28	20232002	PILA-CANALE	407	1995	2018	41.81	8.90
29	20258001	RENNO	755	1995	2018	42.19	8.81
30	20268001	SAMPOLO	837	1996	2018	41.94	9.12
31	20272004	SARTENE	62	1998	2018	41.65	8.98
32	20342001	SOLENZARA	12	1982	2018	41.92	9.40
33	30081002	CHUSCLAN	30	1993	2018	44.13	4.71
34	30189001	NIMES-COURBESSA	59	1982	2018	43.86	4.41
35	30209002	PUJAUT	44	1992	2018	44.00	4.76
36	30258001	NIMES-GARONS	94	1982	2018	43.77	4.42
37	30339001	MONT_AIGOUAL	1567	1996	2018	44.12	3.58
38	30352002	VILLEVIEILLE	41	1992	2018	43.79	4.09

No.	ID	Name	Altitude (m)	Start_year	End_year	Latitude	Longitude
39	34028003	BEDARIEUX	373	1993	2018	43.64	3.15
40	34151005	MARSILLARGUES	4	1989	2018	43.63	4.17
41	34154001	MONTPELLIER-AER	1	1982	2018	43.58	3.96
42	34178001	MURVIEL_LES_BEZ	140	1993	2018	43.48	3.14
43	34205001	LES_PLANS	844	1995	2018	43.79	3.24
44	34209002	BEZIERS-VIAS	15	1998	2018	43.32	3.35
45	34217001	PRADES_LE_LEZ	69	1992	2018	43.72	3.87
46	34274001	ST_MARTIN_DE_LO	214	1999	2018	43.78	3.73
47	34301002	SETE	75	1997	2018	43.40	3.69
48	34306001	SOUMONT	252	1994	2018	43.71	3.35
49	4049001	ST_AUBAN	458	1982	2018	44.06	5.99
50	4230001	VALENSOLE	600	1998	2018	43.84	6.00
51	48004001	ALTIER	900	1999	2018	44.49	3.85
52	5046001	EMBRUN	871	1982	2018	44.57	6.50
53	5055001	LA_FAURIE	825	1998	2018	44.57	5.75
54	5070003	LARAGNE_MONTEGL	565	1993	2018	44.32	5.79
55	5126001	ROSANS	625	1992	2018	44.39	5.46
56	5170001	TALLARD	593	1994	2018	44.45	6.03
57	6004009	ANTIBES	32	1989	2018	43.60	7.11
58	6023004	BREIL_SUR_ROYA	305	1988	2018	43.94	7.51
59	6029001	CANNES	2	1989	2018	43.56	6.95
60	6033002	CARROS	78	1992	2018	43.79	7.21
61	6037002	CAUSSOLS	1268	1988	2018	43.75	6.92

No.	ID	Name	Altitude (m)	Start_year	End_year	Latitude	Longitude
62	6050002	COURSEGOULES_SA	985	1990	2018	43.79	7.05
63	6079002	MANDELIEU_LA_NA	104	1990	2018	43.52	6.90
64	6083005	MENTON	216	1992	2018	43.79	7.49
65	6088001	NICE	2	1982	2018	43.65	7.21
66	6091003	PEILLE	1106	1989	2018	43.78	7.43
67	6152002	VALBONNE-SOPHIA	238	1988	2018	43.62	7.03
68	66074002	EUS	307	1998	2018	42.63	2.44
69	66136001	PERPIGNAN	42	1982	2018	42.74	2.87
70	66137003	LE_PERTHUS	295	1991	2018	42.47	2.86
71	66181001	STE_LEOCADIE	1320	1993	2016	42.44	2.01
72	83007004	AUPS	497	1994	2018	43.64	6.19
73	83019002	BORMES_LES_MIMO	88	1991	2018	43.19	6.38
74	83031001	LE_LUC	80	1982	2018	43.38	6.39
75	83035001	LE_CASTELLET	417	1989	2018	43.25	5.78
76	83042001	COGOLIN_SAPC	31	1998	2018	43.26	6.51
77	83061001	FREJUS	7	1982	2018	43.42	6.74
78	83069001	HYERES	2	1982	2018	43.09	6.15
79	83069003	ILE_DU_LEVANT	118	1995	2018	43.03	6.47
80	83083001	MONTFORT-SUR-AR	141	1998	2018	43.47	6.13
81	83137001	TOULON	3	1982	2018	43.12	5.90
82	83153001	CAP_CEPET	115	1996	2018	43.08	5.94
83	84007005	AVIGNON	34	1998	2018	43.91	4.90
84	84009002	LA_BASTIDE_DES_	381	1995	2018	43.79	5.61

No.	ID	Name	Altitude (m)	Start_year	End_year	Latitude	Longitude
85	84025001	CABRIERES_D_AVI	142	1989	2018	43.88	5.16
86	84031001	CARPENTRAS	99	1964	2018	44.08	5.06
87	84087001	ORANGE	57	1994	2018	44.14	4.86
88	84107002	ST_CHRISTOL	836	1996	2018	44.04	5.49
89	84150001	VISAN	141	1989	2018	44.34	4.91

Supplementary for Chapter 5

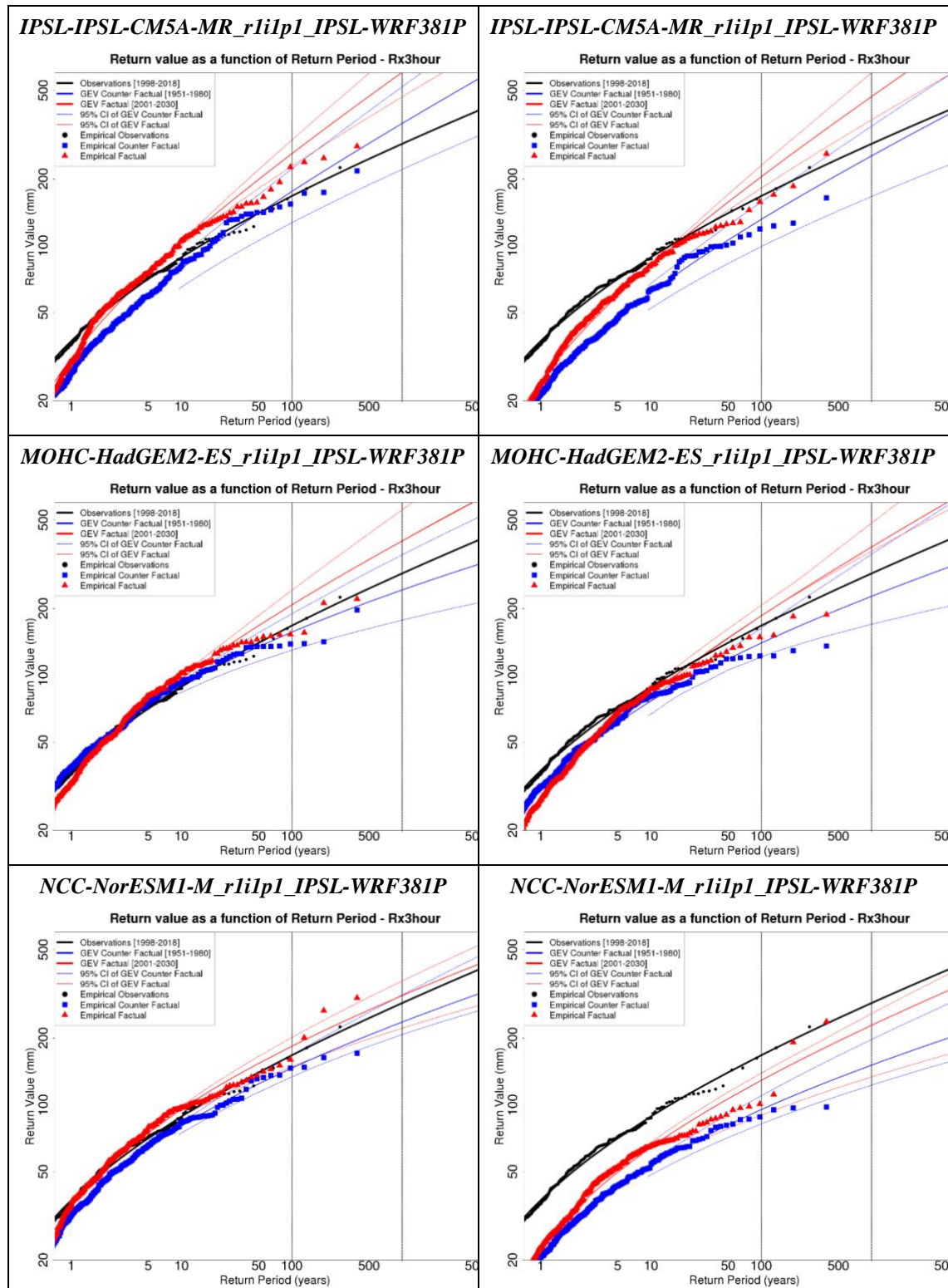
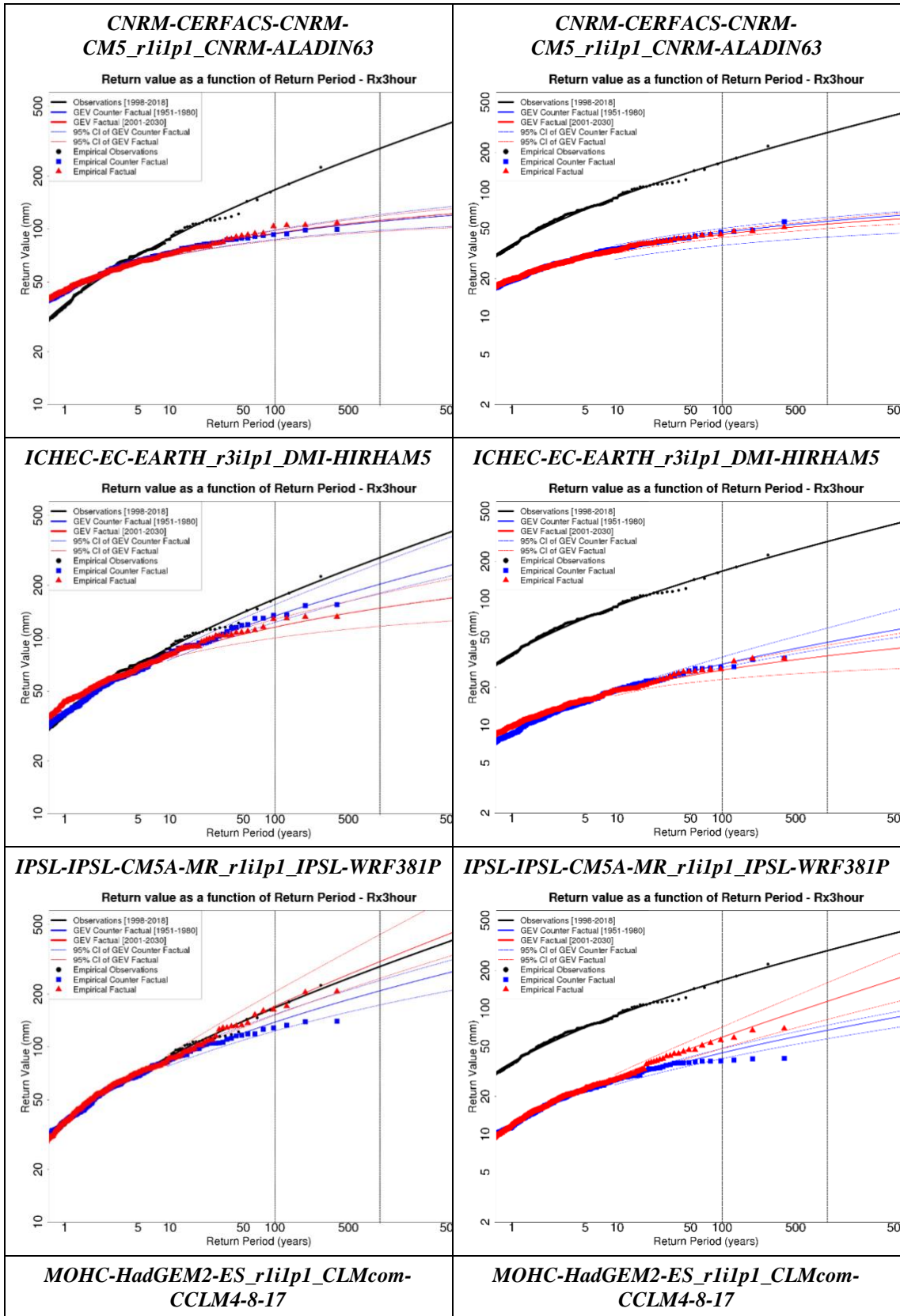
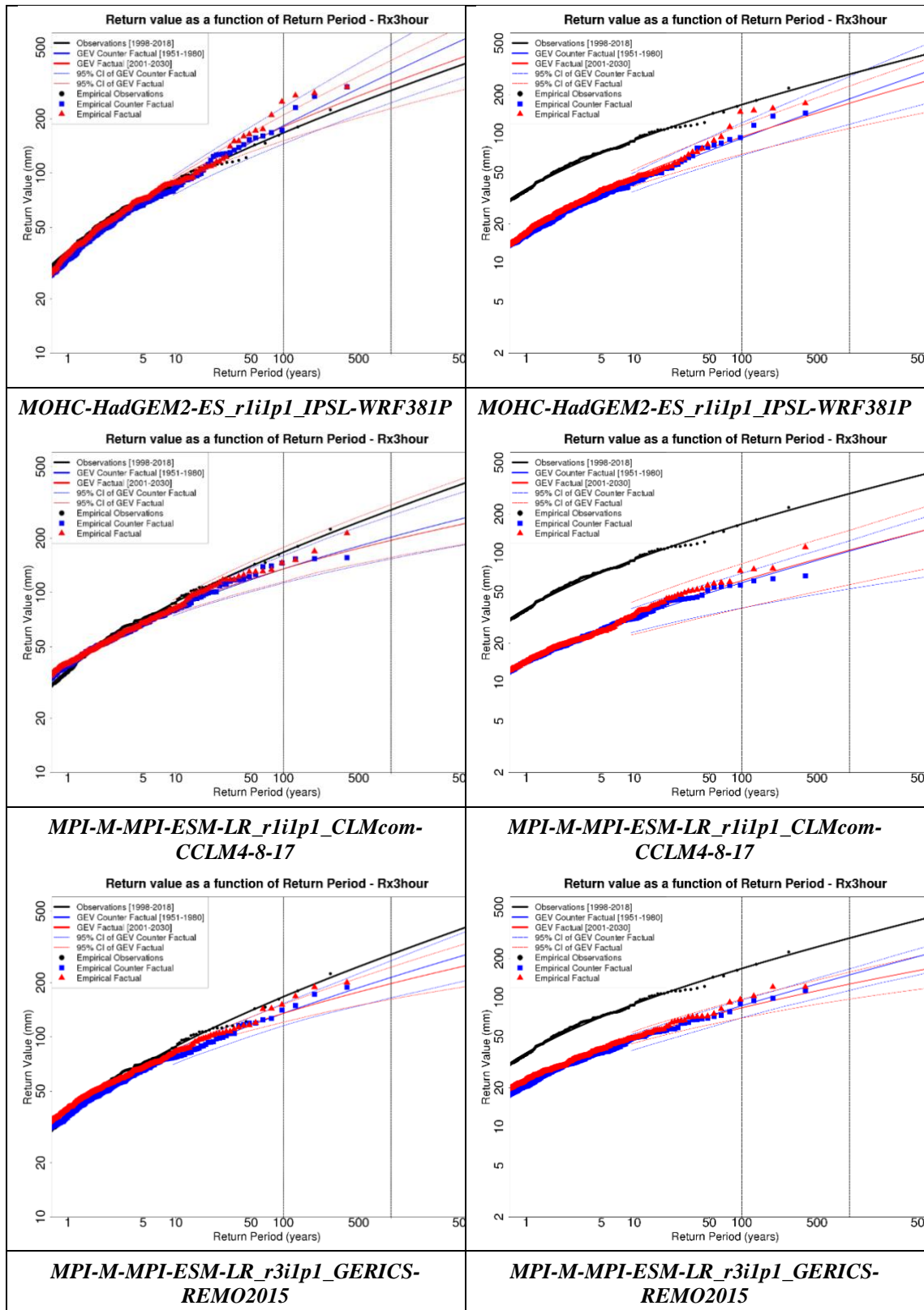


Figure 57. Return value as a function of return period of Rx3hour from individual CPS simulations; the left/right column shows normalized/raw dataset; The black/blue/red curves denote the GEV fits of Observations/Counter Factual/Factual climates; The dashed blue/red curves denote 95% confidence interval of the GEV fits of counterfactual/factual climates.





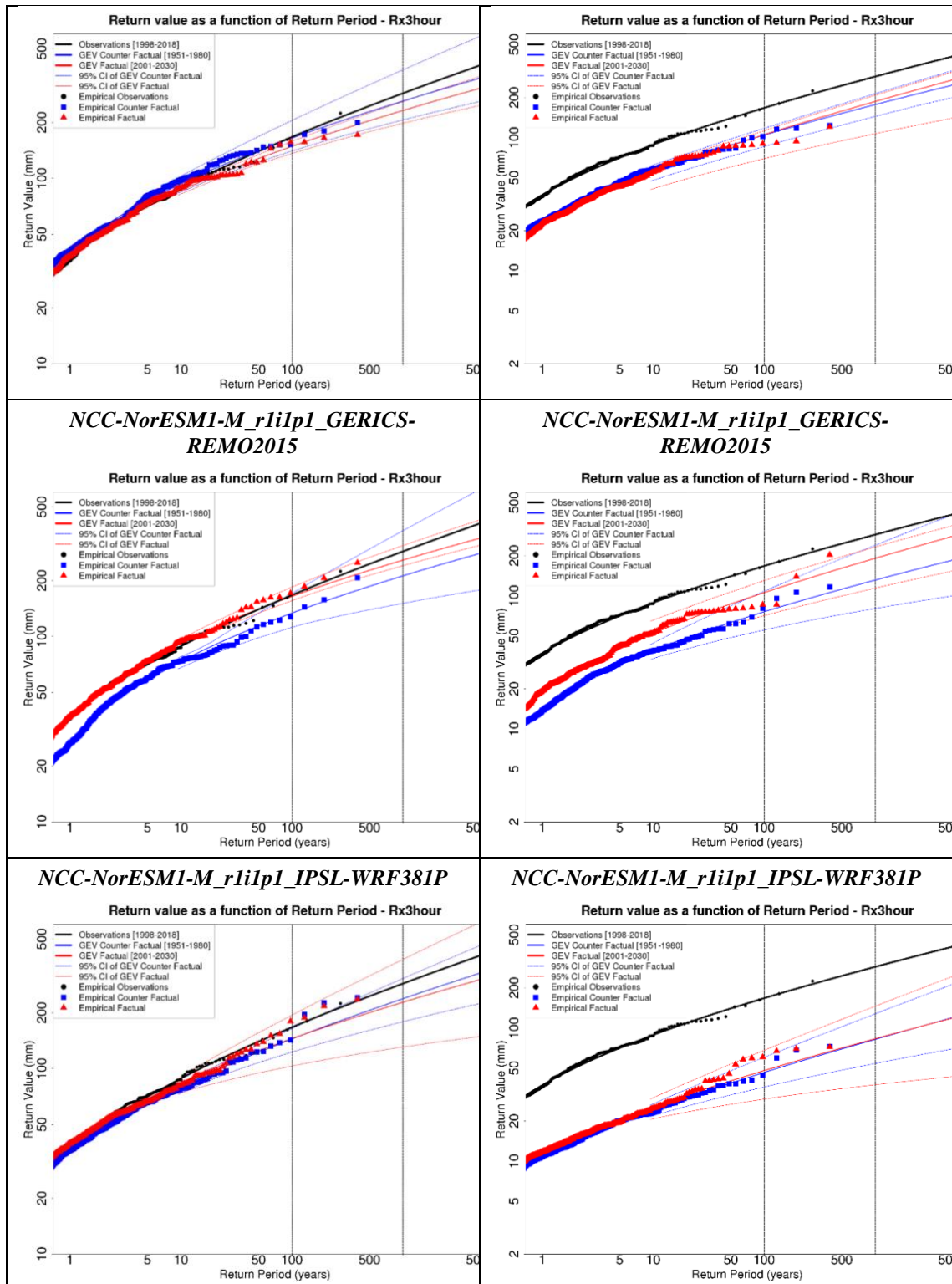


Figure 58. Return value as a function of return period of Rx3hour from individual EUR-11 simulations; the left/right column shows normalized/raw dataset; The black/blue/red curves denote the GEV fits of Observations/Counter Factual/Factual climates; The dashed blue/red curves denote 95% confidence interval of the GEV fits of counter factual/factual climates.

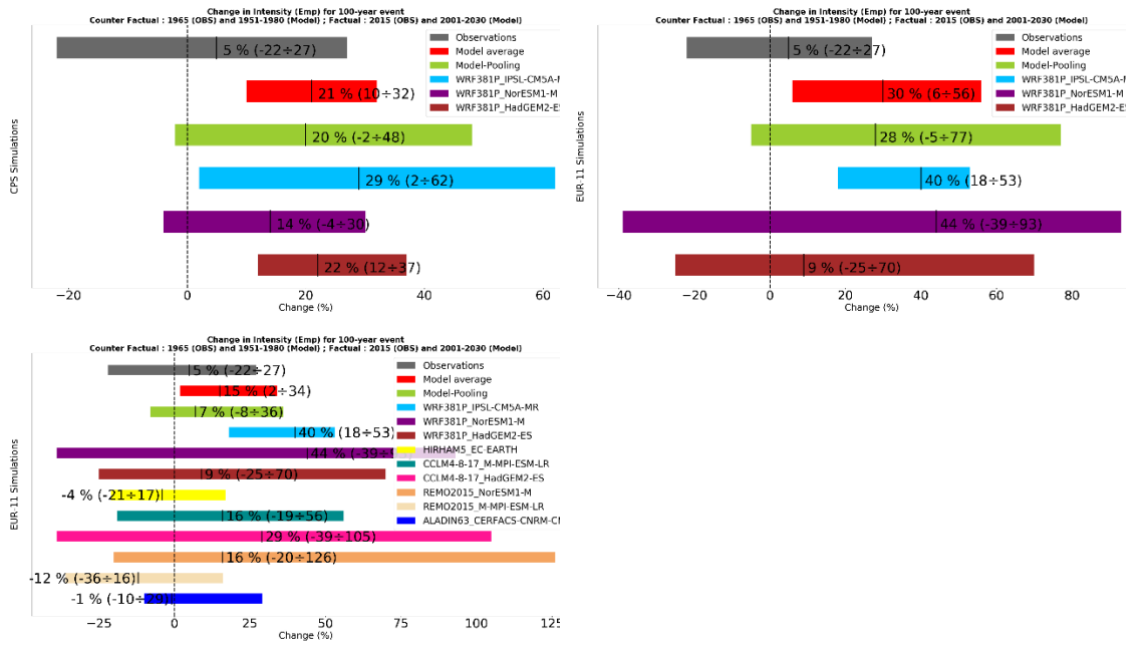
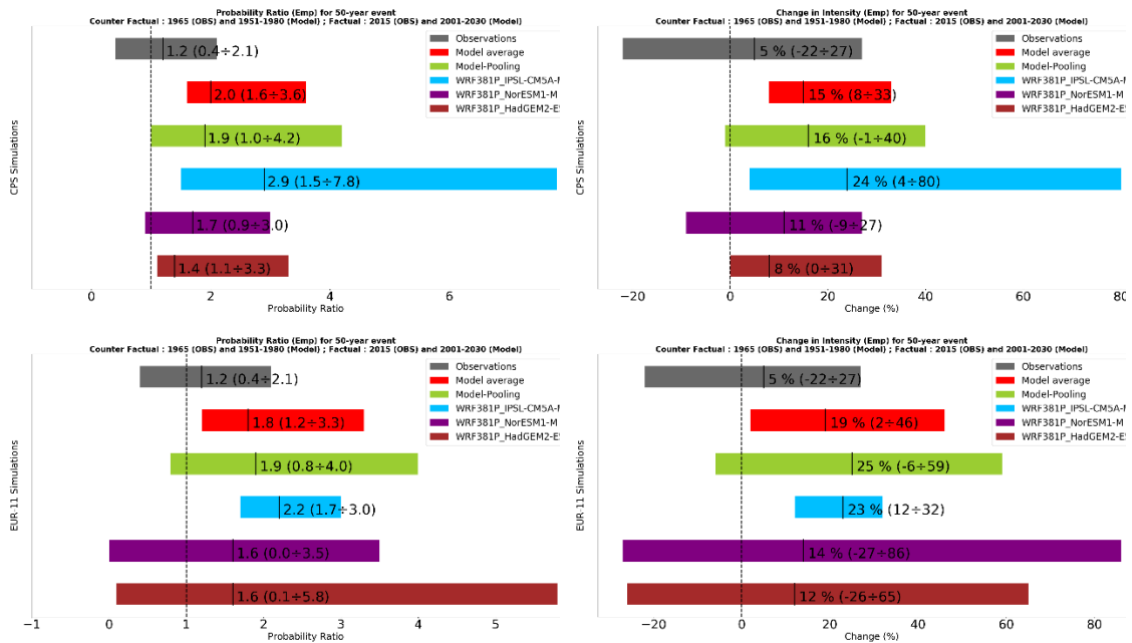


Figure 59. The syntheses of Intensity change of Rx3hour for 100-year event from model pooling and individual simulations from raw data (similar results for normalized data are shown in Figure 45); the top left panel shows results of CPS ensemble; the top right panel shows results of the three EUR-11 driving CPSs; the bottom left shows results of all EUR-11 simulations.



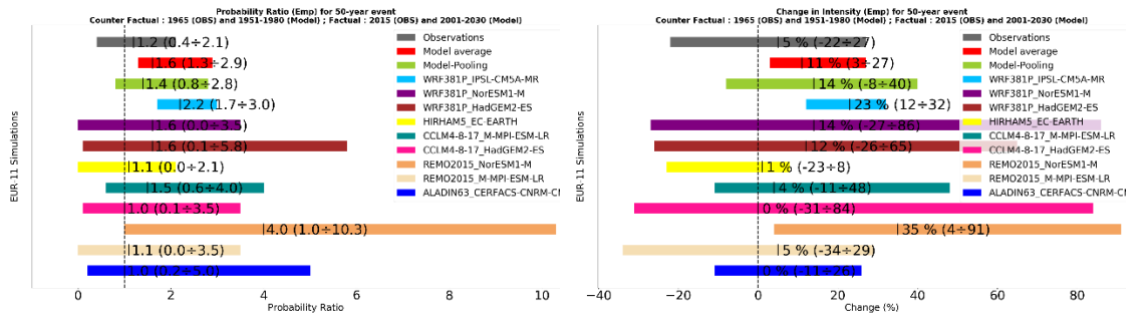


Figure 60. The syntheses of Probability Ratio (left column) and Intensity change (right column) of Rx3hour for 50-year event from model pooling and individual simulations from raw dataset (similar result for normalized data are shown in Figure 46); the top row shows results of the three CPS simulations; the middle row shows results of the three EUR-11 simulations driving the three CPSs; the bottom row shows results of all EUR-11 simulations.

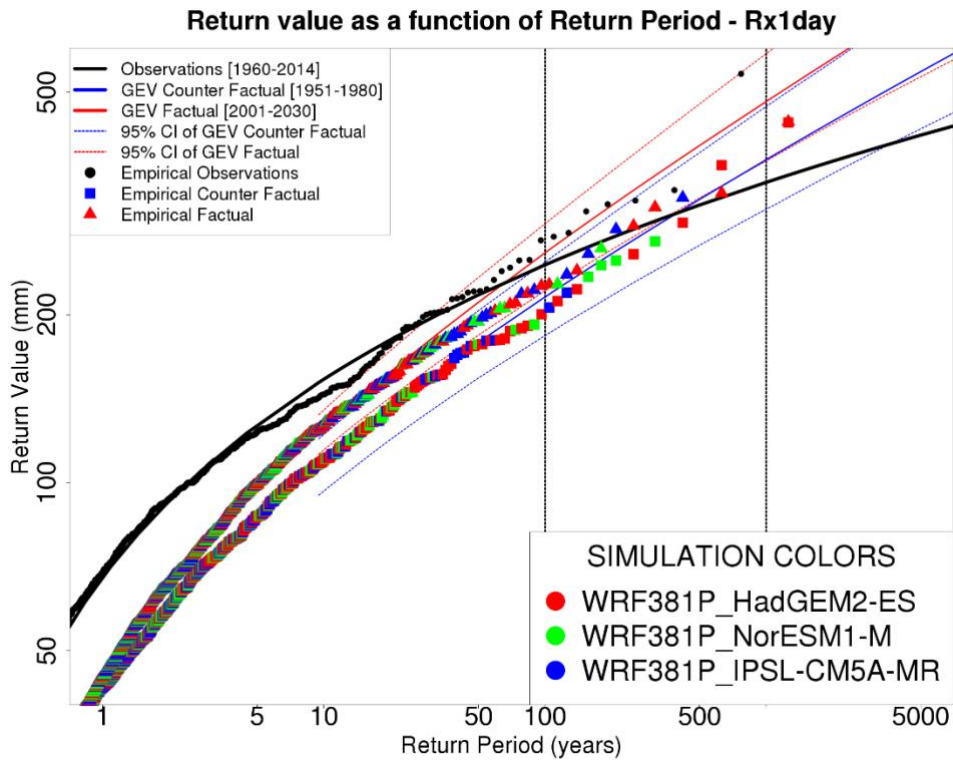


Figure 61. Return value as a function of return period of Rx1day from raw convection – permitting simulations pooling (similar result for normalized data are shown in Figure 48); The black/blue/red curves denote the GEV fits of Observations/Counter Factual/Factual climates; The dashed blue/red curves denote 95% confidence interval of the GEV fits of counter factual/factual climates; The circle/square/triangle points denote precipitation values from observations/counter factual/factual climates; The different colors of points denote different simulations contributing to the pooling procedure.

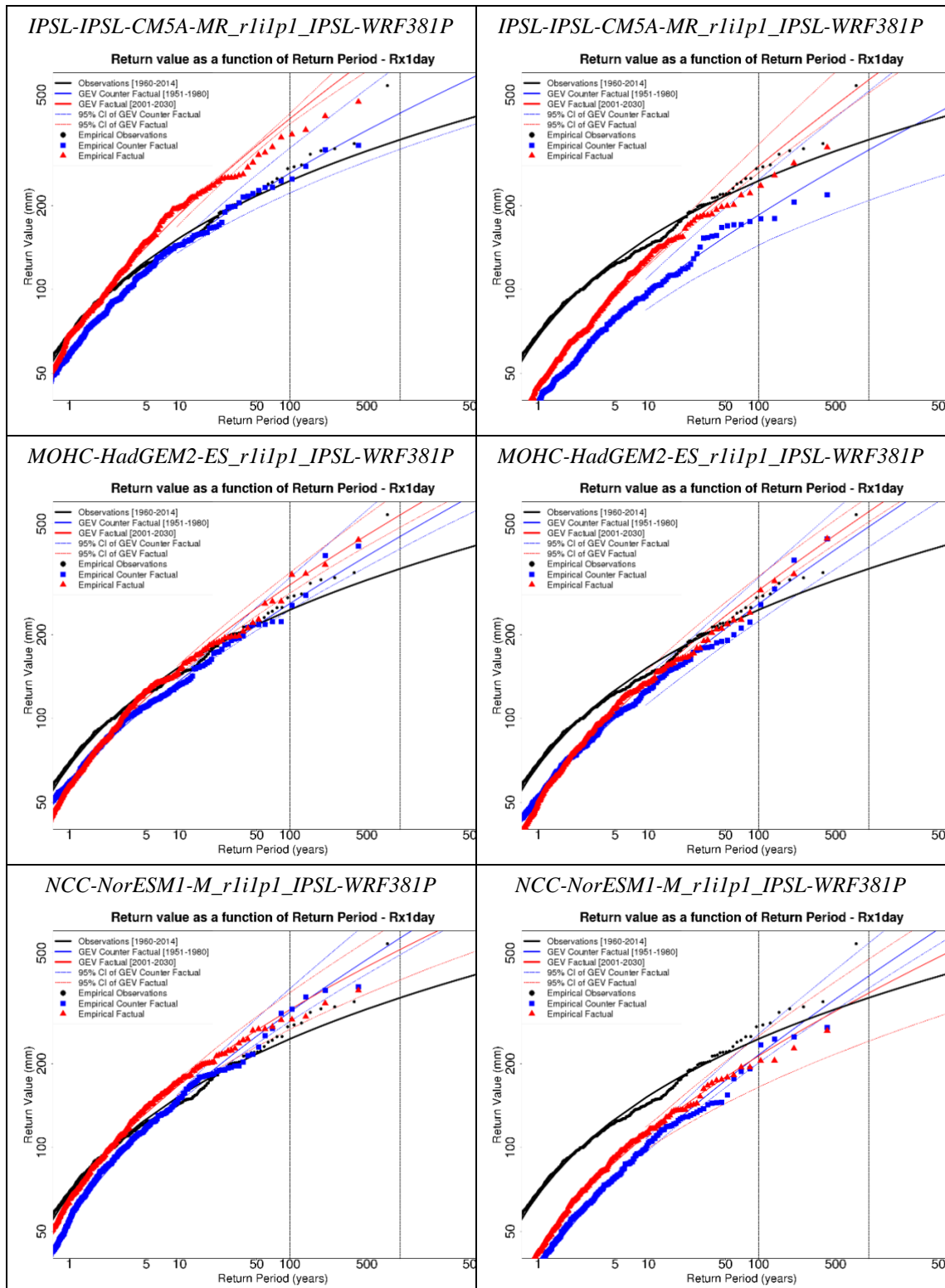


Figure 62. Return value as a function of return period of Rx1day from individual CPS simulations; the left/right column shows normalized/raw dataset; The black/blue/red curves denote the GEV fits of Observations/Counter Factual/Factual climates; The dashed blue/red curves denote 95% confidence interval of the GEV fits of counter factual/factual climates.

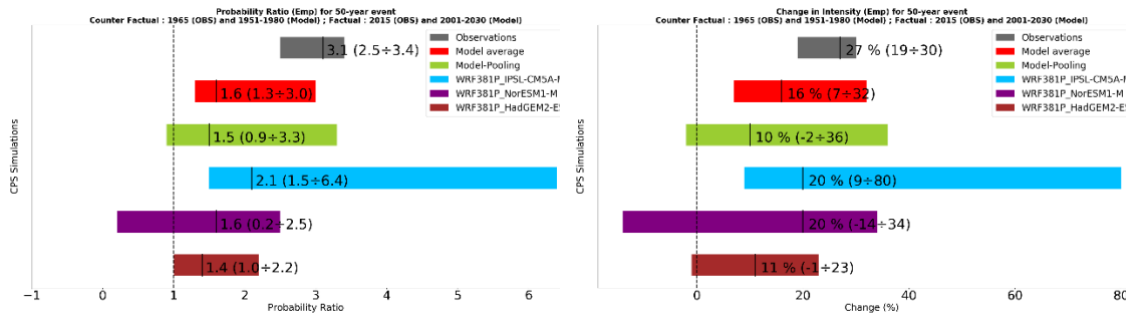


Figure 63. The syntheses of Probability Ratio (left) and Intensity change (right) of *Rx1day* for 100-year event from raw CPS simulations (similar result for normalized data are shown in Figure 49).

Bibliography

- Allen, M., 2003, Liability for climate change: *Nature*, v. 421, no. 6926, p. 891.
- Armon, M., Marra, F., Enzel, Y., Rostkier-Edelstein, D., and Morin, E., 2019, Characterising patterns of heavy precipitation events in the eastern Mediterranean using a weather radar and convection-permitting WRF simulations: *Hydrol. Earth Syst. Sci. Discuss.*, v. 2019, p. 1-38.
- Ban, N., Rajczak, J., Schmidli, J., and Schär, C., 2018, Analysis of Alpine precipitation extremes using generalized extreme value theory in convection-resolving climate simulations: *Climate Dynamics*, p. 1-15.
- Ban, N., Schmidli, J., and Schär, C., 2014, Evaluation of the convection-resolving regional climate modeling approach in decade-long simulations: *Journal of Geophysical Research: Atmospheres*, v. 119, no. 13, p. 7889-7907.
- Bellprat, O., and Doblas-Reyes, F., 2016, Attribution of extreme weather and climate events overestimated by unreliable climate simulations: *Geophysical Research Letters*, v. 43, no. 5, p. 2158-2164.
- Bellprat, O., Guemas, V., Doblas-Reyes, F., and Donat, M. G., 2019, Towards reliable extreme weather and climate event attribution: *Nature communications*, v. 10, no. 1, p. 1732.
- Bevacqua, E., Maraun, D., Hobæk Haff, I., Widmann, M., and Vrac, M., 2017, Multivariate statistical modelling of compound events via pair-copula constructions: analysis of floods in Ravenna (Italy): *Hydrol. Earth Syst. Sci.*, v. 21, no. 6, p. 2701-2723.
- Bevacqua, E., Maraun, D., Voudoukas, M. I., Voukouvalas, E., Vrac, M., Mentaschi, L., and Widmann, M., 2019, Higher probability of compound flooding from precipitation and storm surge in Europe under anthropogenic climate change: *Science Advances*, v. 5, no. 9, p. eaaw5531.
- Bindoff, N. L., Stott, P. A., AchutaRao, K. M., Allen, M. R., Gillett, N., Gutzler, D., Hansingo, K., Hegerl, G., Hu, Y., and Jain, S., 2013, Detection and attribution of climate change: from global to regional.
- Cannon, A. J., and Innocenti, S., 2019, Projected intensification of sub-daily and daily rainfall extremes in convection-permitting climate model simulations over North America: implications for future intensity–duration–frequency curves: *Nat. Hazards Earth Syst. Sci.*, v. 19, no. 2, p. 421-440.
- Chan, S. C., Kendon, E. J., Fowler, H. J., Blenkinsop, S., Ferro, C. A., and Stephenson, D. B., 2013, Does increasing the spatial resolution of a regional climate model improve the simulated daily precipitation?: *Climate dynamics*, v. 41, no. 5-6, p. 1475-1495.
- Chan, S. C., Kendon, E. J., Fowler, H. J., Blenkinsop, S., Roberts, N. M., and Ferro, C. A., 2014, The value of high-resolution met office regional climate models in the simulation of multihourly precipitation extremes: *Journal of Climate*, v. 27, no. 16, p. 6155-6174.
- Chernokulsky, A., Kozlov, F., Zolina, O., Bulygina, O. N., Mokhov, I., and Semenov, V., 2019, Observed changes in convective and stratiform

- precipitation over Northern Eurasia during the last decades: *Environmental Research Letters*.
- Christidis, N., Betts, R. A., and Stott, P. A., 2019, The Extremely Wet March of 2017 in Peru: *Bulletin of the American Meteorological Society*, v. 100, no. 1, p. S31-S35.
- Christidis, N., and Stott, P. A., 2015, Extreme Rainfall in the United Kingdom During Winter 2013/14: The Role of Atmospheric Circulation and Climate Change: *Bulletin of the American Meteorological Society*, v. 96, no. 12, p. S46-S50.
- Christidis, N., Stott, P. A., Jones, G. S., Shiogama, H., Nozawa, T., and Luterbacher, J., 2012a, Human activity and anomalously warm seasons in Europe: *International Journal of Climatology*, v. 32, no. 2, p. 225-239.
- Christidis, N., Stott, P. A., Zwiers, F. W., Shiogama, H., and Nozawa, T., 2010, Probabilistic estimates of recent changes in temperature: a multi-scale attribution analysis: *Climate Dynamics*, v. 34, no. 7, p. 1139-1156.
- , 2012b, The contribution of anthropogenic forcings to regional changes in temperature during the last decade: *Climate Dynamics*, v. 39, no. 6, p. 1259-1274.
- Clapeyron, É., 1834, Mémoire sur la puissance motrice de la chaleur: *Journal de l'École polytechnique*, v. 14, p. 153-190.
- Clausius, R., 1850, Über die bewegende Kraft der Wärme und die Gesetze, welche sich daraus für die Wärmelehre selbst ableiten lassen: *Annalen der Physik*, v. 155, no. 3, p. 368-397.
- Coles, S., 2001, *An introduction to statistical modeling of extreme values*, Springer.
- Colin, J., Déqué, M., Radu, R., and Somot, S., 2010, Sensitivity study of heavy precipitation in Limited Area Model climate simulations: influence of the size of the domain and the use of the spectral nudging technique: *Tellus A: Dynamic Meteorology and Oceanography*, v. 62, no. 5, p. 591-604.
- Coppola, E., Sobolowski, S., Pichelli, E., Raffaele, F., Ahrens, B., Anders, I., Ban, N., Bastin, S., Belda, M., and Belusic, D., 2018, A first-of-its-kind multi-model convection permitting ensemble for investigating convective phenomena over Europe and the Mediterranean: *Climate Dynamics*, p. 1-32.
- Cornes, R. C., van der Schrier, G., van den Besselaar, E. J. M., and Jones, P. D., 2018, An Ensemble Version of the E-OBS Temperature and Precipitation Data Sets: *Journal of Geophysical Research: Atmospheres*, v. 123, no. 17, p. 9391-9409.
- Dash, S., Pattnayak, K., Panda, S., Vaddi, D., and Mamgain, A., 2015, Impact of domain size on the simulation of Indian summer monsoon in RegCM4 using mixed convection scheme and driven by HadGEM2: *Climate dynamics*, v. 44, no. 3-4, p. 961-975.

- de Abreu, R. C., Cunningham, C., Rudorff, C. M., Rudorff, N., Abatan, A. A., Tett, S. F., Dong, B., Lott, F. C., and Sparrow, S. N., 2019, Contribution of Anthropogenic Climate Change to April–May 2017 Heavy Precipitation over the Uruguay River Basin: *Bulletin of the American Meteorological Society*, v. 100, no. 1, p. S37-S41.
- Demeshko, I., Maruyama, N., Tomita, H., and Matsuoka, S., *Multi-GPU Implementation of the NICAM Atmospheric Model*, Berlin, Heidelberg, 2013, Springer Berlin Heidelberg, p. 175-184.
- Diffenbaugh, N., and Scherer, M., 2013, Likelihood of July 2012 US temperatures in preindustrial and current forcing regimes: *Bull Am. Meteorol Soc*, v. 94, no. 9, p. S6-S9.
- Diffenbaugh, N., Swain, D. L., and Touma, D., 2015, Anthropogenic warming has increased drought risk in California: *Proceedings of the National Academy of Sciences*, v. 112, no. 13, p. 3931-3936.
- Dole, R., Hoerling, M., Perlwitz, J., Eischeid, J., Pegion, P., Zhang, T., Quan, X. W., Xu, T., and Murray, D., 2011, Was there a basis for anticipating the 2010 Russian heat wave?: *Geophysical Research Letters*, v. 38, no. 6.
- Drobinski, P., Ducrocq, V., Alpert, P., Anagnostou, E., Béranger, K., Borga, M., Braud, I., Chanzy, A., Davolio, S., Delrieu, G., Estournel, C., Boubrahmi, N. F., Font, J., Grubišić, V., Gualdi, S., Homar, V., Ivančan-Picek, B., Kottmeier, C., Kotroni, V., Lagouvardos, K., Lionello, P., Llasat, M. C., Ludwig, W., Lutoff, C., Mariotti, A., Richard, E., Romero, R., Rotunno, R., Roussot, O., Ruin, I., Somot, S., Taupier-Letage, I., Tintore, J., Uijlenhoet, R., and Wernli, H., 2014, HyMeX: A 10-Year Multidisciplinary Program on the Mediterranean Water Cycle: *Bulletin of the American Meteorological Society*, v. 95, no. 7, p. 1063-1082.
- Ducrocq, V., Braud, I., Davolio, S., Ferretti, R., Flamant, C., Jansa, A., Kalthoff, N., Richard, E., Taupier-Letage, I., Ayrat, P.-A., Belamari, S., Berne, A., Borga, M., Boudevillain, B., Bock, O., Boichard, J.-L., Bouin, M.-N., Bousquet, O., Bouvier, C., Chiggiato, J., Cimini, D., Corsmeier, U., Coppola, L., Cocquerez, P., Defer, E., Delanoë, J., Girolamo, P. D., Doerenbecher, A., Drobinski, P., Dufournet, Y., Fourrié, N., Gourley, J. J., Labatut, L., Lambert, D., Coz, J. L., Marzano, F. S., Molinié, G., Montani, A., Nord, G., Nuret, M., Ramage, K., Rison, W., Roussot, O., Said, F., Schwarzenboeck, A., Testor, P., Baelen, J. V., Vincendon, B., Aran, M., and Tamayo, J., 2014, HyMeX-SOP1: The Field Campaign Dedicated to Heavy Precipitation and Flash Flooding in the Northwestern Mediterranean: *Bulletin of the American Meteorological Society*, v. 95, no. 7, p. 1083-1100.
- Ducrocq, V., Nuissier, O., Ricard, D., Lebeaupin, C., and Thouvenin, T., 2008, A numerical study of three catastrophic precipitating events over southern France. II: Mesoscale triggering and stationarity factors: *Quarterly Journal of the Royal Meteorological Society*, v. 134, no. 630, p. 131-145.

- Dyrddal, A. V., Stordal, F., and Lussana, C., 2018, Evaluation of summer precipitation from EURO-CORDEX fine-scale RCM simulations over Norway: *International Journal of Climatology*, v. 38, no. 4, p. 1661-1677.
- ECMWF, 2017, ERA5: Fifth generation of ECMWF atmospheric reanalyses of the global climate, Copernicus Climate Change Service Climate Data Store (CDS).
- Eden, J. M., Kew, S. F., Bellprat, O., Lenderink, G., Manola, I., Omrani, H., and van Oldenborgh, G. J., 2018, Extreme precipitation in the Netherlands: An event attribution case study: *Weather and climate extremes*, v. 21, p. 90-101.
- Eden, J. M., Wolter, K., Otto, F. E., and van Oldenborgh, G. J., 2016, Multi-method attribution analysis of extreme precipitation in Boulder, Colorado: *Environmental Research Letters*, v. 11, no. 12, p. 124009.
- Feng, Z., Leung, L. R., Houze Jr, R. A., Hagos, S., Hardin, J., Yang, Q., Han, B., and Fan, J., 2018, Structure and Evolution of Mesoscale Convective Systems: Sensitivity to Cloud Microphysics in Convection-Permitting Simulations Over the United States: *Journal of Advances in Modeling Earth Systems*, v. 10, no. 7, p. 1470-1494.
- Fischer, E. M., and Knutti, R., 2015, Anthropogenic contribution to global occurrence of heavy-precipitation and high-temperature extremes: *Nature Climate Change*, v. 5, no. 6, p. 560-564.
- Fosser, G., Khodayar, S., and Berg, P., 2015, Benefit of convection permitting climate model simulations in the representation of convective precipitation: *Climate Dynamics*, v. 44, no. 1-2, p. 45-60.
- Fresnay, S., Hally, A., Garnaud, C., Richard, E., and Lambert, D., 2012, Heavy precipitation events in the Mediterranean: sensitivity to cloud physics parameterisation uncertainties: *Natural Hazards & Earth System Sciences*, v. 12, no. 8.
- Fuhrer, O., Chadha, T., Hoefler, T., Kwasniewski, G., Lapillonne, X., Leutwyler, D., Lüthi, D., Osuna, C., Schär, C., Schulthess, T. C., and Vogt, H., 2018, Near-global climate simulation at 1 km resolution: establishing a performance baseline on 4888 GPUs with COSMO 5.0: *Geosci. Model Dev.*, v. 11, no. 4, p. 1665-1681.
- Fumière, Q., Déqué, M., Nuissier, O., Somot, S., Alias, A., Caillaud, C., Laurantin, O., and Seity, Y., 2019, Extreme rainfall in Mediterranean France during the fall: added value of the CNRM-AROME Convection-Permitting Regional Climate Model: *Climate Dynamics*, p. 1-15.
- Giorgi, F., 2006, Climate change hot-spots: *Geophysical Research Letters*, v. 33, no. 8.
- Giorgi, F., and Mearns, L. O., 1999, Introduction to special section: Regional climate modeling revisited: *Journal of Geophysical Research: Atmospheres*, v. 104, no. D6, p. 6335-6352.

- Gudmundsson, L., and Seneviratne, S. I., 2016, Anthropogenic climate change affects meteorological drought risk in Europe: *Environmental Research Letters*, v. 11, no. 4, p. 044005.
- Hauser, M., Gudmundsson, L., Orth, R., Jézéquel, A., Haustein, K., Vautard, R., Van Oldenborgh, G. J., Wilcox, L., and Seneviratne, S. I., 2017, Methods and model dependency of extreme event attribution: the 2015 European drought: *Earth's Future*, v. 5, no. 10, p. 1034-1043.
- Haylock, M. R., Hofstra, N., Klein Tank, A. M. G., Klok, E. J., Jones, P. D., and New, M., 2008, A European daily high-resolution gridded data set of surface temperature and precipitation for 1950–2006: *Journal of Geophysical Research: Atmospheres*, v. 113, no. D20.
- Hegerl, G., and Zwiers, F., 2011, Use of models in detection and attribution of climate change: *Wiley interdisciplinary reviews: climate change*, v. 2, no. 4, p. 570-591.
- Held, I. M., and Soden, B. J., 2006, Robust responses of the hydrological cycle to global warming: *Journal of climate*, v. 19, no. 21, p. 5686-5699.
- Herring, S. C., Christidis, N., Hoell, A., Hoerling, M. P., and Stott, P. A., 2019, Explaining Extreme Events of 2017 from a Climate Perspective: *Bulletin of the American Meteorological Society*, v. 100, no. 1, p. S1-S117.
- Herring, S. C., Christidis, N., Hoell, A., Kossin, J. P., III, C. J. S., and Stott, P. A., 2018, Explaining Extreme Events of 2016 from a Climate Perspective: *Bulletin of the American Meteorological Society*, v. 99, no. 1, p. S1-S157.
- Herring, S. C., Hoell, A., Hoerling, M. P., Kossin, J. P., III, C. J. S., and Stott, P. A., 2016, Explaining Extreme Events of 2015 from a Climate Perspective: *Bulletin of the American Meteorological Society*, v. 97, no. 12, p. S1-S145.
- Herring, S. C., Hoerling, M. P., Kossin, J. P., Peterson, T. C., and Stott, P. A., 2015, Explaining Extreme Events of 2014 from a Climate Perspective: *Bulletin of the American Meteorological Society*, v. 96, no. 12, p. S1-S172.
- Herring, S. C., Hoerling, M. P., Peterson, T. C., and Stott, P. A., 2014, Explaining Extreme Events of 2013 from a Climate Perspective: *Bulletin of the American Meteorological Society*, v. 95, no. 9, p. S1-S104.
- Hodnebrog, Ø., Marelle, L., Alterskjær, K., Wood, R., Ludwig, R., Fischer, E., Richardson, T., Forster, P., Sillmann, J., and Myhre, G., 2019, Intensification of summer precipitation with shorter time-scales in Europe: *Environmental Research Letters*, v. 14, no. 12, p. 124050.
- Hohenegger, C., Brockhaus, P., and Schaer, C., 2008, Towards climate simulations at cloud-resolving scales: *Meteorologische Zeitschrift*, v. 17, no. 4, p. 383-394.
- Hope, P., Lim, E.-P., Hendon, H., and Wang, G., 2018, The Effect of Increasing CO₂ on the Extreme September 2016 Rainfall Across Southeastern Australia: *Bulletin of the American Meteorological Society*, v. 99, no. 1, p. S133-S138.

- Iacono, M. J., Delamere, J. S., Mlawer, E. J., Shephard, M. W., Clough, S. A., and Collins, W. D., 2008, Radiative forcing by long-lived greenhouse gases: Calculations with the AER radiative transfer models: *Journal of Geophysical Research: Atmospheres*, v. 113, no. D13.
- Imada, Y., Watanabe, M., Mori, M., Kimoto, M., Shiogama, H., and Ishii, M., 2013, Contribution of atmospheric circulation change to the 2012 heavy rainfall in southwestern Japan: *Bulletin of the American Meteorological Society*, v. 94, no. 9, p. S52.
- IPCC, 2014, Climate change 2014 synthesis report. contribution of working groups I, II, and III to the fifth assessment report of the Intergovernmental Panel on Climate Change [Core Writing Team, R.K. Pachauri and L.A. Meyer (eds.)]. IPCC, Geneva, Switzerland, 151 pp.
- Isotta, F. A., Frei, C., Weilguni, V., Perčec Tadić, M., Lassegues, P., Rudolf, B., Pavan, V., Cacciamani, C., Antolini, G., and Ratto, S. M., 2014, The climate of daily precipitation in the Alps: development and analysis of a high-resolution grid dataset from pan-Alpine rain-gauge data: *International Journal of Climatology*, v. 34, no. 5, p. 1657-1675.
- Jacob, D., Petersen, J., Eggert, B., Alias, A., Christensen, O. B., Bouwer, L. M., Braun, A., Colette, A., Déqué, M., Georgievski, G., Georgopoulou, E., Gobiet, A., Menut, L., Nikulin, G., Haensler, A., Hempelmann, N., Jones, C., Keuler, K., Kovats, S., Kröner, N., Kotlarski, S., Kriegsman, A., Martin, E., van Meijgaard, E., Moseley, C., Pfeifer, S., Preuschmann, S., Radermacher, C., Radtke, K., Rechid, D., Rounsevell, M., Samuelsson, P., Somot, S., Soussana, J.-F., Teichmann, C., Valentini, R., Vautard, R., Weber, B., and Yiou, P., 2014, EURO-CORDEX: new high-resolution climate change projections for European impact research: *Regional Environmental Change*, v. 14, no. 2, p. 563-578.
- Janjic, Z., 1996, The surface layer parameterization in the NCEP Eta Model: *World Meteorological Organization-Publications-WMO TD*, p. 4.16-14.17.
- Jézéquel, A., Dépoues, V., Guillemot, H., Rajaud, A., Trolliet, M., Vrac, M., Vanderlinden, J.-P., and Yiou, P., 2020, Singular Extreme Events and Their Attribution to Climate Change: A Climate Service-Centered Analysis: *Weather, Climate, and Society*, v. 12, no. 1, p. 89-101.
- Jézéquel, A., Dépoues, V., Guillemot, H., Trolliet, M., Vanderlinden, J.-P., and Yiou, P., 2018, Behind the veil of extreme event attribution: *Climatic Change*, v. 149, no. 3, p. 367-383.
- Kam, J., Knutson, T. R., Zeng, F., and Wittenberg, A. T., 2018, CMIP5 Model-based Assessment of Anthropogenic Influence on Highly Anomalous Arctic Warmth During November–December 2016: *Bulletin of the American Meteorological Society*, v. 99, no. 1, p. S34-S38.
- Karki, R., Gerlitz, L., Schickhoff, U., Scholten, T., and Böhner, J., 2017, Quantifying the added value of convection-permitting climate simulations in complex terrain: a systematic evaluation of WRF over the Himalayas: *Earth System Dynamics*, v. 8, p. 507-528.

- Kay, A. L., Booth, N., Lamb, R., Raven, E., Schaller, N., and Sparrow, S., 2018, Flood event attribution and damage estimation using national-scale grid-based modelling: Winter 2013/2014 in Great Britain: *International Journal of Climatology*, v. 38, no. 14, p. 5205-5219.
- Kendon, E. J., Ban, N., Roberts, N. M., Fowler, H. J., Roberts, M. J., Chan, S. C., Evans, J. P., Fosser, G., and Wilkinson, J. M., 2017, Do convection-permitting regional climate models improve projections of future precipitation change?: *Bulletin of the American Meteorological Society*, v. 98, no. 1, p. 79-93.
- Kendon, E. J., Roberts, N. M., Senior, C. A., and Roberts, M. J., 2012, Realism of rainfall in a very high-resolution regional climate model: *Journal of Climate*, v. 25, no. 17, p. 5791-5806.
- Kendon, E. J., Stratton, R. A., Tucker, S., Marsham, J. H., Berthou, S., Rowell, D. P., and Senior, C. A., 2019, Enhanced future changes in wet and dry extremes over Africa at convection-permitting scale: *Nature communications*, v. 10, no. 1, p. 1794.
- King, A. D., Karoly, D. J., Donat, M. G., and Alexander, L. V., 2014, Climate change turns Australia's 2013 big dry into a year of record-breaking heat.
- Kirchmeier-Young, M. C., Wan, H., Zhang, X., and Seneviratne, S. I., 2019, Importance of Framing for Extreme Event Attribution: The Role of Spatial and Temporal Scales: *Earth's Future*, v. 7, no. 10, p. 1192-1204.
- Knist, S., Goergen, K., and Simmer, C., 2018, Evaluation and projected changes of precipitation statistics in convection-permitting WRF climate simulations over Central Europe: *Climate Dynamics*, p. 1-17.
- Komurcu, M., Emanuel, K. A., Huber, M., and Acosta, R. P., 2018, High-Resolution Climate Projections for the Northeastern United States Using Dynamical Downscaling at Convection-Permitting Scales: *Earth and Space Science*, v. 5, no. 11, p. 801-826.
- Kotlarski, S., Keuler, K., Christensen, O. B., Colette, A., Déqué, M., Gobiet, A., Goergen, K., Jacob, D., Lüthi, D., van Meijgaard, E., Nikulin, G., Schär, C., Teichmann, C., Vautard, R., Warrach-Sagi, K., and Wulfmeyer, V., 2014, Regional climate modeling on European scales: a joint standard evaluation of the EURO-CORDEX RCM ensemble: *Geosci. Model Dev.*, v. 7, no. 4, p. 1297-1333.
- Langhans, W., Schmidli, J., Fuhrer, O., Bieri, S., and Schär, C., 2013, Long-term simulations of thermally driven flows and orographic convection at convection-parameterizing and cloud-resolving resolutions: *Journal of Applied Meteorology and Climatology*, v. 52, no. 6, p. 1490-1510.
- Lee, K. O., Flamant, C., Duffourg, F., Ducrocq, V., and Chaboureau, J. P., 2018, Impact of upstream moisture structure on a back-building convective precipitation system in south-eastern France during HyMeX IOP13: *Atmos. Chem. Phys.*, v. 18, no. 23, p. 16845-16862.

- Lélé, M. I., Leslie, L. M., and Lamb, P. J., 2015, Analysis of Low-Level Atmospheric Moisture Transport Associated with the West African Monsoon: *Journal of Climate*, v. 28, no. 11, p. 4414-4430.
- Lenderink, Barbero, R., Loriaux, J., and Fowler, H., 2017, Super-Clausius–Clapeyron scaling of extreme hourly convective precipitation and its relation to large-scale atmospheric conditions: *Journal of Climate*, v. 30, no. 15, p. 6037-6052.
- Lenderink, G., and Attema, J., 2015, A simple scaling approach to produce climate scenarios of local precipitation extremes for the Netherlands: *Environmental Research Letters*, v. 10, no. 8, p. 085001.
- Lenderink, G., and Van Meijgaard, E., 2008, Increase in hourly precipitation extremes beyond expectations from temperature changes: *Nature Geoscience*, v. 1, no. 8, p. 511.
- Lewis, S., and Karoly, D., 2014, The role of anthropogenic forcing in the record 2013 Australia-wide annual and spring temperatures.
- Liang, X.-Z., Kunkel, K. E., and Samel, A. N., 2001, Development of a Regional Climate Model for U.S. Midwest Applications. Part I: Sensitivity to Buffer Zone Treatment: *Journal of Climate*, v. 14, no. 23, p. 4363-4378.
- Luu, L. N., Vautard, R., Yiou, P., van Oldenborgh, G. J., and Lenderink, G., 2018, Attribution of Extreme Rainfall Events in the South of France Using EURO-CORDEX Simulations: *Geophysical Research Letters*, v. 45, no. 12, p. 6242-6250.
- Mallakpour, I., and Villarini, G., 2017, Analysis of changes in the magnitude, frequency, and seasonality of heavy precipitation over the contiguous USA: *Theoretical and Applied Climatology*, v. 130, no. 1-2, p. 345-363.
- Marjanac, S., and Patton, L., 2018, Extreme weather event attribution science and climate change litigation: an essential step in the causal chain?: *Journal of Energy & Natural Resources Law*, v. 36, no. 3, p. 265-298.
- Marthews, T. R., Jones, R. G., Dadson, S. J., Otto, F. E. L., Mitchell, D., Guillod, B. P., and Allen, M. R., 2019, The Impact of Human-Induced Climate Change on Regional Drought in the Horn of Africa: *Journal of Geophysical Research: Atmospheres*, v. 124, no. 8, p. 4549-4566.
- Massey, N., Jones, R., Otto, F. E. L., Aina, T., Wilson, S., Murphy, J. M., Hassell, D., Yamazaki, Y. H., and Allen, M. R., 2015, weather@home—development and validation of a very large ensemble modelling system for probabilistic event attribution: *Quarterly Journal of the Royal Meteorological Society*, v. 141, no. 690, p. 1528-1545.
- Meinshausen, M., Smith, S. J., Calvin, K., Daniel, J. S., Kainuma, M. L. T., Lamarque, J. F., Matsumoto, K., Montzka, S. A., Raper, S. C. B., Riahi, K., Thomson, A., Velders, G. J. M., and van Vuuren, D. P. P., 2011, The RCP greenhouse gas concentrations and their extensions from 1765 to 2300: *Climatic Change*, v. 109, no. 1, p. 213.

- Michelangeli, P.-A., Vrac, M., and Loukos, H., 2009, Probabilistic downscaling approaches: Application to wind cumulative distribution functions: *Geophysical Research Letters*, v. 36, no. 11.
- Miguez-Macho, G., Stenchikov, G. L., and Robock, A., 2004, Regional Climate Simulations over North America: Interaction of Local Processes with Improved Large-Scale Flow: *Journal of Climate*, v. 18, no. 8, p. 1227-1246.
- Miguez-Macho, G., Stenchikov, G. L., and Robock, A., 2004, Spectral nudging to eliminate the effects of domain position and geometry in regional climate model simulations: *Journal of Geophysical Research: Atmospheres*, v. 109, no. D13.
- Min, S.-K., Kim, Y.-H., Paik, S., Kim, M.-K., and Boo, K.-O., 2015, Anthropogenic Influence on the 2014 Record-Hot Spring in Korea: *Bulletin of the American Meteorological Society*, v. 96, no. 12, p. S95-S99.
- Min, S.-K., Zhang, X., Zwiers, F. W., and Hegerl, G. C., 2011, Human contribution to more-intense precipitation extremes: *Nature*, v. 470, no. 7334, p. 378-381.
- Nakanishi, M., and Niino, H., 2006, An Improved Mellor–Yamada Level-3 Model: Its Numerical Stability and Application to a Regional Prediction of Advection Fog: *Boundary-Layer Meteorology*, v. 119, no. 2, p. 397-407.
- National Academies of Sciences, E., Medicine, 2016, Attribution of extreme weather events in the context of climate change, National Academies Press.
- Nuissier, O., Ducrocq, V., Ricard, D., Lebeaupin, C., and Anquetin, S., 2008, A numerical study of three catastrophic precipitating events over southern France. I: Numerical framework and synoptic ingredients: *Quarterly Journal of the Royal Meteorological Society*, v. 134, no. 630, p. 111-130.
- Nuissier, O., Joly, B., Joly, A., Ducrocq, V., and Arbogast, P., 2011, A statistical downscaling to identify the large-scale circulation patterns associated with heavy precipitation events over southern France: *Quarterly Journal of the Royal Meteorological Society*, v. 137, no. 660, p. 1812-1827.
- Nuissier, O., Joly, B., Vié, B., and Ducrocq, V., 2012, Uncertainty of lateral boundary conditions in a convection-permitting ensemble: a strategy of selection for Mediterranean heavy precipitation events: *Nat. Hazards Earth Syst. Sci.*, v. 12, no. 10, p. 2993-3011.
- Nuissier, O., Marsigli, C., Vincendon, B., Hally, A., Bouttier, F., Montani, A., and Paccagnella, T., 2016, Evaluation of two convection-permitting ensemble systems in the HyMeX Special Observation Period (SOP1) framework: *Quarterly Journal of the Royal Meteorological Society*, v. 142, no. S1, p. 404-418.
- O’Gorman, P. A., 2012, Sensitivity of tropical precipitation extremes to climate change: *Nature Geoscience*, v. 5, no. 10, p. 697-700.
- Otto, F. E., Massey, N., Van Oldenborgh, G., Jones, R., and Allen, M., 2012, Reconciling two approaches to attribution of the 2010 Russian heat wave: *Geophysical Research Letters*, v. 39, no. 4.

- Pall, P., Aina, T., Stone, D. A., Stott, P. A., Nozawa, T., Hilberts, A. G., Lohmann, D., and Allen, M. R., 2011, Anthropogenic greenhouse gas contribution to flood risk in England and Wales in autumn 2000: *Nature*, v. 470, no. 7334, p. 382.
- Pall, P., Allen, M. R., and Stone, D. A., 2007, Testing the Clausius–Clapeyron constraint on changes in extreme precipitation under CO₂ warming: *Climate Dynamics*, v. 28, no. 4, p. 351-363.
- Perkins, S. E., King, A. D., and Alexander, L., 2014, Increased simulated risk of the hot Australian summer of 2012/13 due to anthropogenic activity as measured by heat wave frequency and intensity.
- Peterson, T. C., Hoerling, M. P., Stott, P. A., and Herring, S. C., 2013, Explaining Extreme Events of 2012 from a Climate Perspective: *Bulletin of the American Meteorological Society*, v. 94, no. 9, p. S1-S74.
- Peterson, T. C., Stott, P. A., and Herring, S., 2012, Explaining Extreme Events of 2011 from a Climate Perspective: *Bulletin of the American Meteorological Society*, v. 93, no. 7, p. 1041-1067.
- Philip, S., Kew, S. F., Oldenborgh, G. J. v., Otto, F., O’Keefe, S., Haustein, K., King, A., Zegeye, A., Eshetu, Z., Hailemariam, K., Singh, R., Jjemba, E., Funk, C., and Cullen, H., 2018, Attribution Analysis of the Ethiopian Drought of 2015: *Journal of Climate*, v. 31, no. 6, p. 2465-2486.
- Polade, S. D., Gershunov, A., Cayan, D. R., Dettinger, M. D., and Pierce, D. W., 2017, Precipitation in a warming world: Assessing projected hydro-climate changes in California and other Mediterranean climate regions: *Scientific Reports*, v. 7, no. 1, p. 10783.
- Prein, Gobiet, A., Suklitsch, M., Truhetz, H., Awan, N., Keuler, K., and Georgievski, G., 2013, Added value of convection permitting seasonal simulations: *Climate Dynamics*, v. 41, no. 9-10, p. 2655-2677.
- Prein, Langhans, W., Fosser, G., Ferrone, A., Ban, N., Goergen, K., Keller, M., Tölle, M., Gutjahr, O., and Feser, F., 2015, A review on regional convection-permitting climate modeling: Demonstrations, prospects, and challenges: *Reviews of Geophysics*, v. 53, no. 2, p. 323-361.
- Prein, A., Gobiet, A., Truhetz, H., Keuler, K., Goergen, K., Teichmann, C., Maule, C. F., Van Meijgaard, E., Déqué, M., and Nikulin, G., 2016, Precipitation in the EURO-CORDEX 0.11° and 0.44° 0.44° simulations: high resolution, high benefits?: *Climate dynamics*, v. 46, no. 1-2, p. 383-412.
- Quintana-Seguí, P., Moigne, P. L., Durand, Y., Martin, E., Habets, F., Baillon, M., Canellas, C., Franchisteguy, L., and Morel, S., 2008, Analysis of Near-Surface Atmospheric Variables: Validation of the SAFRAN Analysis over France: *Journal of Applied Meteorology and Climatology*, v. 47, no. 1, p. 92-107.

- Rahmstorf, S., and Coumou, D., 2011, Increase of extreme events in a warming world: *Proceedings of the National Academy of Sciences*, v. 108, no. 44, p. 17905-17909.
- Ribes, A., Thao, S., Vautard, R., Dubuisson, B., Somot, S., Colin, J., Planton, S., and Soubeyrou, J.-M., 2019, Observed increase in extreme daily rainfall in the French Mediterranean: *Climate dynamics*, v. 52, no. 1-2, p. 1095-1114.
- Rimi, R. H., Haustein, K., Allen, M. R., and Barbour, E. J., 2019, Risks of Pre-Monsoon Extreme Rainfall Events of Bangladesh: Is Anthropogenic Climate Change Playing a Role?: *Bulletin of the American Meteorological Society*, v. 100, no. 1, p. S61-S65.
- Rosier, S., Dean, S., Stuart, S., Carey-Smith, T., Black, M. T., and Massey, N., 2015, Extreme Rainfall in Early July 2014 in Northland, New Zealand—Was There an Anthropogenic Influence?: *Bulletin of the American Meteorological Society*, v. 96, no. 12, p. S136-S140.
- Ruti, P. M., Somot, S., Giorgi, F., Dubois, C., Flaounas, E., Obermann, A., Dell'Aquila, A., Pisacane, G., Harzallah, A., Lombardi, E., Ahrens, B., Akhtar, N., Alias, A., Arsouze, T., Aznar, R., Bastin, S., Bartholy, J., Béranger, K., Beuvier, J., Bouffies-Cloch e, S., Brauch, J., Cabos, W., Calmanti, S., Calvet, J.-C., Carillo, A., Conte, D., Coppola, E., Djurdjevic, V., Drobinski, P., Elizalde-Arellano, A., Gaertner, M., Gal n, P., Gallardo, C., Gualdi, S., Goncalves, M., Jorba, O., Jord , G., L'Heveder, B., Lebeaupin-Brossier, C., Li, L., Liguori, G., Lionello, P., Maci s, D., Nabat, P.,  nol, B., Raikovic, B., Ramage, K., Sevault, F., Sannino, G., Struglia, M. V., Sanna, A., Torma, C., and Vervatis, V., 2016, Med-CORDEX Initiative for Mediterranean Climate Studies: *Bulletin of the American Meteorological Society*, v. 97, no. 7, p. 1187-1208.
- Scaff, L., Prein, A. F., Li, Y., Liu, C., Rasmussen, R., and Ikeda, K., 2019, Simulating the convective precipitation diurnal cycle in North America's current and future climate: *Climate Dynamics*.
- Schaller, N., FRIEDERIKE, E. O., GEERT, J., OLDENBORGH, N. R., Sparrow, S., and MYLES, R. A., 2014, THE HEAVY PRECIPITATION EVENT OF MAY–JUNE 2013 IN THE UPPER DANUBE AND ELBE BASINS.
- Schaller, N., Kay, A. L., Lamb, R., Massey, N. R., Van Oldenborgh, G. J., Otto, F. E., Sparrow, S. N., Vautard, R., Yiou, P., and Ashpole, I., 2016, Human influence on climate in the 2014 southern England winter floods and their impacts: *Nature Climate Change*, v. 6, no. 6, p. 627.
- Scherrer, S. C., Fischer, E. M., Posselt, R., Liniger, M. A., Croci-Maspoli, M., and Knutti, R., 2016, Emerging trends in heavy precipitation and hot temperature extremes in Switzerland: *Journal of Geophysical Research: Atmospheres*, v. 121, no. 6, p. 2626-2637.
- S n si, S., Bougeault, P., Ch ze, J.-L., Cosentino, P., and Thepenier, R.-M., 1996, The Vaison-La-Romaine Flash Flood: Mesoscale Analysis and Predictability Issues: *Weather and Forecasting*, v. 11, no. 4, p. 417-442.

- Seth, A., and Giorgi, F., 1998, The effects of domain choice on summer precipitation simulation and sensitivity in a regional climate model: *Journal of Climate*, v. 11, no. 10, p. 2698-2712.
- Shi, X., and Durran, D., 2016, Sensitivities of Extreme Precipitation to Global Warming Are Lower over Mountains than over Oceans and Plains: *Journal of Climate*, v. 29, no. 13, p. 4779-4791.
- Sippel, S., Otto, F. E. L., Forkel, M., Allen, M. R., Guillod, B. P., Heimann, M., Reichstein, M., Seneviratne, S. I., Thonicke, K., and Mahecha, M. D., 2016, A novel bias correction methodology for climate impact simulations: *Earth Syst. Dynam.*, v. 7, no. 1, p. 71-88.
- Sparrow, S., Huntingford, C., Massey, N., and Allen, M. R., 2013, The use of the very large atmospheric model ensemble to assess potential anthropogenic influence on the UK summer 2012 high rainfall totals: *Bulletin of the American Meteorological Society*, v. 94, no. 9, p. S36-S38.
- Stott, P. A., 2003, Attribution of regional-scale temperature changes to anthropogenic and natural causes: *Geophysical Research Letters*, v. 30, no. 14.
- Stott, P. A., Allen, M., Christidis, N., Dole, R. M., Hoerling, M., Huntingford, C., Pall, P., Perlwitz, J., and Stone, D., 2013, Attribution of Weather and Climate-Related Events, *in* Asrar, G. R., and Hurrell, J. W., eds., *Climate Science for Serving Society: Research, Modeling and Prediction Priorities*: Dordrecht, Springer Netherlands, p. 307-337.
- Stott, P. A., Stone, D. A., and Allen, M. R., 2004, Human contribution to the European heatwave of 2003: *Nature*, v. 432, no. 7017, p. 610.
- Stott, P. A., and Walton, P., 2013, Attribution of climate-related events: understanding stakeholder needs: *Weather*, v. 68, no. 10, p. 274-279.
- Sun, Q., and Miao, C., 2018, Extreme Rainfall (R20mm, RX5day) in Yangtze–Huai, China, in June–July 2016: The Role of ENSO and Anthropogenic Climate Change: *Bulletin of the American Meteorological Society*, v. 99, no. 1, p. S102-S106.
- Sun, X., Xue, M., Brotzge, J., McPherson, R. A., Hu, X. M., and Yang, X. Q., 2016, An evaluation of dynamical downscaling of Central Plains summer precipitation using a WRF-based regional climate model at a convection-permitting 4 km resolution: *Journal of Geophysical Research: Atmospheres*, v. 121, no. 23, p. 13,801-813,825.
- Tabary, P., Dupuy, P., L’Henaff, G., Gueguen, C., Moulin, L., Laurantin, O., Merlier, C., and Soubeyroux, J.-M., 2012, A 10-year (1997–2006) reanalysis of quantitative precipitation estimation over France: methodology and first results: *IAHS Publ.*, v. 351, p. 255-260.
- Thompson, G., Field, P. R., Rasmussen, R. M., and Hall, W. D., 2008, Explicit Forecasts of Winter Precipitation Using an Improved Bulk Microphysics Scheme. Part II: Implementation of a New Snow Parameterization: *Monthly Weather Review*, v. 136, no. 12, p. 5095-5115.

- Tozer, C., Risbey, J., Grose, M., Monselesan, D., Squire, D., Black, A., Richardson, D., Sparrow, S., Li, S., and Wallom, D., 2020, A 1-day extreme rainfall event in Tasmania: Process evaluation and long tail attribution: *Bulletin of the American Meteorological Society*.
- Tramblay, Y., and Somot, S., 2018, Future evolution of extreme precipitation in the Mediterranean: *Climatic Change*, v. 151, no. 2, p. 289-302.
- Trenberth, K. E., 2008, Observational needs for climate prediction and adaptation: *Bulletin of the World Meteorological Organization*, v. 57, no. 1, p. 17-21.
- Trenberth, K. E., Dai, A., Rasmussen, R. M., and Parsons, D. B., 2003, The Changing Character of Precipitation: *Bulletin of the American Meteorological Society*, v. 84, no. 9, p. 1205-1218.
- Uhe, P., Philip, S., Kew, S., Shah, K., Kimutai, J., Mwangi, E., van Oldenborgh, G. J., Singh, R., Arrighi, J., Jjemba, E., Cullen, H., and Otto, F., 2018, Attributing drivers of the 2016 Kenyan drought: *International Journal of Climatology*, v. 38, no. S1, p. e554-e568.
- van der Wiel, K., Kapnick, S. B., van Oldenborgh, G. J., Whan, K., Philip, S., Vecchi, G. A., Singh, R. K., Arrighi, J., and Cullen, H., 2017, Rapid attribution of the August 2016 flood-inducing extreme precipitation in south Louisiana to climate change: *Hydrol. Earth Syst. Sci.*, v. 21, no. 2, p. 897-921.
- van Oldenborgh, G. J., Reyes, F. D., Drijfhout, S., and Hawkins, E., 2013, Reliability of regional climate model trends: *Environmental Research Letters*, v. 8, no. 1, p. 014055.
- Vanden Broucke, S., Wouters, H., Demuzere, M., and van Lipzig, N. P. M., 2019, The influence of convection-permitting regional climate modeling on future projections of extreme precipitation: dependency on topography and timescale: *Climate Dynamics*, v. 52, no. 9, p. 5303-5324.
- Vautard, R., Colette, A., Van Meijgaard, E., Meleux, F., Jan van Oldenborgh, G., Otto, F., Tobin, I., and Yiou, P., 2018, Attribution of wintertime anticyclonic stagnation contributing to air pollution in Western Europe: *Bulletin of the American Meteorological Society*, v. 99, no. 1, p. S70-S75.
- Vautard, R., Yiou, P., Otto, F., Stott, P., Christidis, N., Van Oldenborgh, G. J., and Schaller, N., 2016, Attribution of human-induced dynamical and thermodynamical contributions in extreme weather events: *Environmental Research Letters*, v. 11, no. 11, p. 114009.
- Vautard, R., Yiou, P., van Oldenborgh, G.-J., Lenderink, G., Thao, S., Ribes, A., Planton, S., Dubuisson, B., and Soubeyroux, J.-M., 2015, Extreme fall 2014 precipitation in the Cévennes mountains: *Bulletin of the American Meteorological Society*, v. 96, no. 12, p. S56-S60.
- Vidal, J.-P., Martin, E., Franchistéguy, L., Baillon, M., and Soubeyroux, J.-M., 2010, A 50-year high-resolution atmospheric reanalysis over France with the Safran system: *International Journal of Climatology*, v. 30, no. 11, p. 1627-1644.

- Vié, B., Molinié, G., Nuissier, O., Vincendon, B., Ducrocq, V., Bouttier, F., and Richard, E., 2012, Hydro-meteorological evaluation of a convection-permitting ensemble prediction system for Mediterranean heavy precipitating events: *Nat. Hazards Earth Syst. Sci.*, v. 12, no. 8, p. 2631-2645.
- Vié, B., Nuissier, O., and Ducrocq, V., 2011, Cloud-Resolving Ensemble Simulations of Mediterranean Heavy Precipitating Events: Uncertainty on Initial Conditions and Lateral Boundary Conditions: *Monthly Weather Review*, v. 139, no. 2, p. 403-423.
- Vrac, M., Drobinski, P., Merlo, A., Herrmann, M., Lavaysse, C., Li, L., and Somot, S., 2012, Dynamical and statistical downscaling of the French Mediterranean climate: uncertainty assessment.
- Wahl, T., Jain, S., Bender, J., Meyers, S. D., and Luther, M. E., 2015, Increasing risk of compound flooding from storm surge and rainfall for major US cities: *Nature Climate Change*, v. 5, no. 12, p. 1093-1097.
- Weedon, G. P., Balsamo, G., Bellouin, N., Gomes, S., Best, M. J., and Viterbo, P., 2014, The WFDEI meteorological forcing data set: WATCH Forcing Data methodology applied to ERA-Interim reanalysis data: *Water Resources Research*, v. 50, no. 9, p. 7505-7514.
- Westra, S., Fowler, H. J., Evans, J. P., Alexander, L. V., Berg, P., Johnson, F., Kendon, E. J., Lenderink, G., and Roberts, N. M., 2014, Future changes to the intensity and frequency of short-duration extreme rainfall: *Reviews of Geophysics*, v. 52, no. 3, p. 522-555.
- Yang, Y., Uddstrom, M., and Duncan, M., 2011, Effects of short spin-up periods on soil moisture simulation and the causes over New Zealand: *Journal of Geophysical Research: Atmospheres*, v. 116, no. D24.
- Yiou, P., Jézéquel, A., Naveau, P., Otto, F. E., Vautard, R., and Vrac, M., 2017, A statistical framework for conditional extreme event attribution: *Advances in Statistical Climatology, Meteorology and Oceanography*, v. 3, no. 1, p. 17-31.
- Yuan, X., Wang, S., and Hu, Z.-Z., 2018, Do Climate Change and El Niño Increase Likelihood of Yangtze River Extreme Rainfall?: *Bulletin of the American Meteorological Society*, v. 99, no. 1, p. S113-S117.
- Zhang, W., Villarini, G., Scoccimarro, E., and Vecchi, G. A., 2017, Stronger influences of increased CO₂ on subdaily precipitation extremes than at the daily scale: *Geophysical Research Letters*, v. 44, no. 14, p. 7464-7471.
- Zhang, X., Wan, H., Zwiers, F. W., Hegerl, G. C., and Min, S.-K., 2013, Attributing intensification of precipitation extremes to human influence: *Geophysical Research Letters*, v. 40, no. 19, p. 5252-5257.
- Zhou, C., Wang, K., and Qi, D., 2018, Attribution of the July 2016 Extreme Precipitation Event Over China's Wuhang: *Bulletin of the American Meteorological Society*, v. 99, no. 1, p. S107-S112.

- Zhu, K., Xue, M., Zhou, B., Zhao, K., Sun, Z., Fu, P., Zheng, Y., Zhang, X., and Meng, Q., 2018, Evaluation of Real-Time Convection-Permitting Precipitation Forecasts in China During the 2013–2014 Summer Season: *Journal of Geophysical Research: Atmospheres*, v. 123, no. 2, p. 1037-1064.
- Zittis, G., Bruggeman, A., Camera, C., Hadjinicolaou, P., and Lelieveld, J., 2017, The added value of convection permitting simulations of extreme precipitation events over the eastern Mediterranean: *Atmospheric research*, v. 191, p. 20-33.

Titre: Le rôle du changement climatique induit par l'homme sur les précipitations convectives extrêmes dans le sud de la France : Une approche de simulation par modèle à haute résolution

Mots clés: Extrême, Précipitation, Attribution, Permettant la Convection

Résumé: La zone France-Méditerranée est fréquemment exposée à de fortes précipitations en automne dont l'accumulation quotidienne peut parfois dépasser 300 millimètres. Quelques études montrent une tendance à l'augmentation de la fréquence et de l'intensité de ces événements (par exemple Vautard et al., 2015; Ribes et al., 2019). Cependant, une attribution formelle des événements extrêmes qui lie ces changements au changement climatique induit par l'homme pour cette région n'a jamais été faite. Ce sujet de thèse vise à quantifier le rôle du changement climatique induit par l'homme dans l'altération des propriétés statistiques des précipitations convectives extrêmes survenant sur la région France-Méditerranée, en se concentrant sur la chaîne de montagnes des Cévennes et en utilisant pour la première fois une approche de modèle à haute résolution incluant un modèle permettant la convection. J'analyse d'abord l'ensemble EURO-

CORDEX, qui comprend différentes combinaisons de modèles climatiques globaux et de modèles climatiques régionaux. Ensuite, j'ai effectué une série de simulations numériques avec le modèle WRF à une résolution permettant la convection. J'ai également comparé les simulations avec les observations et les ré-analyses à haute résolution. Les résultats montrent que les modèles régionaux peuvent reproduire des événements extrêmes de pluie convective avec une meilleure concordance avec les observations en augmentant leur résolution horizontale, en particulier à une résolution permettant la convection (environ 3 km). En utilisant ces simulations, je montre que le changement climatique induit par l'homme rend les précipitations quotidiennes et trihoraires sur 100 ans au moins deux fois plus probables dans le climat actuel. Les résultats suggèrent également la nécessité d'utiliser une approche multi-modèle pour réduire les incertitudes dans ce type d'étude d'impact.

Title: The Role of Human-Induced Climate Change on Extreme Convective Precipitation Events in the South of France: A High-Resolution Model Simulation Approach

Keywords: Extreme, Precipitation, Attribution, Convection-permitting

Abstract: The France-Mediterranean area is frequently exposed to heavy precipitation events in the autumn whose daily accumulation can sometimes exceed 300 millimeters. There are a few studies showing the increasing trend in the frequency and intensity of these events (e.g. Ribes et al., 2019; Vautard et al., 2015). However, a formal extreme event attribution that links those changes to human-induced climate change for this area has never been done. This PhD subject aims at quantifying the role of human-induced climate change in altering the statistical properties of extreme convective precipitation event occurring over the France-Mediterranean focusing on the Cevennes mountain range and using a high-resolution model approach including convection-permitting model for the first time. I first analyze the EURO-CORDEX ensemble,

which includes different combinations of global climate models and regional climate models. Then I conducted a set of numerical simulations with the WRF model at a convection-permitting resolution. I also compared the simulations with observations and high-resolution re-analyses. The results show that regional models can reproduce extreme convective rainfall events in better agreement with observations by increasing their horizontal resolution, especially to convection-permitting resolution (approx. 3 km). By using these simulations, I show that human-induced climate change consistently makes the 100-year of 3-hourly and daily precipitation event at least 2 times more likely under current climate. The results also suggest the need of using multi-model approach to reduce the uncertainties in this type of impact study.